



**UNIVERSITÀ DEGLI STUDI DI ROMA
"TOR VERGATA"**

FACOLTA' DI INGEGNERIA

DOTTORATO DI RICERCA IN

Ingegneria delle Strutture e Geotecnica

XXI Ciclo

**Ottimizzazione e Miglioramento del Comportamento a Fatica di Ponti
a Piastra Ortotropia**

Zhonghui QIAN

A.A. 2009/2010

Docente Guida: Prof. Antonio Grimaldi, Prof. Donato Abruzzese

Coordinatore: Prof. Franco Maceri

Z.H. QIAN

**OTTIMIZZAZIONE E MIGLIORAMENTO DEL COMPORTAMENTO A FATICA DI PONTI
A PIASTRA ORTOTROPA**

Tesi, luglio 2010



DIPARTIMENTO DI INGEGNERIA CIVILE

UNIVERSITA' DEGLI STUDI DI ROMA "TOR VERGATA"

DOTTORATO DI RICERCA IN INGEGNERIA DELLE STRUTTURE E GEOTECNICA

DOTTORATO DI RICERCA IN INGEGNERIA DELLE STRUTTURE

XXI CICLO

UNIVERSITÀ DEGLI STUDI DI ROMA "TOR VERGATA"

**OTTIMIZZAZIONE E MIGLIORAMENTO DEL COMPORTAMENTO A
FATICA DI PONTI A PIASTRA ORTOTROPA**

Tesi presentata per il conseguimento del titolo di

Dottore di Ricerca in Ingegneria delle Strutture

da

Zhonghui QIAN

Coordinatore del Corso di Dottorato

Prof. Franco Maceri

Tutore del candidato

Prof. Ing. Antonio Grimaldi

Co-tutore

Prof. Ing. Donato Abruzzese

Dipartimento di Ingegneria Civile

Luglio 2010

ACKNOWLEDGEMENTS

The author would like to express his most sincere gratitude and deepest appreciation to Prof. Donato ABRUZZESE, Prof. Antonio GRIMALDI and Ing. Sante CAMO, who spent much time to guide the investigation. Their guidance, insight, patience and encouragement not only help the author on this dissertation, but also regarding his professional career. They provided the author many chances to participate intensive courses and conferences, both in Italy and other countries.

The author would like to express his great appreciation to Prof. Jianli YUAN for his continuous concern and guidance during the past years.

The author would like to express his deep appreciation to the technician Fedinando MIELE and Dr. Lorenzo MICCOLI. Special thanks are given to Prof. Vincenzo Tagliaferri, Dr. Massimiliano Barletta, Ing. Daniele Carnevale and Ing. GIANLUCA for the collaboration of laboratory tests.

The author would like to express his appreciation to Prof. Ben YEN, Prof. Richard SAUSE, Prof. John W. FISHER, Dr. Cheng CHEN, and Dr. Sougata ROY for their great help when he visited Lehigh University.

The author would like to thank Dean Marina TESAURO, and Ms. Claudia FIORANI and Ms. Belinda CAPARRO for their continuous support when he arrived in Rome. The author also would like to thank all the faculty and staff of Department of Civil Engineering who helped him during his studies.

Many thanks are given to Mr. Yan Chu FONG, Dr. Jun XIAO and many other friends for the encouragement and help during these years.

Finally, the author would like to express his deepest thanks to his parents and his wife Beibei Liu for their constant and strong encouragement and support.

TABLE OF CONTENTS

1. INTRODUCTION	1
1.1 Historical Development of Analytical Methods and Design.....	1
1.2 The Advantages of Orthotropic Deck in Bridge Engineering.....	4
1.3 Orthotropic Deck Plate in Bridge Structure.....	6
1.4 Optimization Technologies.....	8
1.5 Research Objectives.....	9
1.5.1 Geometric optimization of orthotropic deck.....	9
1.5.2 Fatigue enhancement.....	10
2. ANALYSIS METHODS OF ORTHOTROPIC DECK	15
2.1 Classical Theories.....	15
2.1.1 Introduction of orthotropic plate theories.....	16
2.1.2 Orthotropic plate theory.....	18
2.1.2.1 Determination of rigidities in various specific cases.....	20
2.1.2.2 Application of the theory to the calculation of gridworks.....	24
2.1.3 The Pelikan-Esslinger Method.....	27
2.1.3.1 Open rib of orthotropic deck.....	28
2.1.3.2 Closed rib of orthotropic deck.....	32
2.1.3.3 The Pelikan-Esslinger method in AISC.....	36
2.2 Finite Element Methods.....	38
2.2.1 Advantages of FEM.....	39
2.2.2 Disadvantages of FEM.....	41
2.2.3 Application of FEM in orthotropic deck.....	41
2.3 Fatigue Behaviors.....	43

3. INFLUENCES OF GEOMETRIC PROPERTIES TO ORTHOTROPIC DECKS51

3.1 Finite Element Analysis54

 3.1.1 Introduction54

 3.1.2 Numerical modeling55

 3.1.2.1 Detailed dimensions55

 3.1.2.2 Boundary conditions.....56

 3.1.2.3 Load cases56

3.2 Deck Behaviors57

 3.2.1 Behaviors of deck plate58

 3.2.2 Behaviors of diaphragm65

3.3 Influence of Cutout.....73

 3.3.1 Introduction73

 3.3.2 The four different shapes of cutout.....78

 3.3.3 Results of Static analysis80

 3.3.3.1 The Stress performance in the diaphragm80

 3.3.3.2 The deflection and stress in the deck plate86

 3.3.4 Discussions.....92

3.4 Influence of Bulkhead96

 3.4.1 Introduction96

 3.4.2 The four different models with or without bulkhead.....100

 3.4.3 Results of Static analysis102

 3.4.3.1 Behaviors of the diaphragm.....102

 3.4.3.2 Behaviors of the deck plate114

 3.4.4 Discussions.....121

3.5 Influence of Deck Plate124

 3.5.1 Introduction124

3.5.2 Thickness influence of the deck plate.....	126
3.5.3 Discussions.....	130
3.6 Future research	131
4. FATIGUE EVALUATION OF ORTHOTROPIC DECK	135
4.1 Design Codes.....	140
4.1.1 European codes.....	141
4.1.1.1 British standard (BS5400).....	141
4.1.1.2 Eurocode 3	144
4.1.1.3 DNV offshore specifications	147
4.1.2 American specifications	150
4.1.3 Recommendations of IIW.....	154
4.1.4 Japanese specifications	158
4.1.5 Chinese codes	160
4.1.6 Discussions.....	161
4.2 Nominal Stress Approach.....	165
4.2.1 Fatigue cumulative damage law	165
4.2.1.1 Linear fatigue cumulative damage law.....	166
4.2.1.2 Nonlinear fatigue cumulative damage law	166
4.2.2 Traditional nominal stress approach.....	168
4.2.2.1 Assumptions of nominal stress approach.....	169
4.2.2.2 Traditional nominal stress approach	169
4.3 Hot Spot Stress Approach	171
4.3.1 The definitions of the structural hot spot stress method	171
4.3.2 Recent investigations of structural hot spot stress method.....	176
4.3.3 Discussions.....	178

4.4 Method of Analysis	179
4.4.1 Global model analyses of the orthotropic deck	179
4.4.1.1 Global model	179
4.4.1.2 Results of global model analyses.....	180
4.4.2 Submodel analyses of the rib-to-deck plate connections.....	180
4.4.2.1 Submodel.....	180
4.4.2.2 Results of submodel analyses	184
4.4.3 Structural hot-spot stresses	196
4.4.4 Three-step approach	199
4.4.5 Conclusions	200
5. FATIGUE ENHANCEMENT TECHNIQUES.....	205
5.1 Stress Methods	207
5.1.1 Shot peening	207
5.1.2 Hammer peening	209
5.1.3 Needle peening	211
5.1.4 Ultrasonic impact treatment	212
5.1.5 Laser peening	214
5.1.6 Fluid bed peening	215
5.1.7 Discussions	220
5.2 Geometric Methods	222
5.2.1 Buur Grinding.....	222
5.2.2 TIG dressing	224
5.3. Fatigue Tests Applied FBP	226
5.3.1 Material tests	226
5.3.2 Surface treatment.....	228

5.3.3 Fatigue tests	233
5.3.3.1 Loading spectrum	233
5.3.3.2 Test results	235
5.3.4 Discussions and conclusions	239
6. CONCLUSIONS AND RECOMMENDATIONS	243
6.1 Conclusions	243
6.2 Recommendations	245
REFERENCES.....	247

ABSTRACT

Orthotropic deck bridges are widely used in bridge engineering, especially for long span bridges. Although orthotropic deck bridges have many advantages, it is found that they are sensitive to produce fatigue cracking under the repeating vehicle loading since there are a large number of welded connections in the deck structure. Among of these connections, rib-to-deck plate connection, rib-to-diaphragm connection and rib-to-diaphragm-to-deck plate (RDDP) connection are the three typical welded connections that are more sensitive to the fatigue cracking due to the high concentrated stress and high residual stress.

Fatigue analysis of an orthotropic deck is a complex and uncertain process due to many factors which can influence the fatigue cracking. A state-of-the-art literature review of the fatigue codes/specifications was conducted to identify their advantages, disadvantages and limitations in this study. Meanwhile, the stress performances of a typical orthotropic deck were analyzed through Finite Element analysis (FEA) and, then, the fatigue resistance evaluation was carried out by the structural hot spot stress method. In addition, a fatigue improvement technique, the Fluid Bed Peening (FBP) was illustrated, and fatigue tests of the specimens treated by FBP were conducted in the laboratory.

The primary two goals of this study are to analyze the stress performances of the orthotropic deck and to develop an approach for improving the fatigue behaviors through FE method and analytical techniques, by doing parametric studies of various geometric parameters and the structural hot spot stress method. Many FE models were developed in order to analyze the stress influences of cutout geometry, with or without bulkhead, and the thickness of deck plate. The different applied loadings, which to simulate the different vehicle locations on the pavement, were used in order to obtain the maximum stress range. Then, submodels were developed based on the global analyses in order to obtain accurate stresses for calculating fatigue resistance, using the structural hot spot stress method. The fatigue analysis was done by the use of the

structural hot spot stress method to quantify stress ranges for which there is no “nominal stress” database (that which is available in design codes for stress away from the concentration). Based on the analyses, a three-step approach is concluded and some suggestions are provided to bridge designers in this study which can be helpful for improving the design of orthotropic decks.

Furthermore, a relatively new fatigue enhancement technique, FBP, is discussed based on simple fatigue tests. FBP as a technique of surface treatments can definitely improve the surface performance, and demands less operational parameters. Fatigue tests of four different groups were carried out under cyclic constant amplitude fatigue loading in the laboratory in order to study the effect of treatment of FBP. It is found that FBP not only can improve the fatigue life, but also sometime can remedy small fatigue cracks.

SOMMARIO

Gli Orthotropic deck bridges sono ampiamente usati nell'ingegneria dei ponti, soprattutto per i ponti di grande luce. Anche se gli orthotropic deck bridges presentano molti vantaggi, si è scoperto che essi sono particolarmente vulnerabili nei confronti ai fenomeni di fatica che provocano la formazione di incrinature per i carichi ciclici dei veicoli quando esiste un elevato numero di connessioni saldate nella struttura dell'impalcato. Tra queste tipologie di connessioni le rib-to-deck plate, i rib-to-diaphragm e i rib-to-diaphragm-to-deck plate (RDDP) sono le tre connessioni saldate più ricorrenti che sono più sensibili a fenomeni di incrinatura da fatica a causa di alte concentrazioni di tensioni e di valori elevati di tensioni residue.

L'analisi a fatica di un orthotropic deck bridge è un processo complesso e incerto a causa dei numerosi fattori che possono influenzare il cracking a fatica. Nel presente lavoro è stato condotto uno studio sullo stato dell'arte della letteratura corrente e delle normative e delle istruzioni sul comportamento a fatica, per conoscere meglio i vantaggi e gli svantaggi, nonché le limitazioni di questa tipologia strutturale. Inoltre, è stato analizzato lo stato tensionale di un tipico orthotropic deck mediante un codice agli elementi finiti (FEA) ed è stato possibile valutare la resistenza a fatica attraverso il metodo dello "structural hot spot stress". È stata studiata approfonditamente la tecnica Fluid Bed Peening (FBP) per il miglioramento a fatica, ed in presto sono stati condotte prove a fatica in laboratorio su campioni trattati con FBP.

I due obiettivi principali di questo studio sono stati quelli di analizzare la risposta tensionale degli orthotropic deck bridges e di sviluppare un approccio per migliorare i comportamenti a fatica attraverso il metodo FE e le tecniche di analisi, attraverso gli studi parametrici sulle caratteristiche geometriche e il metodo di structural hot spot stress. Numerosi modelli FE sono stati sviluppati al fine di analizzare l'influenza delle tensioni su ritaglio di geometria, con o senza paratie, e lo spessore del deck plate. Sono stati applicate diverse condizioni di carico, che sono state usate per simulare le diverse posizioni dei veicoli sulla carreggiata, in modo da ottenere i valori tensionali

massimi. Inoltre, sono stati sviluppati sottomodelli sulla base di analisi globali al fine di ottenere accurate sollecitazioni per il calcolo della resistenza a fatica, utilizzando il metodo dello structural hot spot stress. L'analisi a fatica è stata condotta con l'uso del metodo di structural hot spot stress per quantificare il range di tensioni per i quali non vale la "tensione nominale" da normativa (quella che è disponibile nei codici di progettazione per lo stress di distanza dalla concentrazione). Sulla base di queste analisi, è stato condotto un approccio in tre fasi e sono indicati alcuni suggerimenti per supportare i progettisti nel dimensionamento e verifica degli orthotropic deck bridges.

Inoltre, è stata utilizzata una tecnica relativamente nuova, FBP, per il miglioramento degli elementi strutturali soggetti a fatica. Infatti l'FBP, come tecnica di trattamento della superficie, può migliorare significativamente le prestazioni degli elementi strutturali soggetti a fatica, e richiede meno parametri operativi. Sono state eseguite prove a fatica su quattro diversi gruppi, sotto carico ciclico di ampiezza di fatica costante in laboratorio per studiare l'effetto del trattamento di FBP. Il risultato è che l'FBP non solo può migliorare il comportamento a fatica, ma a volte può anche porre rimedio a piccole cricche provocate dai fenomeni a fatica.

CHAPTER 1

INTRODUCTION

At present, the orthotropic deck is used more and more in bridge engineering, especially for long span bridges. For instance, the longest cable-stayed bridge span: Sutong Changjiang Highway Bridge (in China) utilizes orthotropic box girder.

The word “ORTHOTROPIC” is derived from the phrase “ORTHOgonal anisoTROPIC”. As the name implies, the properties of an orthotropic deck are different in orthogonal directions. Orthotropic decks are the part of the superstructures which are made completely of steel, and lies immediately below the wearing surface. There are many orthotropic decks now, which have been built over the years since the 1930’s. They have been applied to suspension bridges, cable-stayed bridges, plate girder bridges, box girder bridges, arch bridges, movable bridges, truss bridges, floating bridges, and pedestrian structures.

1.1 Historical Development of Analytical Methods and Design

When Europe was being re-built after World War II, steel was in short supply. Orthotropic decks were constructed with thin deck plates and were designed for strength with little regard for fatigue details. A typical example is that the Kurpfalz Bridge over the River Neckar (1950) in Mannheim, while the Cologne-Muelheim Bridge (1951) over the Rhine is the first suspension bridge which used orthotropic deck.

Orthotropic deck bridges developed very quickly in Europe due to the need of reducing the self weight of long span and lifting bridges. It is well known that concrete deck is relatively heavy, while orthotropic deck might be expected to weigh about 50% as much as concrete deck.

In the 1950s and 1960s, open rib longitudinal stiffeners were commonplace in orthotropic decks. But today most of ribs are closed ribs. To attenuate large

deflections in wide highway bridges, orthotropic box girder was developed to utilize their suspension torsional resistance. In 1982, the publication of British Standard BS5400 was a milestone because it provided rules for stability problems. The completion of Great Belt East Bridge (Denmark) in 1998 represented the advanced technology of orthotropic deck and box girder structure in bridge engineering. On 6 March 2009, the new Italian government announced that the project of Messina Bridge (see Figure 1-1) using orthotropic deck would be resurrected. If completed, the bridge would be the longest suspension bridge in the world, which the main span of 3,300m would surpass the Akashi Kaikyo Bridge (1,991m main span, Japan).

Orthotropic deck took root in the United States in the early 1960's (San Mateo-Hayward Bridge, in California). They were not widely accepted due to lacking design rules and little practical experiences. At present, compared to the other bridge types, the percentage of orthotropic deck in U.S.A. remain very low, while 25% of them are in California. One of the most famous projects is the Golden Gate Bridge which was redecked with orthotropic deck in 1985. Figure 1-1 shows it in comparison to the proposed strait Messina Bridge.



FIGURE 1-1 Messina Bridge and Golden Gate Bridge (www.skyscrapercity.com).

Today, Japan has a large number of orthotropic deck bridges which are among the longest in the world. For example, there are more 1,000 spans applied to the orthotropic viaducts in Tokyo. In recent years, China has built many long span orthotropic deck bridges, such as Jiangyin Changjiang Highway Bridge (1,385m main span, suspension bridge, 1999), Yunyang Changjiang Bridge (1,450m main span, suspension bridge, 2005), Sutong Changjiang Highway Bridge (1088m main span, cable-stayed bridge, 2008, as shown in Figure 1-2), and so on.

The development tendency of orthotropic deck is still going forward all over the world.



FIGURE 1-2 Sutong Changjiang Highway Bridge (www.stbridge.com.cn).

Instability and fatigue are two major problems for orthotropic deck bridges. The dead weight of the deck system and the vehicle loading cause the bending moments, both to the deck plate and the longitudinal ribs. In recent years, many of orthotropic bridges applied slender types, thus, the instability problems should be paid more attention, both out-of-plane deformation and in-plane deformation. The deck plates in the positive moment areas of long span bridges are primarily suffered the flexural compressive stress under the vehicle load, thus, it attracts many researchers' attention in recent years.

Although the problem due to compressive stress has been realized for years, buckling

problem has not been prevented in orthotropic bridges. Tvergaard [1] started to study the buckling problem in 1970's, and he investigated the sensitivity of stiffened plates to geometric imperfections via numerical methods. Troitsky [2] presented several methods to analyze the stiffened plates. The problem is still being studied in recent years. Jen [3] and Matthew [4] investigated local buckling problem of trapezoidal rib orthotropic bridges based on experimental tests and numerical analysis. Figure 1-3 shows six different buckling modes of stiffened plates.

Both instability problem and fatigue problem are very important to the orthotropic deck bridge, but this paper mainly focuses on the fatigue problem and will be discussed detailed in the following chapters.

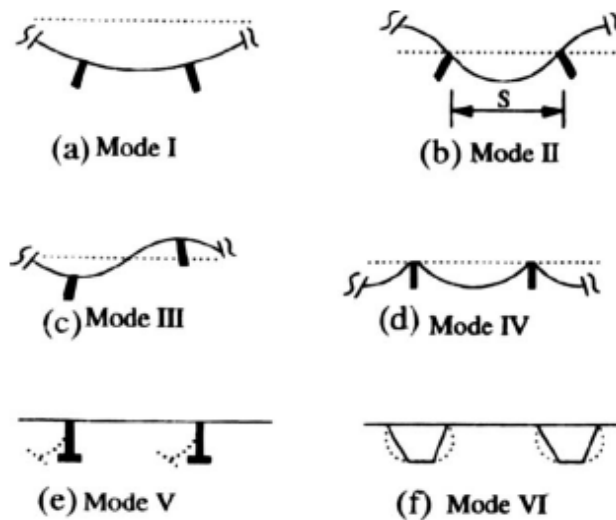


FIGURE 1-3 Various buckling modes of stiffened plates.

1.2 The Advantages of Orthotropic Deck in Bridge Engineering

Today, more and more orthotropic decks are used in bridge engineering because they are better understood relative to their fatigue performance and more practical experience in its fabrication has been gained. Orthotropic decks have many advantages as follows.

Light weight. A concrete deck weighs 2 times as much as an orthotropic steel deck due to thick and heavy concrete used. A lighter weight superstructure usually has

better seismic performance, therefore, results smaller or fewer substructures, such as columns, piers and foundations. Orthotropic deck provides a much lighter weight to long span bridges compared to concrete deck, especially for suspension bridges and cable-stayed bridges. In addition, light weight is very important to movable bridges, such as lifting bridges. An orthotropic deck technology advanced it became clear that such decks are ideally suited for lifting bridge construction for two main reasons: a) they are light and require less power from prime movers to lift and let down the leaf(s); they also require smaller ballast for the same reason; b) they deliver the entire floor load (when the bridge is lifted) to the girders directly through the deck plate, with much less difficulty than their earlier counterparts, the open grid decks or concrete filled grid decks. The internal forces in the trunnions are also reduced.

High strength. Orthotropic deck plate acting as part of load carrying components leads to higher safety reserve compared to the one dimensional beam structure. Meanwhile, high strength steels can be used to the decks.

Durability. A well designed and manufactured orthotropic deck bridge could offer a service life more than 100 years. Improvements in design life are further expected. With improved knowledge of the performance in orthotropic decks, it is a good choice for long span bridges, including self supported (not suspension) plate or box girders.

Rapid construction. Orthotropic deck is manufactured in workshop and transported to construction site to be erected. The construction time on site is much shorter than other competing technologies. In some areas traffic can be placed on an orthotropic deck before it is completely joined longitudinally.

Integration with bridge framing in rehabilitation projects. As mentioned before, orthotropic deck is made in the workshop. It is easily adaptable to existing framing which in prior time supported a concrete deck. There are many examples in the United States.

Life-cycle economy. The initial cost of orthotropic deck bridge is very high compared to competing technologies. However, an orthotropic deck has a lighter weight superstructure, and it can reduce seismic loads on the substructure. Therefore, it brings smaller foundation sizes, columns, and piers, which in turn causes less cost.

Furthermore, a good orthotropic deck bridge can last more than 100 years, and needs less maintenance. Orthotropic decks are highly competitive when compared to other bridge types on life-cycle costs basis.

Orthotropic decks are widely applied to replace old original concrete decks due to the light self weight. Meanwhile, there is no interruption during the replacement of bridge deck. One of the most famous examples is the Golden Gate Bridge as mentioned before. In recent years, there are many long span bridges redecked with orthotropic decks, such as Triborough Bridge and Whitestone Bridge.

Although orthotropic deck bridges have many advantages, they have some drawbacks. One of the biggest barriers to using orthotropic decks is the willingness of bridge owners to believe the reputed longevity of orthotropic decks on the basis of current theory of fatigue even if recently tested in several experiments. The use of hot spot stress technique is yet foreign to the staffer of bridge authorities. High initial cost is the main cause of its rejection as a viable alternate.

1.3 Orthotropic deck plate in bridge structure

An orthotropic deck usually consists three main components, deck plate, floor beam (or crossbeam) and longitudinal rib (or stiffener), as shown in Figure 1-3 [5]. Fatigue failure is likely to occur at welded connections especially where rib runs across a floor beam (diaphragm). Here the details present complex geometries with significant stress concentrations. Design of orthotropic decks is primarily how the engineer manages to reduce stress when geometries are complex so as to reduce stress concentration below the endurance limit.

Two types of longitudinal rib are used in orthotropic decks, as shown in Figure 1-4. The upper figure shows an “open” flat plate rib in a typical bridge framing. The lower figure shows a “closed” trapezoidal rib, which is inaccessible inside once welded to the deck plate.

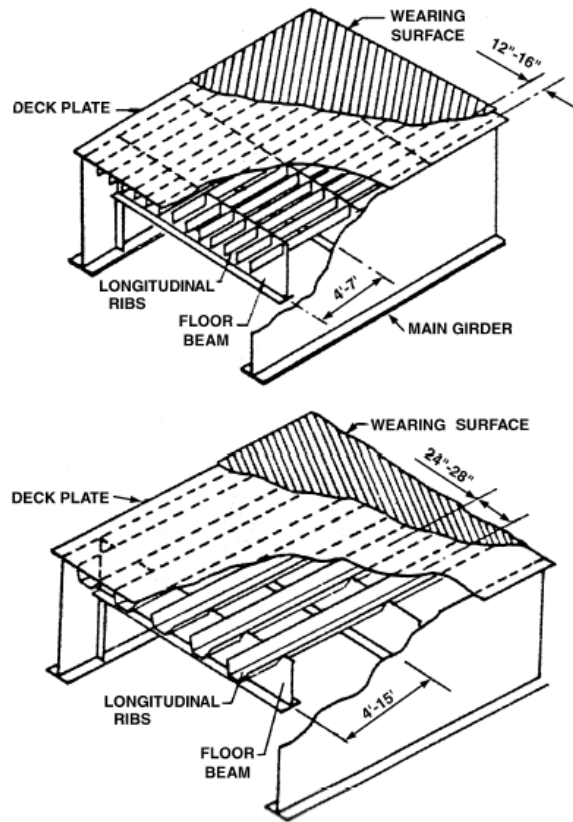


FIGURE 1-4 Typical components of orthotropic deck bridges (M. S. Troitsky, 1987).

Figure 1-5 illustrates several types of open-ribs (on the left) and closed ribs (on the right), which have been used in the evolution of this design technology. Both have an impact on the design of the “cutout” which will be discussed in Chapter 2.

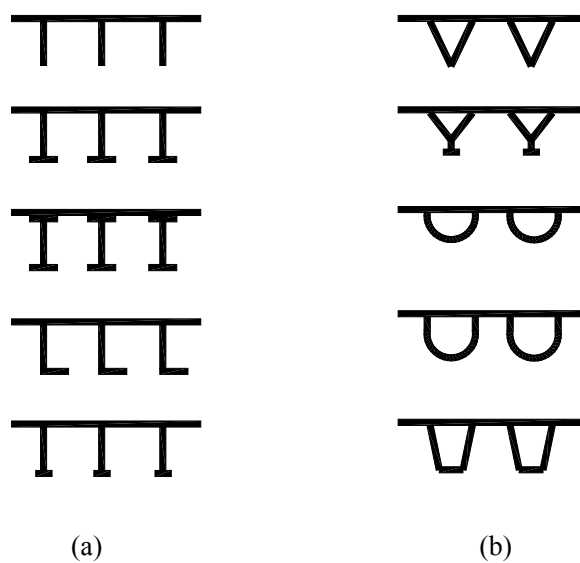


FIGURE 1-5 Rib typologies: (a) open-ribs; (b) closed ribs.

1.4 Optimization Technologies

The evolution of the technology has shown that the design of an orthotropic deck is governed by fatigue and not by strength. Welded connections in orthotropic deck (see Figure 1-6) [6] are subject to fatigue cracking like in other steel structures. Cutout geometries play an important role in the severity of stress concentration. The development of computer science, Finite Element Method (FEM) plays a more and more important role in the improvement of these geometries so that fatigue effects can be minimized. With more powerful computer, bridge designer can develop better bridge models and compare geometric design in a short time.

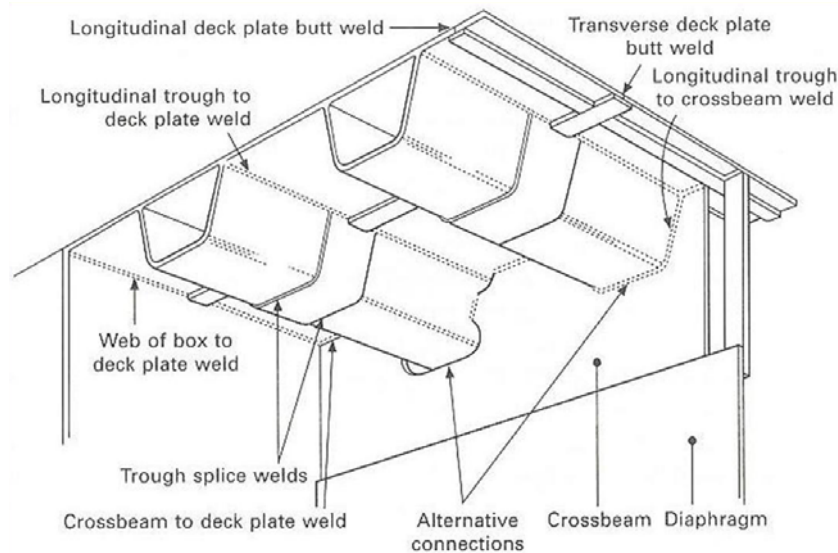


FIGURE 1-6 Welded connections in orthotropic deck (T. Gurney, 2006).

For the purpose of increasing the longevity of orthotropic decks, fatigue enhancement techniques can be utilized in the welded connections. In general, fatigue enhancement methodologies can be categorized as follows: (1) those that introduce beneficial compressive stress; (2) those that reduce stress concentration; (3) those that remove defects in components; and (4) those that increase the rigidity in the connection, or that in some way reduce the stress concentration in hot spots. While these techniques have not been used in orthotropic decks, it is seen that they may contribute to lower fabrication costs by removal of the cut-out, while helping to keep deck weight low.

1.5 Research Objectives

The primary goal of this research is to develop an approach to improve the fatigue behaviors of orthotropic deck bridge through FEM and analytical techniques, by doing parametric studies of various geometric parameters. Furthermore, the fatigue enhancement technique, Fluid Bed Peening (FBP), is discussed based on a series of simple fatigue tests.

1.5.1 Geometric optimization of orthotropic deck

The structure of orthotropic deck is very complex. The early analytical methods such as Pelikan-Esslinger method can't assess the details where the concentrated stress existed, for instance, at the cutout and welded connections. It is well known that these details are very critical according to the studies conducted for the development of actual projects. The FEM technique is highly suitable to study stress concentrations of a multitude of designs in which single parameters are made to vary while others are held constant. This type of analysis will eventually evolve in an optimized design of a particular orthotropic deck. In past years, a large amount of experiments were carried out all over the world. Advanced Technology for Large Structural Systems (ATLSS) center at Lehigh University (U.S.A.) is continuing to investigate the fatigue performance of orthotropic deck through full-scale specimens and obtains fruitful results [7]. The redecking of the Williamsburg Bridge [8, 9], the Bronx Whitestone Bridge, and the Verrazzano Bridge were tested ATLSS center under the guide of Fisher. The prototypes to be tested were first developed by FE techniques. More and more FE software are applied to study the performances of orthotropic deck. Conner [10] studied the influence of traditional cutout to orthotropic deck via FEM. In the past few years, some important connections were studied by building fine meshed submodels. Figure 1-7 shows the FE model with cracks developed by Kornel Kiss [11].

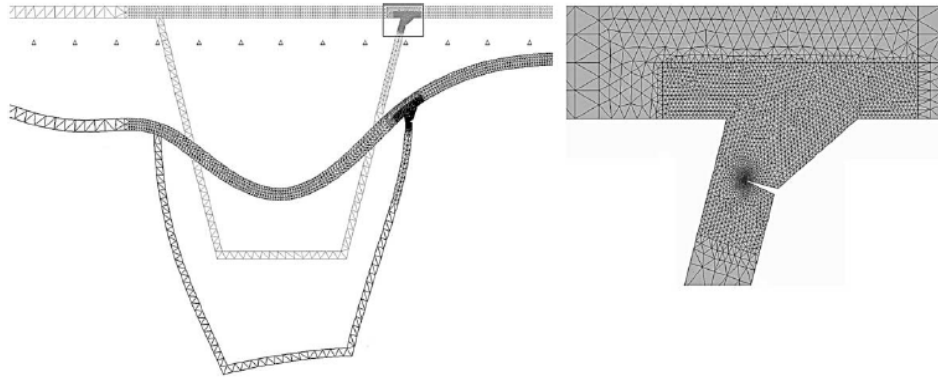


FIGURE 1-7 Submodel of rib-to-deck plate connection (Kornel Kiss, 2002).

In this research, FEM is applied to analyze the stress performance of orthotropic deck. Many Finite Element (FE) models would be developed in order to analyze the influences of cutout, bulkhead, and deck plate [12]. The applied loading is developed to obtain maximum stress range. Furthermore, submodels are developed based on the global analyses in order to obtain accurate stresses for calculating fatigue resistance, using the structural hot spot stress method.

These analyses provide the loading background to fatigue life. The fatigue analysis is done by the use of structural hot spot stress approach in order to quantify stress ranges for which there is no “nominal stress” database (that which is available in design codes for stress away from the concentration). Based on this research, some suggestions are provided to bridge designers which can be helpful for improving the design of orthotropic decks.

1.5.2 Fatigue enhancement

Another method for improving the longevity of orthotropic deck is to increase the fatigue resistance of the welded joint. The International Institute of Welding (IIW) provides quantitative values of how much one fatigue category can be improved for various enhancement procedures such as burr grinding, TIG dressing, peening, blasting, stress relieving, and others [13]. However, high accuracy in selection of operational parameters is demanded by traditional methods, such as shot peening [14].

Otherwise, over shot peening can increase the defects of surface and cause initial cracks [15, 16].

FBP, a relatively new method, as a technique of surface treatments can dramatically improve the surface performance, and demands less operational parameters. Material tests done by M. Barletta et al. [17, 18] showed that FBP can optimize the roughness of material surface significantly. Figure 1-8 shows the optimized effect of surface roughness treated by FBP [18]. Furthermore, it is easy to control because less operational parameters are demanded. Thereby, fatigue tests are carried out in the laboratory to study the effect of treatment of FBP in this research. Fatigue enhancement techniques not only can be used to postpone the initiation of fatigue cracking, but also sometime can remedy small fatigue cracks [19]. This will be discussed detailed in Chapter 5.

As a result, an approach for optimizing and enhancing the fatigue behaviors of orthotropic decks is provided in this research.

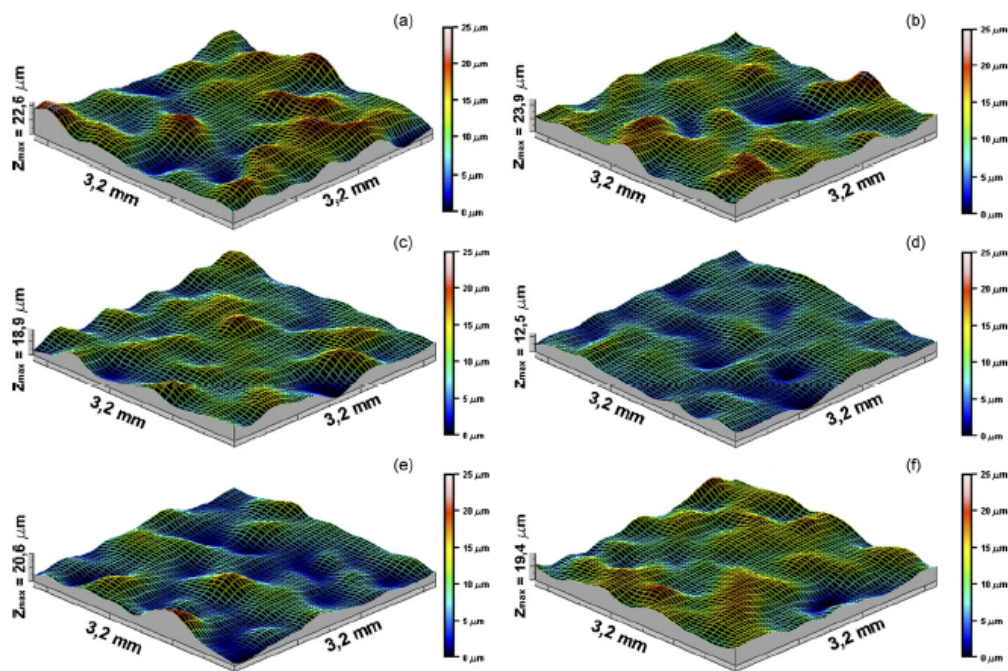


FIGURE 1-8 Surface roughness after treated 30 min:(a) 110°; (b) 130°; (c) 150°; (d) 170°; (e) 200°; (f) 230° (M. Barletta et al., 2007).

References

- [1] Tvergaard V, Needleman A. Buckling of eccentrically stiffened elastic-plastic panels on two simple supports or multiply supported, *Int. J. Solids Structures*, 1975, Vol. 11: 647-663.
- [2] Troitsky MS. *Stiffened Plates, Bending, Stability and Vibrations*, Elsevier, 1976, New York.
- [3] Jen W. *Strength of steel orthotropic deck with trapezoidal shaped longitudinal stiffeners*. Lehigh University, 2006.
- [4] Yarnold MT, Wilson JL, Jen W, Yen BT. Local buckling analysis of trapezoidal rib orthotropic bridge deck systems. *Bridge Structures*, 2007; 3(2): 93-103.
- [5] Troitsky MS. *Orthotropic Bridges - Theory and Design (2nd ed.)*. Cleveland, OH: James F. Lincoln Arc Welding Foundation, 1987.
- [6] Gurney T. *Cumulative damage of welded joints*. Woodhead Publishing Limited, 2006.
- [7] Fisher JW. Evolution of fatigue-resistant steel bridge. Distinguished Lectureship. Transportation Research Board, 76th Annual Meeting, Washington DC, January 12-16. Paper No. 971520.1-22, 1997.
- [8] Bocchieri WJ, Fisher JW. Williamsburg Bridge Replacement Orthotropic Deck As-built Fatigue Test. ATLSS Report No. 98-04. May, 1998.
- [9] Connor RJ, Fisher JW. Results of Field Measurements on the Williamsburg Bridge Orthotropic Deck. ATLSS Report No. 01-01. January, 2001.
- [10] Connor RJ. Influence of cutout geometry on stresses at welded rib to diaphragm connections in the steel orthotropic bridge decks. *Journal of the Transportation Research Board*, 2004; No.1892, 78-87.
- [11] Kiss K, Dunai L. Fracture mechanics based fatigue analysis of steel bridge decks by two-level cracked models. *Computers and Structures*, 2002; 80: 2321–2331.
- [12] Abruzzese D, Grimaldi A, Qian ZH. Fatigue Behaviors of Cutout at Crossbeam of Trapezoidal Rib Orthotropic Deck; *International Orthotropic Bridge Conference, U.S.A.*, 2008: 256-266.
- [13] Haagensen P.J, Maddox S J. IIW recommendations post weld improvement steel and

aluminium structures. IIW Commission XIII-1815-00. International Institute of Welding, 2002.

[14] Guagliano M, Vergani L. An approach for prediction of fatigue strength of shot peened components, *Engineering Fracture Mechanics*, 2004; Vol. 71: 501-512

[15] Mutoh Y, Fair GH, Noble B, Waterhouse RB. The effect of residual stresses induced by shot-peening on fatigue crack propagation in two high strength aluminum alloys. *Fatigue Fract Eng Mater Struct*, 1987; Vol. 10(4): 216–72.

[16] Tekeli S. Enhancement of fatigue strength of SAE 9245 steel by shot peening. *Mater Lett.*, 2002; Vol. 57: 604–608.

[17] Barletta M, Lambiase F, Tagliaferri V. Improvement of fatigue behaviour high strength aluminium alloys by Fluid Bed Peening (FBP). *Key Engineering Materials*, 2007; Vol.344: 87-95.

[18] Barletta M, Bolelli G, Guarino S, Lusvarghi L. Development of matte finishes in electrostatic (EFB) and conventional hot dipping (CHDFB) fluidized bed coating process. *Progress in Organic Coatings*, 2007; Vol. 59: 53–67.

[19] Qian ZH, Abruzzese D. Fatigue Failure of Welded Connections at Orthotropic Bridges. *Frattura ed Integrità Strutturale. Gruppo Italiano Frattura*, 2009; 9: 105-112.

CHAPTER 2

STRUCTURAL ANALYSIS OF ORTHOTROPIC DECK

An orthotropic plate is defined as a plate having elastic properties in orthogonal direction, as shown in Figure 2-1 [1]. A large amount of investigations had been carried out on orthotropic steel deck systems in the last century, including elastic analysis of stiffened plates, buckling analysis of deck plate components, and strength evaluation of orthotropic deck and components. The development of theory optimizes the design and the manufacture to the orthotropic deck plate. Moreover, the appearance of FE software brings a great break through for analyzing the complex details in orthotropic decks.

2.1 Classical Theories

Orthotropic deck not only acts as deck plate, but also part of main girder. It is the upper flange for floor beam and longitudinal beam, as well as for main girder. Orthotropic deck is often studied by dividing into three different structural systems:

(1) Main girder system; Deck plate and longitudinal ribs act as the upper flange of main girder.

(2) Deck system; It is composed by deck plate, floor beams and longitudinal ribs. Deck plate acts as the common upper flange of floor beams and longitudinal ribs. The system is supported by the main girders, and only undertakes vehicle loading. The real bearing capacity of this structure is much higher than the results calculated by small deflection elastic theory due to the high plastic reserved capacity.

(3) Deck plate system; It includes only deck plate which acts as homogeneous and continuous plate supported by longitudinal ribs and floor beams. Vehicle loading affects directly on the system, and delivers to longitudinal ribs and floor beams.

Although the deck plate has constant thickness and same material, the different elastic modulus and different Poisson ratios bring the different properties in the orthogonal

directions. Thus, the deck plate is called orthotropic deck.

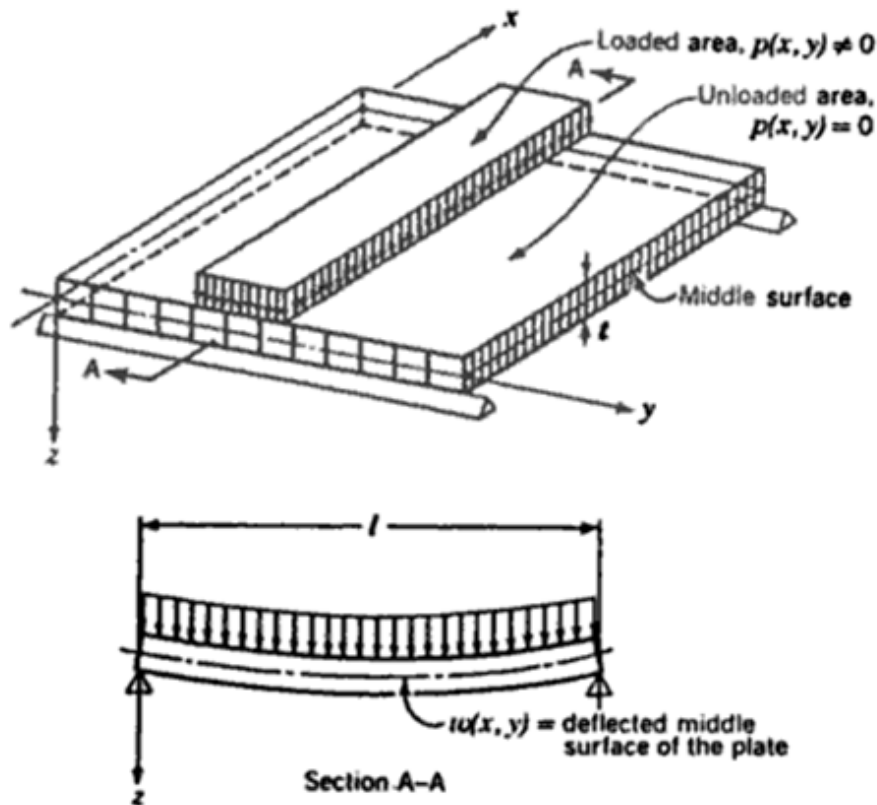


FIGURE 2-1 Basic designation of orthotropic deck plate as an anisotropic system (Xanthakos, 1994).

2.1.1 Introduction of orthotropic plate theories

Gehring and Boussinesq introduced firstly the analysis of an isotropic plate, and Huber presented the complete solution for isotropic plate. The famous Huber's equation is presented as Equation (2.1) which providing the relationship between the lateral deflection and the loading of an orthotropic deck.

$$D_x \frac{\partial^4 w}{\partial x^4} + 2H \frac{\partial^4 w}{\partial x^2 \partial y^2} + D_y \frac{\partial^4 w}{\partial y^4} = p(x, y) \quad (2.1)$$

Where, w is the lateral deflection of the middle surface of the plate at point (x, y) as shown in Figure 2-1; D_x , D_y and H are rigidity coefficients, and $p(x, y)$ is the load density at any point expressed as a function of the coordinate x and y .

The basic hypothesis proposed by Huber to calculate the overall bending deflections and bending stresses in a stiffened plate, is to replace it by an equivalent orthotropic plate of constant thickness having the same orthogonal stiffness characteristics. It is called the Method of Elastic Equivalence (MEE).

Guyon [2] utilized the method to analyze a deck without torsional stiffness of the longitudinal rib. Massonnet [3] extended Guyon's method to include the torsional stiffness. Morice, Little and Rowe [4] applied the previous theory to concrete bridges. The design technique is concluded by Rowe [5] which is based on a set solution of the governing partial differential equation at a stage before the widespread availability of computers. The governing differential equations for large deflection orthotropic plate theory are the equilibrium equation and the compatibility equation. Considering the idealized initial imperfection, boundary conditions and load application, Paik and Thayamballi [6] solved the governing differential equations. Cornelius [7] treated the orthotropic deck as equivalent to a continuum without considering the spacing between floor beams.

For the purpose of design, various methods have been developed:

- (1) The Pelikan-Esslinger method [8], based on Huber's equation, is simplified but sufficient accurate. It assumes that the deck system is a continuous orthotropic plate, rigidly supported by longitudinal main girders and elastically supported by the floor beams. The parameters expressing certain rigidities of the orthotropic deck are disregarded in the method, as the parameters are considered of little importance during the design. The method does not provide the information on the load carrying strength of the deck panel and the stress status of details, for example, the stress near the cutout.
- (2) The equivalent gird method is assumed to perform as an integral unit. It assumes that the deck plated slit between the longitudinal ribs, which are treated as individual beams between panel points of the grid system, with the deck plate strips acting as the upper flanges. The effect of the deck plate rigidity perpendicular to the ribs is disregarded and should be considered separately.
- (3) The equivalent orthotropic plate method (orthotropic slab method) in the AISC

manual [9] and James F. Lincoln Electric manual [10], assumes that the rigidities of both the floor beams and the longitudinal ribs are uniformly distributed throughout the deck in the direction perpendicular to the respective member. Therefore, the actual discontinuous structure of the steel plate deck is represented as an idealized substitute orthotropic slab.

- (4) The thin-walled-beam method, as an elastic analysis method, accounts for the torsional distortion effects of box girders with an orthotropic deck [11]. It is also referred as the folded plate theory [12].

Furthermore, the design of orthotropic deck can be solved by Finite Difference and Finite Element techniques.

2.1.2 Orthotropic Plate Theory

Timoshenko [13] elaborated thoroughly the orthotropic plate theory in 1959, and Figure 2-2 shows the stress state of an orthotropic deck. Timoshenko assumed that the material of the plate has three planes of symmetry with respect to its elastic properties. Taking these planes as the coordinate planes, the relations between the stress and strain components for the case of plane stress in the xy plane can be represented by the following equations:

$$\begin{aligned}\sigma_x &= E'_x \varepsilon_x + E'' \varepsilon_y \\ \sigma_y &= E'_y \varepsilon_y + E'' \varepsilon_x \\ \tau_{xy} &= G \gamma_{xy}\end{aligned}\tag{2.2}$$

where, E'_x , E'_y and E'' are elastic modulus, and G is shear modulus.

Considering the bending of a plate made of such a material, it is assumed as before that linear elements perpendicular to the middle plane (xy plane) of the plate before bending remain straight and normal to the deflection surface of the plate after bending. Hence, the following expressions can be used for the components of strain:

$$\varepsilon_x = -z \frac{\partial^2 w}{\partial x^2} \quad \varepsilon_y = -z \frac{\partial^2 w}{\partial y^2} \quad \gamma_{xy} = -2z \frac{\partial^2 w}{\partial x \partial y}$$

The corresponding stress components, from Equations. (2.2), are

$$\begin{aligned}\sigma_x &= -z \left(E'_x \frac{\partial^2 w}{\partial x^2} + E'' \frac{\partial^2 w}{\partial y^2} \right) \\ \sigma_y &= -z \left(E'_y \frac{\partial^2 w}{\partial y^2} + E'' \frac{\partial^2 w}{\partial x^2} \right) \\ \tau_{xy} &= -2Gz \frac{\partial^2 w}{\partial x \partial y}\end{aligned}\quad (2.3)$$

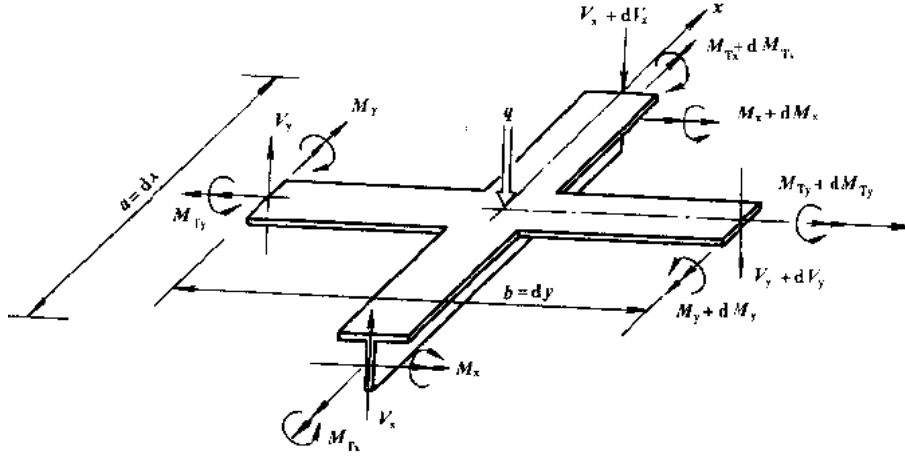


FIGURE 2-2 Forces of orthotropic plate (Timoshenko, 1959).

With these expressions for stress components, the bending and twisting moments are

$$\begin{aligned}M_x &= - \left(D_x \frac{\partial^2 w}{\partial x^2} + D_1 \frac{\partial^2 w}{\partial y^2} \right) \\ M_y &= - \left(D_y \frac{\partial^2 w}{\partial y^2} + D_1 \frac{\partial^2 w}{\partial x^2} \right) \\ M_{xy} &= -2D_{xy} \frac{\partial^2 w}{\partial x \partial y}\end{aligned}\quad (2.4)$$

in which

$$D_x = \frac{E'_x h^3}{12} \quad D_y = \frac{E'_y h^3}{12} \quad D_1 = \frac{E'' h^3}{12} \quad D_{xy} = \frac{Gh^3}{12} \quad (a)$$

It is obtained the following equation for anisotropic plates:

$$D_x \frac{\partial^4 w}{\partial x^4} + 2H \frac{\partial^4 w}{\partial x^2 \partial y^2} + D_y \frac{\partial^4 w}{\partial y^4} = q(x, y) \quad (2.5)$$

in which

$$H = D_1 + 2D_{xy}$$

2.1.2.1 Determination of rigidities in various specific cases

The expressions (a) given for the rigidities need minor modifications according to the natural material utilized. Common values of the rigidities in some practical cases are presented in the following.

a) Reinforced concrete slabs

Let be E_s Young's modulus of steel, E_c that of the concrete, ν_c Poisson's ratio for concrete, and $n = E_s/E_c$. In terms of the elastic constants we have approximately

$\nu_c = E''/\sqrt{E'_x E'_y}$. For a slab with two-way reinforcement in the directions x and y , it is assumed that:

$$\begin{aligned} D_x &= \frac{E_c}{1-\nu_c^2} [I_{cx} + (n-1)I_{nx}] \\ D_y &= \frac{E_c}{1-\nu_c^2} [I_{cy} + (n-1)I_{ny}] \\ D_1 &= \nu_c \sqrt{D_x D_y} \\ D_{xy} &= \frac{1-\nu_c^2}{2} \sqrt{D_x D_y} \end{aligned} \tag{2.6}$$

With the expression given for D_{xy} it is obtained:

$$H = \sqrt{D_x D_y}$$

b) Plywood

For a plate glued together of three or five plies, the constants which can be used are given in Table 2-1.

TABLE 2-1 Elastic Constants for Plywood (unit=10⁶psi).

Material	E'_x	E'_y	E''	G
Maple, 5-ply	1.87	0.60	0.073	0.159
Afara,3-ply	1.96	0.165	0.043	0.11
Gaboon, 3- ply	1.28	0.11	0.014	0.085
Brich, 3- and 5-ply	2.00	0.167	0.077	0.17
Brich with bakelite membranes	1.70	0.85	0.061	0.10

c) Corrugated sheet

Figure 2-3 shows the form of the corrugation, and the thickness is obtained that

$$z = f \cdot \sin \frac{\pi x}{l}$$

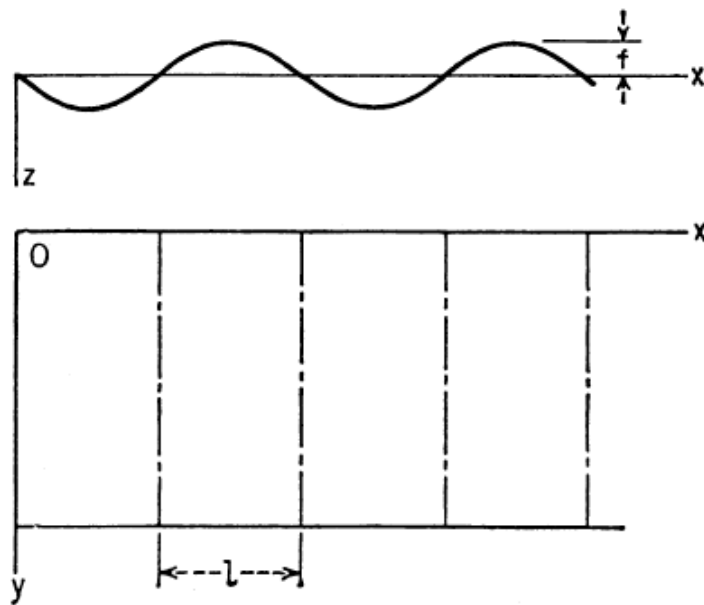


FIGURE 2-3 The form of the corrugation (Timoshenko, 1959).

It is assumed that s is the length of the arc of one-half a wave, then

$$\begin{aligned}
 D_x &= \frac{l}{s} \frac{Eh^3}{12(1-\nu_c^2)} \\
 D_y &= EI \\
 D_1 &\approx 0 \\
 H = 2D_{xy} &= \frac{s}{l} \frac{Eh^3}{12(1+\nu)}
 \end{aligned}
 \tag{2.7}$$

d) Plate reinforced by equidistant stiffeners in one direction

For a plate reinforced symmetrically with respect to its middle plane, as shown in Figure 2-4, it is taken:

$$\begin{aligned}
 D_x = H &= \frac{Eh^3}{12(1-\nu^2)} \\
 D_y &= \frac{Eh^3}{12(1-\nu^2)} + \frac{E'I}{a_1}
 \end{aligned}
 \tag{2.8}$$

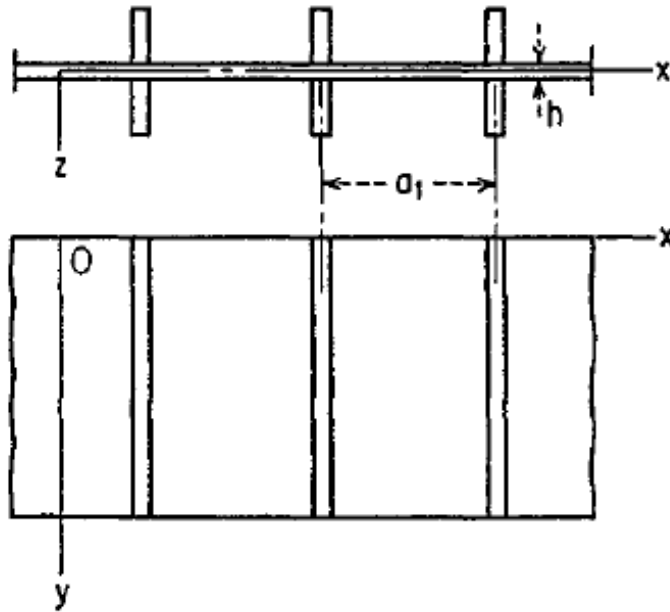


FIGURE 2-4 Plate reinforced by equidistant stiffeners in one direction
(Timoshenko, 1959).

in which E and ν are the elastic constants of the plate, E' the Young modulus, and I the moment of inertia of a stiffener, taken with respect to the middle axis of the cross section of the plate.

e) Plate cross-stiffened by two sets of equidistant stiffeners

Provided the reinforcement is still symmetrical about the plate, then

$$\begin{aligned}
 D_x &= \frac{Eh^3}{12(1-\nu^2)} + \frac{E'I_1}{b_1} \\
 D_y &= \frac{Eh^3}{12(1-\nu^2)} + \frac{E'I_2}{a_1} \\
 H &= \frac{Eh^3}{12(1-\nu^2)}
 \end{aligned}
 \tag{2.9}$$

where, I_1 is the moment of inertia of one stiffener, and b_1 is the spacing of the stiffeners in direction x , and I_2 and a_1 are the respective values for the stiffening in direction y .

f) Slab reinforced by a set of equidistant ribs

In the case, as shown in Figure 2-5, the theory established can give only a rough idea of the actual state of stress and strain of the slab. Suppose E be the modulus of the material (for instance, concrete), I the moment of inertia of a T section of width a_1 and $\alpha = h/H$. Then it is assumed that

$$\begin{aligned}
 D_x &= \frac{Ea_1h^3}{12(a_1 - t + \alpha^3 t)} \\
 D_y &= \frac{EI}{a_1} \\
 D_1 &= 0
 \end{aligned}
 \tag{2.10}$$

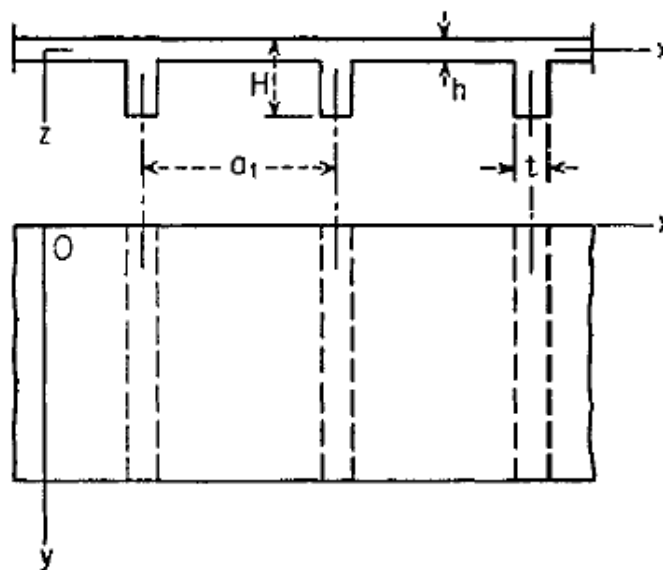


FIGURE 2-5 Slab reinforced by a set of equidistant ribs (Timoshenko, 1959).

The effect of the transverse contraction is neglected in the foregoing formulas. The torsional rigidity, finally, may be calculated by means of the expression

$$D_{xy} = D'_{xy} + \frac{C}{2a_1}$$

where, D'_{xy} is the torsional rigidity of the slab without the ribs and C the torsional rigidity of one rib.

2.1.2.2 Application of the theory to the calculation of gridworks

Equation (2.5) can be applied to the grid system as well, as shown in Figure 2-6.

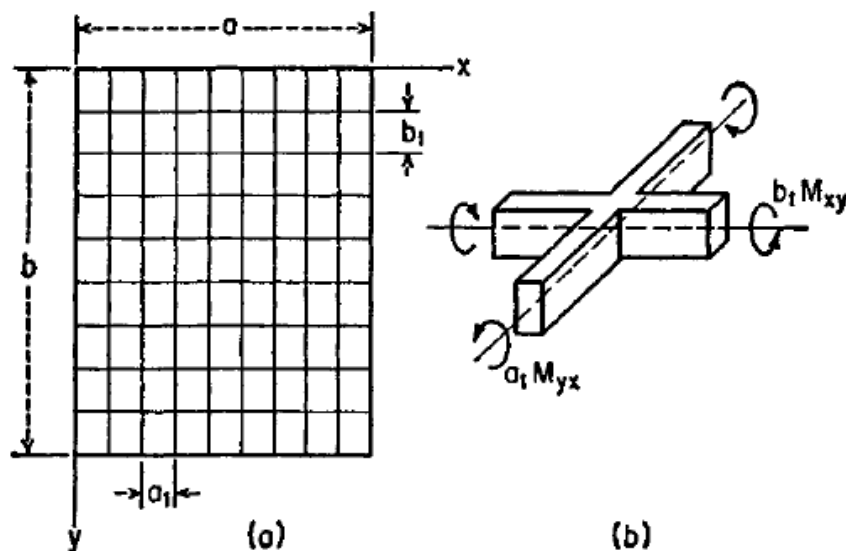


FIGURE 2-6 Application of the theory to the calculation of grid-works
(Timoshenko, 1959).

This consists of two systems of parallel beams spaced equal distances apart in the x and y directions and rigidly connected at their points of intersection. The beams are supported at the ends, and the load is applied normal to the xy plane. If the distances a_1 and b_1 between the beams are small in comparison with the dimensions a and b of the grid, and if the flexural rigidity of each beam parallel to the x axis is equal

to B_1 and that of each beam parallel to y axis is equal to B_2 , then they can be substituted in Equation (2.5)

$$D_x = \frac{B_1}{b_1} \quad D_y = \frac{B_2}{b_2}$$

The quantity D_1 in this case is zero, while the quantity D_{xy} can be expressed in terms of the torsional rigidities C_1 and C_2 of the beams parallel to the x and y axes, respectively. Therefore, it is considered the twist of an element as shown in Figure 2-6 and we obtain the following relations between the twisting moments and the twist $\partial^2 w / \partial x \partial y$:

$$M_{xy} = \frac{C_1}{b_1} \frac{\partial^2 w}{\partial x \partial y} \quad M_{yx} = -\frac{C_2}{a_1} \frac{\partial^2 w}{\partial x \partial y} \quad (2.11)$$

Substituting these expressions in the equation of equilibrium, it is found that in the case of the system represented in Figure 2-6a the differential equation of the deflection surface is

$$\frac{B_1}{b_1} \frac{\partial^4 w}{\partial x^4} + \left(\frac{C_1}{b_1} + \frac{C_2}{a_1} \right) \frac{\partial^4 w}{\partial x^2 \partial y^2} + \frac{B_2}{a_1} \frac{\partial^4 w}{\partial y^4} = q \quad (2.12)$$

which is of the same form as Equation (2.5).

In order to obtain the final expressions for the flexural and torsional moments of a rib, the moments should be multiplied, such as given by Equations (2.4) and valid for the unit width of the grid, by the spacing of the ribs. The variation of the moments, for example M_x and M_{xy} , may be assumed parabolic between the points $(m-1)$ and $(m+1)$ and the shaded area of the diagram (as shown in Figure 2-7) may be assigned to the rib (m) running in the direction x . Then, observing the expressions (2.4), it is obtained the following approximate formulas for both moments of the rib (m) :

$$\begin{aligned}
M_x &= -\frac{B_1}{24} \left[\left(\frac{\partial^2 w}{\partial x^2} \right)_{m-1} + 22 \left(\frac{\partial^2 w}{\partial x^2} \right)_m + \left(\frac{\partial^2 w}{\partial x^2} \right)_{m+1} \right] \\
M_{xy} &= \frac{C_1}{24} \left[\left(\frac{\partial^2 w}{\partial x \partial y} \right)_{m-1} + 22 \left(\frac{\partial^2 w}{\partial x \partial y} \right)_m + \left(\frac{\partial^2 w}{\partial x \partial y} \right)_{m+1} \right]
\end{aligned}
\tag{2.14}$$

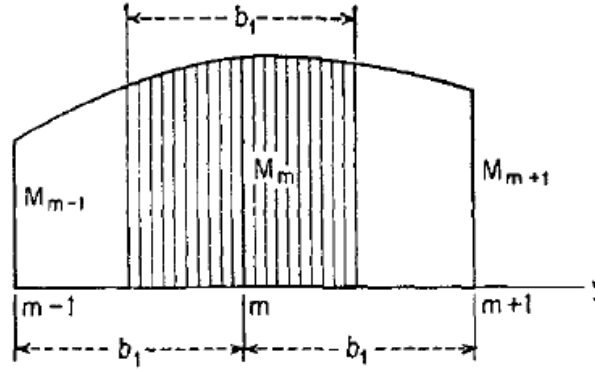


FIGURE 2-7 Diagram of moment between $(m-1)$ and $(m+1)$ (Timoshenko, 1959).

For ribs of the direction y , it needs to interchange x and y in the foregoing expressions and replace B_1 by B_2 and C_1 by C_2 ; $(m-1)$, (m) , and $(m+1)$ then denote three successive joints on a rib having the direction x .

Two parameters largely defining the elastic properties of a grid and often used in calculation are

$$\lambda = \sqrt[4]{\frac{B_2 b_1}{B_1 a_1}} \quad \mu = \frac{1}{2} \frac{\frac{C_1}{b_1} + \frac{C_2}{a_1}}{\sqrt{\frac{B_1 B_2}{a_1 b_1}}}$$

The parameter λ multiplied by the side ratio a/b (Figure 2-7) yields the relative carrying capacity of a rectangular plate in the directions x and y , whereas the parameter μ characterizes the torsional rigidity of a grid as compared with its flexural rigidity.

Equation (2.12) has been extensively used in investigating the distribution of an arbitrarily located single load between the main girders of a bridge stiffened in the transverse direction by continuous floor beams.

2.1.3 The Pelikan-Esslinger Method

The Pelikan-Esslinger method [8] was proposed by Germany researchers W. Pelikan and M. Esslinger in 1950s, then it was widely used and adopted as well by “Design manual for orthotropic steel plate deck bridges” (1963) [9].

The detailed analysis of the orthotropic deck is well documented in the design manual [9]. This method is also based on the application of Huber's equation. Some assumptions are presented prior to apply P-E method to calculate the deflections and stresses of orthotropic deck:

- a) the distance between the ribs should be very small compared to the length of plate edge, that means stiffeners should be put closely;
- b) the distribution of the ribs (both longitudinal or transverse) should be uniform;
- c) the plate stiffness keeps the same while the loading and boundary conditions change;
- d) the material of the ribs and the plate should be the same;
- e) the connections of the rib and the plate should be tight and deep-set.

The design procedure is divided into two stages (as shown in Figure 2-8).

In the first stage, it is assumed that floor beams and the main girders are infinitely rigid. The deck plate is supported by the floor beams, as shown in Figure 2-8a. The moments of longitudinal ribs and transversal floor beams are calculated in this stage.

In the second stage, the moments calculated in the first step is modified according to the results of the floor beams considering the elastic deformation, see Figure 2-8b. It is in good agreement to the practical situation, shown in Figure 2-8c.

The longitudinal flexural rigidity D_y is much larger than the transversal flexural rigidity D_x , therefore, it is assumed that $D_x \approx 0$; The torsional rigidity H of open rib orthotropic deck is also very small, thus, it is assumed that $H \approx 0$. According to the above, it is obtained that

- a) open rib orthotropic deck: $D_x = 0$, $H = 0$;

b) closed rib orthotropic deck: $D_x = 0$.

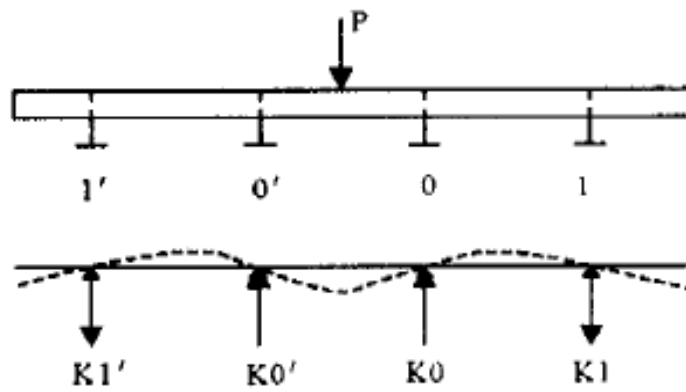
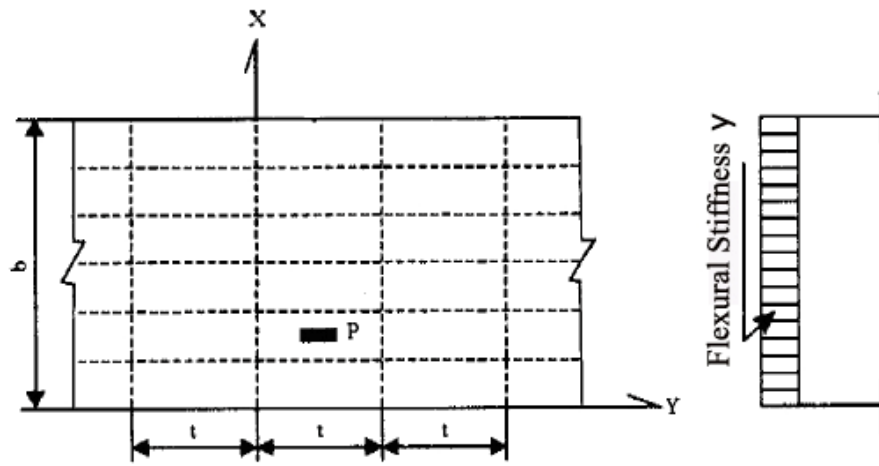
2.1.3.1 Open rib orthotropic deck

a) Solutions of continuous beam supported rigidly

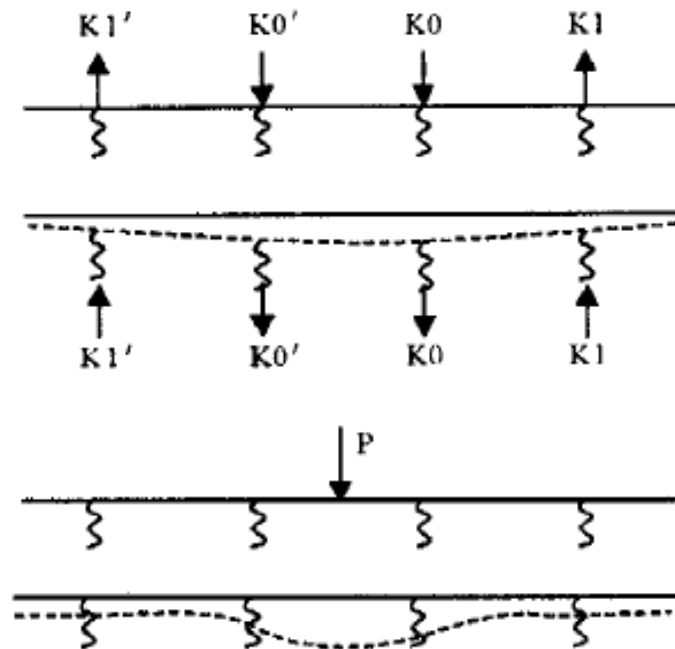
For an open rib orthotropic deck, it is assumed that $D_x = 0$, $H = 0$, then

$$D_y \frac{\partial^4 w}{\partial y^4} = q(x, y) \quad (2.15)$$

Figure 2-9 shows the influence lines of internal forces at the continuous beam supported rigidly.



(a) The first step.



(b) The second step.

FIGURE 2-8 Flowchart of the Pelikan-Esslinger method.

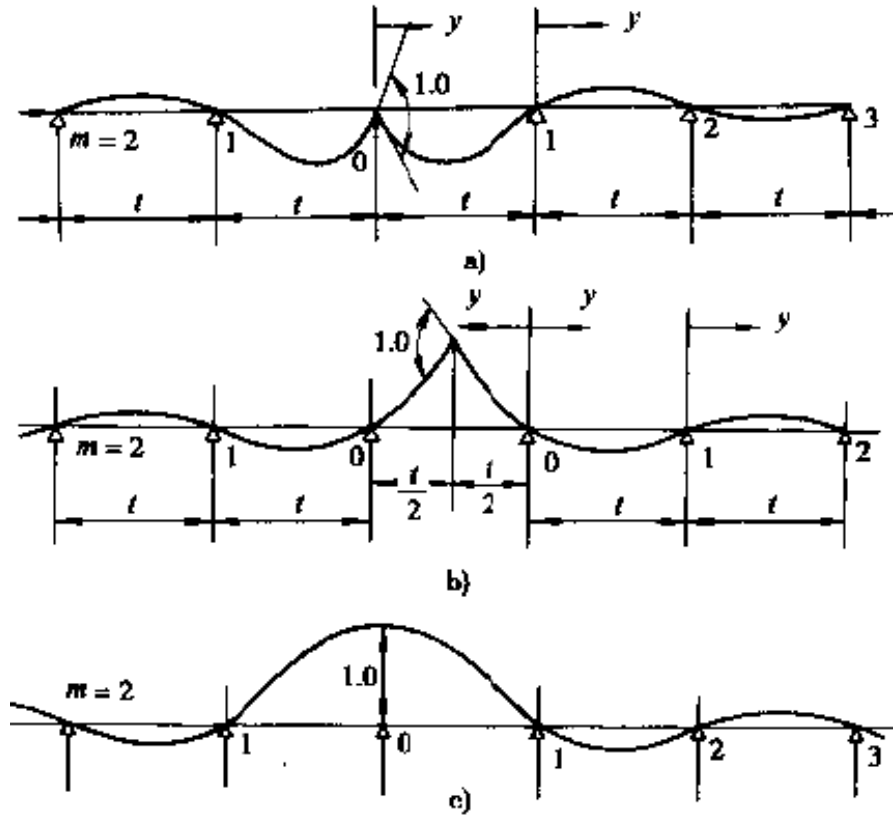


FIGURE 2-9 The influence lines of continuous beam.

1) Moment in the middle of the longitudinal ribs M_m

When the concentrated loading P acts between the area 0-0, the moment of the center point can be calculated by

$$\left(\frac{M_m}{P_t}\right)_{0-0} = 0.1830\left(\frac{y}{t}\right) + 0.3170\left(\frac{y}{t}\right)^2 \quad (2.16)$$

The maximal value of the influence line M_m occurs at $y/t = 0.5$:

$$\left(\frac{M_m}{P_t}\right)_{\max} = \left[0.1830\left(\frac{y}{t}\right) + 0.3170\left(\frac{y}{t}\right)^2\right]_{\frac{y}{t}=0.5} = 0.1708 \quad (2.17)$$

For the other situations:

$$\left(\frac{M_m}{P_t}\right)_{m-(m+1)} = (-0.2679)^m \left[-0.1830\left(\frac{y}{t}\right) + 0.3170\left(\frac{y}{t}\right)^2 - 0.1340\left(\frac{y}{t}\right)^3\right] \quad (2.18)$$

2) Moment M_s at the supporting point of longitudinal rib

The moment can be calculated by

$$\left(\frac{M_s}{P_t}\right)_{m-(m+1)} = (-0.2679)^m \left[-0.5\left(\frac{y}{t}\right) + 0.866\left(\frac{y}{t}\right)^2 - 0.366\left(\frac{y}{t}\right)^3 \right] \quad (2.19)$$

Maximal M_s occurs at $d/t = 0.3804$, then

$$\left(\frac{M_s}{P_t}\right)_{\max} = -0.085 + 0.1494\left(\frac{c}{t}\right)^2 \quad (2.20)$$

3) Reaction at the node R_o

Through the calculation based on the influence lines, it is obtained that:

for Span “0-1”

$$\left(\frac{R_o}{P}\right)_{0-1} = \left[1 - 2.19\left(\frac{y}{t}\right)^2 + 1.1962\left(\frac{y}{t}\right)^3 \right] \quad (2.21)$$

for Span “m-(m+1)”

$$\left(\frac{R_o}{P}\right)_{m-(m+1)} = (-0.2679)^{m-1} \left[-8038\left(\frac{y}{t}\right) + 1.3923\left(\frac{y}{t}\right)^2 - 0.5885\left(\frac{y}{t}\right)^3 \right] \quad (2.22)$$

b) Modify according to the deflection of floor beam

It is assumed that the floor beams are rigid in the first stage, therefore the moments in the rib should be modified. The additional moment of floor beam in direction x can be calculated by

$$\Delta M_t = Q_0 t a \frac{Q_{1x}}{Q_o} \sum_{m=0}^{\infty} \frac{K_m}{p} \frac{\overline{\eta_{im}}}{t} \quad (2.23)$$

While the decreased moment of transverse stiffener in direction x can be calculated by

$$\Delta M_q = Q_0 \left(\frac{b}{\pi}\right)^2 \frac{Q_{1x}}{Q_o} \left[\frac{K_0}{P} - \sum_{m=0}^{\infty} \frac{K_m}{p} \overline{\vartheta}_{0m} \right] \quad (2.24)$$

2.1.3.2 Closed rib orthotropic deck

For open rib orthotropic deck, it is assumed that $D_x = 0$, $H = 0$, then

$$2H \frac{\partial^4 w}{\partial x^4 \partial y^4} + D_y \frac{\partial^4 w}{\partial y^4} = q(x, y) \quad (2.25)$$

The solution is

$$2H \frac{\partial^4 w}{\partial x^4 \partial y^4} + D_y \frac{\partial^4 w}{\partial y^4} = 0 \quad (2.26)$$

$$w = \sum_{n=1}^{\infty} (C_1 sh \alpha y + C_2 ch \alpha y + C_3 \alpha y + C_4) \sin \frac{n\pi x}{b}$$

in which

$$\alpha = \sqrt{\frac{2H}{D_y} \frac{n\pi}{b}}$$

a) Three-moment equation of continuous plate

Figure 2-10 shows a simple supported plate with different loads. Through the calculation, it is assumed that

$$M_0 \alpha_1 + 2M_1 \alpha_2 + M_2 \alpha_1 = 0 \quad (2.27)$$

while

$$C = \frac{\alpha_2}{\alpha_1} = \frac{\alpha t ch \alpha t - sh \alpha t}{sh \alpha t - \alpha t}$$

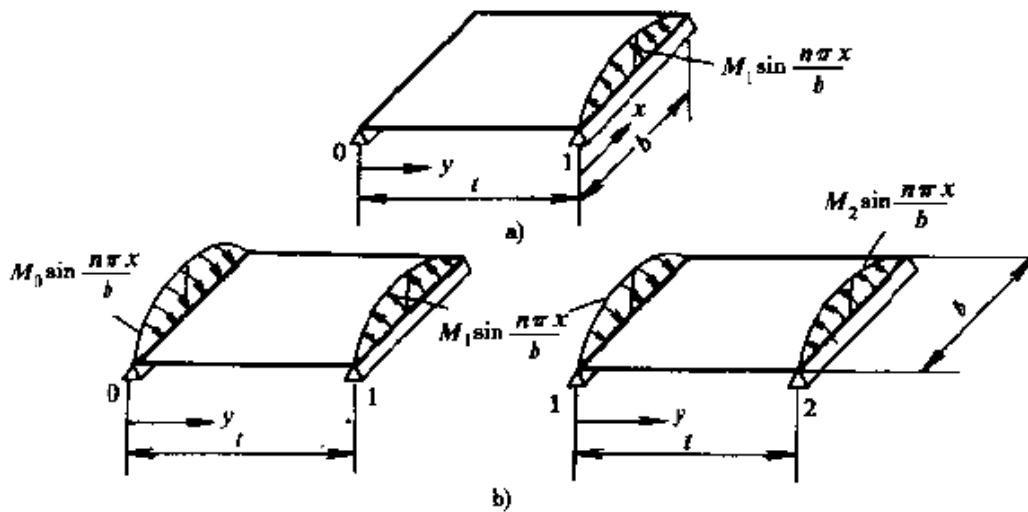


FIGURE 2-10 Single plate for calculating transverse coefficient K .

then

$$M_0 + 2CM_1 + M_2 = 0$$

Due to the moment decreases with the extending of span, then

$$M_1 = kM_0, M_2 = k_1M_1 = k^2M_0, \dots$$

Therefore,

$$\begin{aligned} M_0(1 + 2Ck + k^2) &= 0 \\ k &= -C + \sqrt{C^2 - 1} \end{aligned} \quad (2.28)$$

b) The moments of supported surfaces

Different loads on the plate are shown in Figure 2-11.

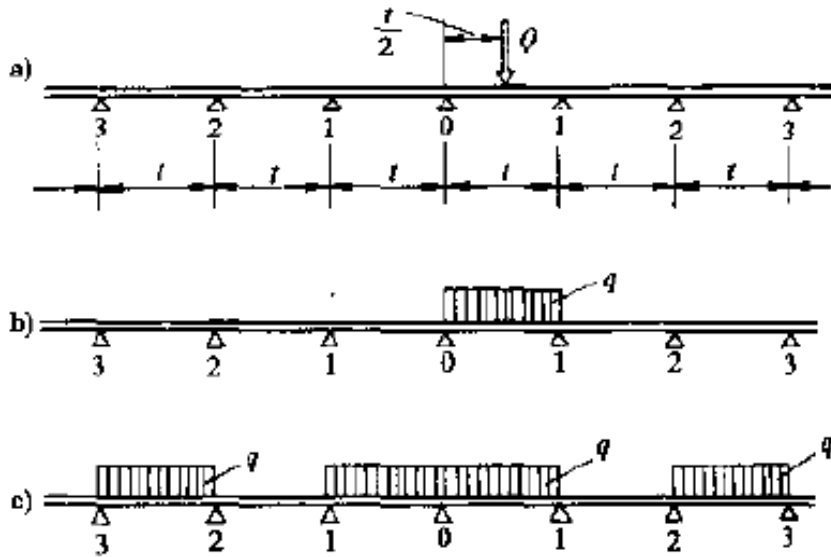


FIGURE 2-11 Different loading conditions on supported lines.

For load case a:

$$\begin{aligned} M_0^{0-1} &= Qt \frac{k}{2\alpha^*(1-k)} \left[1 - \frac{1}{ch \frac{\alpha t}{2}} \right] \\ M_0^{0-2} &= kM_0^{0-1} \end{aligned} \quad (2.29)$$

For load case b:

$$M_0^{0-1} = \frac{qt^2}{2} \frac{k}{2\alpha^*(1-k)} \left[1 - \frac{\alpha t}{2} \operatorname{th} \frac{\alpha t}{2} \right] \quad (2.30)$$

$$M_0^{1-2} = kM_0^{0-1}$$

While the loads act the full line:

$$M_0 = 2M_0^{0-1}(1 + k^2 + k^3 + \dots) = \frac{2M_0^{0-1}}{1-k}$$

For load case c:

$$M_0 = 2M_0^{0-1}(1 + k^2 + k^4 + \dots) = \frac{2M_0^{0-1}}{1-k^2} \quad (2.31)$$

c) The moment in the middle of the supports

Figure 2-12 shows the different loads between two nodes in the plate.

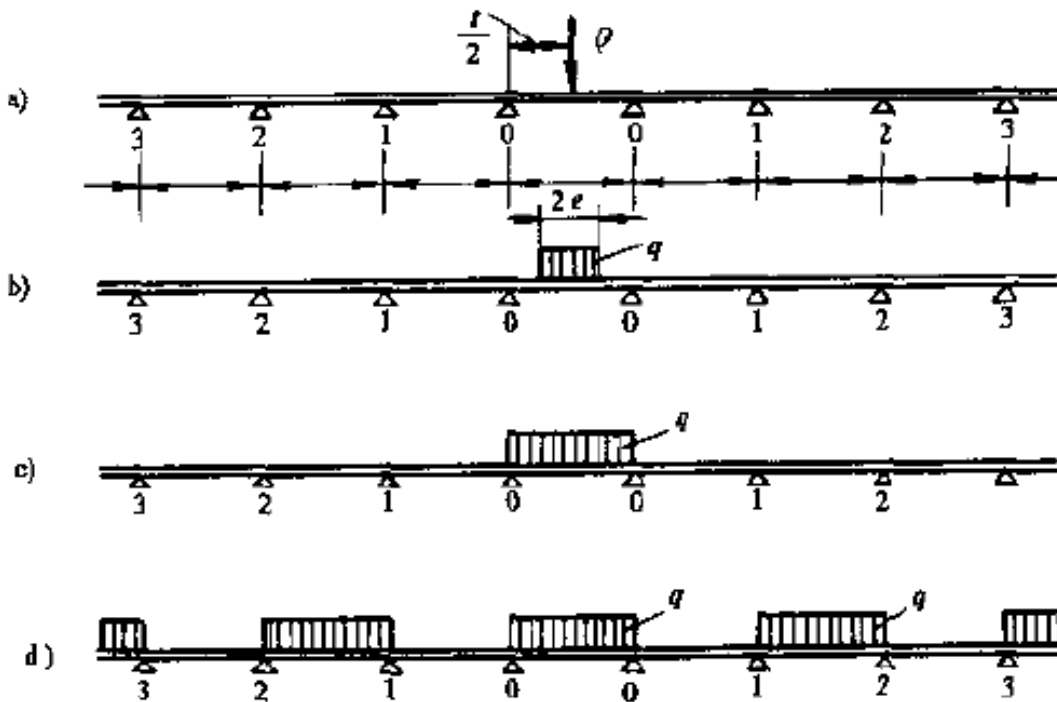


FIGURE 2-12 Different loading conditions in the middle of plate.

For load case a:

$$M_m^{0-0} = Qt \left[\frac{1}{2\alpha t} \operatorname{th} \frac{\alpha t}{2} + \frac{M_0^*}{t} \left(1 - \frac{1}{\operatorname{ch} \frac{\alpha t}{2}} \right) \right] \quad (2.32)$$

For load case b:

$$M_m^{0-0} = Qt \left\{ \frac{1}{2\alpha^2 te} \left[1 - \frac{ch\alpha \left(\frac{t}{2} - e \right)}{ch \frac{\alpha t}{2}} + \frac{M_0^*}{t} \left(1 - \frac{sh\alpha e}{\alpha e} \frac{1}{ch \frac{\alpha t}{2}} \right) \right] \right\} \quad (2.33)$$

For load case c:

$$M_m^{0-0} = qt \left[1 - \frac{ch \frac{\alpha t}{2} - 1}{(\alpha t)^2 ch \frac{\alpha t}{2}} + \frac{M_0^*}{t} \left(1 - \frac{2}{\alpha t} ch \frac{\alpha t}{2} \right) \right]$$

For load case d:

$$M = M_m^{0-0} + 2(1 + k^3 + k^5 + \dots) = M_m^{0-0} + \frac{2k}{1 - k^2} M_0^{0-1} \quad (2.34)$$

d) The moment of closed rib

Similar to the open rib deck, the moment of closed rib deck can be calculated by

$$M_y = \sum_{n=1}^{\infty} Q_n \sin \frac{n\pi x}{b} \eta_n = Q_0 t \sum_{n=1}^{\infty} \frac{Q_{nx}}{Q_0} \frac{\eta_n}{t} \quad (2.35)$$

where, η_n is the longitudinal distance of the influence area of the deck plate.

The actual moment M_R of the deck rib can be calculated based on the result of the center moment of the longitudinal rib, as shown in Figure 2-13:

$$M_R = (a + e) M_y \quad (2.36)$$

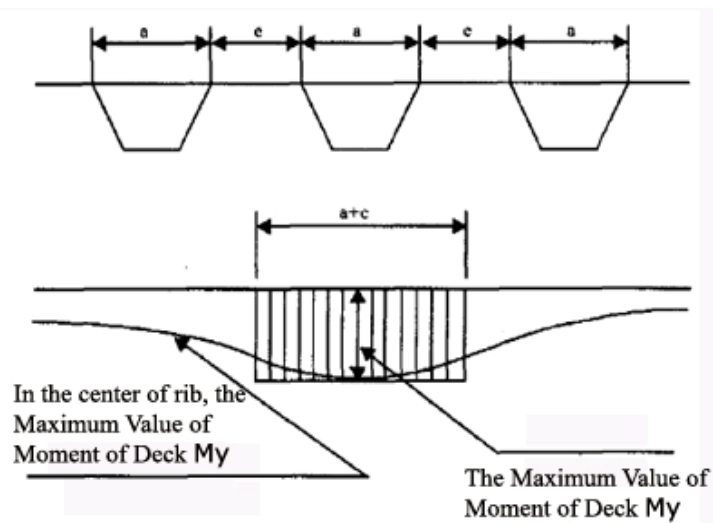


FIGURE 2-13 Moment of the closed rib.

2.1.3.3 The Pelikan-Esslinger method in AISC

As expressed in the 1963 AISC Design Manual for Orthotropic Steel Plate Deck Bridges [9], the simplifications attributed to Esslinger and Pelikan are as follows:

a) Open ribs

- 1) The deck plate is treated as a beam - i.e. the plate is given rigidity in the short direction from rib to rib. Deflection and flexure (at 25.9 ksi/178.6MPa) and shear criteria governed, giving a 3/8 inch (0.95cm) thickness over a 12 inch (30.48cm) rib spacing, for a 12 kip (53.4kN) wheel load.
- 2) The wheel load is distributed to adjacent ribs as in a beam on elastic foundations.
- 3) Effective width of deck plate (used to calculate the rib/deck plate composite properties over major rib carrying load) is a function of its share of the wheel load and of the “effective” rib span. It is usually larger than the actual rib spacing. The effective rib span is always 0.7 times the actual span.
- 4) Ribs “near” the floor beam support are treated as resting on rigid foundations; ribs “near” floor beam mid span are treated as resting on flexible foundations. Ribs near mid span will have larger positive moments and smaller negative moments than those near floor beam support. The AISC manual gives Moment Relief formulae all based on sinusoidal deflection of the floor beam.

In short, concepts of orthotropy are abandoned in favor of partial compatibility between beams. Global transverse rigidity is ignored; influence lines for beams are invoked.

b) Closed ribs

- 1) The torsional rigidity of the deck plate is governed by G , K and μ as defined by the following equation:

$$H = \frac{1}{2} \left(\frac{\mu GK}{a + e} \right) \quad (2.37)$$

Where G is the shear modulus for steel, K is a factor representing the physical properties and geometries of the rib such:

$$K = \frac{4A^2}{(u/t_r) + (a/t_p)} \quad (2.38)$$

Where

A is the area enclosed by the closed rib;

u is the entire length of the closed rib plate;

a is the rib width where it is joined to the deck plate;

t_r is the thickness of the rib plate;

t_p is the thickness of the deck plate;

e is the spacing between ribs stems of adjacent ribs – i.e. $a + e =$ rib spacing;

μ is a number less than 1 which accounts for the reduction of the torsional rigidity due to the flexibility of the deck plate. The AISC manual provides lengthy formulae for evaluating this factor for four closed rib geometries, and

H is the distributed rigidity per unit width of deck.

- 2) The transverse rigidity of the deck plate and the ribs are ignored.
- 3) Esslinger/Pelikan solved the Huber differential equation and provided charts for longitudinal moments for various loads and spans.
- 4) Adjustments are made to moments based on floor beam rigidity in the same way as is done for open ribs.

Torsional moments at the deck floor beam support were not sought. Also, the introduction of a stiffening intermediate diaphragm that is not supported on the girders, but merely spreads the load to more ribs represents a complication that was not dealt with by Pelikan and Esslinger.

What Should be Noted

The effective width of a discrete stiffened plate is smaller than that of a fully continuous orthotropic plate. It should be recognized that only the deck plate is continuous.

Trough shaped stiffeners are not fully effective in torsion because of cross-section distortion. Guidance is available on suitable methods of accommodating the reduction in rigidity.

In principle, the design of the deck should be verified separately for static strength and fatigue resistance. For static strength, the individual components of the deck need to be checked for the following stresses, in combination:

- a) Longitudinal stresses from participation in overall bending of the superstructure;
- b) Transverse stresses from participation in bending of the cross girder;
- c) Longitudinal stresses and shear stresses from bending of the stiffened plate between cross girders;
- d) Transverse bending of the deck plate between trough webs.

In practice, adequacy is demonstrated by experience rather than by calculation of the very complex elastic stress fields.

The flanges of bridge cross-sections are usually relatively wide with respect to their spans. The effects of shear lag need, therefore, to be included in the bending analysis. Shear lag effects cause the stress distribution over the cross-section to be non-linear. The maximum stress values occur at the flange-to-web junctions. The effective width is defined by the condition that the stresses at the flange-to-web junction, according to engineering bending theory, must be identical to the maximum stresses calculated by applying the mathematical theory of elasticity.

2.2 Finite Element Methods

Although traditional classic theories are very important to the design of orthotropic deck bridge, the assumptions and simplifications make the solutions existing errors,

especially at details. For example, the Pelikan-Esslinger method can be used to calculate accurately the stresses of longitudinal ribs, while it can not calculate the stresses around the cutout in the diaphragm. The Pelikan-Esslinger method can be applied to the preliminary design or the checking of FEM analysis. More precise method is necessary for calculating the stresses of critical connections, especially near the positions where support vehicle loads.

With the development of the science and technology, more and more numerical analysis methods can be used to calculate the stress state in the orthotropic deck. Finite Strip method was presented by Cheng, Y. K [14] in 1969. It was developed by Powell and Ogden [15] through a large number of investigations, and now is called Finite Element Method (FEM). There are many software can be used to carry out the analysis of orthotropic deck, such as SAP2000, LUSAS, ABQUAS and ANSYS. More complicated problems can be solved, and more accurate results can be obtained taking account into the more advanced computer.

2.2.1 Advantages of FEM

FE analysis calculating by powerful computer is one of the most effective methods in numerical analysis. FEM provides a large number of advantages, such as fast modeling, accurate analyzed results and economic compared to laboratory tests.

Fast modeling. The Modeling of a structure provided by FE software costs much less time than the test in laboratory. A structural model developed by FEM often takes a few weeks or even several days while takes several months in laboratory. Once the model is built, it is easy to modify in FE software through changing the parameters, thus, plenty of time is saved. For example, different load cases to an orthotropic deck can be applied to the same model and can be computed even in one running.

Accurate analyzed results. Almost any kind of details can be simulated in FE software through different models. Both elastic analysis and plastic analysis can be carried out by FE analysis. A great number of different meshed elements are provided

in FE software, from one-dimension to three-dimension, as shown in Figure 2-14. Each kind of element has several different meshes, and it can make the model more close to the real project. Figure 2-15 shows different meshes in two-dimension structures. Given good meshes to an orthotropic deck, better analyzed results can be obtained for the critical connections.

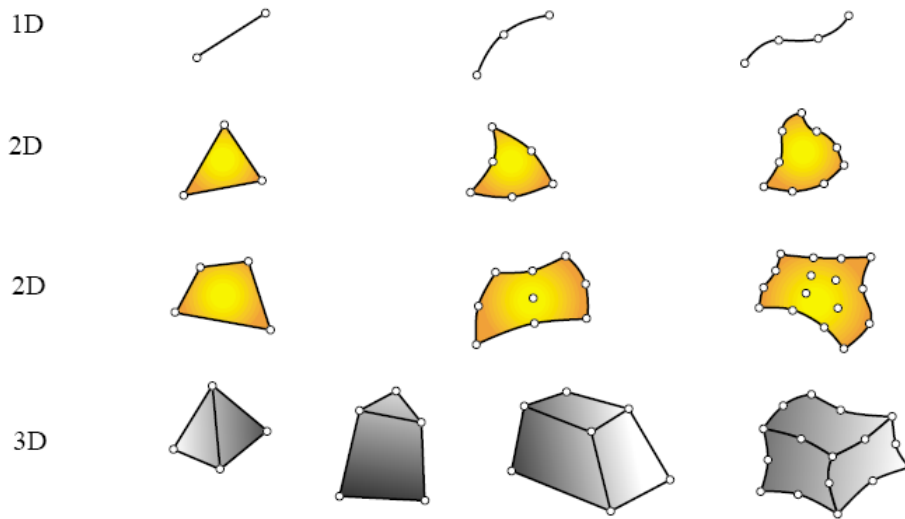


FIGURE 2-14 Different mesh elements

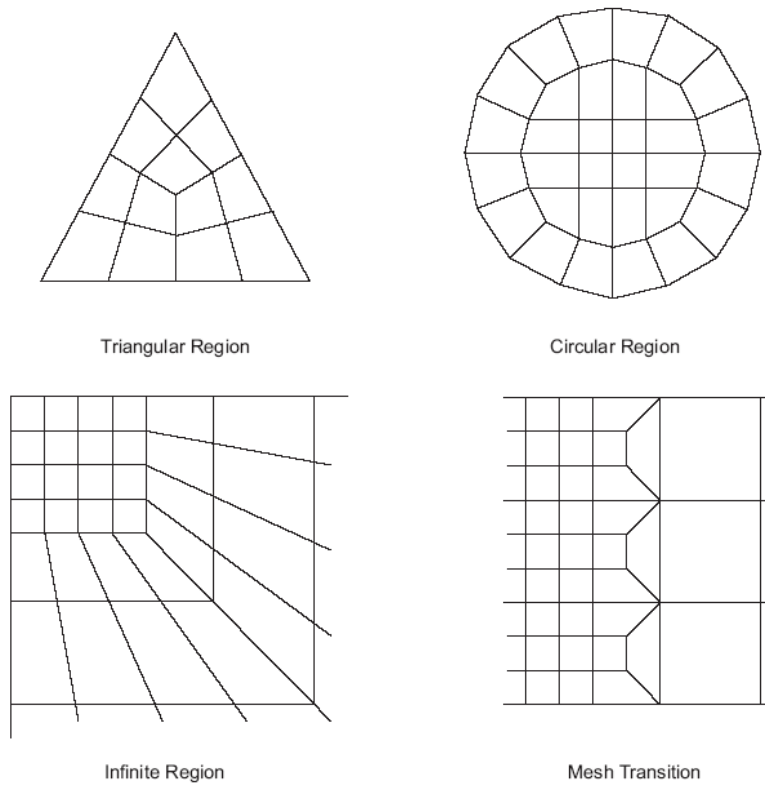


FIGURE 2-15 Different meshes of 2D structures

Economy. Laboratory test of an orthotropic deck is always very expensive, especially for prototype test. It needs a large number of machines, materials, and labor forces, therefore, it costs too much. However, numerical analysis via FE software is very economic compared with the laboratory test. A powerful computer is not too expensive to afford for a research group or a design office today, it usually costs about 2000 euro to 4000 euro. Costs related with software range from several thousands euro per year to several ten thousands euro per year. Many cases can be analyzed in one year through a powerful computer and software, thus, a mass of money can be saved.

2.2.2 Disadvantages of FEM

Although FEM provides many advantages in analyzing orthotropic decks, there are several disadvantages should be noted to the bridge designers.

Reasonable assumptions should be provided to develop an orthotropic deck model, such as boundary conditions and load cases. Improper assumptions would cause the analyzed results deviating from the real situation. In addition, different meshes provide different results, and sometimes may be very obvious, thus, the designers or users must be very familiar with the software. Considerable time and effort must be paid to build a detailed model with fine meshes, especially for a 3D model.

A good designer not only must be competent in the use of FE software, but also has a thorough comprehension to orthotropic decks.

2.2.3 Application of FEM in orthotropic deck

Both laboratory test and FEA are important to the study of the stress behaviors in an orthotropic deck structure. FEA is preferred by bridge designers because it is a fast and efficient way to calculate the stresses in an orthotropic deck. Also, FEM is a way provided to verify the results of laboratory tests.

Tinawi [16] calculated the deflections and stresses of the deck plate by FEM. Although the results were not very precise, they were strongly useful for bridge designers. Figure 2-16 shows the deflections obtained from FEA and compared with the results of the laboratory tests.

With the development of computer science and FE software, more and more investigations, especially for the fatigue evaluation of orthotropic deck, are carried out recently by researchers via FEA.

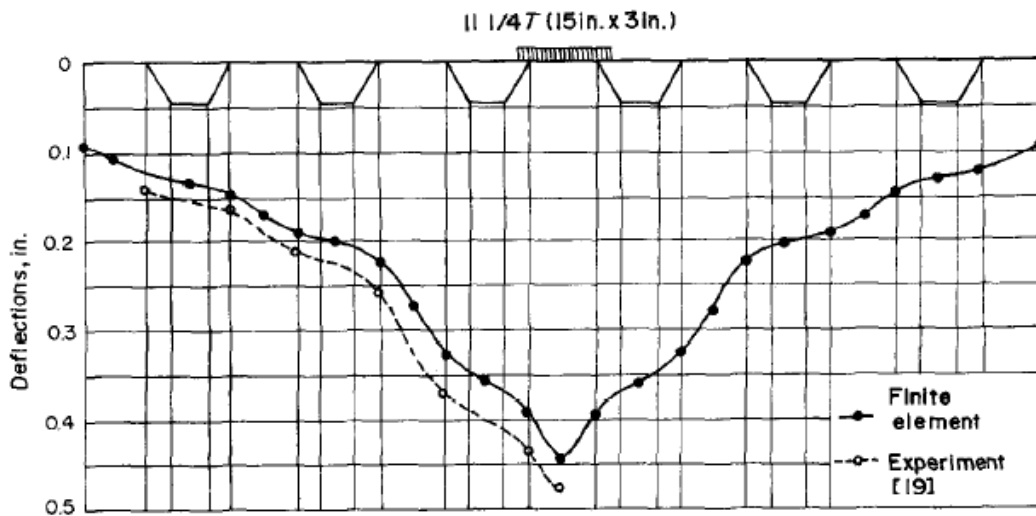


FIGURE 2-16 Deflections of orthotropic deck plate (R. Tinawi, 1976)

Mahmoud et al. [17] developed a detailed FE model to study the potential for fracture of the detail through linear and nonlinear analyses, as shown in Figure 2-17. Battista et al. [18] estimated the fatigue life with the aid of refined numerical model and in situ experimental strain measurements, taking into account all the built-in structural alterations, changes in volume of traffic and in vehicles loading which have occurred during this bridge's 32 years of service life. Furthermore, Kiss et al. [19] simulated crack growth by the numerical integration of the Paris formula, using K factors obtained from two-level cracked models of the bridge deck.

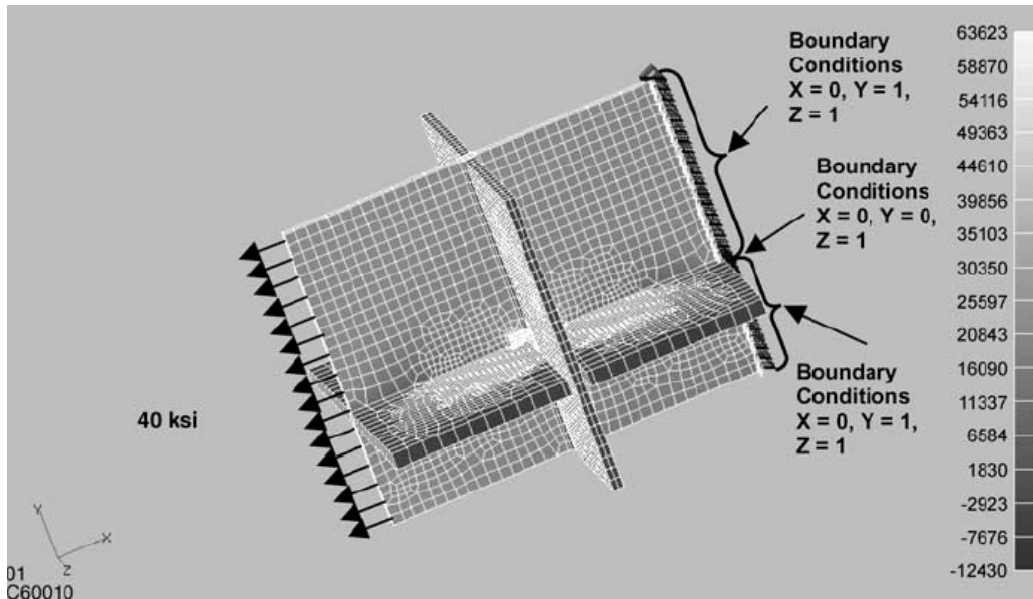


FIGURE 2-17 FE model with load and boundary conditions (Mahmoud et al, 2005).

2.3 Fatigue Behaviors

Fatigue cracking is a common problem in orthotropic steel bridges, as well as in other steel structures. Most of the cracks occur at welded connections due to the high stress concentration, high residual stress, and more initial flaws at welds. As well, the wearing surfacing of an orthotropic deck is inclined to occur fatigue cracking.

Rib-to-deck plate connection is one of the welded connections which are sensitive to fatigue cracking at an orthotropic deck bridge, while rib-to-diaphragm connection and rib-to-diaphragm-to-deck plate connection are other two connections ease to occur fatigue cracks. Figure 2-18 shows the cracks in the cope that has been repaired by drilling a stop hole [20]. The crack is caused by incompatibility between the curvature of the superstructure and the orthotropic steel deck that is bolted onto the floor beams.



FIGURE 2-18 Fatigue cracks at the floor beam of Throgg's Neck Bridge in New York
(W. Chen and L. Duan, 2000)

The behaviors of wearing surfacing on orthotropic steel decks under heavy truck traffic and environmental conditions are highly complex. The AASHTO Bridge Design Specifications first incorporated provisions for the design of orthotropic deck bridges in 1970s, however, this and subsequent editions as well as the technical literature provided few requirements or guidelines for the design of the wearing surfacing. Little information is available today to help bridge designers to find suitable materials and design methods for the orthotropic deck wearing surfacing.

An orthotropic deck plate requires a wearing surfacing for skid resistance, smooth riding and corrosion protection. The wearing surfacing suffers the heavy impact of loaded truck wheels imposed by the passage of millions of trucks during its service life. Thus, fatigue failure often occurs in the wearing surfacing above the webs of main girder or longitudinal ribs under cyclic traffic loading due to roller compaction, large temperature reduction and maintenance. Furthermore, interfacial dis-bonding between the wearing surfacing and underlying steel plate has been experienced. Figure 2-19 shows fatigue cracks of wearing surface on an orthotropic deck, and Figure 2-20 shows a detail of a visual observation [21].



FIGURE 2-19 Visual observations indicating deck plate cracking fixed bridge
(Dong et al., 2004)



FIGURE 2-20 Visual observations indicating deck plate crack (Dong et al., 2004)

Good performance of the wearing surfacing depends on the stiffness of deck plate, the properties of materials composed the wearing surfacing and the repeated vehicle loading crossing the bridge. Among of these, the properties of materials are more related with wearing surfacing itself. The following properties of the wearing surfacing should be considered in order to design a long lifespan wearing surfacing:

- Skid resistance: provide a safe skid-resistant surface with polish resistance aggregates for millions of wheel passages during the service life of the surfacing.
- Smooth ride quality: provide a smooth riding surface to the orthotropic deck.
- High bond strength: ensure high bond strength to the steel deck plate to provide composite action between the surfacing and the deck plate to reduce fatigue stresses

in the deck and in the surfacing, and to resist delaminations from shear stresses caused by flexure and by differential temperature expansion and contraction. The deflection and stress performances are showed in Figure 2-21 and Figure 2-22 [22].

- Resistance to cracking: provide fatigue resistance against material cracking under millions of repetitive truck wheels.
- Resistance to deformation: be resistant to shoving, rutting, and raveling by millions of wheel passages and high temperature extremes.
- Durable: be resistant to environmental factors, such as sunlight, oxidation, and temperature changes, and impervious to saltwater and to fuel and oil droppings from traffic.
- Waterproof: be impervious to the passage of water through the surfacing.
- Protected from corrosion: in addition to being impervious, provide a corrosion-resisting coating to protect the steel deck plate.

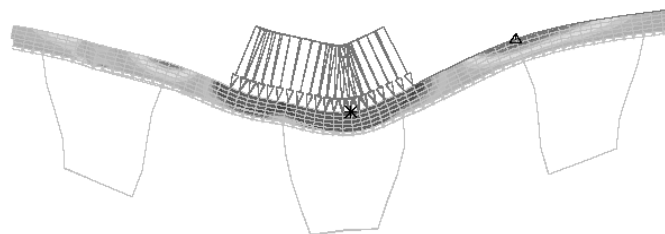


FIGURE 2-21 Tensile and compressive wearing surface stresses due to transverse bending of deck (C. Seim, T. Ingham, 2004).

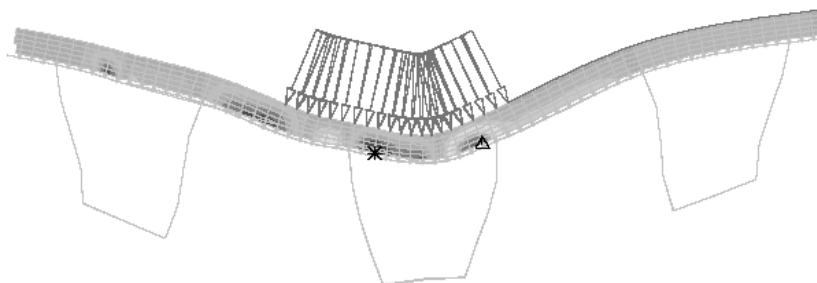


FIGURE 2-22 Shear and interface bond stresses due to transverse bending of deck (C. Seim, T. Ingham, 2004).

Stress behaviors of deck structure which carried by FE analysis will be discussed in Chapter 3, and fatigue evaluations based on the stress results are presented in Chapter 4. However, fatigue behaviors of wearing surface will not be discussed detailed in this study.

References:

- [1] Xanthakos DP. Theory and design of bridges. John Wiley & Sons, Inc. 1994.
- [2] Guyon Y. Calcul De Ponts Larges a Prouties Multiples Solidarisees Par des Entretoises. Ann. De Ports et Chavsees de France, 1946; 24(5):553-612.
- [3] Massonnet C. Methods of Calculation of Bridges with Several Longitudinal Beams TakingInto Consideration Their Torsional Resistance. International Association for Bridge and Structural Engineering Publications, 1950; 10: 147-182.
- [4] Morice PB, Little G, Rowe RE. Design curves for the effects of concentrated loads on concrete bridge decks. Publication DB11a, Cement and Concrete Association, 1956.
- [5] Rowe RE. Concrete bridge design. C. R. Books, London, 1962.
- [6] Paik JK, Thayamballi AK. Ultimate limit state design of steel plated structures. John Wiley & Sons, 2003.
- [7] Cornelius W. Die berechnung der ebener flachentragwerke mit hilfe der theorie der orthogonal anisotropen platten. Der Stahlbau, 1952; 2: 21-26.
- [8] Pelikan W, Esslinger M. Die Stahlfahrbahn Berechnung und Konstruktion. MAN ForschHeft, 1957, 7.
- [9] American Institute of Steel Constrction (AISC). Design manual for orthotropic steel plate deck bridge, New York, U.S.A., 1963.
- [10] Troitsky MS. Orthotropic Bridges Theory and Design. The Forms F. Lincoln Arc Welding Foundation, 1987.
- [11] Vlasov VZ. Thin-walled elastic beams. Israel Program for Scientific Translation, NSF, Jerusalem, 1967. (in English; orginal Russian edition, 1959)
- [12] De Fries-Suene A, Scordelis AC. Direct stiffness solution for folded plates. J. Strut. Div. ASCE, 1964; 90 (ST4): 15-47.
- [13] Timoshenko S, Woinowsky-Krieger S. Theory of plates and shells. McGraw-Hill Book Company, 1959.
- [14] Cheung YK. The finite strip method in the analysis of elastic plates with two opposite simply supported ends. Proc. Inst. Civ. Eng., May 1968: 1-7.
- [15] Powell GH, Ogden DW. Analysis of orthotropic steel plate bridge decks. J. Strut. Div.

ASCE 1969; 95: 909–922.

- [16] Tinawi R, Redwood RG. Orthotropic bridge decks with closed stiffeners - analysis and behaviour. *Computers & Structures*, 1977; 7: 683-699.
- [17] Mahmoud HN, Connor RJ, Fisher JW. Finite Element Investigation of the Fracture Potential of Highly Constrained Details in Steel Plate Members. *Computer-Aided Civil and Infrastructure Engineering*, 2005; 20: 383–392.
- [18] Battista RC, Pfeila MS, Carvalho E. ML. Fatigue life estimates for a slender orthotropic steel deck. *Journal of Constructional Steel Research*, 2008; 64: 134–143.
- [19] Kiss K, Dunai L. Fracture mechanics based fatigue analysis of steel bridge decks by two-level cracked models. *Computers and Structures*, 2002; 80: 2321–2331.
- [20] Chen W, Duan L. *Bridge Engineering Handbook*. Boca Raton: CRC Press, 2000.
- [21] De Jong FBP. Overview fatigue phenomenon in orthotropic bridge decks in the Netherlands. *Orthotropic Bridge Conference*, Sacramento, California, USA, 2004: 489-512.
- [22] Seim C, Ingham T. Influence of wearing surfacing on performance of orthotropic steel plate decks. *Transportation Research Record: Journal of the Transportation Research Board*, National Research Council, Washington, D.C., 2004; 1892: 98–106.

CHAPTER 3

INFLUENCES OF GEOMETRIC PROPERTIES TO ORTHOTROPIC DECKS

Fatigue problem is one of the most important issues when a bridge designer designs an orthotropic deck. The factors which affect the fatigue life of steel structures can be listed as following:

Stress. Stresses produced by traffic loading, welding or thermal gradients can cause fatigue cracking. Both in-plane stress and out-of-plane stress are important to calculate the fatigue life of an orthotropic deck bridge.

Geometry. Geometric factors determine the position where fatigue cracking occurs. Meanwhile, the magnitude of concentrated stress (influenced by geometry) strongly affects how quickly the fatigue cracking may initiate and propagate. The geometric factors include deck plate, longitudinal rib, diaphragm, cutout, bulkhead, and other details in the orthotropic deck.

Environment. Environmental factors include corrosive liquids or gases, climate and irradiation. Fortunately, these factors can be ignored in most of cases if good protection is provided. However, special attention should be paid to orthotropic bridges in cold areas, especially to the wearing surfacing.

Materials. Material properties determine how the bridge reacts to some of the factors in the other three categories.

Different combinations of the above factors make the fatigue design of orthotropic deck complicated. Bridge designers should employ the suitable combination to continue the fatigue design.

In welded structures, it is inevitable that built-in stresses exist at potential crack locations, such as residual stress. In addition, geometric configuration provides stress concentration as mentioned before. It is noted that stress range is the most important stress factor to fatigue life of welded structures according to many previous investigations. As a result, applied stress range becomes the only significant stress

factor in the nominal stress approach which is widely used to assess the fatigue life. Initial flaws, such as discontinuities, are unavoidable in welded connections. Discontinuities are often very difficult to be detected, but their presence eliminates any significant period of crack initiation. It is especially true when residual stress is very high.

Orthotropic deck bridges and their components behave elastically under the fatigue loading. Therefore, the difference of materials will not cause obvious gap to fatigue lives.

Based the previous discussion, it is clear that the fatigue life of an orthotropic deck bridge is often determined by the following two factors: geometry and stress range. Figure 3-1 shows the factors affecting the fatigue life of an orthotropic deck.

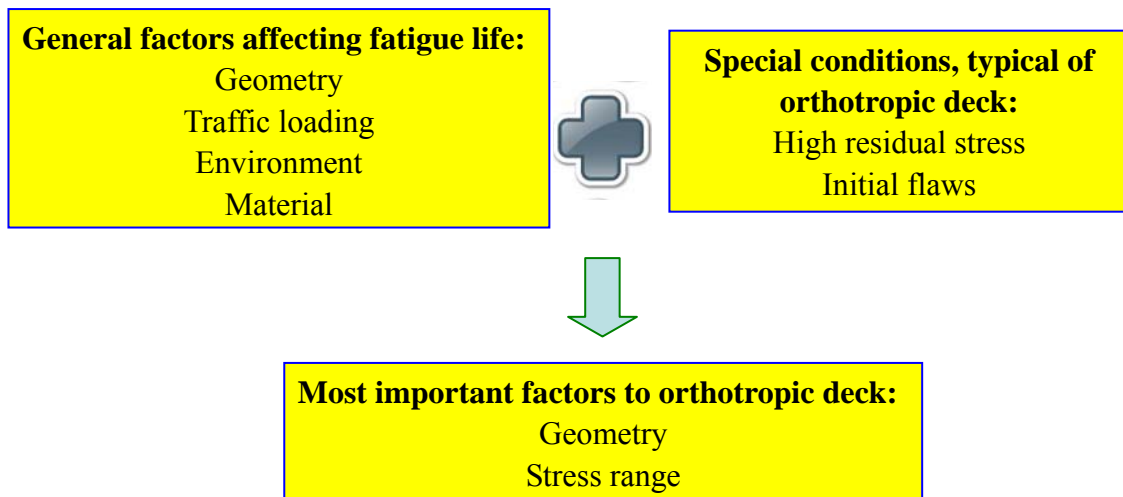


FIGURE 3-1 Factors affecting the fatigue life of orthotropic deck.

Between the two most important factors, geometry is the parameter which can be optimized by a bridge designer during the design stage. Therefore, the geometric influences will be discussed in detail in this study based on numerical analysis of an orthotropic deck. The FE model of the orthotropic deck is shown in Figure 3-2.

In recent, a few practical cases of orthotropic deck bridges demonstrated that fatigue fracture should be adverted due to concentrated stress, out-of-plane stress and residual welding stress at diverse connection details [1, 2]. An orthotropic deck is mainly composed by deck plate, diaphragms and longitudinal ribs, and it has various critical

connection details, such as rib-to-diaphragm, rib-to-deck plate and rib-to-diaphragm-to-deck plate.

A reasonable design can bring considerably advantage to the fatigue resistance. The geometry of orthotropic deck, such as composition of the deck, has a significant influence to the fatigue behavior. The design of orthotropic deck is often being discussed and developed, for example, from open rib to closed rib, from triangle rib to trapezoidal rib, with or without cutout, and with or without bulkhead. Nowadays, some of them are still in discussions, and needs further studies.

Diaphragm, one of the three main parts in orthotropic deck, is sensitive to fatigue cracking due to the existing of many critical connections, such as cutout and bulkhead. The geometry of the cutout at the intersection of longitudinal ribs and transversal diaphragm plates has a significant impact to the stress state in the region of the welded rib-to-diaphragm connection [3]. Therefore, the design of cutout is important to the fatigue life of an orthotropic deck since high concentrated stress occurs at/near it. Diverse shapes of cutouts can produce distinct stress status at the rib-to-diaphragm connections where occur peak stresses easily. The European code [4] and the American specification [5] provide some different geometric cutouts. Meanwhile, the bulkhead is another issue in the design due to the complicated stress performance at the connection details.

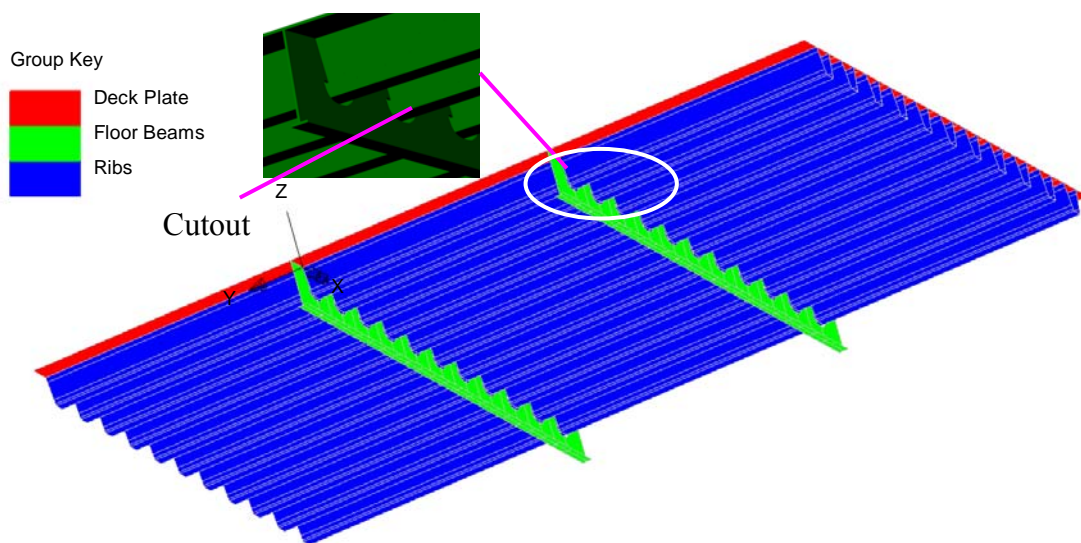


FIGURE 3-2 Orthotropic deck model.

In this chapter, the geometric influences to the stress performance are discussed concretely based on FE analyses.

3.1 Finite Element Analysis

3.1.1 Introduction

The Finite Element program is the tool that has contributed to revolutionary leaps in design and research in the field of Mechanics. The field includes work on materials in any state or medium, such as plasma, fluid, solid, heat transfer, two-phase, and many others. There are a large number of software programs that can be applied to structural mechanics. Software companies continue to make improvements to render their codes more user-friendly and to enable more design engineers to solve more complex problems. In this study, all FE models are developed by LUSAS 14 which is very powerful to analyze bridge structures.

Conventional laboratory tests are often high cost and time consumed. FE method is an economical and accurate method for analyzing complex structure systems. Furthermore, different load cases can be calculated simultaneously and contours of the analyzed results offer extreme detailed information for each part of the structure. For work applicable to orthotropic decks, it is sufficient to have a software program that can do analyses in the elastic domain without considerations to material or geometric nonlinearity. First order displacements are sufficient.

In recent years, many investigations [6, 7] have already been carried out by FE software in order to study the behaviors of orthotropic deck bridges. Although FE method provides many advantages, it should be noted that a perfect model of an orthotropic deck is difficult to be developed due to the complication of the structure. For instance, different meshed dimensions near cutouts or connection details can produce diverse stress performance. Therefore, a good mesh is necessary to the orthotropic deck model, especially at/near the critical positions.

3.1.2 Numerical modeling

3.1.2.1 Detailed dimensions

In order to study the stress performance and the fatigue behavior of critical connections of an orthotropic deck, FE model was built with linear thin shell elements in this study, as shown in Figure 3-3 (detailed meshes are shown in respective paragraph). The FE model is intended to simulate the orthotropic deck as part of the long span bridge. The deck model consists of 11 trapezoidal longitudinal ribs which are commonly used in orthotropic deck bridges, supported by 2 diaphragms. The dimension of deck plate is 9000 mm*6900 mm, the height of diaphragm is 500 mm, and the space of diaphragms is 3000 mm. The cross section of a longitudinal rib is 300 mm (top width, and the bottom width is 200 mm)*300 mm (height), the span of the two longitudinal ribs is 600 mm.

The thickness of the deck plate is 16 mm, the thickness of longitudinal rib is 8 mm, and the diaphragm is 14 mm.

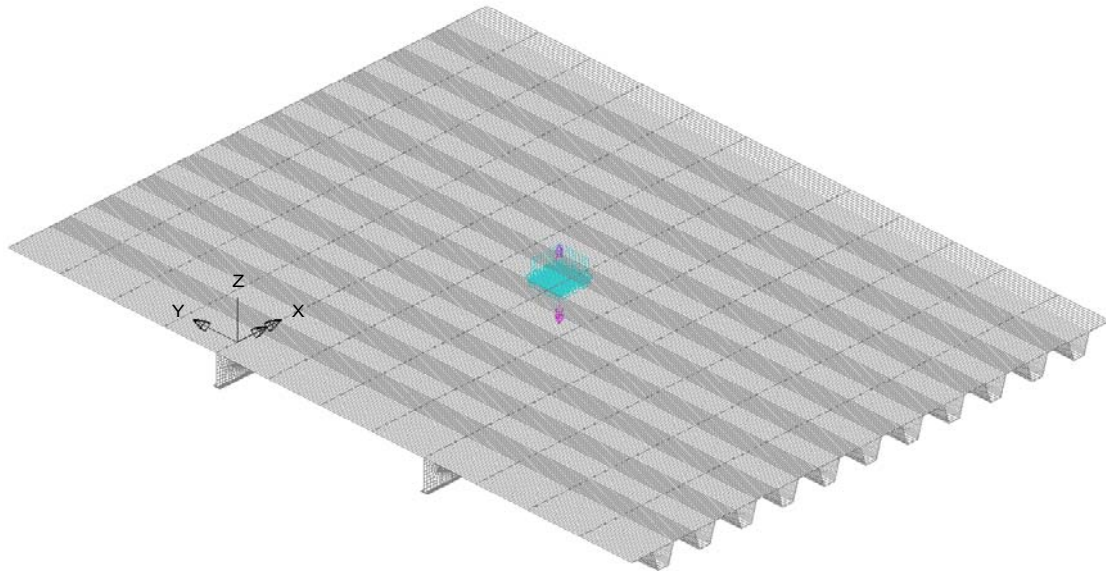


FIGURE 3-3 The mesh of the orthotropic deck model.

3.1.2.2 Boundary conditions

The boundary conditions adopted in the FE model try to simulate the actual status because the actual displacements of the boundaries in orthotropic deck are considered. Both of the vertical and horizontal translations are constrained on the two transversal boundaries (along X direction), and all rotations of the two boundaries are free. Meanwhile, both of the vertical translations are constrained on the two longitudinal boundaries since the diaphragms can restrain the vertical deflection, while all the others are free. The vertical and transverse translations and rotations about Y- and Z-axis are constrained for all nodes at the end of the diaphragms.

3.1.2.3 Load cases

The load applied to the model is 105 kN which distributes on a square surface 400 mm*400 mm. This “fatigue load”, according to the Italian code [8], is 30% less than the peak load applied on the deck plate for local loads, i.e. 150 kN. Considering the distribution function of wearing surfacing, the load area used for numerical analysis is variable. Figure 3-4 displays how to evaluate the calculating area in different orthotropic decks (a is thickness of wearing surfacing, h is thickness of deck plate and b is width of wheel load; the distribution angle is 45°). With the development of wearing surfacing material, thinner wearing surfacing is applied in bridge construction. In this study, one kind of new materials, polymer concrete, is assumed being used in the model of the orthotropic deck, and the thickness is only 25 mm. Consequently, the actual load area is 464 mm*464 mm.

In addition, three different load cases are applied in the analyses. Load case 1 acts in the middle of orthotropic deck, both in the longitudinal direction and the transversal direction; load case 2 locates between the middle rib (R6) and the closed tooth; and load case 3 locates at the tooth nest to the middle rib (R6), as shown in Figure 3-5.

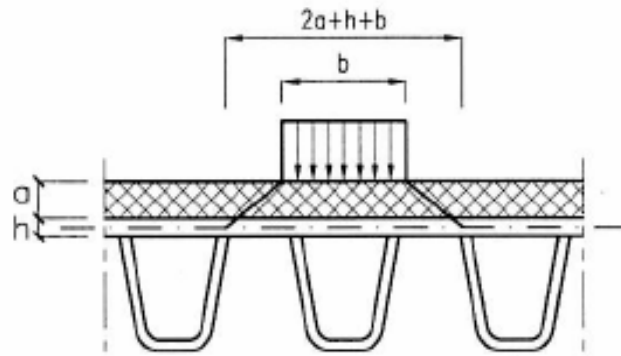


FIGURE 3-4 Load distribution in the wearing surfacing (Norme Tecniche per le Costruzioni, 2008).

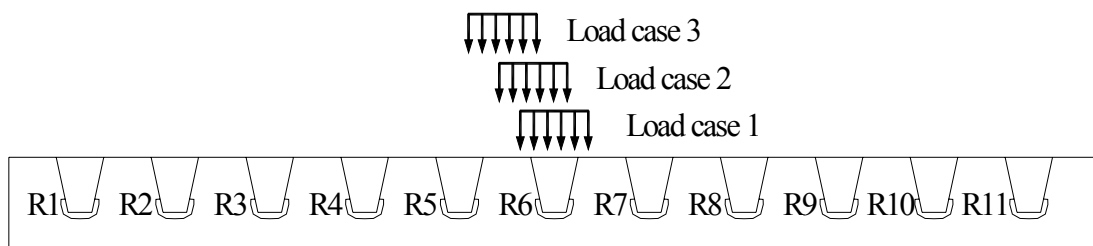


FIGURE 3-5 Wheel load distributions in the transverse direction.

3.2 Deck Behaviors

A numerical model developed from Eurocode 3 [4] is used to analyze the behaviors of orthotropic deck. Figure 3-6 shows the fine mesh in the diaphragm.

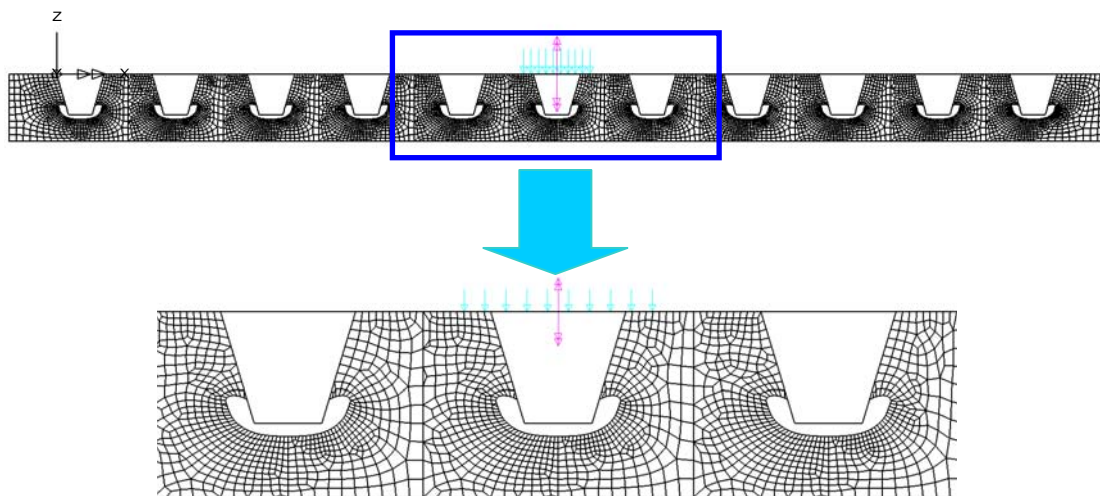


FIGURE 3-6 Fine mesh in the diaphragm.

The behaviors of the main components are studied via FE analysis. Figure 3-7 shows the global deformation of the orthotropic deck model under the simulated vehicle loading. It is found that the deformation far from the loading position is very small, and almost can be ignored.

The behaviors of deck plate, diaphragm and other welded connections are discussed in the following paragraphs.

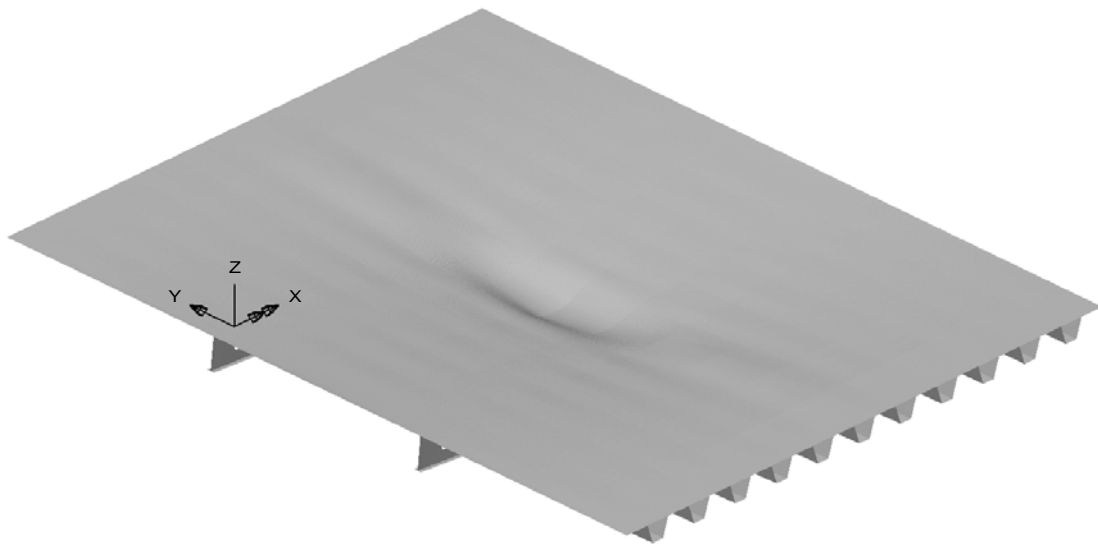


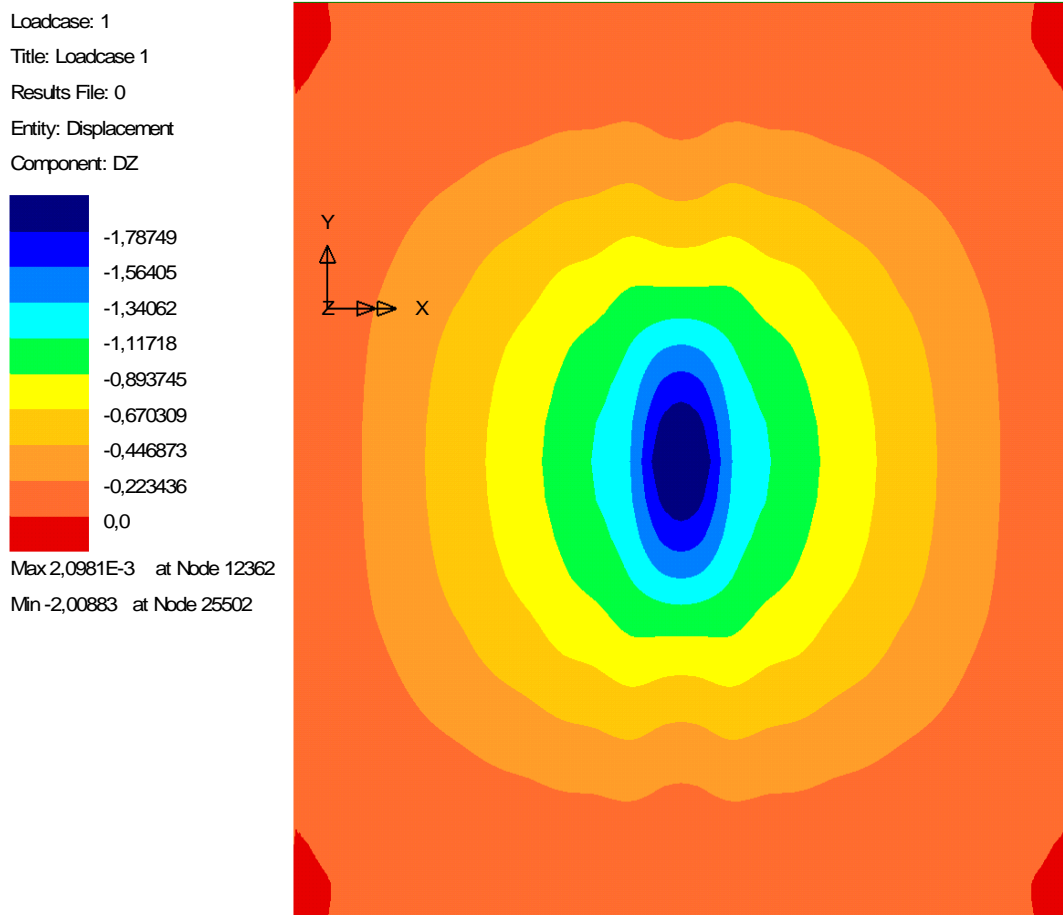
FIGURE 3-7 Deformation of the global orthotropic deck.

3.2.1 Behaviors of deck plate

Figure 3-8 shows the vertical deflection of the deck plate suffering the three different load cases. The deflection of the deck plate mainly locates near the loading position due to the restriction of longitudinal ribs and diaphragms. The deflection far from the loading position can almost be ignored. In addition, it is found that load cases has a strong influence to the stress performance of the deck plate.

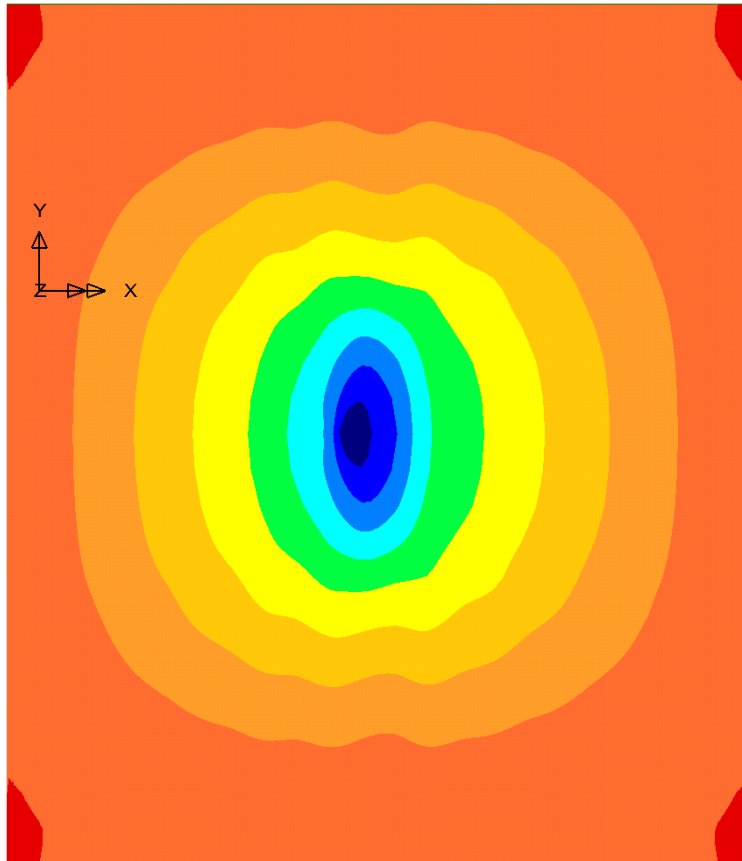
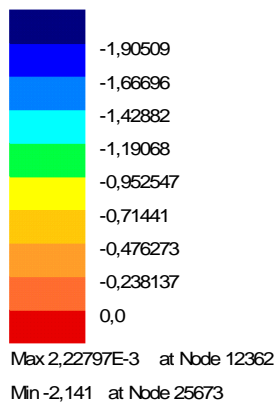
Figure 3-9 displays the stress contours of the deck plate suffering the three different load cases. Large stresses occur only between the two neighboring ribs next to the loading location. It is found that obvious difference of the stress distributions exist at

the deck plate under the three load cases. As shown in Figure 3-9, it is evident that both of the longitudinal rib and the loading location influence the stress performance of the deck plate significantly. The stress trace at the deck plate demonstrates that both the rib and the diaphragm restrict effectively at the deck plate. High stress area mainly locates at the middle span. Moreover, both maximal and minimal stresses are found in the high stress area. As well, it is found that the forms of the high stress area change greatly with diverse load cases.

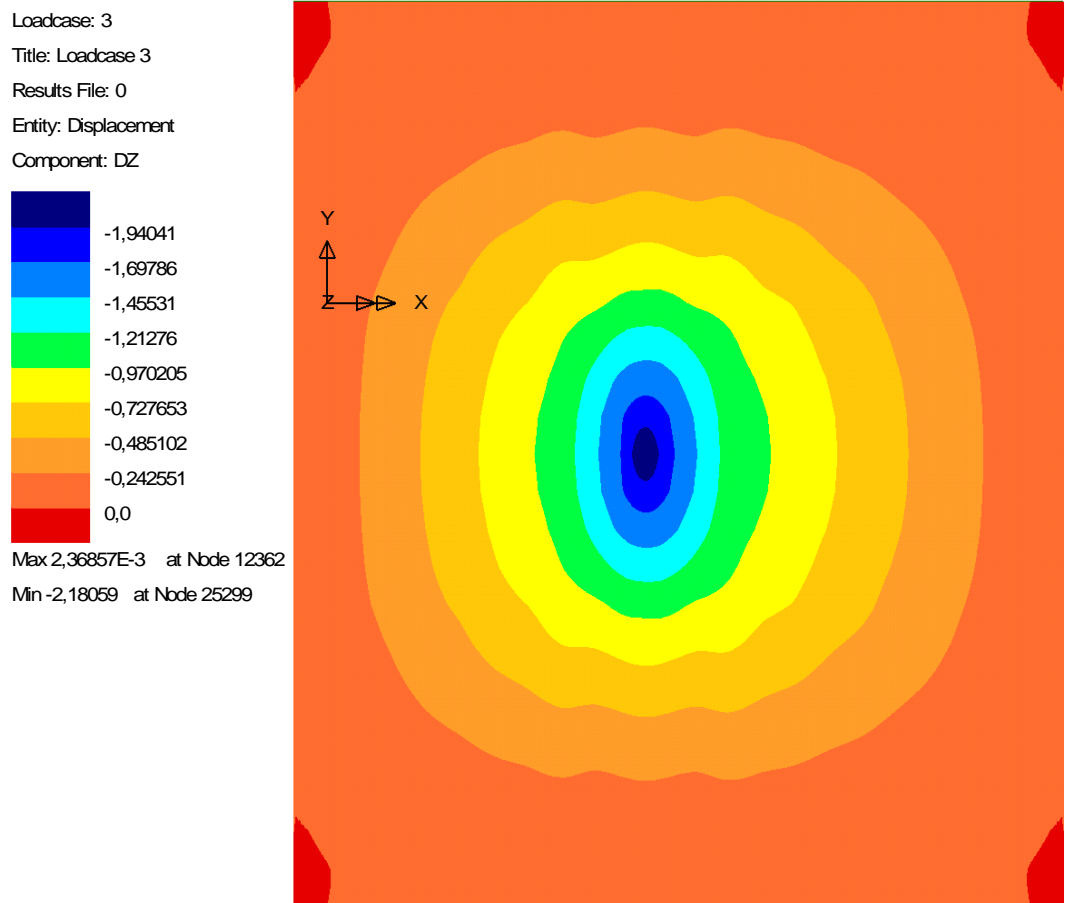


a. Load case 1;

Loadcase: 2
Title: Loadcase 2
Results File: 0
Entity: Displacement
Component: DZ



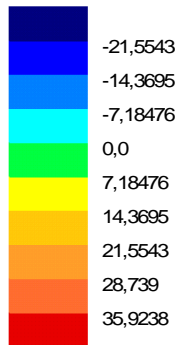
b. Load case 2;



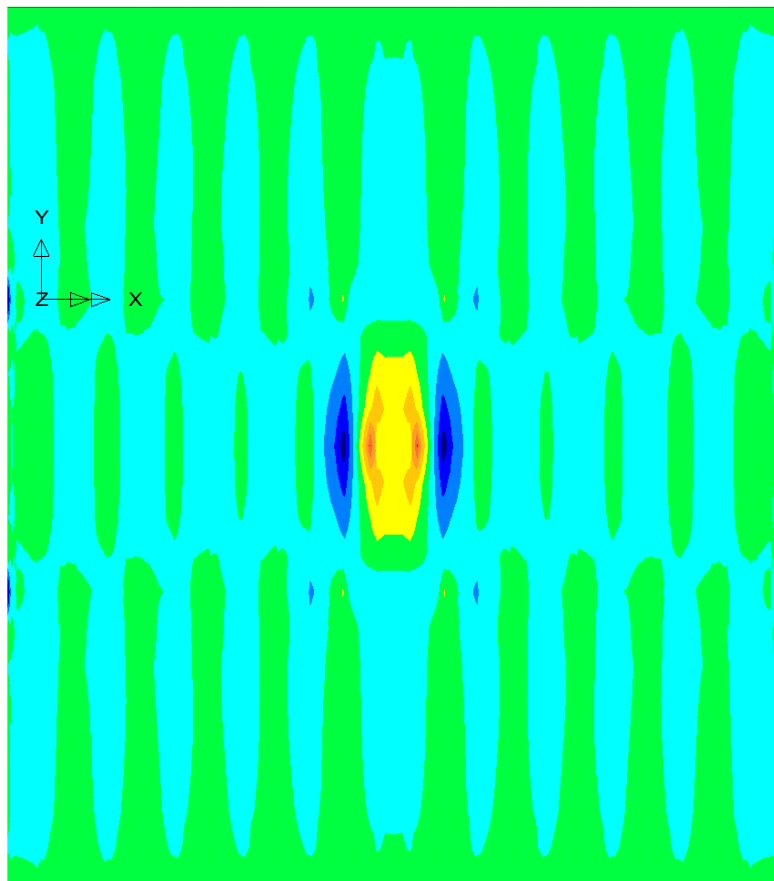
c. Load case 3;

FIGURE 3-8 Vertical displacements of deck plate suffering the different loads.

Loadcase: 1
Title: Loadcase 1
Results File: 0
Entity: Bottom Stress
Component: SX

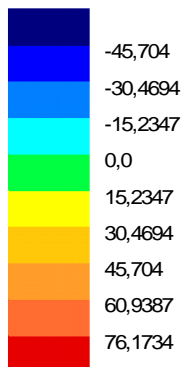


Max 37,1012 at Node 25676
Min -27,5615 at Node 2993

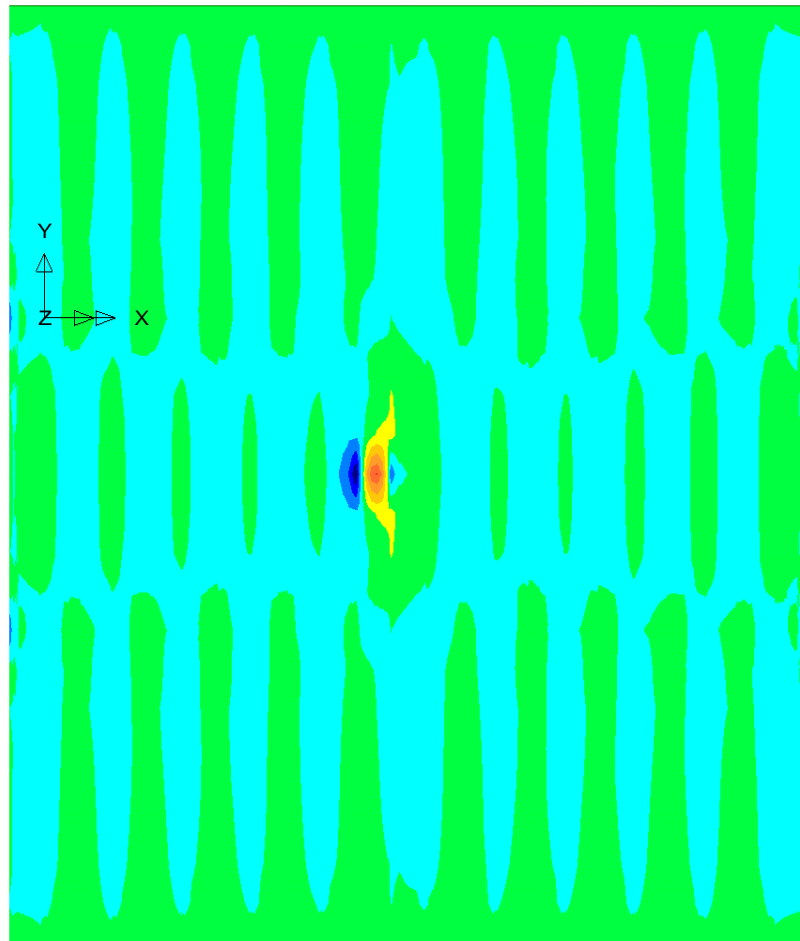


a. Load case 1;

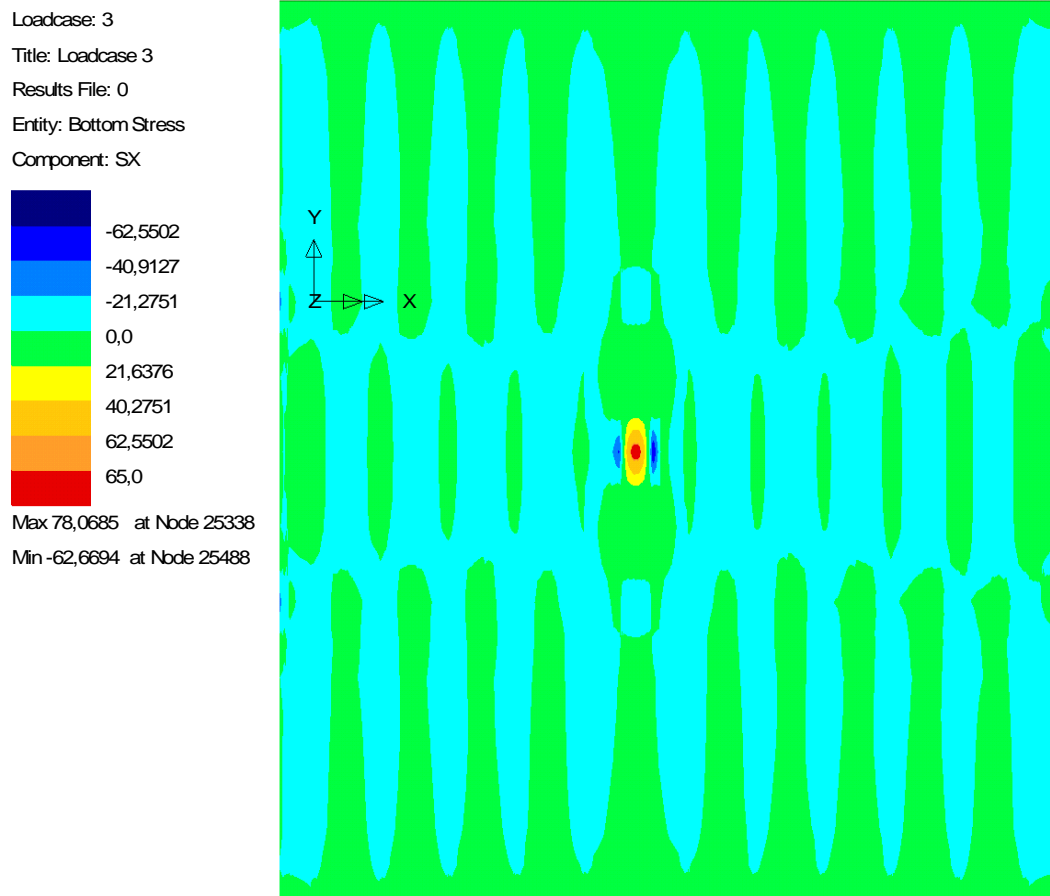
Loadcase: 2
Title: Loadcase 2
Results File: 0
Entity: Bottom Stress
Component: SX



Max 78,0067 at Nobe 25672
Min -59,1054 at Nobe 25067



b. Load case 2;



c. Load case 3;

FIGURE 3-9 Bottom stresses of the deck plate suffering the different loads.

3.2.2 Behaviors of diaphragm

An orthotropic deck has ribs oriented longitudinally running in the direction of the traffic and is integral with the sub-floor structure. An orthotropic deck may also “float” and is weakly connected to supporting members. They respond to the imposed load with effects which are primarily in the orthogonal directions, and involve localized distortions at the diaphragm. Immediately under the wheel, stresses in three orthogonal directions invariably also develop.

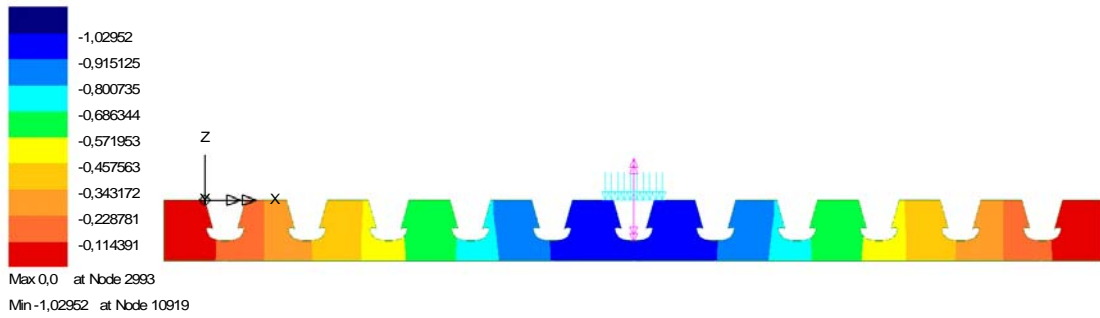
Over the last 15 years the engineering community has come to realize that the most important aspect during the design of an orthotropic deck is not how wheel loads are shared by adjacent ribs or what rib moments can be expected over the floor beam at mid-span or near support, which was the achievement of Pelikan and Esslinger, but on what effects occur at the intersections of the rib and the diaphragm, and how these effects impact on hot spots in the plane of the diaphragm and on their survivability.

Laboratory testing and the application of FEA shed much light on the behavioral effects along diaphragm and how the rigidity of the floor beam, of the diaphragm and of the deck plate interplay in ways that are often in conflict. For example, an increase in diaphragm thickness may improve RDDP stress ranges, but could exacerbate them at the cutout or at the welded all around detail.

Figure 3-10 shows the vertical (in-plane) displacements of the diaphragm under the three different load cases, while Figure 3-11 shows the horizontal (out-of-plane) displacements. The large deformation occurs near the loading location. The in-plane deflection decreases with the increasing of the distance from the loading position. The same phenomenon is found to the out-of-plane displacement.

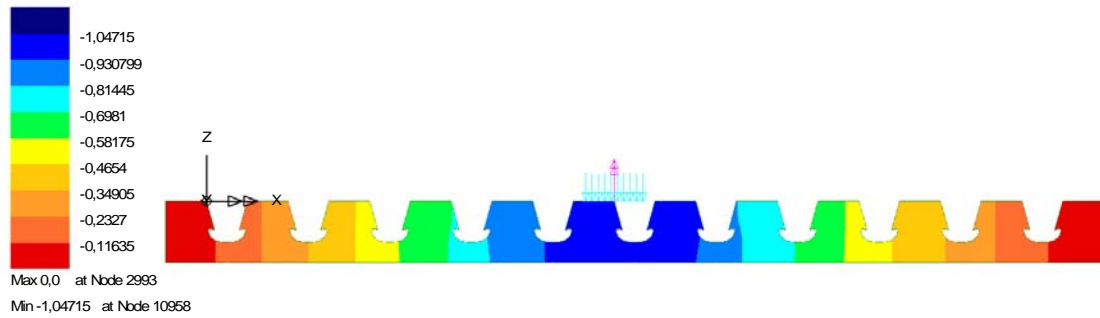
Figure 3-12 displays the stress contours of the diaphragm under the three load cases. The stress decreases with the increasing of the distance from the loading position. It should be noted that there are many connections existing concentrated stresses, such as in rib-to-diaphragm connections.

Loadcase: 1
 Title: Loadcase 1
 Results File: 0
 Entity: Displacement
 Component: DZ



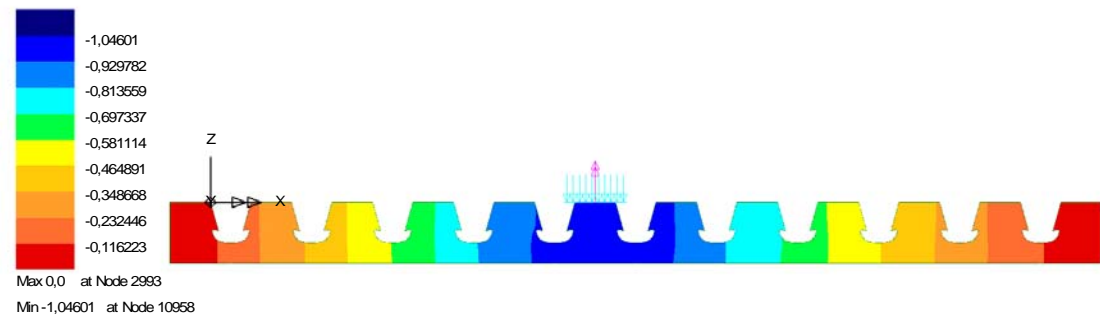
a. Load case 1;

Loadcase: 2
 Title: Loadcase 2
 Results File: 0
 Entity: Displacement
 Component: DZ



b. Load case 2;

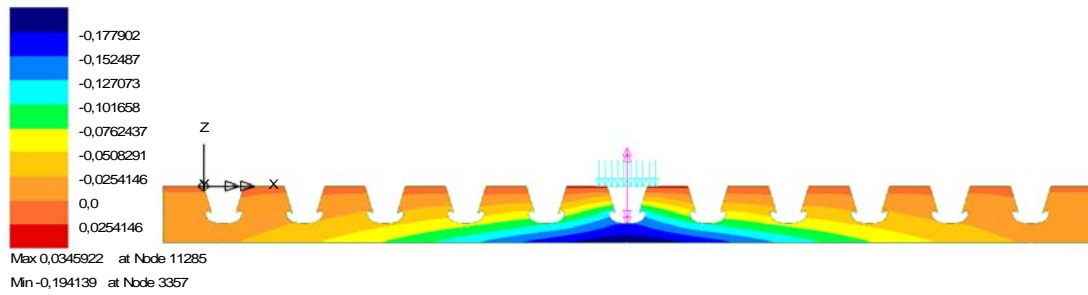
Loadcase: 3
 Title: Loadcase 3
 Results File: 0
 Entity: Displacement
 Component: DZ



c. Load case 3;

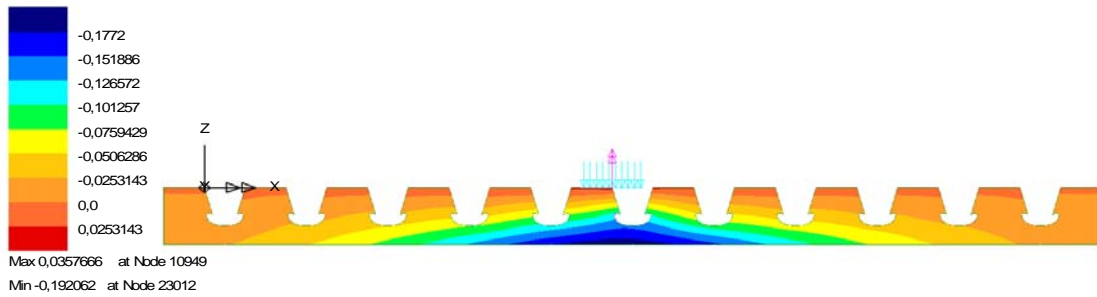
FIGURE 3-10 Vertical deflections of the diaphragm.

Loadcase: 1
 Title: Loadcase 1
 Results File: 0
 Entity: Displacement
 Component: DY



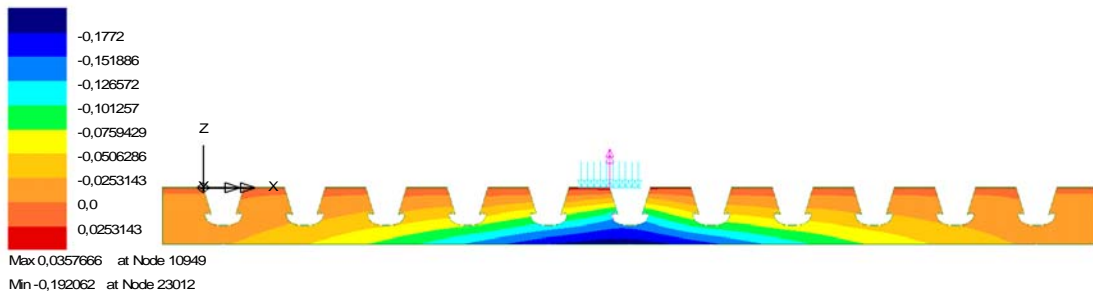
a. Load case 1;

Loadcase: 2
 Title: Loadcase 2
 Results File: 0
 Entity: Displacement
 Component: DY



b. Load case 2;

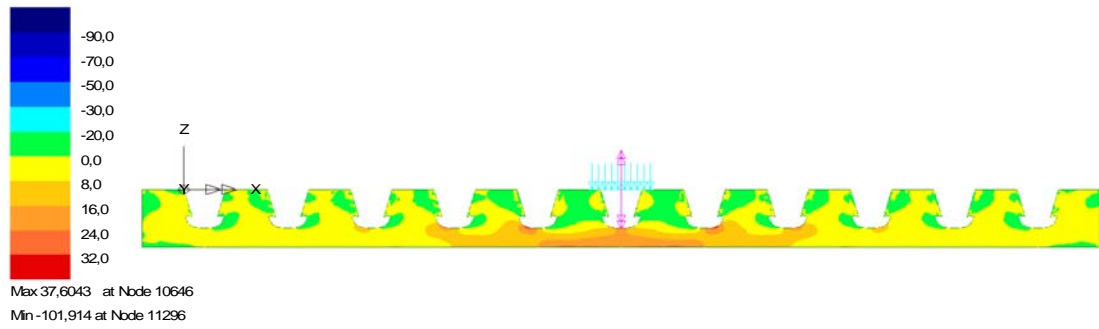
Loadcase: 2
 Title: Loadcase 2
 Results File: 0
 Entity: Displacement
 Component: DY



c. Load case 3;

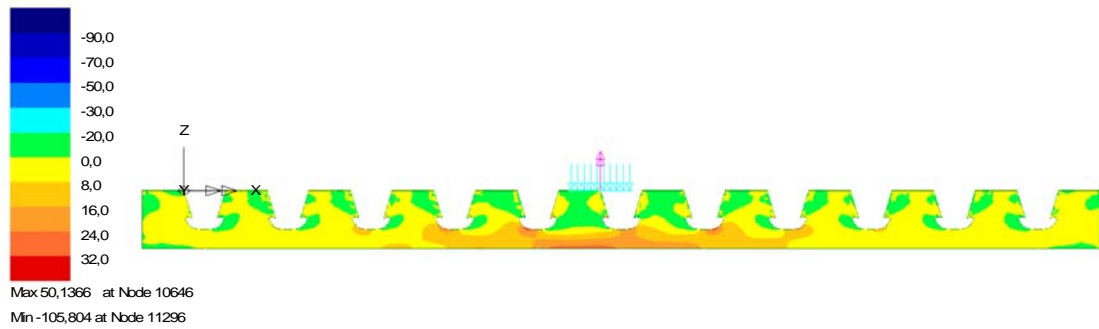
FIGURE 3-11 Horizontal displacements of the diaphragm.

Loadcase: 1
Title: Loadcase 1
Results File: 0
Entity: Bottom Stress
Component: SX



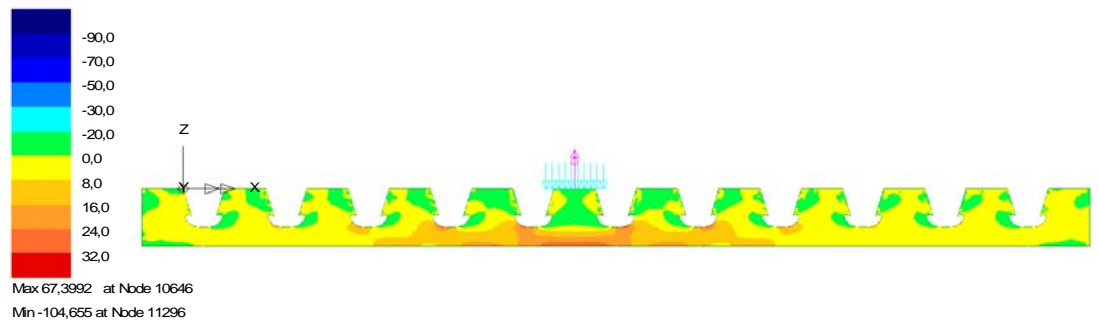
a. Load case 1;

Loadcase: 2
Title: Loadcase 2
Results File: 0
Entity: Bottom Stress
Component: SX



b. Load case 2;

Loadcase: 3
Title: Loadcase 3
Results File: 0
Entity: Bottom Stress
Component: SX



c. Load case 3;

FIGURE 3-44 Stress distributions of the diaphragm.

The local mechanisms that impact all rib/diaphragm details along the floor beam or diaphragm are:

- Ribs' rotation at supports with out of plane impacts on the diaphragm;
- VQ/I effects on rib, diaphragm and deck plate connections;
- Vertical displacement of the tooth;
- Rib distortion effects at the diaphragm due to rib torsional rotation.

These deformations are shown by diagrams illustrating the mechanism and the effect on the hot spots.

a) Rib rotation at support and diaphragm out-of-plane bending, as shown in Figure 3-13.

b) VQ/I effects.

The VQ/I effects exist in any structural member where there are loads transverse to the axis of such member. In orthotropic decks where discontinuities exist by virtue of the rib passing through the web these effects take on a peculiar form which was in part illustrated in Figure 3-45 when a bulkhead is present.

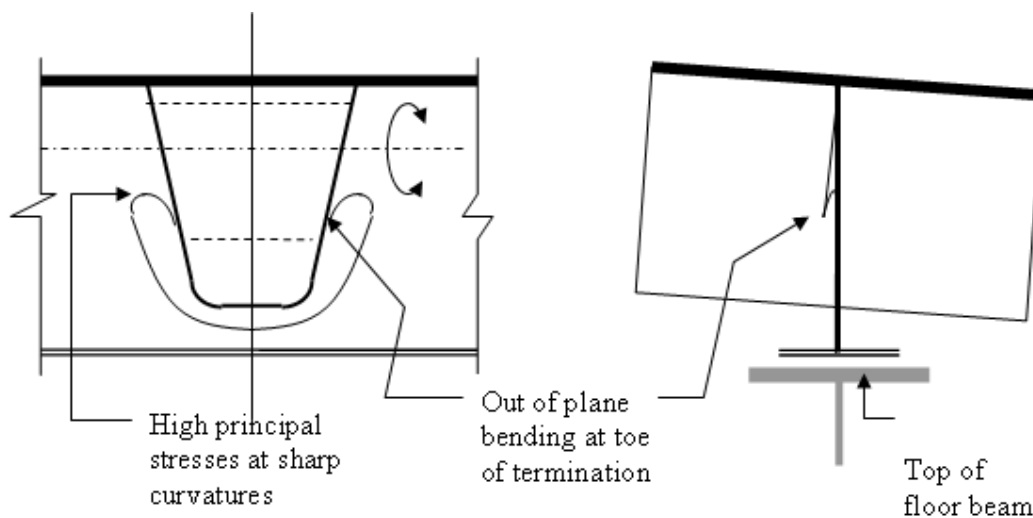
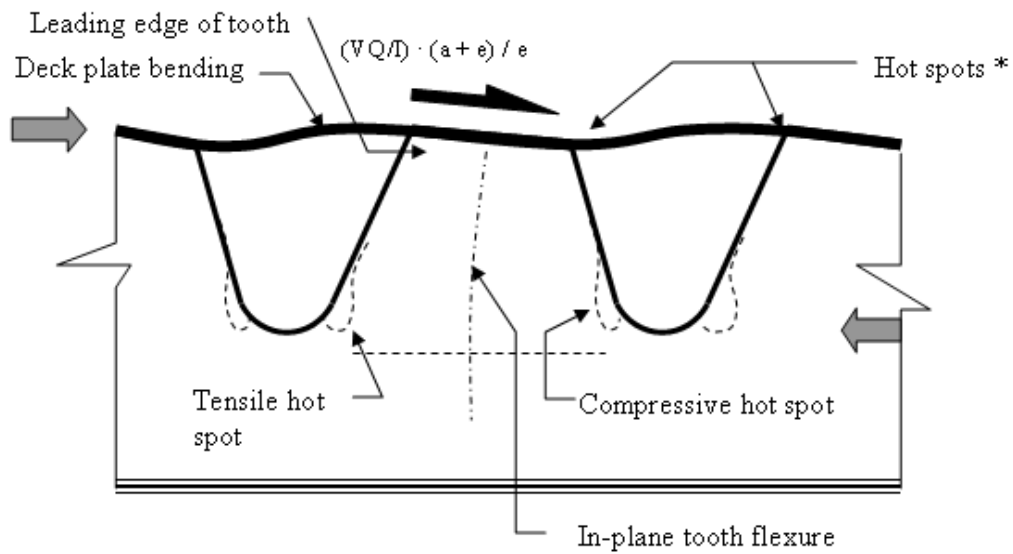
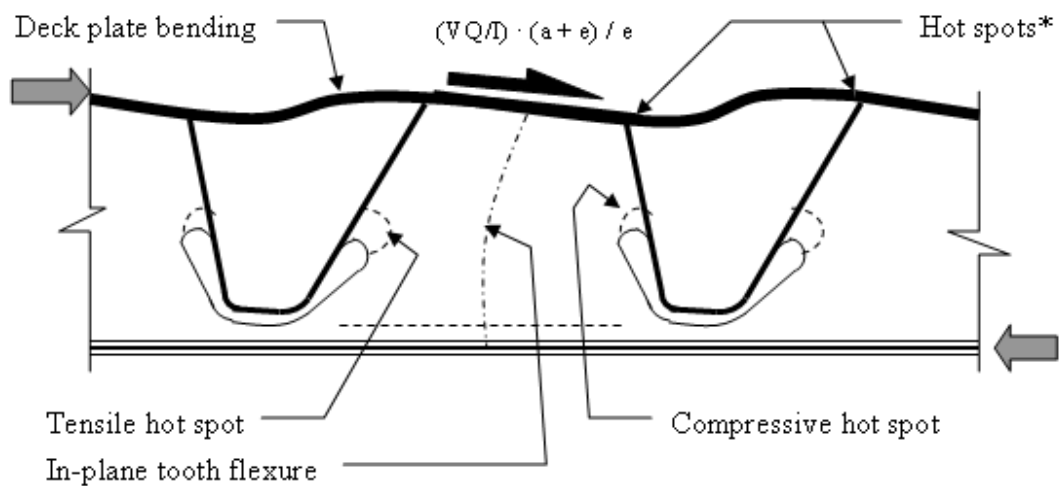


Figure 11

FIGURE 3-13 Rib rotation at support and out-of-plane bending at diaphragm.



a



b

FIGURE 3-14 VQ/I effect at the diaphragm.

* Hot spots come from both flexure of the deck plate, including from wheel load as well as deformation due to VQ/I effects. But they also come from the compression due to engagement of the deck plate by the tooth.

Figure 3-14 shows the VQ/I effect at the diaphragm in the condition obtaining in a simply supported floor beam, where Figure 3-45 shows the case of a cantilevered floor beam.

The VQ/I effects at the hot spots indicated are more severe in the detail of the cutout (Figure 3-14b) because the tooth is much weaker in-plane than the detail in Figure 3-14a. However, FE analysis shows that stresses at the bottom of the deck plate are more concentrated at the leading edge of the tooth (where they are compressive) than at the trailing edge where they are tensile. Also, laboratory tests of full scale models show greater damage at the RDDP of the leading edge.

The bulkhead detail is not shown under this behavior as the stresses were already shown in Figure 3-45. It is common knowledge that the bulkhead helps counteract the damaging effects of this behavior at the RDDP, but it shifts hot spots to the terminations of the bulkhead where abrupt discontinuities exist (see Figure 3-15).

c) Vertical shortening of the tooth.

The size of cutout and the thickness of diaphragm impact on the stresses at the RDDP connection. Figure 3-16 shows how loading over a tooth impacts on the bending of the deck plate.

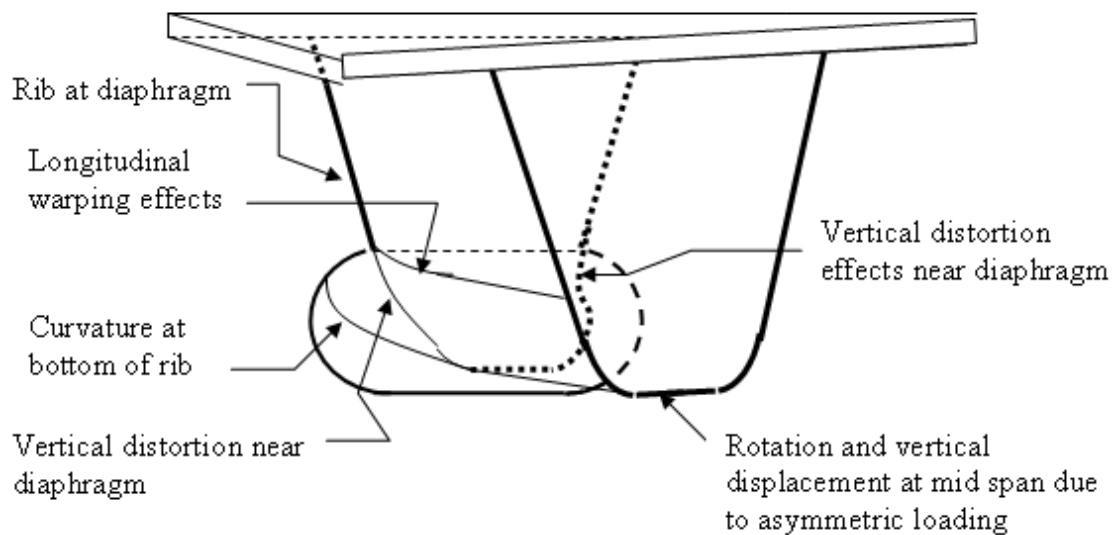


FIGURE 3-15 Stress state at/near the bulkhead detail.

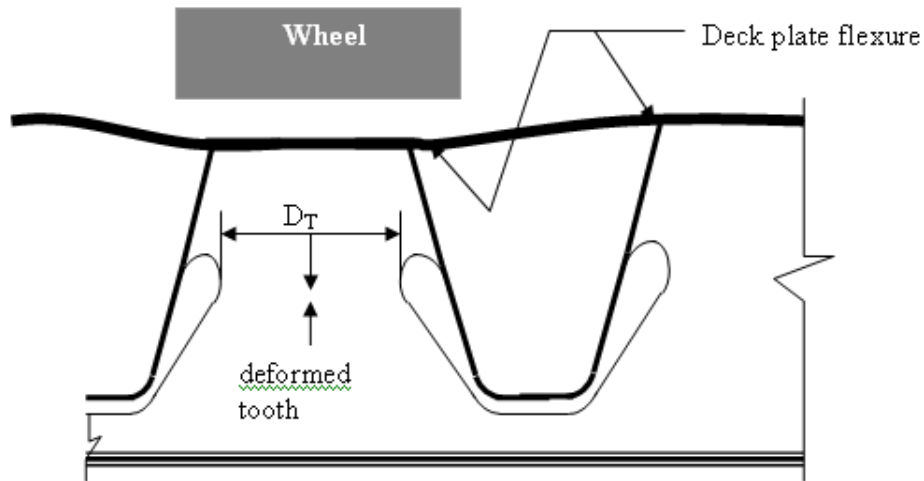


FIGURE 3-16 The impaction of vehicle loading on the tooth.

It is noted that to limit vertical displacements the total remaining tooth depth D_T should be as large as possible with the smallest cut out as feasible with minimum consistent transition requirements at rib. A thick diaphragm tooth reduces this effect while it may increase out-of-plane effects by smaller amounts.

d) Rib distortion at diaphragm.

This is a very important phenomenon that was completely ignored until recently. In a closed rib system, the rotation of the rib when the wheel is at mid-span and eccentric about the axis of the rib causes the rib to rotate about its center of rotation with consequent lateral displacement at mid-span. However the diaphragm represents a fixed boundary (in the plane of rotation).

When there is a cut-out with or without a bulkhead the boundary is partially fixed and it has discontinuities that impose out of plane deformations in the rib stems which engender high stresses relative to the available fatigue resistances.

Figure 3-15 shows that these stresses are both longitudinal and also at the intersection of two hypothetical planes; that of the diaphragm and of the ribs stem. They are shown in a diagram where the cut out is in the order of $h/3$ with an abrupt transition which is deemed in many cases inappropriate to provide sufficient resistance to

fatigue stresses engendered by the distortion.

It is noted, by mere observation of the curvatures in Figure 3-15, that a shallower cut-out would create more severe effects at the cut-out termination. Also, while one stem displays tension due to distortion on the outside face of the rib, the opposite stem displays compression on the outside and the stresses at the inside faces of the stems are reversed. Therefore, as wheels pass on opposite sides of the rib center line, reversal of stresses occur in both stems at these hot spots.

In order to make the cut-out detail to work well in combination with a bulkhead, diaphragm and bulkhead, would both require transitions to address the vertical distortion effects. While this is a possibility, difficult fabrication problems are envisioned.

It should be noted that all the numerical analysis presented in this chapter are based on the global FE model, while the results of submodel analysis will provide more information to the welded connections.

3.3 Influences of Cutout

3.3.1 Introduction

Diaphragm (or floor beam) is one of the three main parts in an orthotropic deck, and cutout is significant to the stress performance of the diaphragm since it may change the magnitude of the stress concentration. Different cutout shapes will evidently change the stress status in the diaphragm, therefore, a suitable typology of cutout can obviously improve the fatigue life of the diaphragm.

Lehrke [9] investigated the in-plane behavior in the diaphragm during the third phase of the European Coal and Steel Community (ECSC) research. Numerical analysis and experimental tests showed that a reduction of the stress concentration at the edges of the cope hole by increasing the notch radius of the cope hole (see Figure 3-17), and the shape of cutout affects significantly the stress performance.

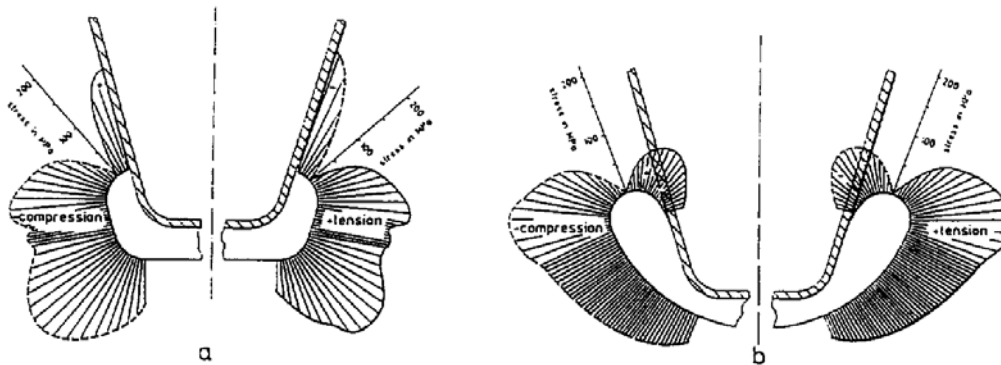


FIGURE 3-17 Stress distributions along the edges of different cutouts (Lehrke, 1990).

Caramelli et al. [10] studied several types of cutout through FE analysis, as shown in Figure 3-18. It is concluded that an optimal shape of the cutout (including a cope hole) is such that the cut area is minimum, and the radius of the free edge is maximum. Therefore, circular cope hole seems to be the optimal shape.

Connor [11] investigated the effect of altering the geometry of certain variables through a FE parametric study. Several FE models are built to analyze the influences of cutout parameters, as shown in Figure 3-19. It is found that larger cutout geometries provide less resistance to out-of-plane displacements induced by longitudinal rib rotations. Therefore, out-of-plane stresses are decreased. However, cutouts that are excessively deep will increase in-plane stresses at the rib-to-diaphragm (rib-to-diaphragm) welded connection.

Fryba et al. [12] studied some possible cutouts in the closed rib railway bridge, as shown in Figure 3-20. It is found that the circular and apple forms are almost equivalent (see Figure 3-20a~d) and are recommended for railway bridges. The apple form provides better stress distribution than the circular, but only if there is no shear stress. The details with no additional cutouts (Figure 3-20e and f) show good fatigue behaviors but they require advanced welding technology to weld the details with the smallest possible residual stresses. The asymmetrical detail (Figure 3-20g) displayed poor fatigue behaviors. Therefore, it is not recommended to be used on railway bridges. The radii of cutouts should be 40-50mm: not too small (as this produces

stress concentrations) and not too large (as this weakens the girder by reducing the cross-sectional area).

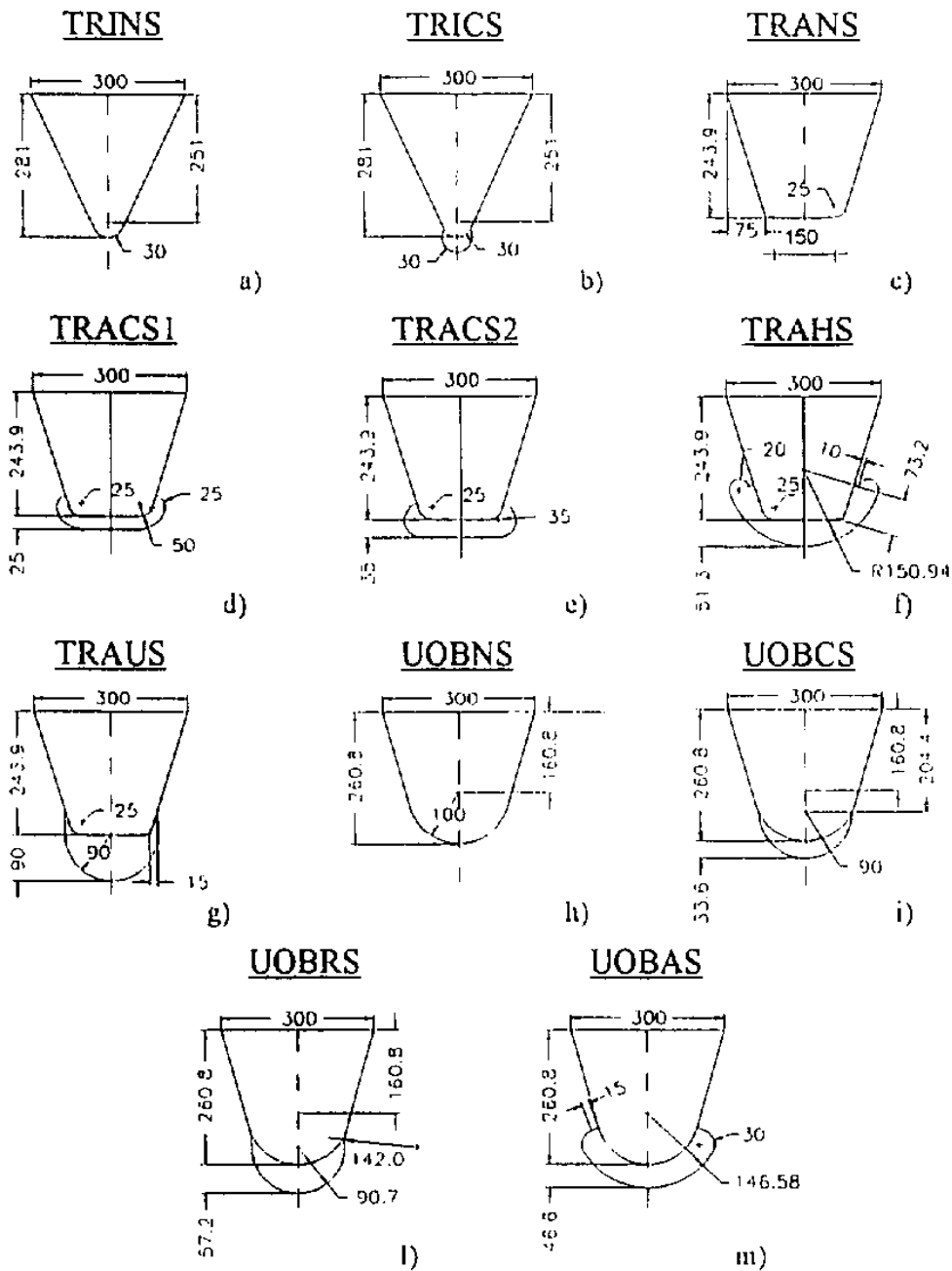


FIGURE 3-18 Different shapes of cutouts studied by numerical analysis (Caramelli et al., 1990).

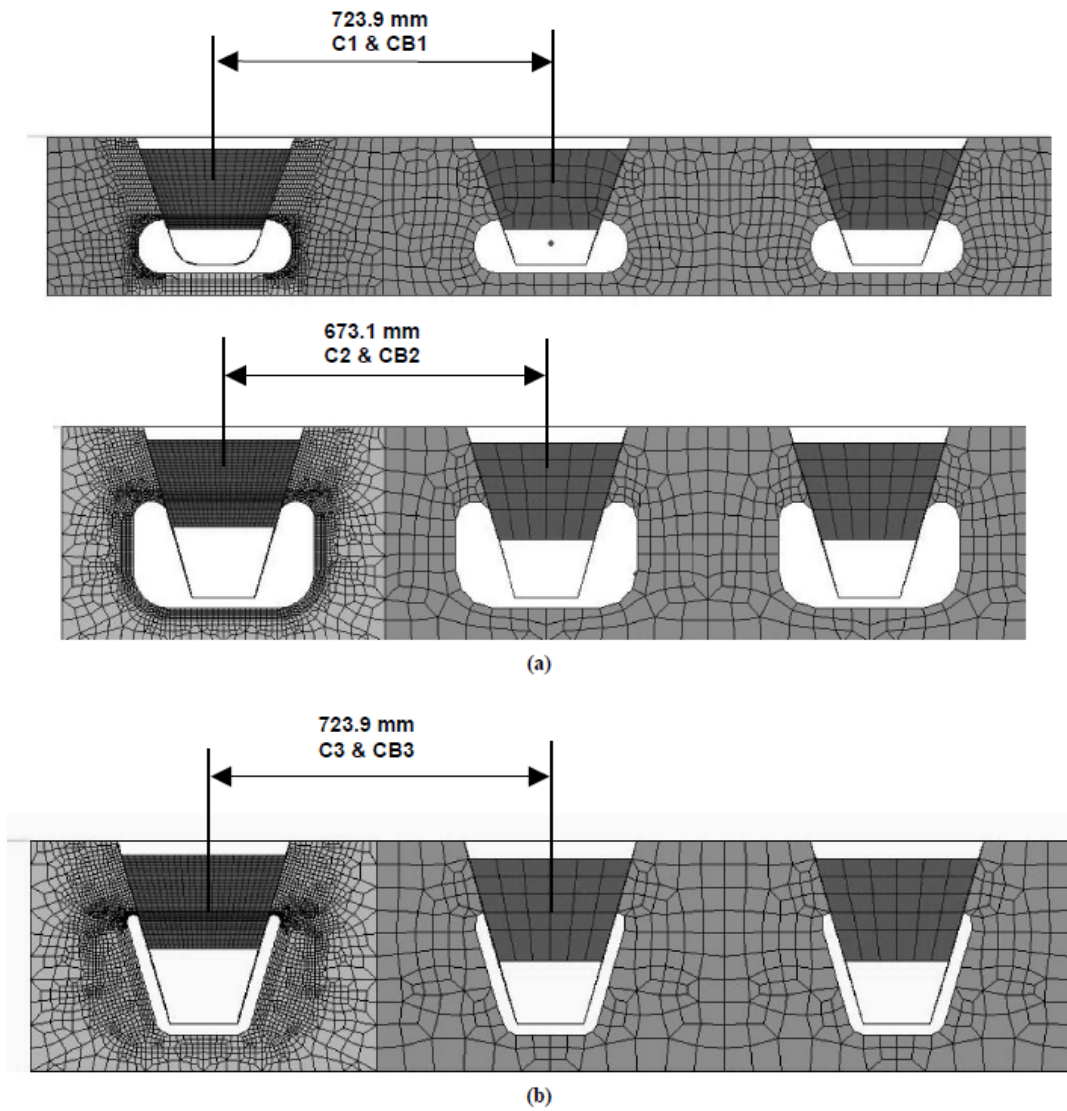


FIGURE 3-19 Different cross sections of flexible diaphragm (Connor, 2004).

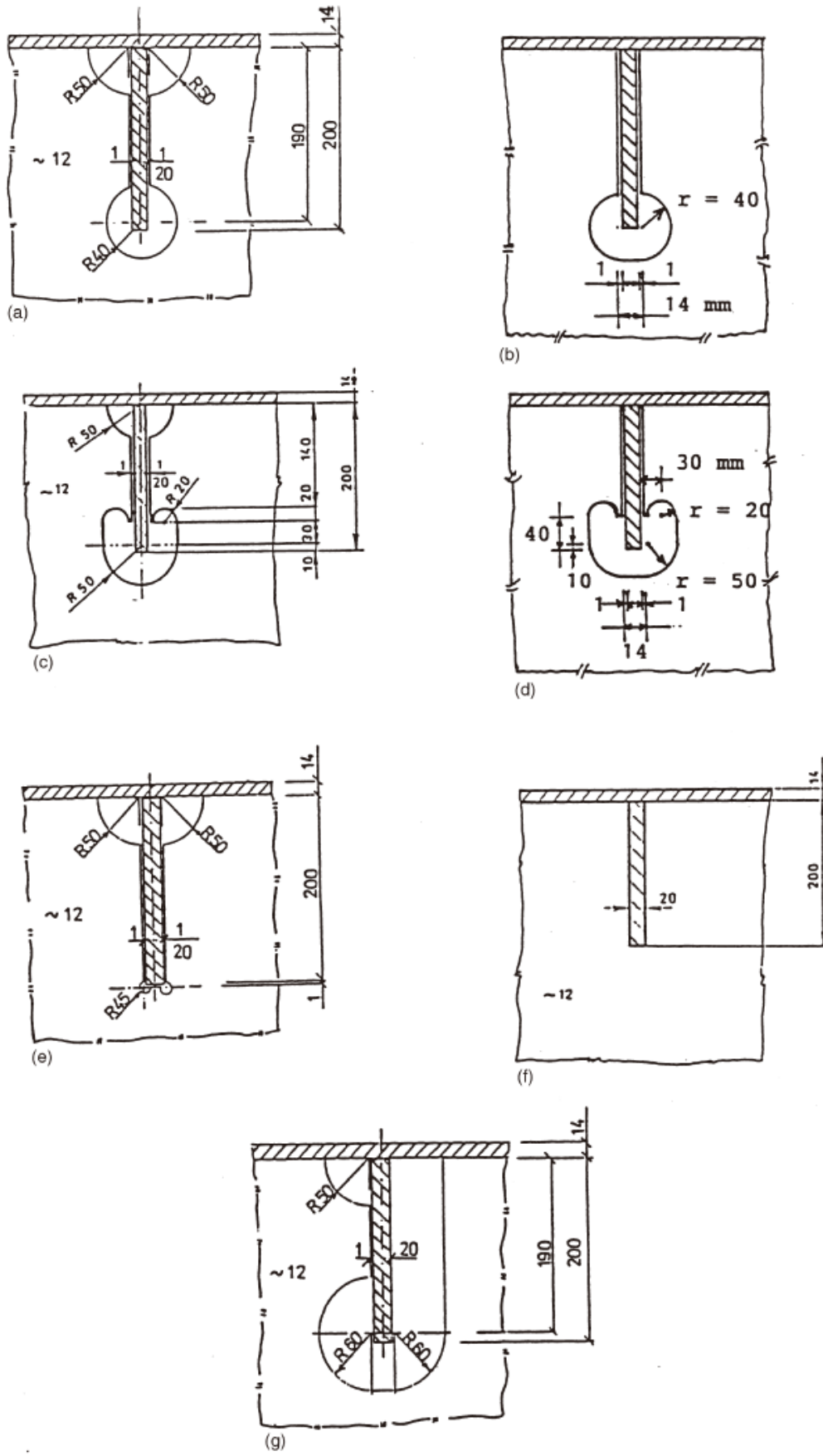


FIGURE 3-20 Different shapes of cutout to the closed ribs (Fryba et al., 1996).

3.3.2 The four different shapes of cutout

In this study, four different typologies of cutout in the diaphragm of orthotropic deck, as shown in Figure 3-20 (*a.* Pfeil et al., 2005 [13]; *b.* Yarnold et al., 2007 [14]; *c.* Eurocode 3, 2004 [4]; *d.* AASHTO, 2005 [15].), are investigated via FE method (LUSAS). It is noted that type *d* is developed based on type *b*. In addition, bulkhead is not included in these four orthotropic deck bridge models. The deflection and stress performances in diaphragm, deck plate and longitudinal rib are analyzed and compared based on the results of numerical analysis.

In order to investigate the stress performances and fatigue behaviors of different cutouts in diaphragm, FE models are built with linear thin shell elements. The FE model is intended to simulate orthotropic deck as part of the long span bridge.

General parameters are provided in Chap. 3.1.2. For different shapes of cutout, it is difficult to appraise which is more suitable due to the different dimensions of cutout. Height of cutout and height of lower clearance are important to both in-plane and out-of-plane stresses [11]. Considering width of cutout may influence the out-of-plane stress, in this study also this important parameter (width of cutout) is taken into account in the modeling.

In the four numerical models, the three same parameters are applied, height of cutout, height of lower clearance, and width of cutout. The height of cutout is 75 mm, the height of lower clearance is 35 mm, and the width of cutout is 240 mm. Figure 3-21 shows the detailed dimensions and meshes for the four different cutouts which are analyzed in this study.

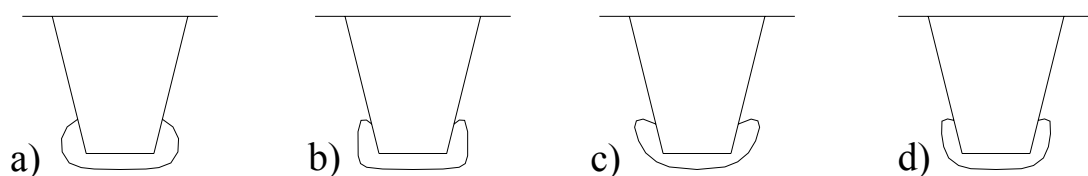
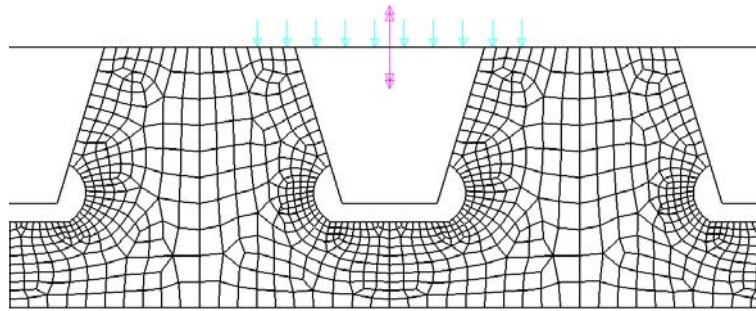
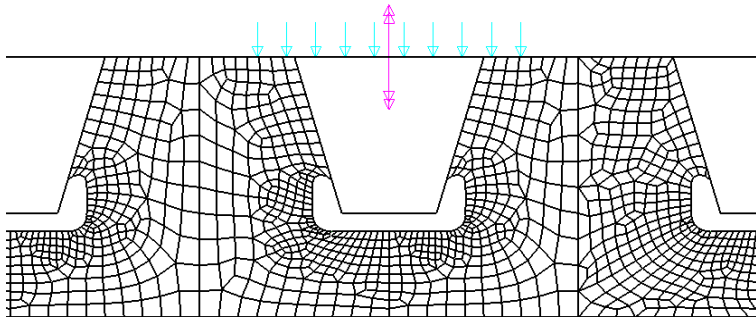


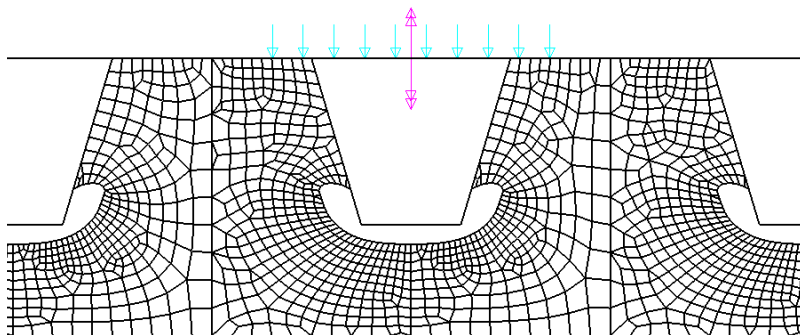
FIGURE 3-20 Typologies of cutouts at diaphragm of orthotropic deck.



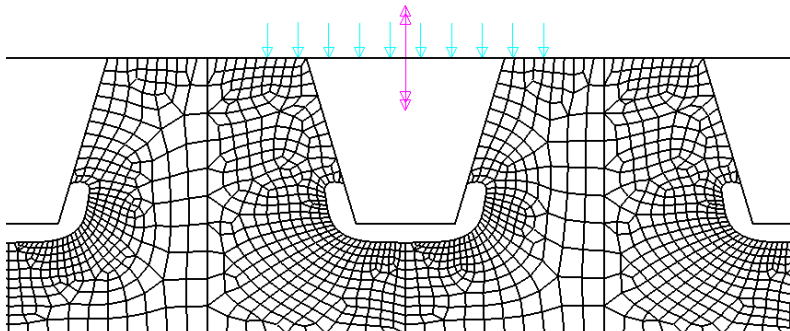
a



b



c



d

FIGURE 3-21 Detailed meshes around the cutouts.

3.3.3 Results of static analysis

3.3.3.1 The Stress performance in the diaphragm (rib-to-diaphragm connection)

The stress performance in the diaphragm of the orthotropic deck is affected by the cutout shape, especially the area near the cutout. Figure 3-22 shows the stress distribution contours of the diaphragm suffering different loading, and Table 3-1 presents the maximal and minimal stresses in the diaphragm (always exist at the rib-to-diaphragm connections).

Through the analysis, it is found that the stress distribution in the diaphragm with different cutout is similar when the deck plate suffers the same load case. The maximal stress often occurs at the rib-to-diaphragm connection, thus causes fatigue cracking easily near the connection. Moreover, high stress concentration is also produced at the bottom corner of the cutout.

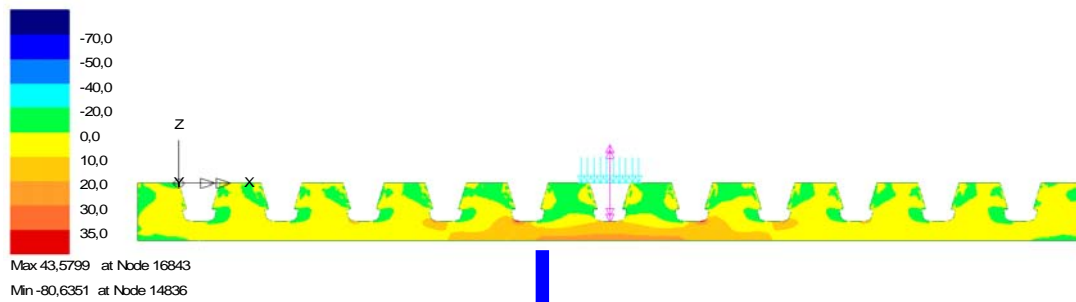
As shown in Figure 3-22, the stress far away from the load is much smaller than that near the loading location, and this is similar to the stress distribution in deck plate studied by Tinawi [16]. The stress near the loading position is much larger than the stress far away, especially in the region between the two adjacent ribs next to the loading. However, the concentrated stresses at the rib-to-diaphragm connections of the other cutouts are also high (despite it may be much smaller compared to the maximal stress).

In addition, other high stresses exist around the rib-to-diaphragm connection. It is in good agreement with the fatigue cracking discovered in the actual orthotropic decks.

TABLE 3-1 Peak stresses of different cutouts in diaphragm (MPa).

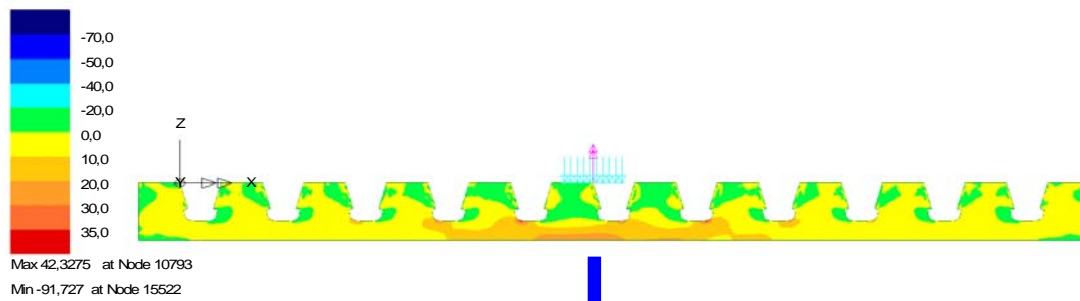
Group	Max. Stress				Min. Stress			
	a	b	c	d	a	b	c	d
Loadcase1	79.3	109.8	37.6	43.6	-59.5	-164.7	-101.9	-80.6
Loadcase2	67.8	115.6	50.1	42.3	-96.0	-174.5	-105.8	-91.7
Loadcase3	69.8	122.0	67.4	49.7	-103.3	-185.3	-104.7	-87.4

Loadcase: 1
Title: Loadcase 1
Results File: 0
Entity: Bottom Stress
Component: SX



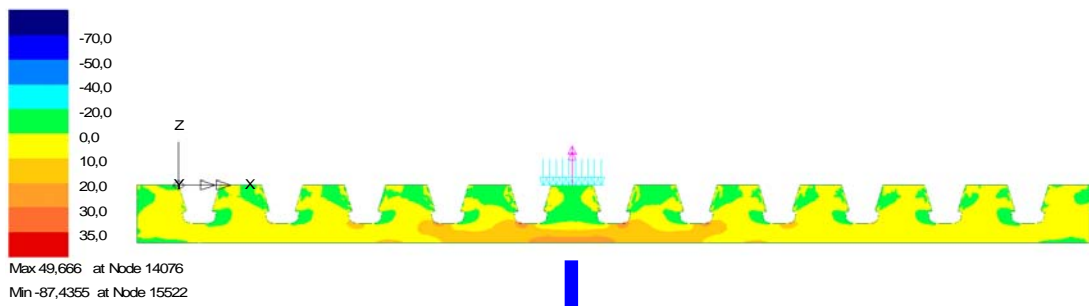
a. Load case 1;

Loadcase: 2
Title: Loadcase 2
Results File: 0
Entity: Bottom Stress
Component: SX



b. Load case 2;

Loadcase: 3
Title: Loadcase 3
Results File: 0
Entity: Bottom Stress
Component: SX



c. Load case 3;

Figure 3-22 Stress contours in the diaphragm.

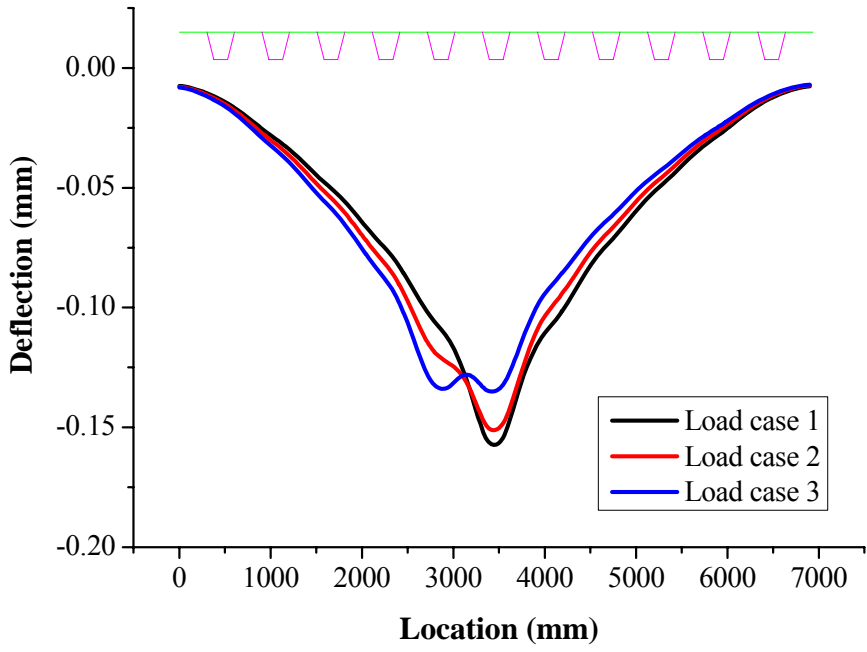
Table 3-1 presents the maximal and minimal stresses based on the static analysis, all of them are located at/near the rib-to-diaphragm connections or the bottom corner of the cutouts. Apparent difference can be found that these stresses are much higher than the stresses in deck plate and any other part of deck structure. Both the change of cutout and loading location can influence the maximal stress significantly.

The fatigue cracking is ease to occur at the cutout *b* due to the high concentrated stress, while the other three typologies behave much better. This kind of cutout was used for the orthotropic deck bridges in the last century and should be monitored timely in order to detect fatigue cracking. The maximal stress in cutout *d*, developed from cutout *b*, is much smaller. In general, the cutout *c* and *d* are better than the other two typologies.

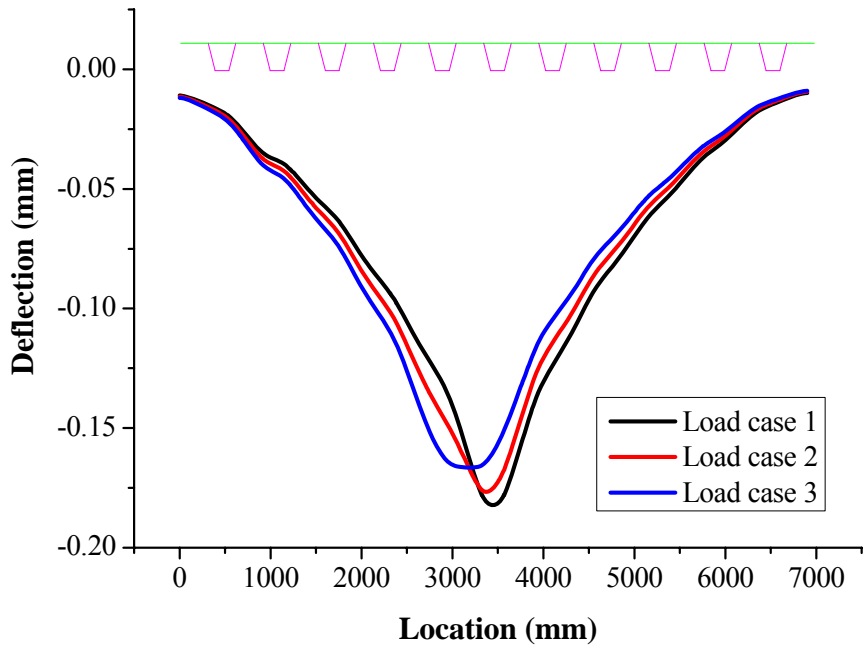
Based on the static analysis, it is known that for different load cases, the stress distributions are similar in the diaphragm with the same cutout. The main peak stress areas exist at the rib-to-diaphragm connections and at the bottom corners of cutouts. However, there are some differences when suffering different load cases. For example, the distributions of the stresses at the bottom of diaphragm near the vehicle loading location present little difference.

Furthermore, the vertical deflection distributions of the four different typologies are almost the same. Moreover, the smoothness level of the cutout edge, especially at the important parts, is very significant to the stress concentration around the cutout.

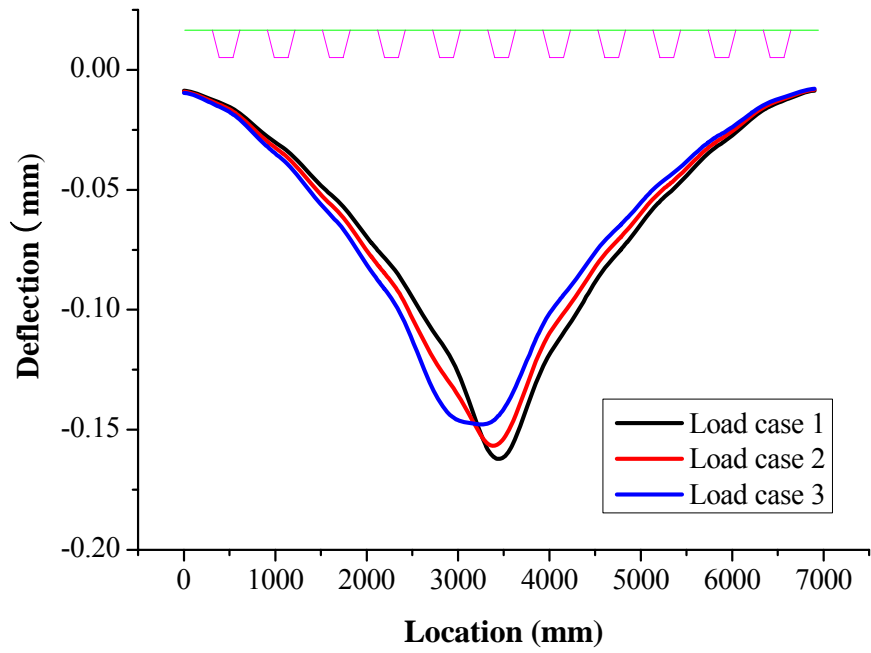
Recently, some researchers become interesting to the out-of-plane displacement of orthotropic deck [17, 18]. The rotation of the longitudinal rib can produce out-of-plane deformation to the diaphragm, but the influence to the fatigue resistance is still in discussion. Figure 3-23 shows the out-of-plane displacements in the diaphragm (150 mm from the bottom of the diaphragm). It is found that the displacements of the four different diaphragms are similar. The peak displacement of load case 1 is the largest, while that of load case 3 is the smallest.



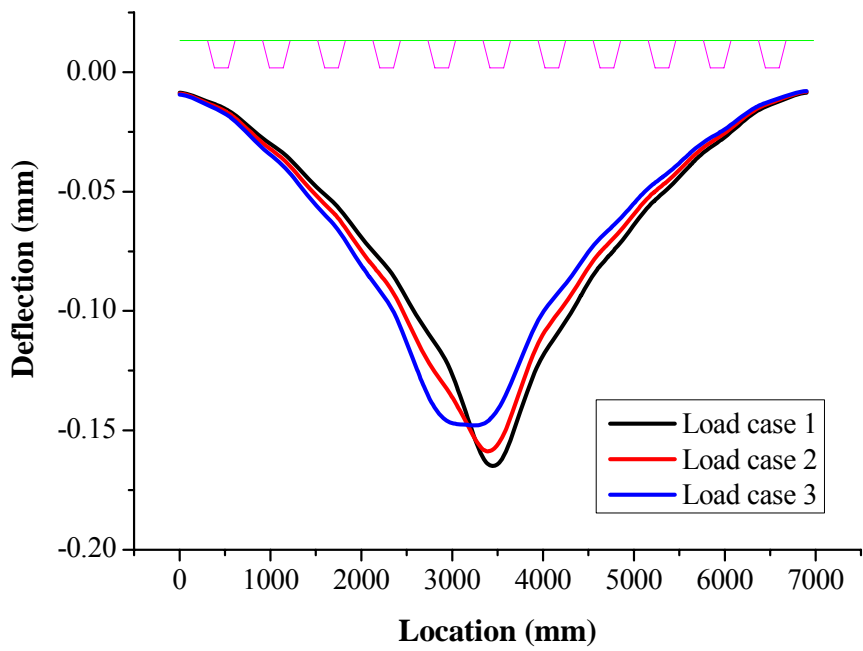
Cutout a;



Cutout b;



Cutout c;



Cutout d;

FIGURE 3-23 Out-of-plane displacements at the diaphragm.

3.3.3.2 The deflection and stress in the deck plate

The contours of deflection and stress in the deck plate with different cutouts are very similar, the distributions are shown in Figure 3-8 and 3-9.

Based on the static analysis, it is known that the contour of the vertical deflection distributes as ellipse, and there are notches at the longitudinal ends (the diaphragms), far from the load. Large deflection occurs around the loading location, between the two neighboring ribs of the load in the diaphragm, and its range is similar with the stress distribution. The deflection out of the two ribs is small, and can be ignored. The maximal deflections for the four different cutouts are very close. Table 3-2 shows the maximal deflections at the deck plate. Furthermore, it is found that the load case has an evident influence to the deflection of the deck plate due to the restriction of the longitudinal ribs.

TABLE 3-2 Maximal deflections of different cutouts at deck plate (mm).

Load case	Maximal Deflection			
	a	b	c	d
Load case 1	-1.92	-2.06	-2.01	-2.00
Load case 2	-2.02	-2.18	-2.14	-2.14
Load case 3	-2.07	-2.24	-2.18	-2.20

Similar with the distribution of the deflection in the deck plate, the peak stress occurs only between the two neighboring ribs next to the loading position. Table 3-3 presents the peak stresses in the deck plate of the four orthotropic deck. It is found that the peak stresses varies with the changing of the cutout despite the deflection of the deck plate are close. The stress variation is not very big, but enough clear. In addition, the variations of load case 2 and 3 are bigger than that of load case 1.

TABLE 3-3 Peak stresses of different cutouts at deck plate (MPa).

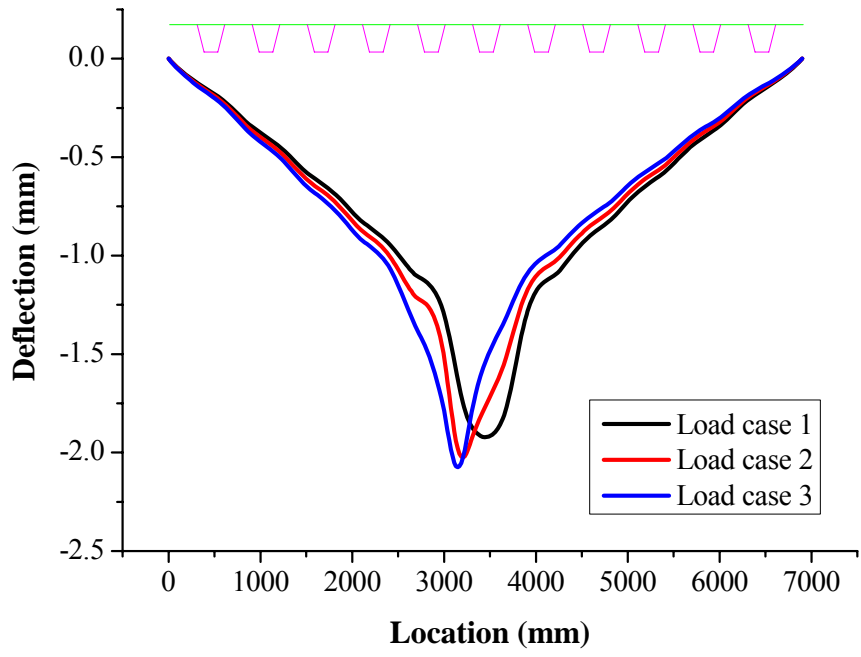
Group	Max. Stress				Min. Stress			
	a	b	c	d	a	b	c	d
Load case 1	28.2	35.9	37.1	37.2	-23.4	-28.9	-27.6	-27.7
Load case 2	62.0	75.9	78.8	77.9	-46.2	-59.6	-59.1	-59.6
Load case 3	62.7	79.9	78.1	80.0	-29.5	-49.3	-62.7	-46.0

Figure 3-24 shows the transversal deflections at the center of the middle span suffering the different load cases. It is obvious that the cutout has almost no influence to the deflection of the deck plate. Both the distribution and the peak stress are almost the same. However, it is found that the middle part of the deflection curve for load case 1 is not as sharp as the curves of load case 2 and 3.

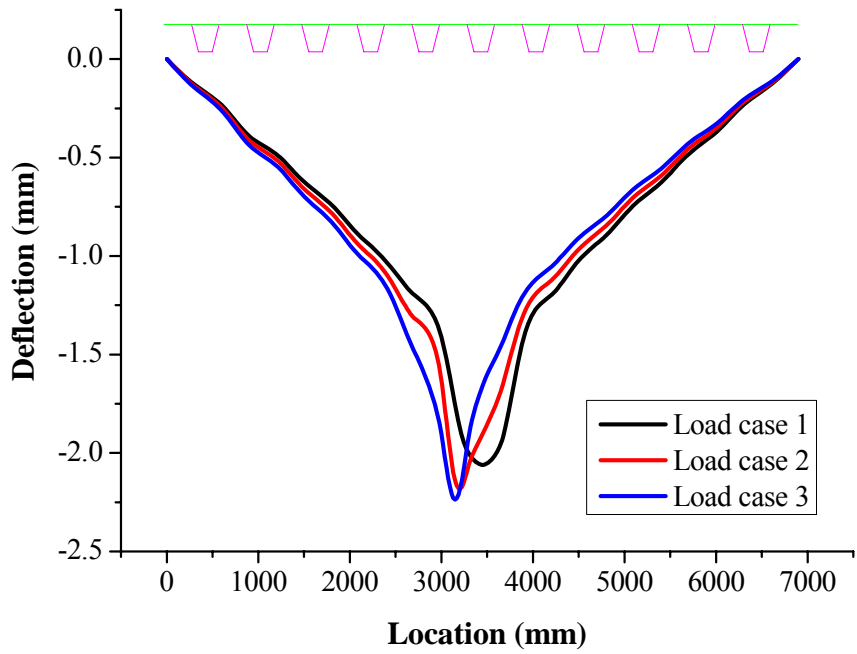
Figure 3-25 shows the transversal stresses at the center of the middle span suffering the different load cases. The cutout influences the stress performance of the deck plate. The transversal peak stress in load case 1 is much smaller than the other two load cases due to the restriction of the longitudinal ribs. It should be noted that the peak stress always occurs at the rib-to-deck plate connection [19]. This can be used to explain why the welded connection is sensitive to the fatigue cracking in real projects. It is proposed to analyze several different shapes of cutout in the stage of the preliminary design, not only the four shapes discussed in the study, but also other different shapes because a reasonable design of the cutout can improve greatly the fatigue life of an orthotropic deck.

Based on the numerical analysis, several conclusions are listed below:

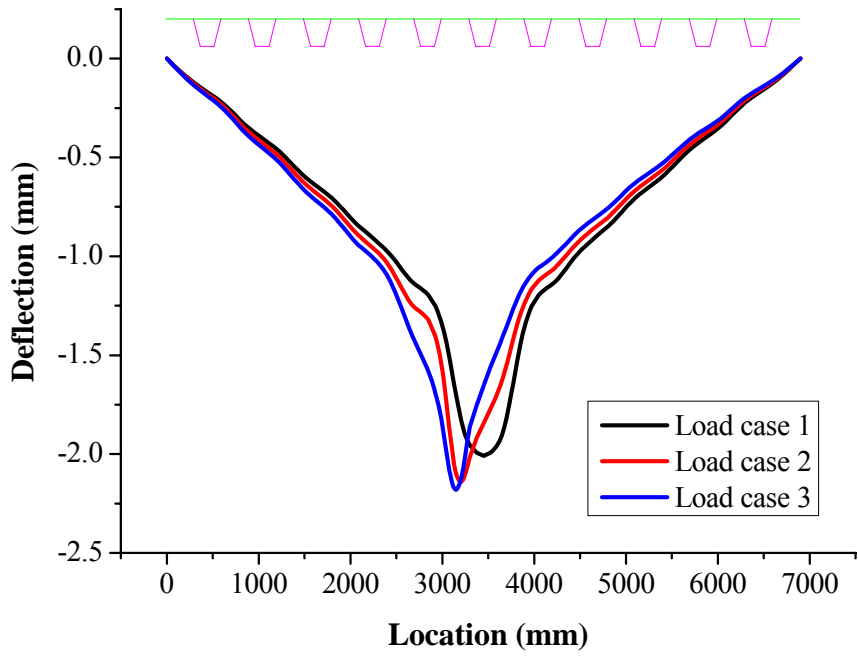
- The shape of cutout has an important influence to the stress, and particularly to the peak stress on the edge of cutout;
- The stress performances of the critical connection in the deck plate are in good agreement with the fatigue cracking in the actual projects;
- The shape of cutout influences slightly to the deformations of the diaphragm, the deck plate and the ribs.



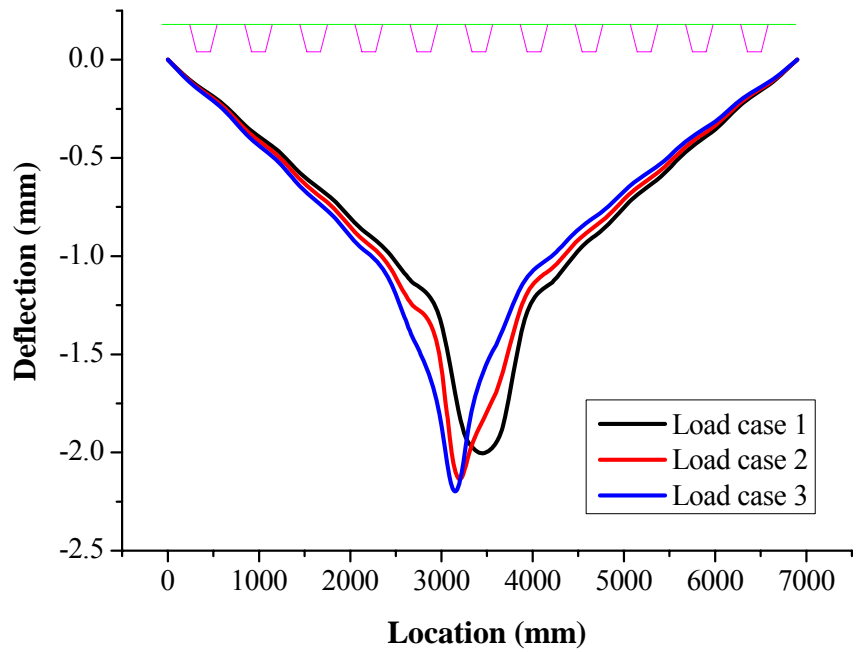
Cutout a



Cutout b

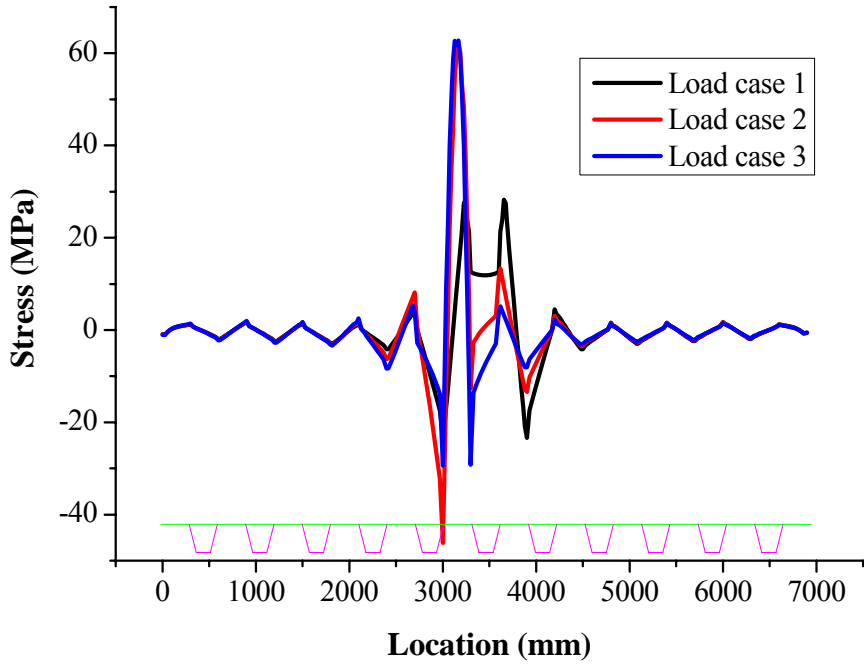


Cutout c

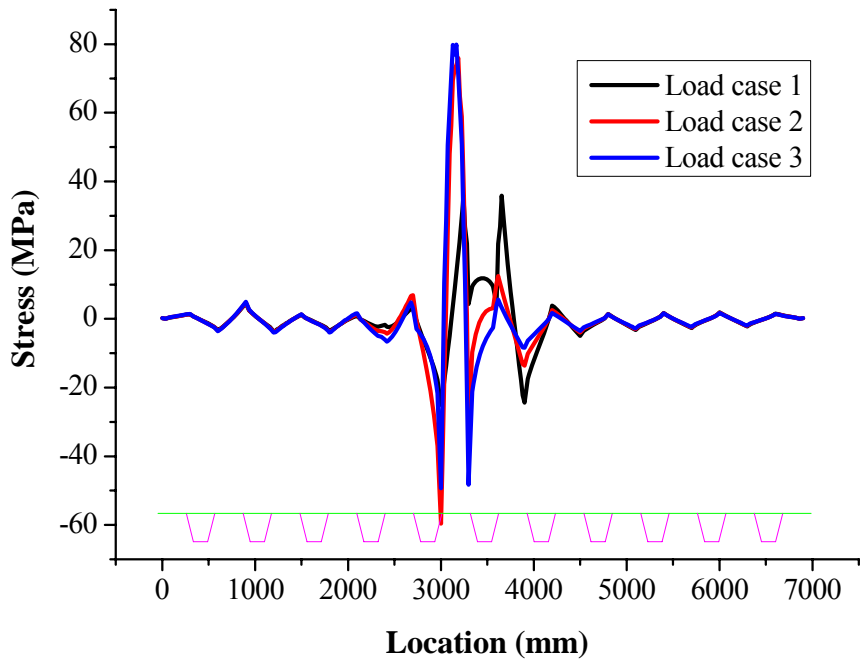


Cutout d

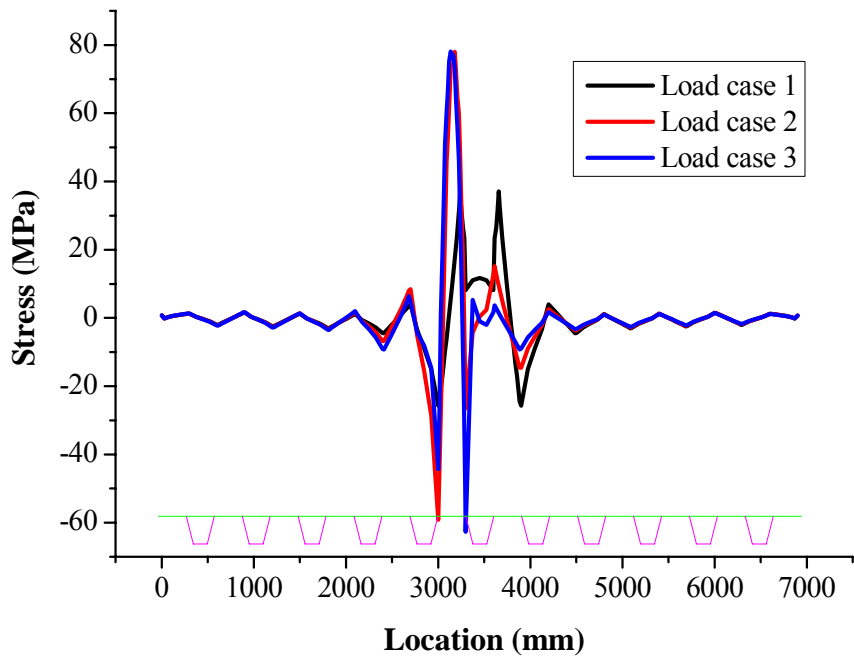
FIGURE 3-24 The deflection distributions at the middle of deck plate.



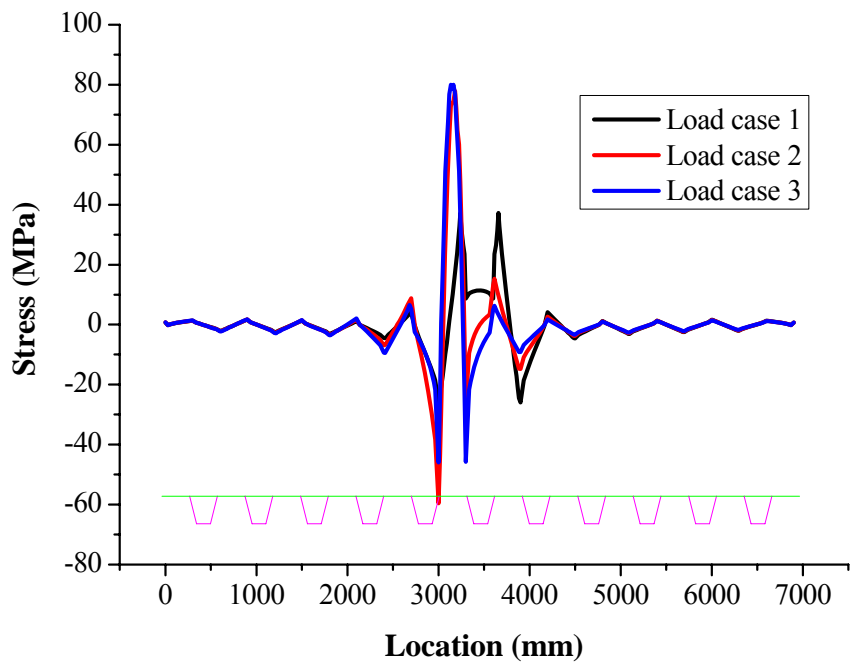
Cutout a



Cutout b



Cutout c



Cutout d

FIGURE 3-25 The stress distributions at the middle of deck plate.

3.3.4 Discussions

It is noted that in the 1950's when the practice of using orthotropic decks advanced forward, structural steel was 228MPa. High strength material (345MPa) has been used starting in the early 1990's, yet rib sections have hardly changed, while deck plate thickness is on the increase. A major reason for this is that one rib displacement, relative to another, impacts on the performance of the wearing surfacing. The other reason is that design of orthotropic decks is governed by fatigue mainly where the ribs interact with the floor beam and diaphragm.

While it was recognized that a cutout was needed to preclude high localized out-of-plane stresses at the bottom of the rib, due to the rotation of the rib at the support, intuition as to how stresses flowed around the plane of the diaphragm ruled the design practice. These criteria in combination with a scarce fatigue database, which treats stresses at the toe of weld to be perpendicular to the weld, steered engineers to conceive of the details as illustrated in Figure 3-26.

Figure 3-26 shows that the concerns of the bridge engineers were that the in-plane stresses should continue to flow in the web without causing excessive stress concentrations by a large hole in the web. The bulkhead was seen as a solution to this concern. The cutout was placed at the bottom of the rib, far from the deck plate and was made shallow to achieve in-plane stress flow without excessive stress concentration around the hole.

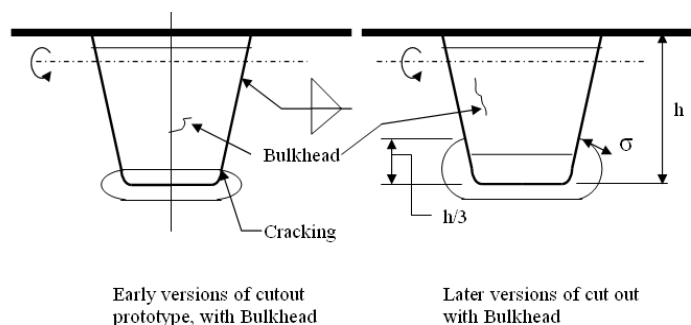


FIGURE 3-26 Development of cutout in orthotropic deck.

The length of the cutout by “trial and error” was intended to minimize the out of plane effects engendered by rib rotation about a transverse horizontal axis.

Decks with shallow and cutouts (the early version) did not fair well. Rib stems were failing below the top edge of the cutout. Although analytical tool were available as far back as the 1970 (finite difference solutions) to determine the cause of these failures, intuition provided the next speculative piece of the puzzle. In the United States, it was postulated that the Poisson effect tended to increase the width of the rib flange causing the stem to deflect outward with a fixed point at the diaphragm upper cut line or the bottom of the bulkhead.

This real or imagined phenomenon was given the name of “Ostapenko Effect”, and led to the criterion that the height of the cutout above the bottom of the rib needed to be 1/3 the height of the rib. This paradigm was written into the AASHTO Code. It is noted that the early as well as the later cutout version maintained the edge of the cutout perpendicular to the stem such that the principal stress in the diaphragm would be perpendicular to the rib-to-diaphragm weld for which there is a fatigue resistance database. Also, contrary to customary practice, the AASHTO Code prescribed fillet welds for the rib to diaphragm connection. The non-prescribed practice was to provide a “wrap-around” at the weld termination.

In Europe and Canada there were parallel developments in a design without a cutout in which a round bellied rib was welded all around to the diaphragm from end to end. Practitioners that developed this design determined that, as a rule of thumb, when the depth of the diaphragm and the rib depth have a ratio $d/h \approx 2$ the design would succeed. Obviously this is predicated on specific rib rigidities and floor beam spacing. It is clear from Figure 3-27 that the concern was not to create high out-of-plane bending stresses in the diaphragm, and that should the ratio d/h be significantly less than 2, this could be remedied by a more rigid and heavier rib that would rotate less, or in part by the use of an intermediate diaphragm that would spread the load to more ribs.

The advantages and disadvantages of such design are described in the following:

a) Advantages

- A detail so fabricated would be less cost. The history of the cutout design shows that smooth transitions need to be made with associated grinding. Estimates range from 25 to 40% less costly when considering the cost of the diaphragm connection to the rib. Total difference in deck costs have been reported as 15%. The validity of these figures should be taken cautiously as they represent the opinions of a small sample of fabricators.
- From the point of view of stresses at the rib-to-diaphragm-to-deck plate (RDDP), this design is a much better than the cutout design without the bulkhead because it reduces the rotation of the tooth (see Figure 3-27), within its own plane, as it engages the deck plate. This reduced the tooth's rotation (or leading edge vertical displacement), which in turn reduces bending of the deck plate spanning over the trough of the rib, thus helping the longevity of the RDDP detail. Another advantage is that the wheel load cannot cause as large a vertical displacement of one tooth relative to its neighbor, as would a design with the cutout. This also helps reduce deck plate bending at the RDDP.

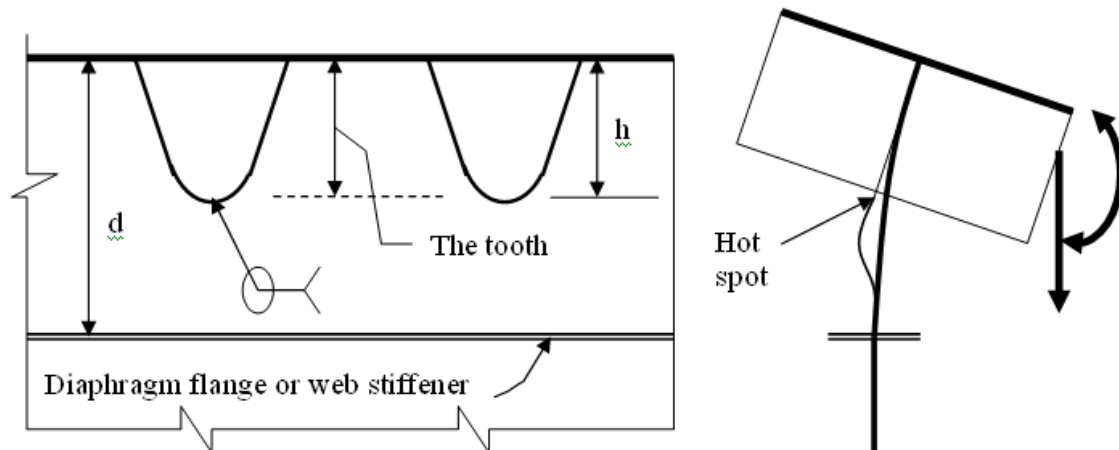


FIGURE 3-27 Out-of-plane bending in the diaphragm.

So, the advantage is not only in reducing internal effect at the RDDP and eliminating the stresses at the transition of the cutout, but also of eliminating a significant number

of designs where a bulkhead might be needed otherwise.

b) Disadvantages

The context of this assessment is based on fatigue criteria that are not in full agreement with the present AASHTO Code relative to compressive cycling. In the AASHTO Code compressive cycling that may cause damage will eventually be unable to cause further crack propagation, and only the largest cycles from the load spectrum that overcome compression due to dead load are evaluated as causing fatigue damage.

Other codes dealing with welded structures consider compressive cycling equally damaging as tensile cycling. In orthotropic decks the point at the bottom of the rib is subject to several stress conditions as illustrated in Figure 3-28, which make the present AASHTO premise unconservative. This evaluation assumes it prudent to consider compressive cycling to be fully damaging because the rib material is thin and any propagation by one mode could continue in a different mode.

It is noted that at the bottom convergence of the rib and diaphragm there are orthogonal stresses and shears. The vertical effects in the diaphragm and the longitudinal stresses in the rib are not in phase with the shears in the diaphragm and the in-plane effects due to floor beam bending. This is called non proportional loading.

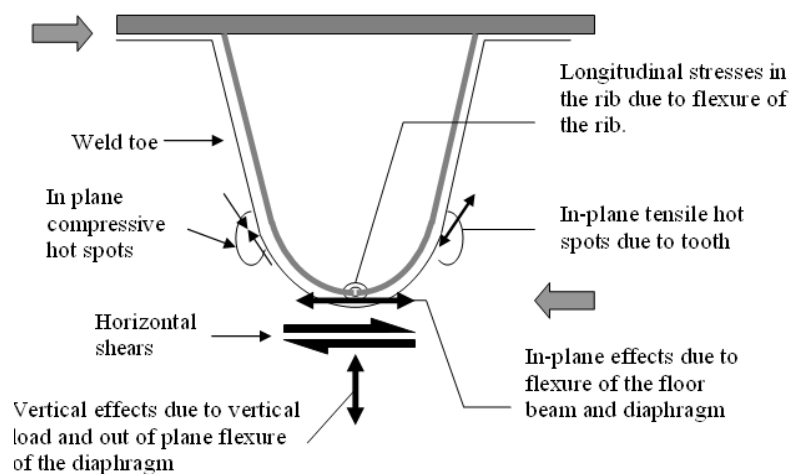


FIGURE 3-28 Stress conditions at the bottom of longitudinal rib.

There are also hot spots on both sides of the belly at the end of the tangent part of the rib where it meets the curved part. The principal stresses there are not perpendicular to the weld toe.

Notwithstanding the good performance of these designs over the last 30 years in many bridges, with some exemplary failures due to improper joining, the data come from field experience and not from testing to failure with known loading. While such performance may be indicative of good design it is not of long enough duration to guarantee good performance past 100 years and may be satisfactory only for limited spans when applying rib proportions used in past practice.

The disadvantages of this design are that:

- The rib needs to be made considerably stronger than in the case of the cutout to reduce longitudinal stresses at the bottom of the rib to a category somewhat below C (AASHTO).
- The evaluation criteria necessary for this detail have not been codified and may be more stringent than what is presently available.

3.4 Influences of Bulkhead

3.4.1 Introduction

Bulkhead is widely utilized to orthotropic deck bridges in U.S.A., while much less are applied in Europe. By the turn of the century (2000) a major full scale test was conducted at ATLSS center (Lehigh University) aimed at assessing the performance of a prototype designed for the Williamsburg Bridge deck replacement, in New York. Figure 3-29 [20] shows the laboratory test. Figure 3-30 displays that the cross-section of full scale setup in laboratory (Test Program 1 and 2).

Cracks originated from the end lack-of-fusion at the termination of the connection, as shown in Figure 3-31a, and either propagated through the through the throat of the

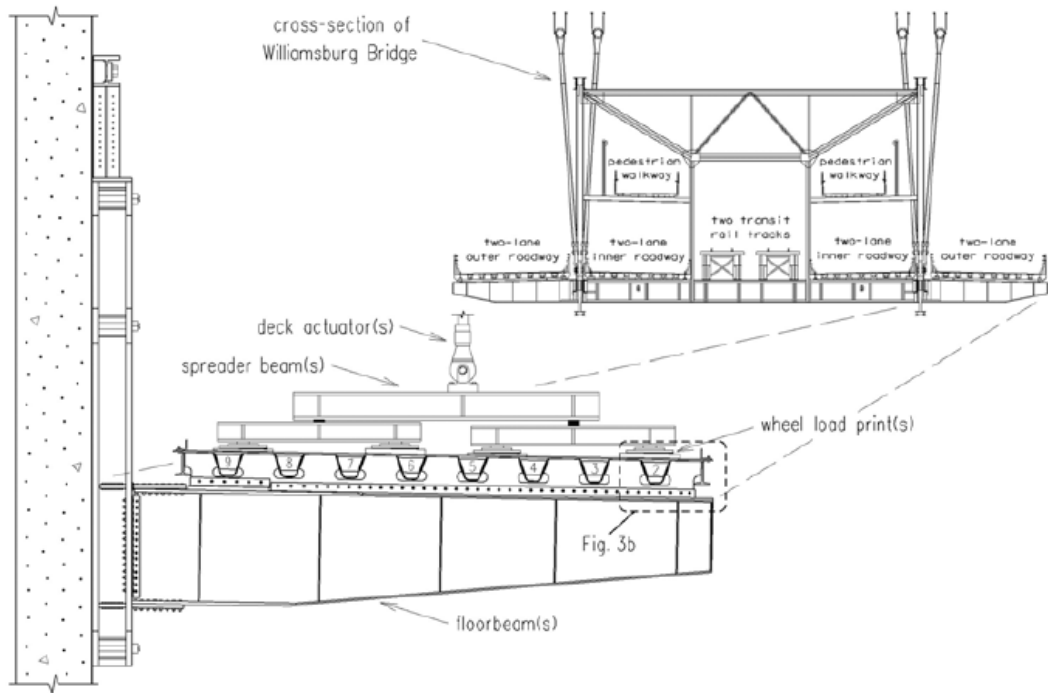
back-to-back fillet welds, in a direction that was parallel to the axis of the rib-to-bulkhead connection, or directly through the adjacent rib wall and into the diaphragm plate on each side of the bulkhead plate.

Figure 3-31b shows that cracks in the rib-to-bulkhead connections initiated either from the end lack-of-fusion at the termination of the connection or from the weld root away from the ends. Crack development in the latter case is believed to be caused by a combination of high in-plane diagonal tension stresses in the welds that were higher than anticipated, and the local effect of vertical compression stresses induced by wheel load prints that were close proximity.

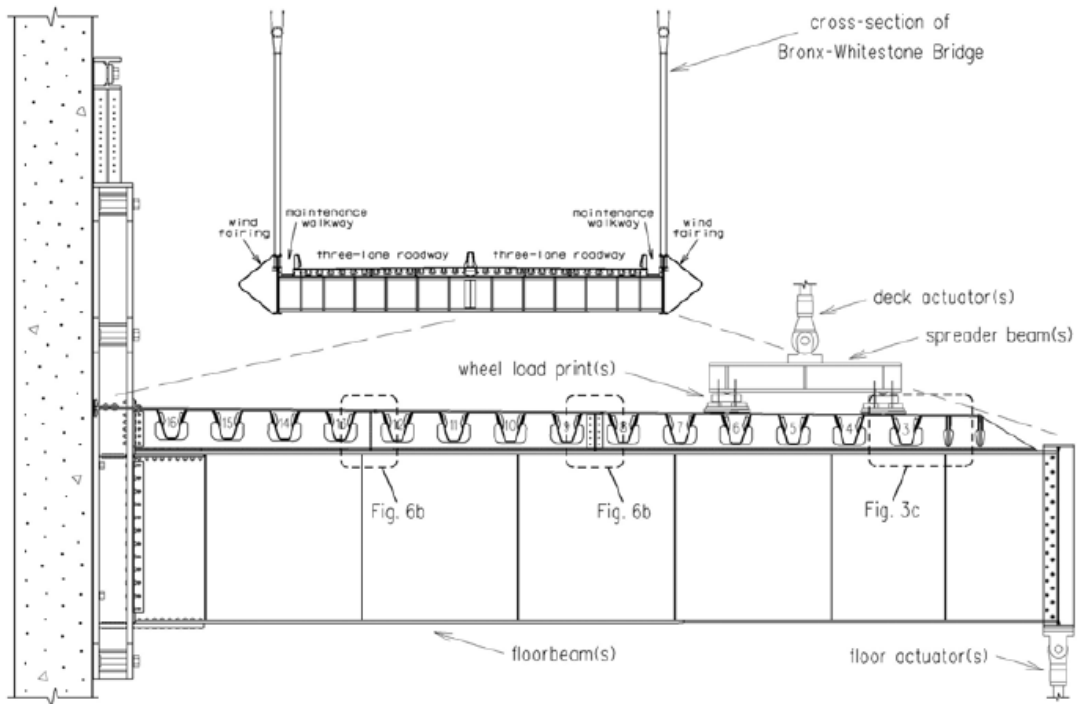
Furthermore, full-scale test of Bronx-Whitestone Bridge redecking was also conducted at ATLSS center.



FIGURE 3-29 Fatigue test of Williamsburg Bridge at ATLSS center.

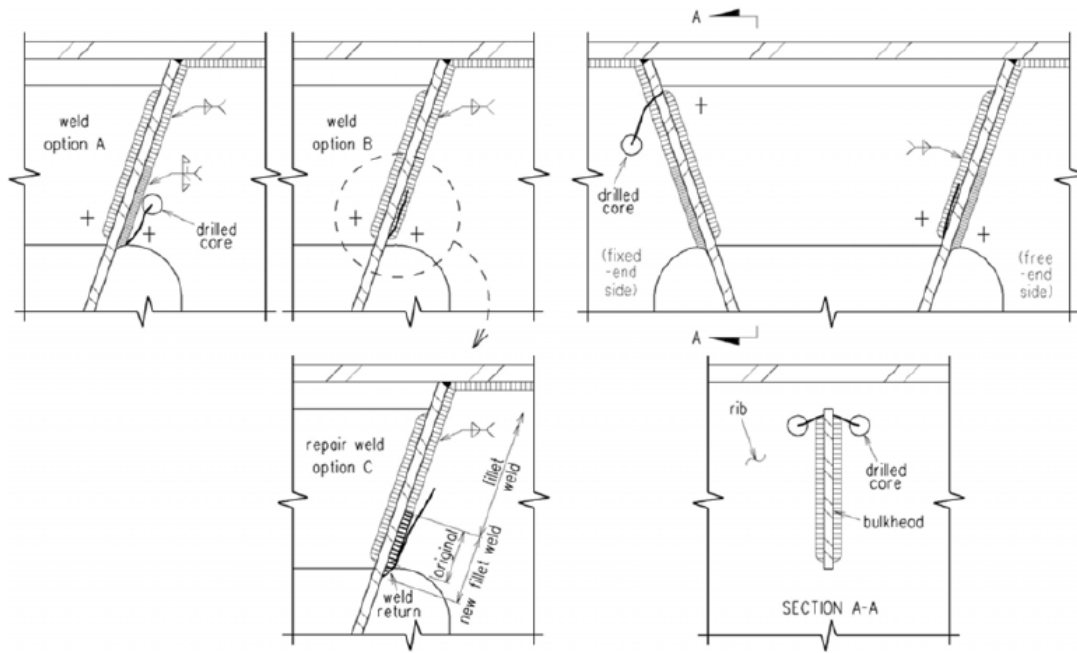


a. Test Program 1;

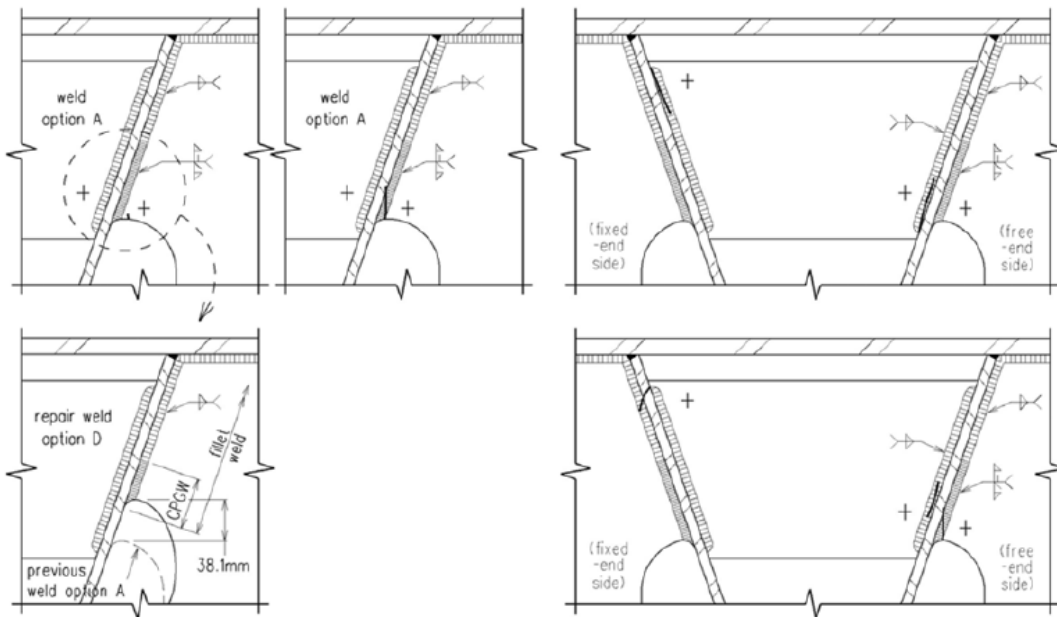


b. Test Program 2;

FIGURE 3-30 Cross-section of full scale setup in laboratory (Tsakopoulos, 2005).



a. 8mm diaphragm;



b. 13mm diaphragm.

FIGURE 3-31 Fatigue crack development in diaphragm during Test Program 1 (Tsakopoulos, 2005).

3.4.2 The four different models with or without bulkhead

The geometry of cutout has a significant influence to the stress performance based on the previous FE analysis. As well, it is found that both the cutouts originated from Eurocode 3 and developed from AASHTO are two suitable designs. Therefore, these two cutouts are chosen to analyze the influence of the bulkhead.

The four different geometries in the diaphragm are shown in Figure 3-32 (a. Eurocode3 cutout without bulkhead; b. Eurocode3 cutout with bulkhead; c. Cutout developed from AASHTO without bulkhead; d. Cutout developed from AASHTO with bulkhead). Detailed meshes in the diaphragms are shown in Figure 3-33.

The height of cutout, the width of cutout and the height of lower clearance are important to both in-plane and out-of-plane stresses, thus, these three parameters are designed the same in the diaphragm (see CHAP. 3.3.2). The bulkhead is 230 mm height, and the distance from the deck plate to the top of bulkhead is 50 mm while the distance from the bottom of bulkhead to the bottom of the longitudinal rib is 20 mm. All the other parameters can be found in the previous FE models.

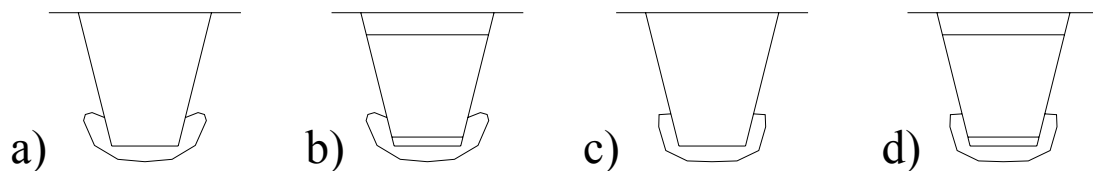
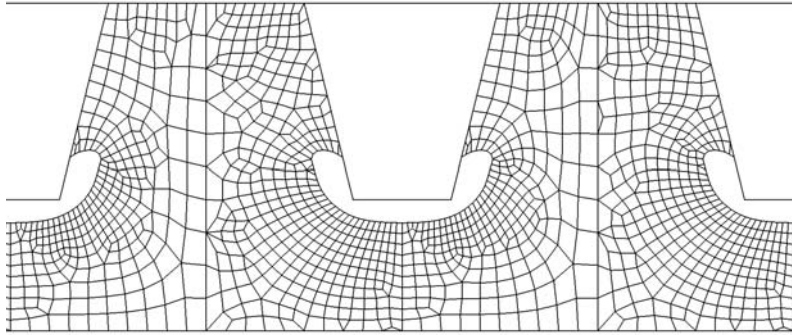
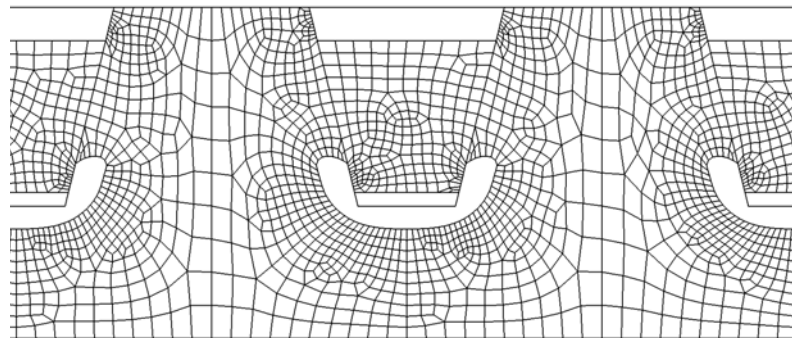


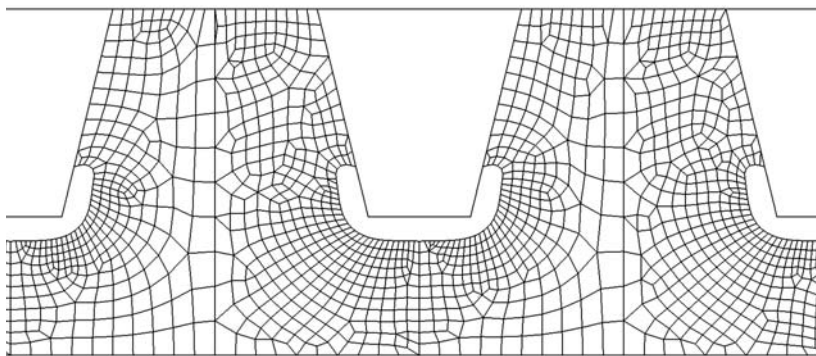
FIGURE 3-32 Different geometries at the diaphragm.



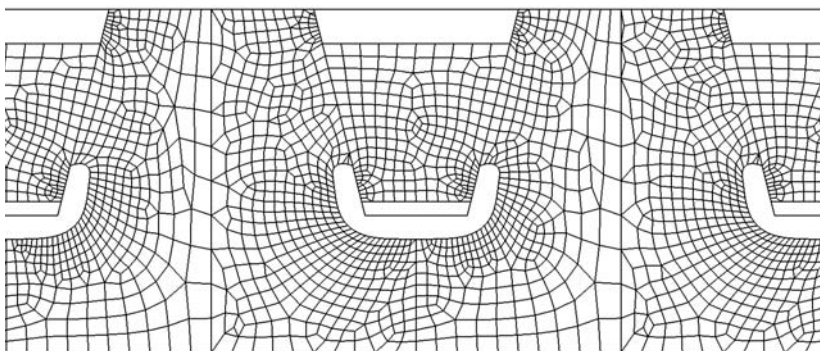
a



b



c



d

FIGURE 3-33 Meshes in the diaphragm.

3.4.3 Results of static analysis

Rib-to-diaphragm, rib-to-diaphragm-to-deck plate, bulkhead-to-diaphragm and rib-to-deck plate are the connections which are ease to produce peak stress range under vehicle loading. Both in-plane and out-of-plane behaviors of these details under three different load cases to the four typologies are emphasized and compared in this study. Furthermore, the thickness influence of deck plates, a hot issue in the design of orthotropic deck, is as well discussed based on the numerical analysis results.

3.4.3.1 Behaviors of the diaphragm

Diaphragm is an important part in an orthotropic deck, and there are plenty of sensitive connections. Numerical analysis was carried out by FE program (LUSAS), and the results are discussed in the following.

The distributions of the displacements and the stresses in the orthotropic deck with bulkhead are similar to the deck without bulkhead. Figure 3-34, 3-35 and 3-36 show the displacement and stress distributions in the diaphragm. Figure 3-37 shows the stress status (SZ) in the diaphragm, and it is found that peak stress exist at the critical connections, such as rib-to-diaphragm connection.

Based on the results of FE analysis, it is found that Rib 5 is one of the most dangerous longitudinal ribs, thus, it is focused in this study. The peak stresses usually occur at the sensitive connections, such as rib-to-diaphragm connection. It is in good agreement with other investigation [21]. The stress results of the critical connections suffering three load cases are presented in Table 3-4. It is found that load case 2 and 3 are more dangerous than load case 1. In general, load case 3 is the most critical for typology A, C and D as the maximal stress existed at Rib 5, while for typology B, load case 2 is the most hazardous. Meanwhile, when there is no bulkhead, the stress of the left rib-to-diaphragm-to-deck plate connection is much higher than that of the right. However, when there is bulkhead in the diaphragm, it is contrary.

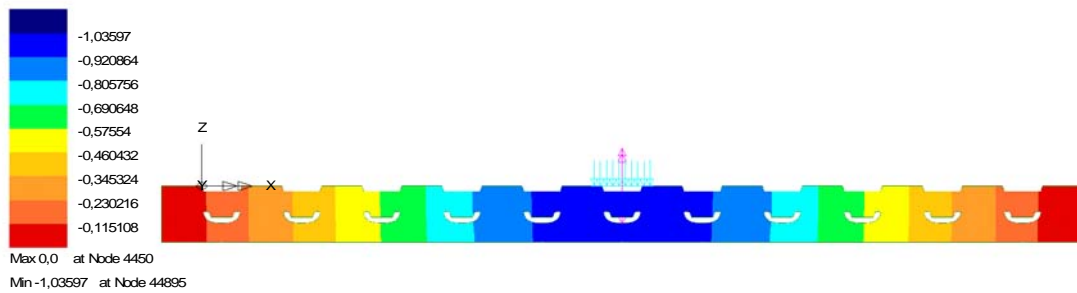
Furthermore, with the comparison among the four typologies of orthotropic deck, it is demonstrated that bulkhead is helpful to decrease the peak stress at the sensitive detail. The maximal stress occurs at typology C (load case 3), and it is at the left of rib-to-diaphragm connection. In addition, typology D, cutout developed from AASHTO and with bulkhead, is the optimized design among all of the four typologies according to the peak stresses based on Table 3-4. It should be noted that all the above analysis are based on the in-plane stress results, while out-of-plane stress is not considered.

Based on the numerical analysis, it is found that high concentrated stresses are occurred at cutout and connection details. The stresses far away from these positions are much smaller and more difficult to produce fatigue cracking. It is obvious that the peak stress exists at or near the connections related with the longitudinal rib for all the four different typologies. For the typologies without bulkhead (A and C), the high stress areas are very small, and inconvenient to be tested in field measurements. Nevertheless, the high stress areas are larger in the other two typologies with bulkhead (B and D), however, the maximal stresses are lower.

TABLE 3-4 Stresses at the Rib 5 connections under the three load cases.

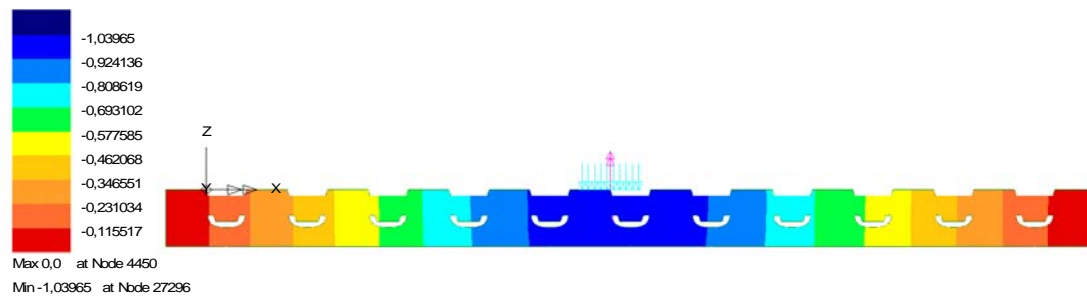
R5	Rib-to-Diaphragm-to-Deck Plate (MPa)		Rib-to-Diaphragm (MPa)		
	Left	Right	Left	Right	
	Loadcase1	22.6	-4.4	-50.1	-44.7
A	Loadcase2	26.9	-10.1	-67.8	-50.4
	Loadcase3	29.2	-6.8	-83.1	-53.8
	Loadcase1	15.6	-35.4	0.4	-1.9
B	Loadcase2	18.1	-62.7	10.6	-1.7
	Loadcase3	14.8	-49.6	17.3	-1.4
	Loadcase1	20.1	-6.4	-48.0	-16.5
C	Loadcase2	23.7	-13.9	-68.2	-16.1
	Loadcase3	25.2	-12.0	-86.1	-17.7
	Loadcase1	20.9	-28.0	5.3	-24.1
D	Loadcase2	25.0	-41.8	20.5	-39.9
	Loadcase3	24.5	-37.9	34.0	-47.9

Loadcase: 1
 Title: Loadcase 1
 Results File: 0
 Entity: Displacement
 Component: DZ



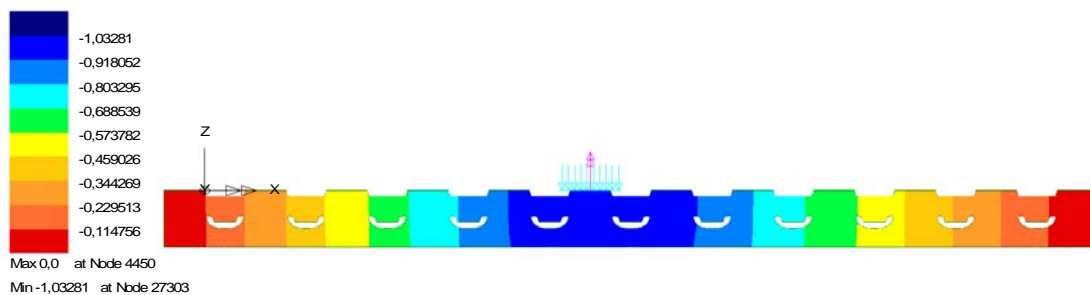
a. Load case 1;

Loadcase: 2
 Title: Loadcase 2
 Results File: 0
 Entity: Displacement
 Component: DZ



b. Load case 2;

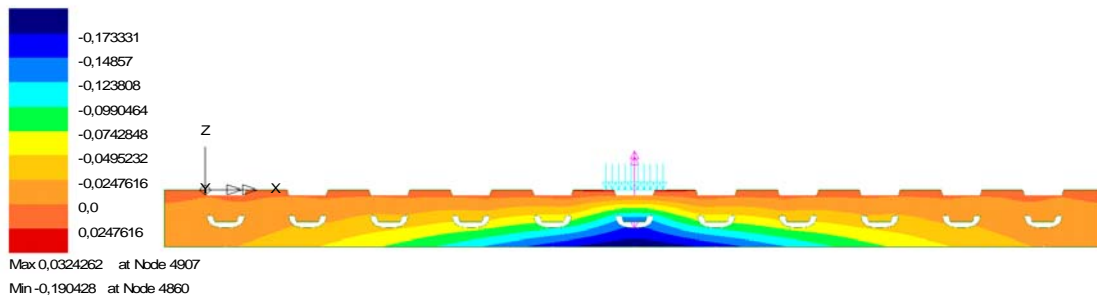
Loadcase: 3
 Title: Loadcase 3
 Results File: 0
 Entity: Displacement
 Component: DZ



c. Load case 3;

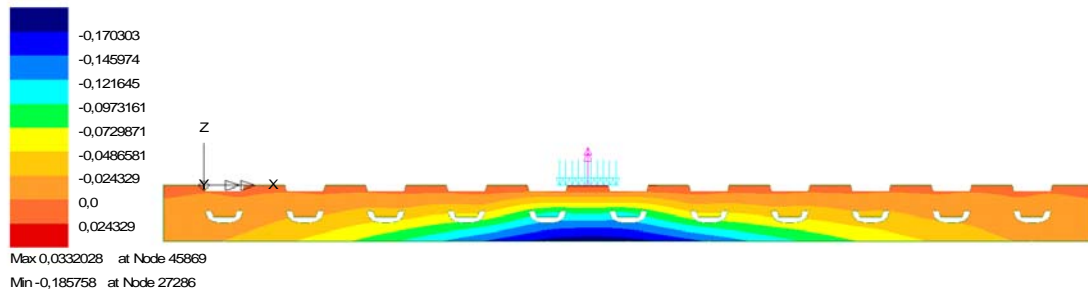
FIGURE 3-34 Vertical displacements in the diaphragm.

Loadcase: 1
 Title: Loadcase 1
 Results File: 0
 Entity: Displacement
 Component: DY



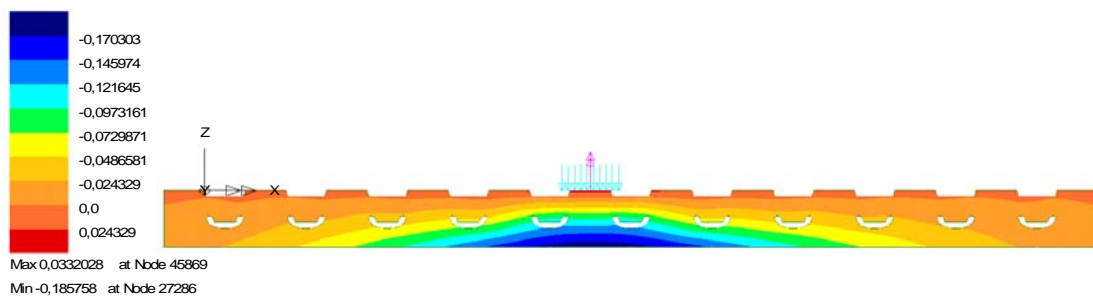
a. Load case 1;

Loadcase: 3
 Title: Loadcase 3
 Results File: 0
 Entity: Displacement
 Component: DY



b. Load case 2;

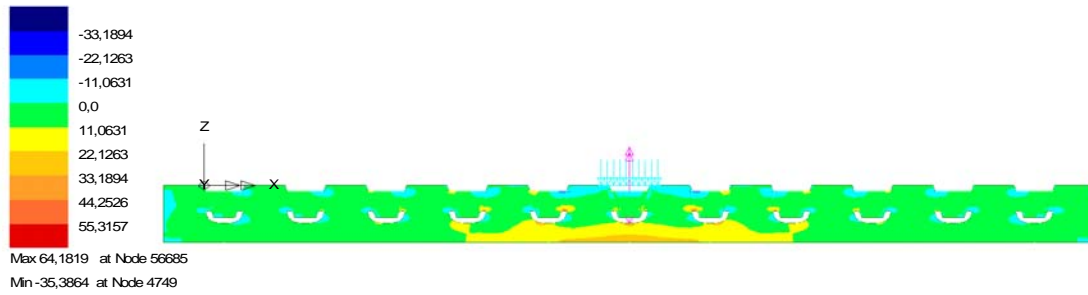
Loadcase: 3
 Title: Loadcase 3
 Results File: 0
 Entity: Displacement
 Component: DY



c. Load case 3;

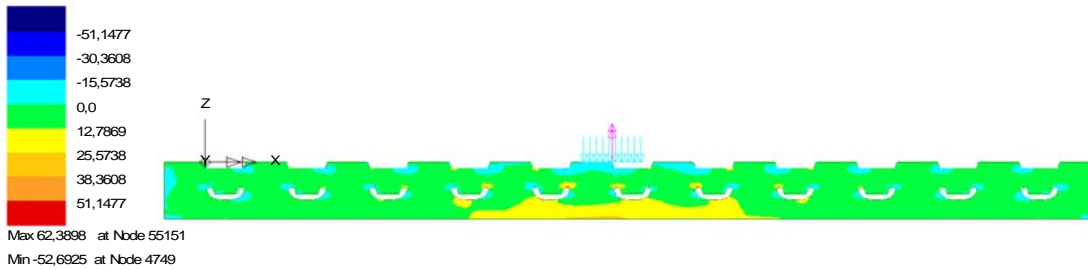
FIGURE 3-35 Out-of-plane deformations in the diaphragm.

Loadcase: 1
Title: Loadcase 1
Results File: 0
Entity: Bottom Stress
Component: SX



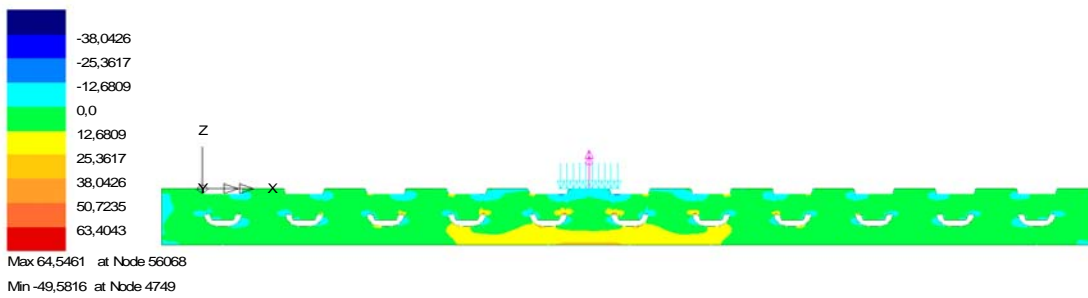
a. Load case 1;

Loadcase: 2
Title: Loadcase 2
Results File: 0
Entity: Bottom Stress
Component: SX



b. Load case 2;

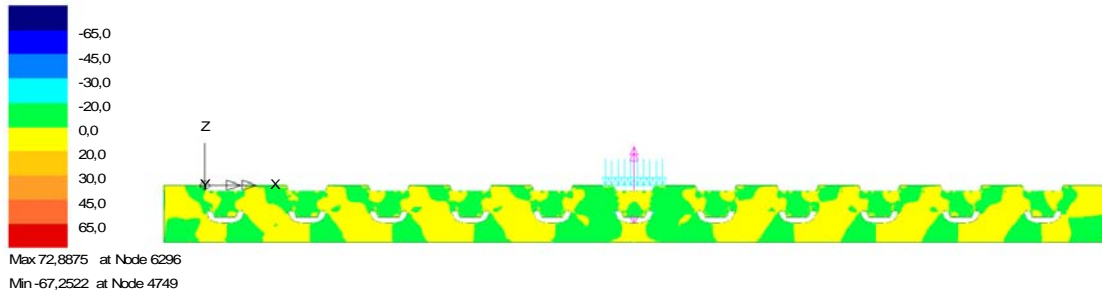
Loadcase: 3
Title: Loadcase 3
Results File: 0
Entity: Bottom Stress
Component: SX



c. Load case 3;

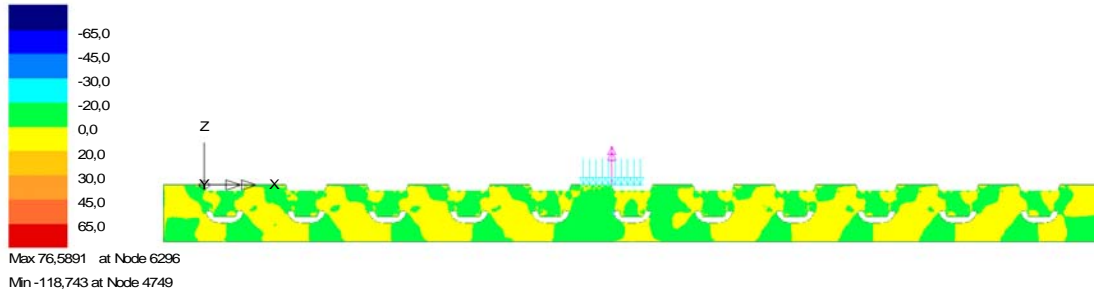
FIGURE 3-36 Stress (SX) in the diaphragm.

Loadcase: 1
Title: Loadcase 1
Results File: 0
Entity: Bottom Stress
Component: SZ



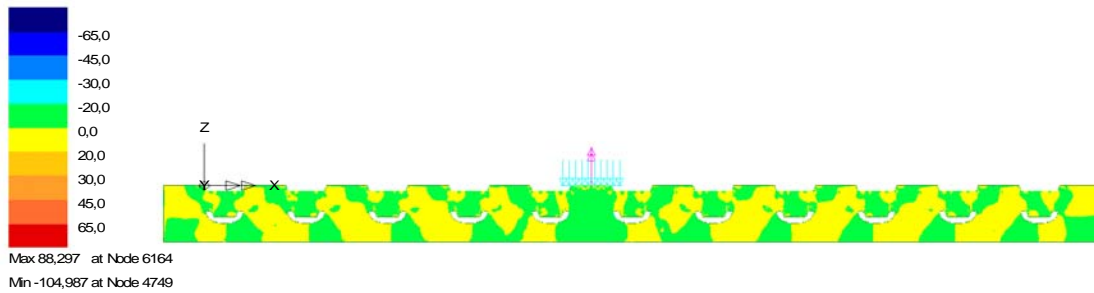
a. Load case 1;

Loadcase: 2
Title: Loadcase 2
Results File: 0
Entity: Bottom Stress
Component: SZ



b. Load case 2;

Loadcase: 3
Title: Loadcase 3
Results File: 0
Entity: Bottom Stress
Component: SZ



c. Load case 3;

FIGURE 3-37 Stress (SZ) in the diaphragm.

Table 3-5 presents the stresses at the bulkhead connections of Rib 5 under the three different load cases, and Figure 3-28 shows the sensitive locations of peak stress around it. It is found that the maximal stresses are produced at/near the bulkhead-to-diaphragm connections when the vehicle loads are not located in the longitudinal rib (load case 1), the similar phenomenon is found at the rib-to-diaphragm connections. The concentrated stresses both for load case 2 and 3 are larger than the stresses of load case 1, while the difference between load case 2 and 3 is minor. Compared with the peak stresses at the bottom of the rib-to-diaphragm connections, the peak stresses at the top of bulkhead-to-diaphragm connections are much smaller. Taking account into the out-of-plane distortion at the diaphragm, the fatigue behavior becomes more complex.

TABLE 3-5 Stresses at the bulkhead connections of Rib 5 under the three load cases.

R5	Top of Bulkhead-to-Diaphragm (MPa)		Bottom of Bulkhead-to-Diaphragm (MPa)	
	Left	Right	Left	Right
Loadcase1	22.7	-11.7	-4.4	59.1
B Loadcase2	22.9	-13.1	-6.5	62.4
Loadcase3	20.0	-7.3	-7.1	59.2
Loadcase1	19.4	-4.4	-14.2	60.8
D Loadcase2	20.3	-3.0	-17.6	69.4
Loadcase3	19.6	-2.9	-19.0	74.0

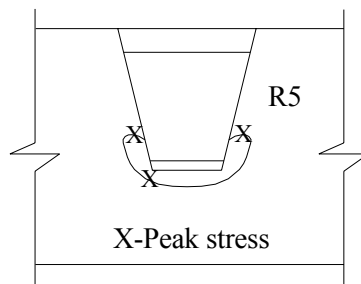


FIGURE 3-38 Peak stresses around R5.

Figure 3-39 shows the in-plane displacement (vertical deflection) in the diaphragm (near the cutout, 150 mm from the bottom of the diaphragm) of typology B and D. Combined with the previous results, it is concluded that the bulkhead has a small influence to the in-plane displacement of the diaphragm.

The out-of-plane displacement distributions at the middle diaphragm of typology B and D are shown in Figure 3-40. It is found that the bulkhead almost also has small influence to the out-of-plane distortion, therefore, it could change the peak stress range. Meanwhile, the loading position influences the out-of-plane distortion obviously.

The out-of-plane stress distributions of typology B and D (near the cutout, 150 mm from the bottom of the diaphragm) are shown in Figure 3-41. From Figure 3-41a, it is known that the differences among the four different typologies are clear, and it can be noted that the bulkhead increases the in-plane stress. Load case can influence the out-of-plane stress at the diaphragm. Combined with the previous results, the out-of-plane stress distributions of the four typologies and the three load cases are similar. It is in good agreement with the out-of-plane displacement distributions. Meanwhile, the stress appears the shape of fluctuation due to the loss of section in the diaphragm.

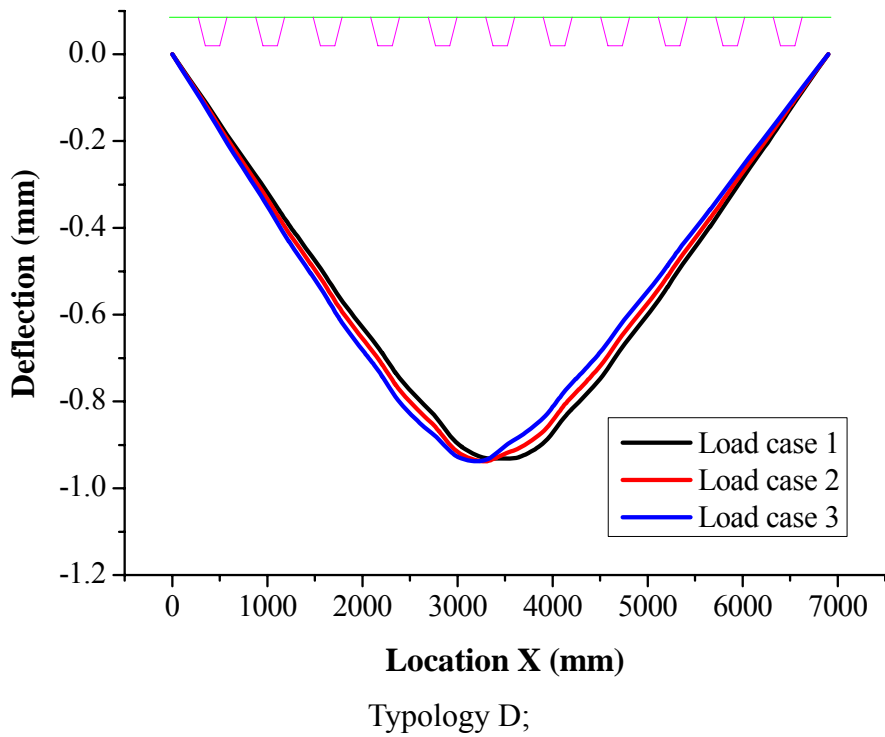
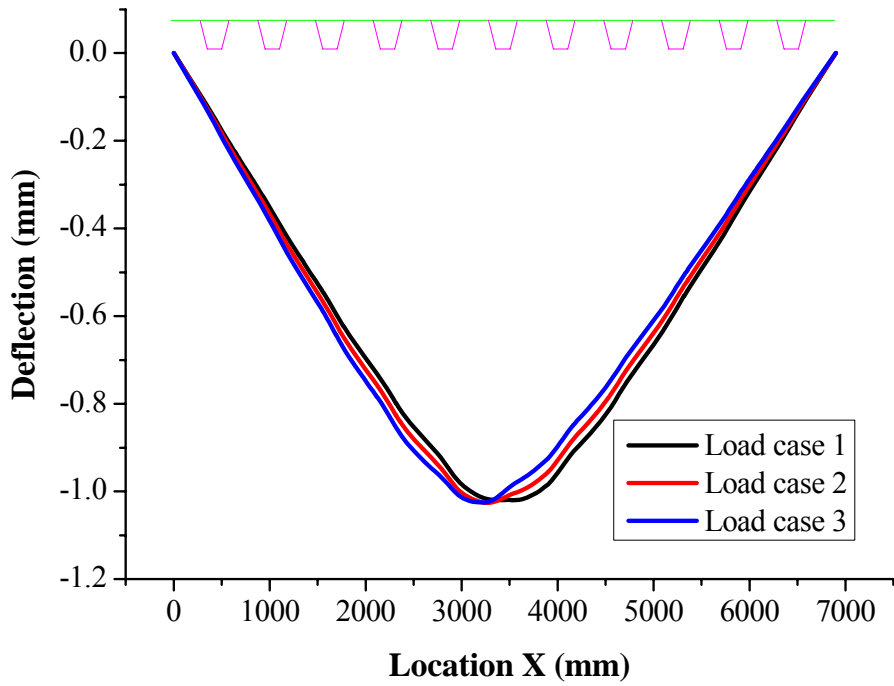


FIGURE 3-39 In-plane displacements at the diaphragm.

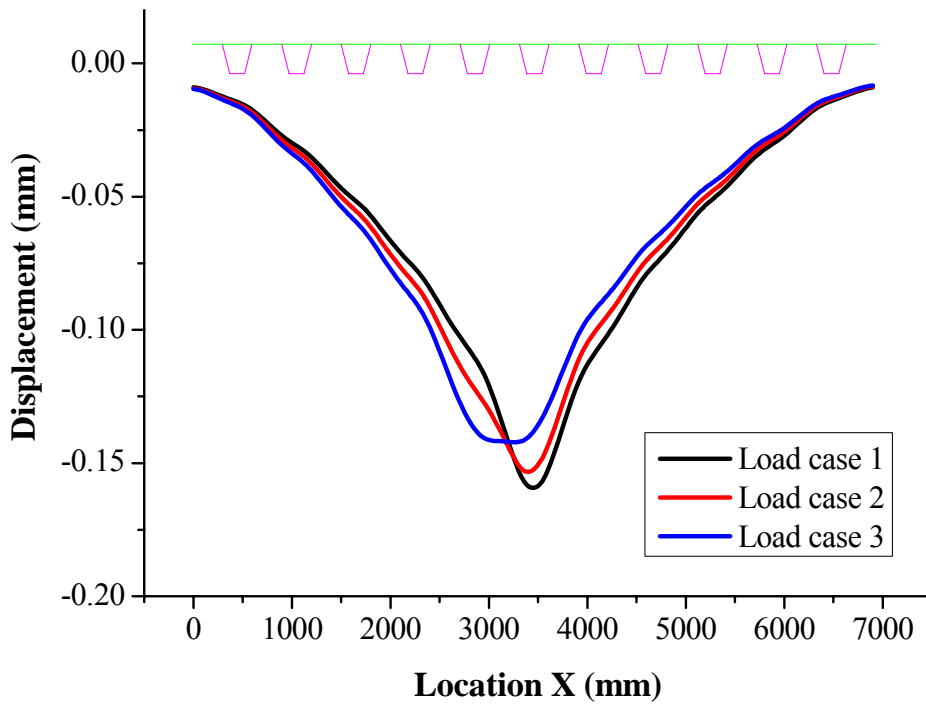
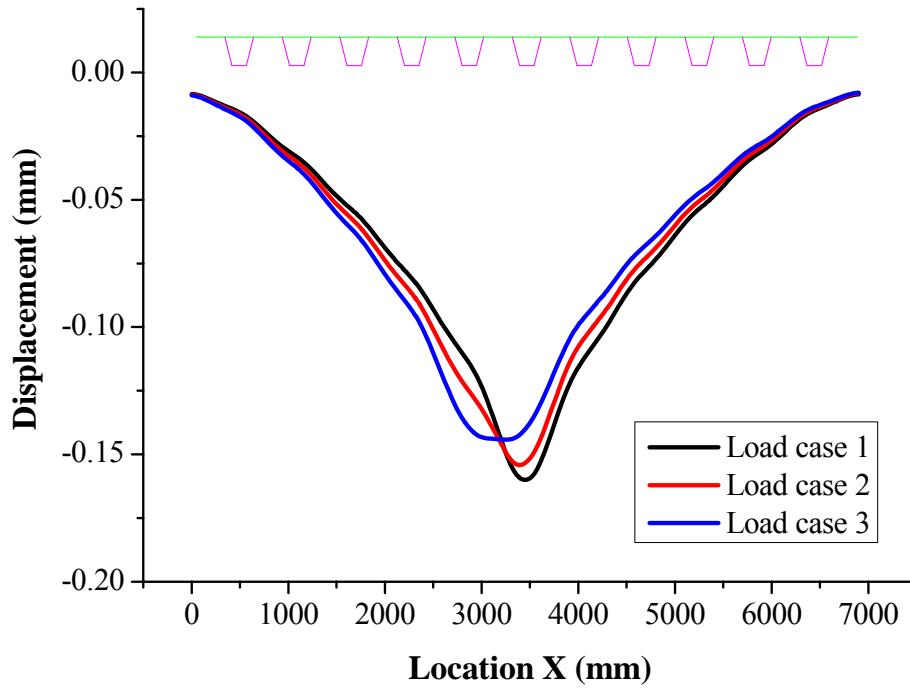
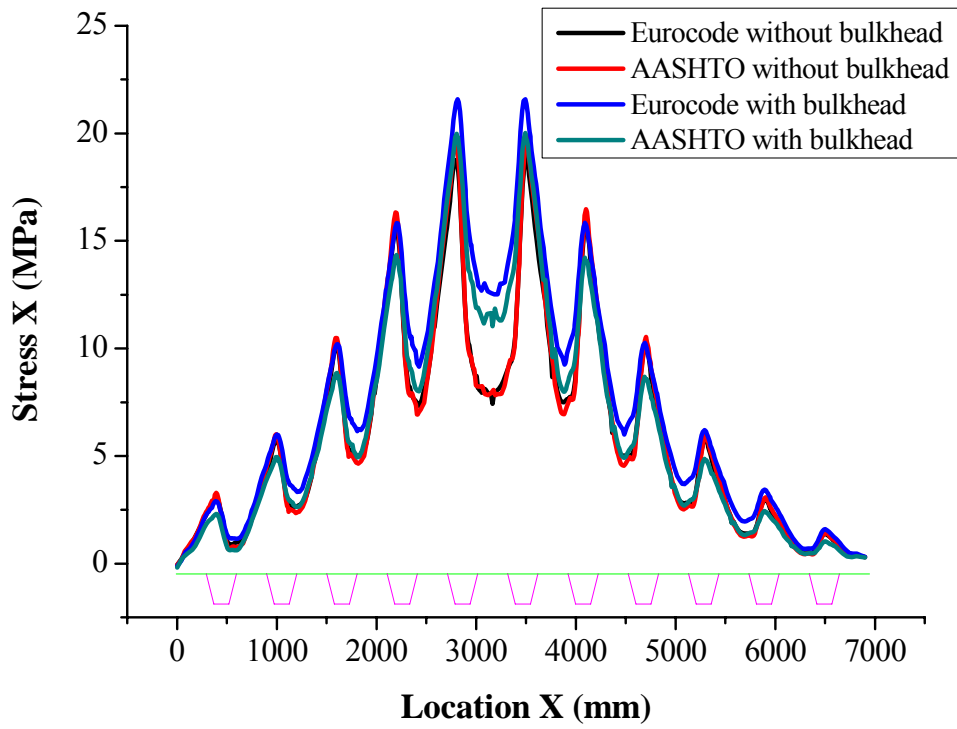
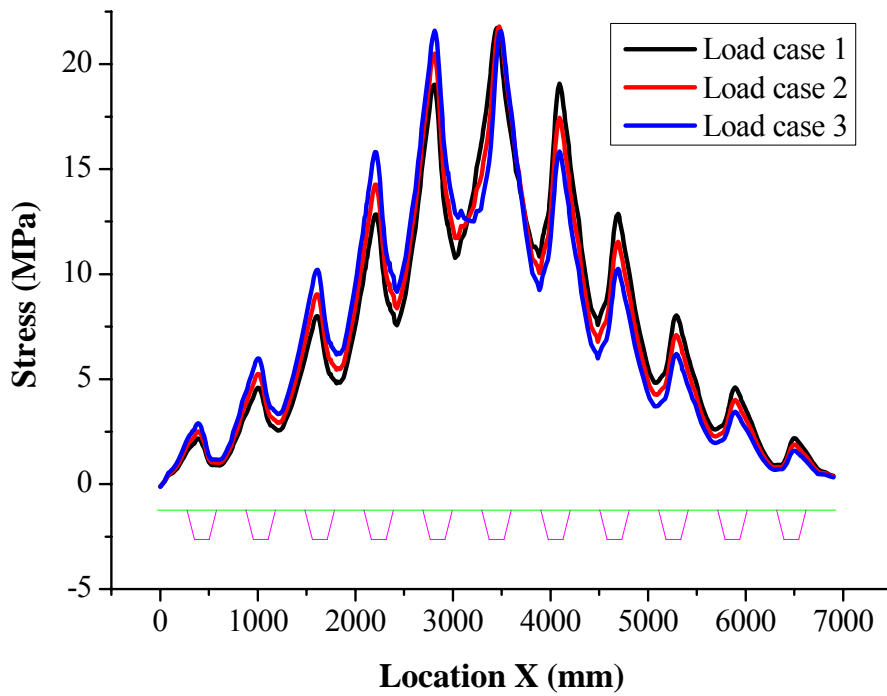


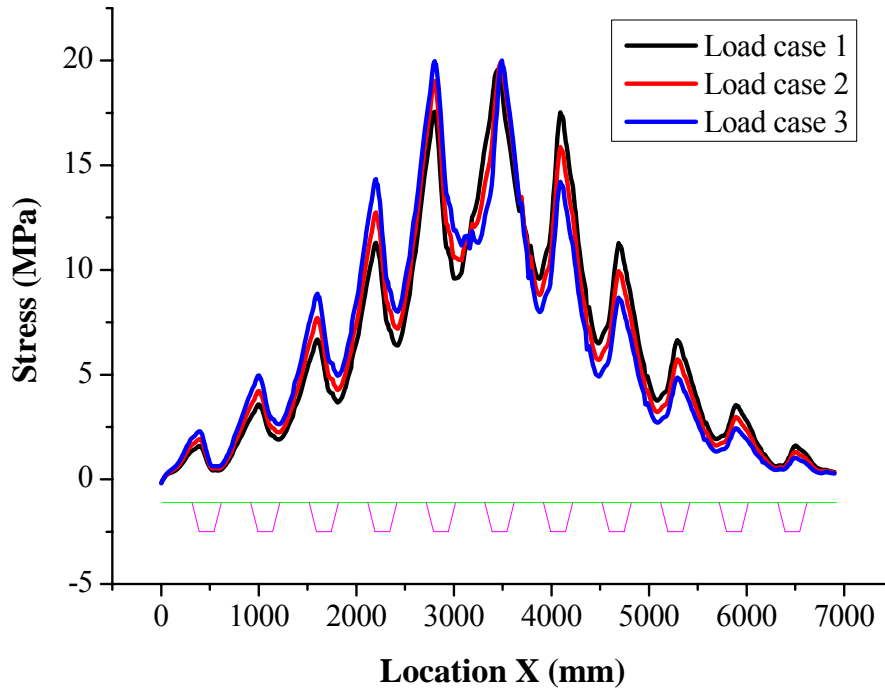
FIGURE 3-40 Out-of-plane displacements at the diaphragm.



a. Different geometries;



Typology B;



Typology D;

FIGURE 3-41 Stresses at the diaphragm.

3.4.3.2 Behaviors of the deck plate

Figure 3-42 shows the stress performance at the center of the middle span of the deck plate. Both the influences of cutout and bulkhead can be ignored from according to Figure 3-25 and 3-42. The stress distributions in transversal direction are almost the same. Nevertheless, the loading position influences significantly the stress performance. The peak stresses of load case 2 and 3 are much higher than that of load case 1. The values of the stresses and the displacements at the deck plate of typology B and D are presented in Table 3-6. Compared to the previous results, there is no big difference between the deck with and without bulkhead. It shows that the bulkhead has minor influence to the deck plate.

Another point which should be noted is that the maximal stresses of all these three different load cases are produced near or exactly at the rib-to-deck plate connections. For load case 1, symmetrical loading, both maximal and minimal stress are exactly at

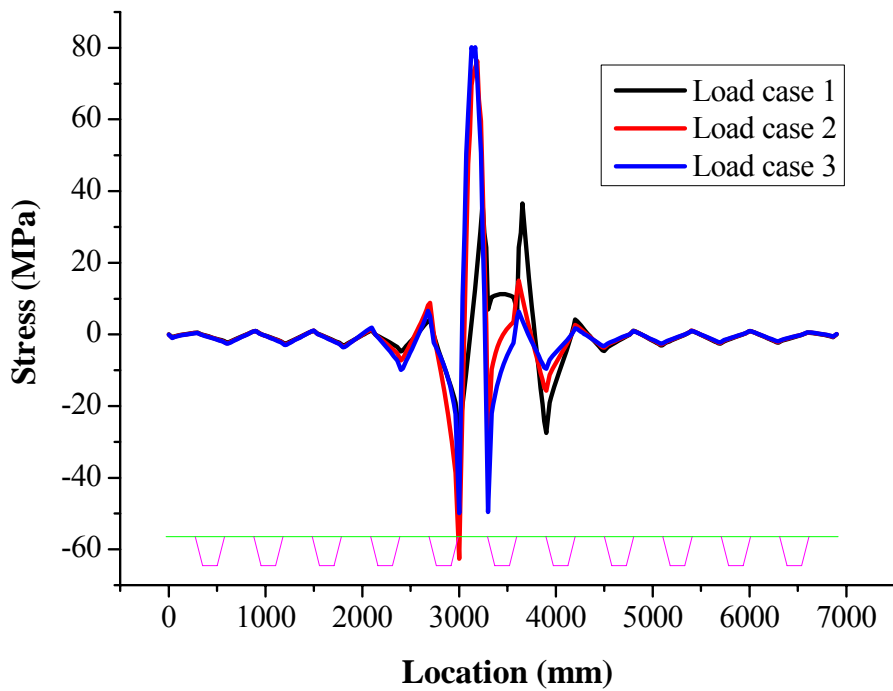
the rib-to-deck plate connections, while for load case 2 and 3, asymmetrical loading, the maximal stresses are produced at the middle of the rib and maximal negative stresses occur at the rib-to-deck plate connections. This reveals why plenty of fatigue cracks are ease to occur at this position both in laboratory tests and actual projects. Although the high stress area becomes smaller in load case 2 and 3, the maximal stress becomes higher. Furthermore, the slope of stress changes suddenly at the peak stress, therefore, it is difficult to be measured in laboratory tests or field measurements.

The stress in the longitudinal direction is discussed based on the counters of numerical analysis, as shown in Figure 3-43. It is evident that the load case influences the logitudinal stress significantly. The high stress region changes with the moving of the vehicle loading, and also for the peak stress.

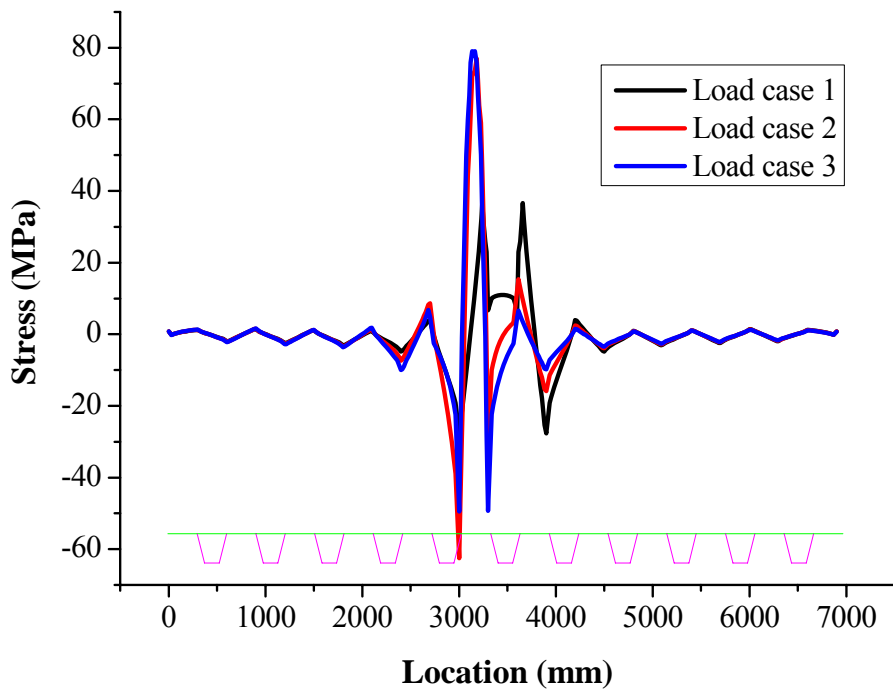
The vertical displacement of the deck plate is discussed as well, as shown in Figure 3-44. Similar to the stress results, the influence of the bulkhead to the displacement of deck plate can be ignored. However, the load position has obvious influence to the displacement as well as to the stress. The vertical dispalcement of load case 1 is evidently smaller than the other two load cases. Meanwhile, the peak deflections for the three different load cases are changed, as shown in Table 3-6, for example, the maximal deflection of load case 3 is 9% more than the load case 1 (Typology B).

TABLE 3-6 Peak stresses and displacements at the deck plate.

Typology	Load Case	Maximal Stress (MPa)	Minimal Stress (MPa)	Maximal Displacement (mm)
	Loadcase1	36.6	-27.5	-2.00
B	Loadcase2	76.2	-62.6	-2.13
	Loadcase3	80.2	-49.9	-2.18
	Loadcase1	36.6	-29.3	-1.91
D	Loadcase2	76.9	-62.6	-2.03
	Loadcase3	79.1	-49.5	-2.07



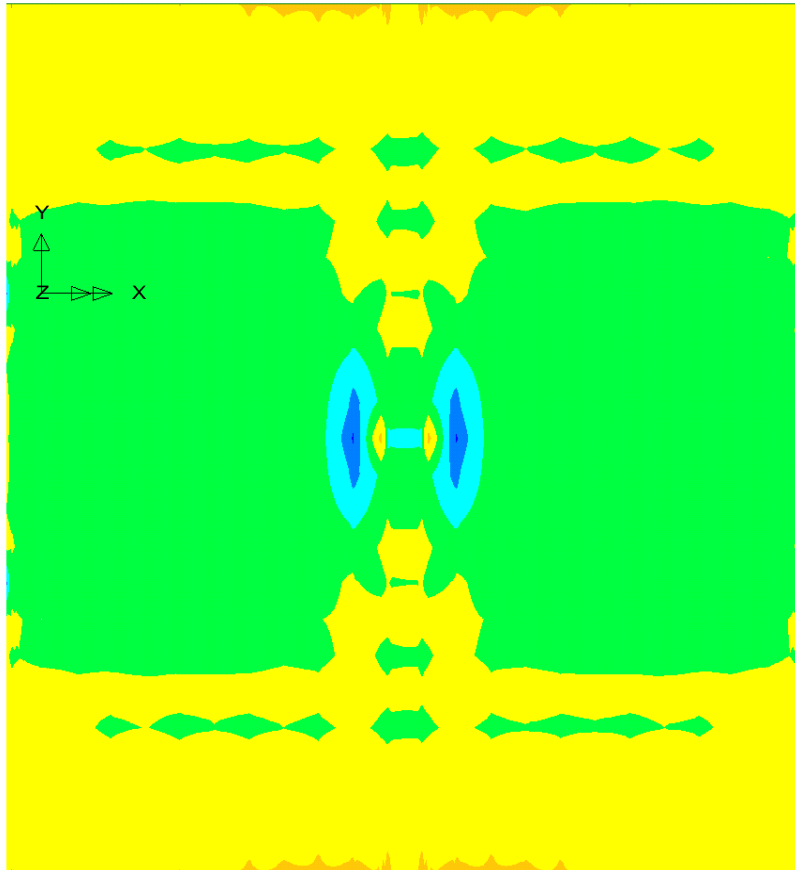
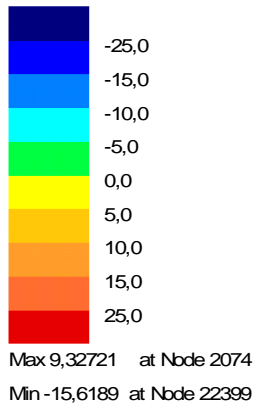
Typology B;



Typology D;

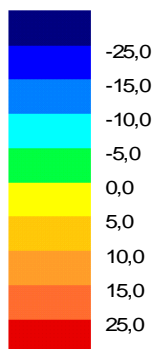
FIGURE 3-42 Stressess at the center deck plate of the middle span.

Loadcase: 1
Title: Loadcase 1
Results File: 0
Entity: Bottom Stress
Component: SY

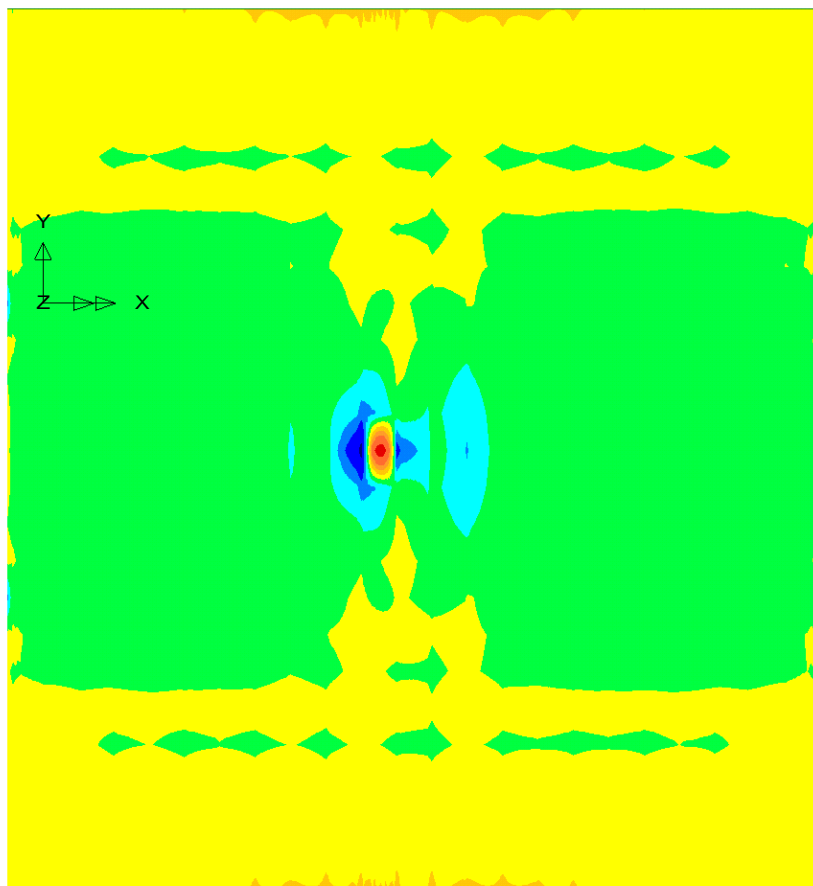


a. load case 1;

Loadcase: 2
Title: Loadcase 2
Results File: 0
Entity: Bottom Stress
Component: SY

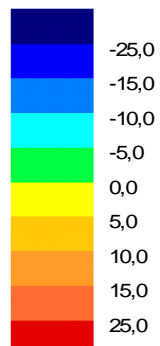


Max 31,5632 at Node 54943
Min -28,5698 at Node 22399

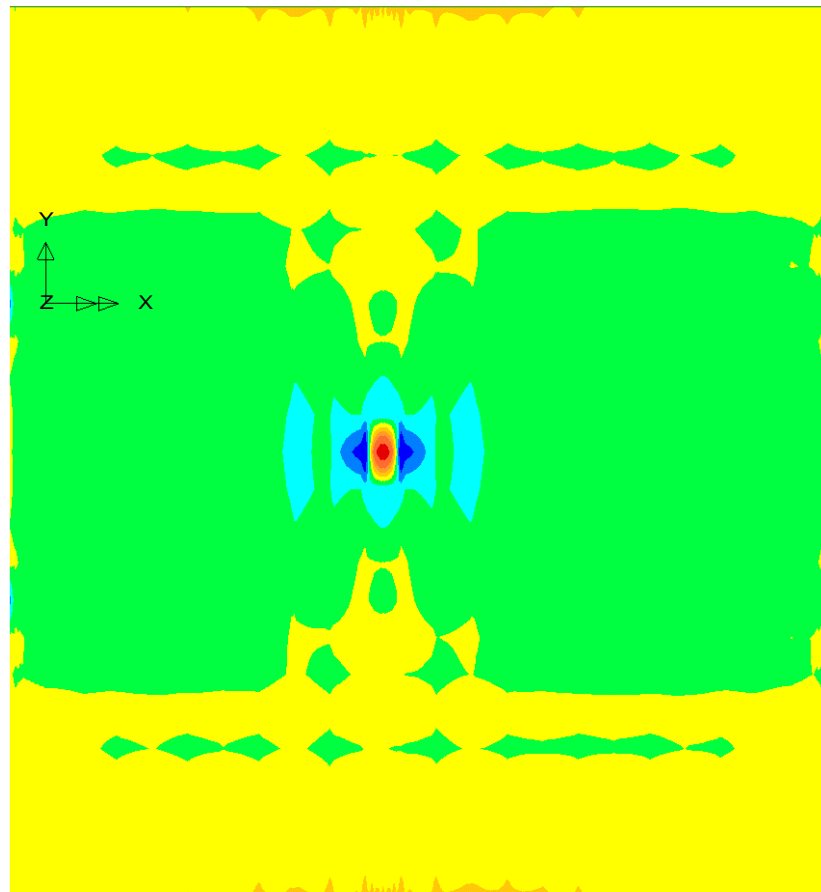


b. load case 2;

Loadcase: 3
Title: Loadcase 3
Results File: 0
Entity: Bottom Stress
Component: SY



Max 34,5131 at Nbdle 54943
Min -25,1009 at Node 22399



c. load case 3;

FIGURE 3-43 Stress (SY) in the deck plate.

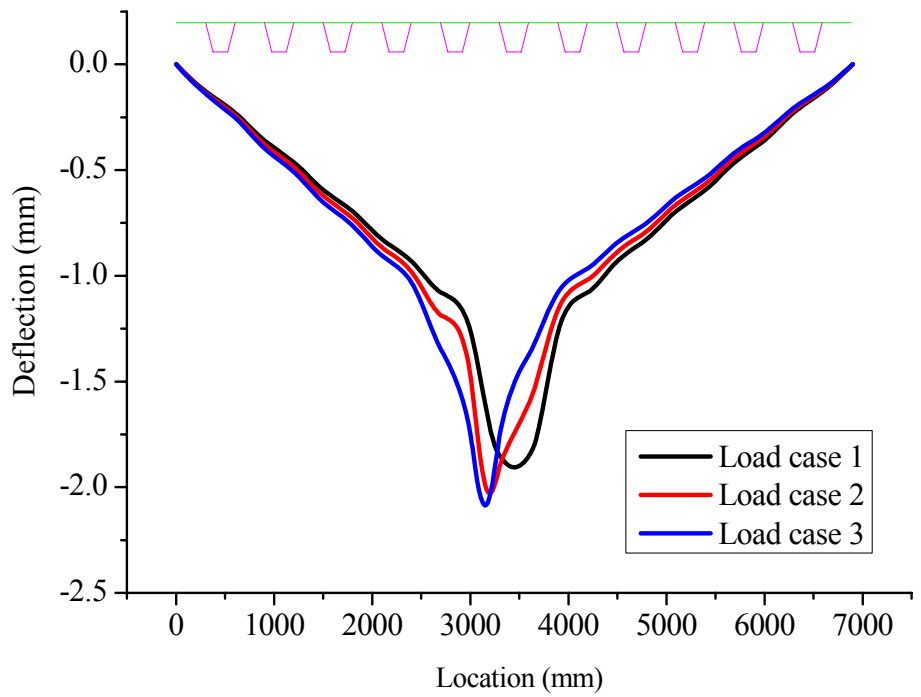
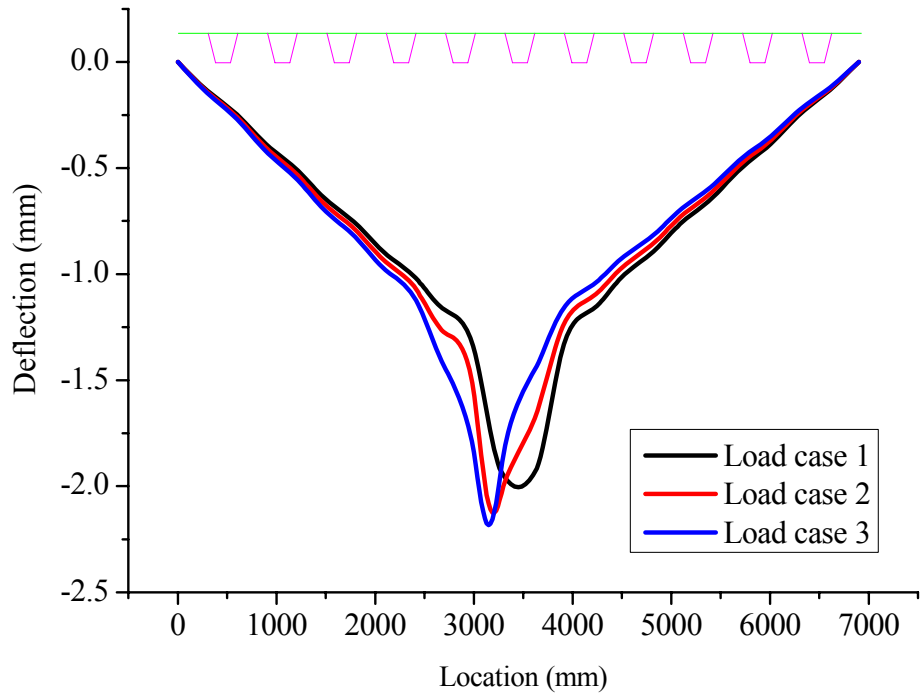


FIGURE 3-44 Deflections at the center deck plate of the middle span.

3.4.4 Discussions

According to the numerical results of this study, the conclusions can be drawn as following:

- a) Bulkhead can reduce the stress at the rib-to-diaphragm-to-deck plate connection and the rib-to-diaphragm connection, while it can increase the stress at the rib-to-bulkhead connection.
- b) Load case has an important influence to the stress performance of orthotropic deck, especially for the peak stress.
- c) Connection details, such as rib-to-diaphragm-to-deck plate, rib-to-diaphragm and rib-to-deck plate, are sensitive to fatigue cracking due to high concentrated stress and residual stress.

Other studies about the bulkhead were carried out in the past years. Laboratory test of Williamsburg Bridge [1] indicated that the prevailing ideology was poorly conceived:

- a) The bulkhead did not behave like a funnel constricting the stress flow, but due to its disconnection to the deck plate, it acted more like a beam in double curvature (contraflexure) due to the discontinuous horizontal shear. The resulting stresses are graphically illustrated in Figure 3-45.
- b) The weakest ligaments in the continuum were the tensile parts in the diaphragm and bulkhead showing root cracking in the Bulkhead and toe cracking in the Diaphragm (called by some researchers as type *b* weld termination cracking, see Figure 3-46). Complete connection penetration welds where root cracking takes place, instead of fillet welds, would have made the prototype more long lasting.
- c) The preponderant stresses in the diaphragm and bulkhead were in-plane stresses, not out-of-plane. The out-of-plane components provide approximately 15 to 20 percent of the combined stresses depending on the thickness of the diaphragm.

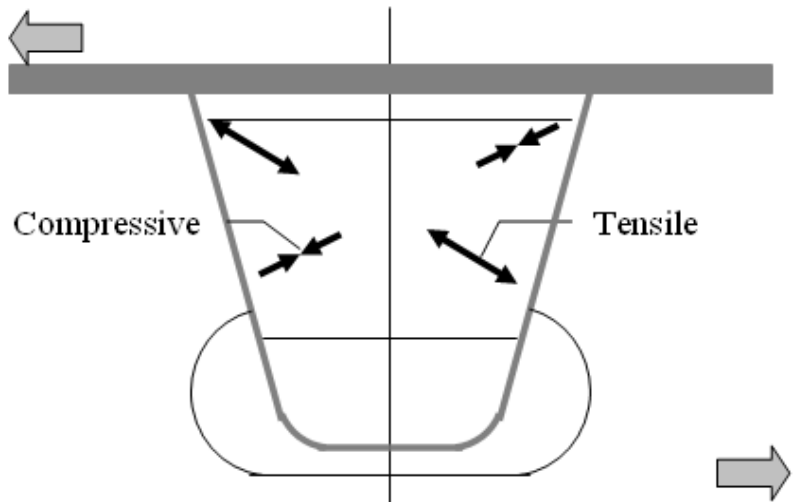


FIGURE 3-45 Stress state at bulkhead.

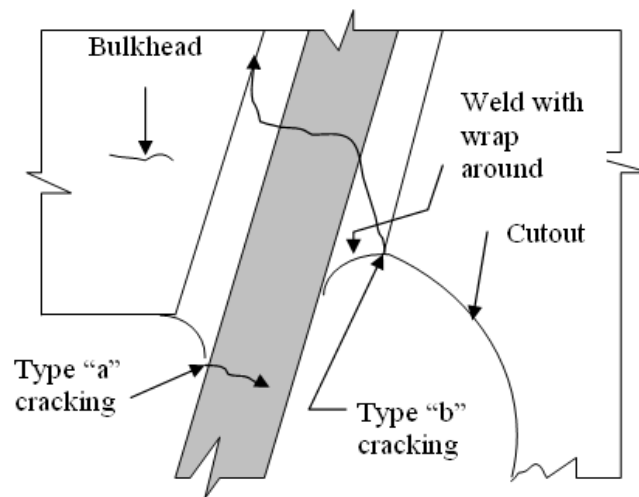


FIGURE 3-46 Cracking types near the bulkhead.

Armed with the above knowledge, engineers who were studying the redecking of the Bronx-Whitestone Bridge conducted analytical parametric studies using FE techniques. The studies indicated, following the illustration in Figure 3-47, that:

- a) Where, following the AISC Manual the longitudinal stress σ_{lr} , would be compressive, regardless of wheel position relative to the center line of the rib, the real response of the rib could be tensile or compressive depending on transversal

wheel position applied in the bays adjacent to the diaphragm. This is because wheel eccentric loading produces torsion, displacing laterally the rib at mid span but with restraint at the diaphragm. Tensile and compressive stresses could alternate on each face of each rib stem, depending on wheel transversal position.

- b) Where the AASHTO Code displayed lack of awareness of the vertical stress in the ribs stem σ_{vr} , following the Pelikan-Esslinger method, FE analyses indicated that the perpendicular edge of the cut out to the rib represented an abrupt transition to these stresses requiring a transition as illustrated in Figure 3-47. AASHTO's convention that a two inch radius is nearly as bad as an abrupt transition which was too conservative, and laboratory testing should provide better data.
- c) While the bulkhead gave the advantage of reducing in plane diaphragm displacements, which is an advantage for the RDDP detail, the internal abrupt transition of the bulkhead presented hot spot stress and fabrication problems, and extra cost.
- d) It was realized that a thickening of the diaphragm, while it would increase the out of plane bending of the diaphragm plate (where resistance is high), it would reduce the in-plane stresses as well as at other hot spots elsewhere in greater proportion, where resistance is low. Optimum diaphragm thickness depends on the entire geometry configuration. The trend is towards thicker diaphragm to reduce the RDDP stresses, when bulkhead is not used.

Tests reported in August 2007 from the UC San Diego indicate that behavior as predicted by FE analyses relative to ribs' stresses σ_{vr} could occur in other major structures fabricated with an abrupt transition cutout, with bulkhead, and were the source of concern. These cracks were not at the toe in the diaphragm but in the toe at the rib stem (such cracks are called by some researches type "a" weld termination cracking see Figure 3-46). Note that type "a" cracking could emanate from either face of the rib, depending which weld toe is lower in the bulkhead/diaphragm arrangement.

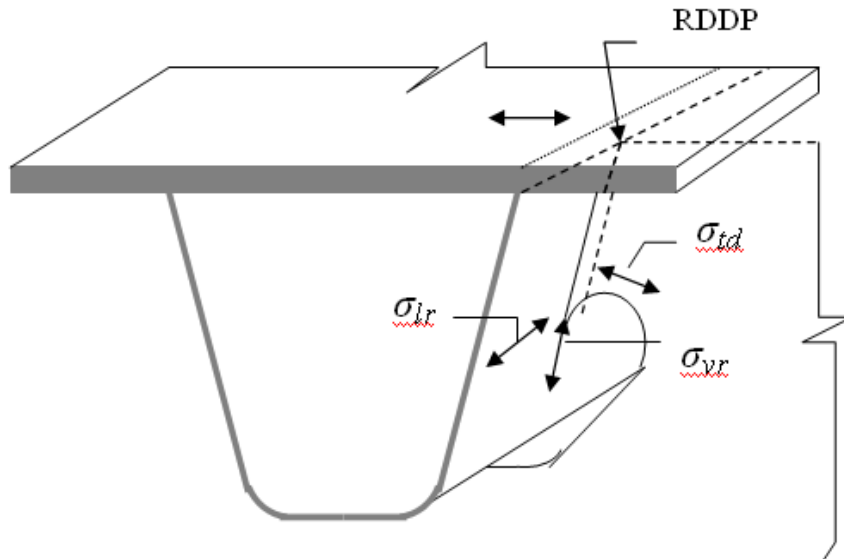


FIGURE 3-47 Stress performance around the RDDP connection.

3.5 Influences of Deck Plate

3.5.1 Introduction

Deck plate plays an important role to the other parts of orthotropic deck because it suffers the vehicle loading directly. The different thicknesses of deck plates can cause significant change to the critical welded connections. Usually, the thicker plate can provide better performance to the deck system. However, it should be noted that a thicker deck plate also means heavier self weight, and costs more.

The deflections of the closed ribs and the open ribs are demonstrated in Figure 3-48 [22]. Under the concentrated load, the superiority of the closed ribs is obvious. In the same test, the behaviors of the deck plates for different positions of the concentrated load show that the orthotropic deck with closed ribs provides the most efficient design.

The behaviors of orthotropic decks has been studied more than 30 years through FE method. Tinawi [17] applied FE analysis to the deck plate and compared with experimental tests. Results of deflections and stresses are showed in Figure 3-49 and 3-50.

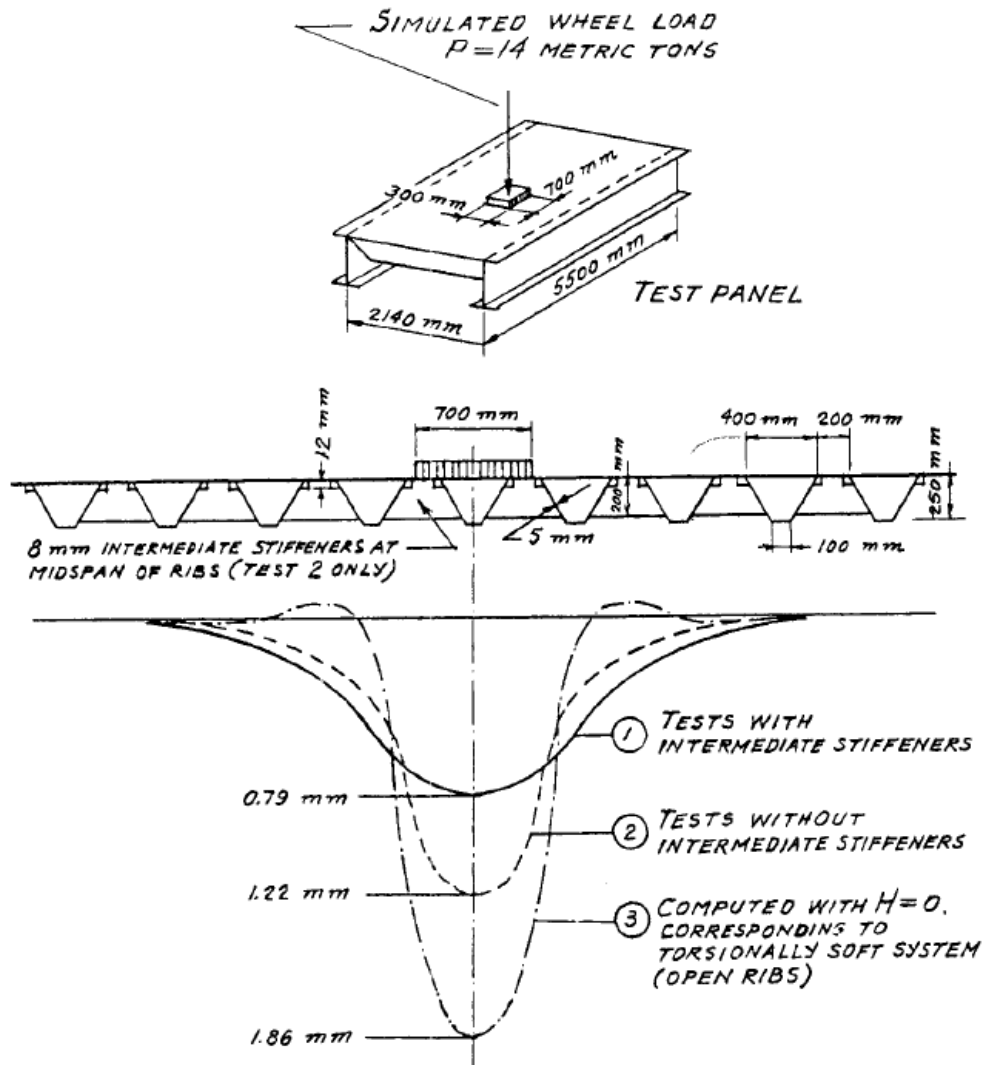


FIGURE 3-48 Results of tests comparing the deflection effects of orthotropic decks with closed and open ribs (Troitsky, 1967).

As shown in Figure 3-49, the theoretical and experimental deflections across the middle span of the deck are in good agreement. However, the computed results appear consistently stiffer. It is probably attributed to the rubber pad stiffeners which permitted the whole panel to undergo a nearly rigid body movement.

As shown in Figure 3-50, it is found when the load is placed between two longitudinal ribs, considerable rotation and bending of adjacent sections occur simultaneously which give rise to rather large variation of stresses at the bottom of the ribs.

With the development of computer science, more precise model of the orthotropic deck can be developed today.

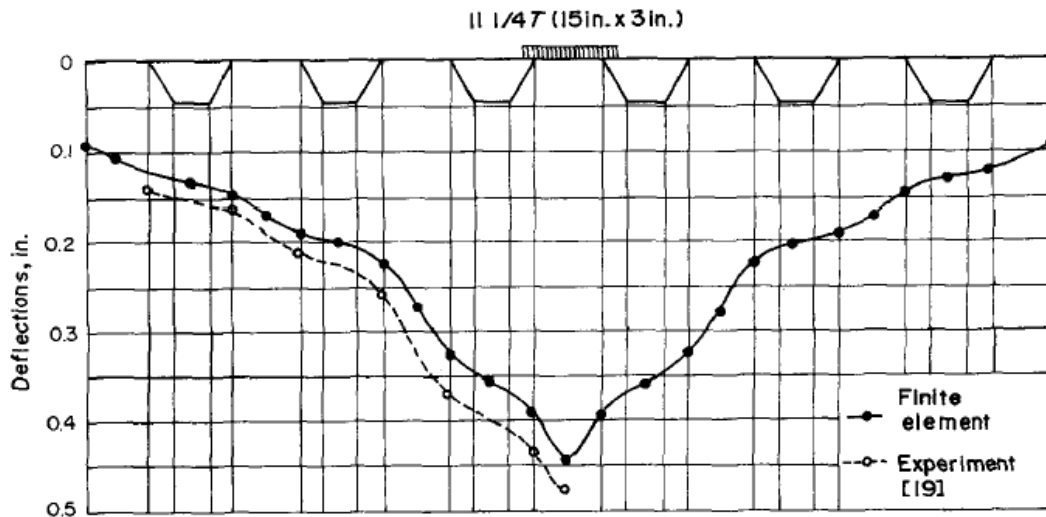


FIGURE 3-49 Deflection results of FE analysis (Tinawi, 1976).

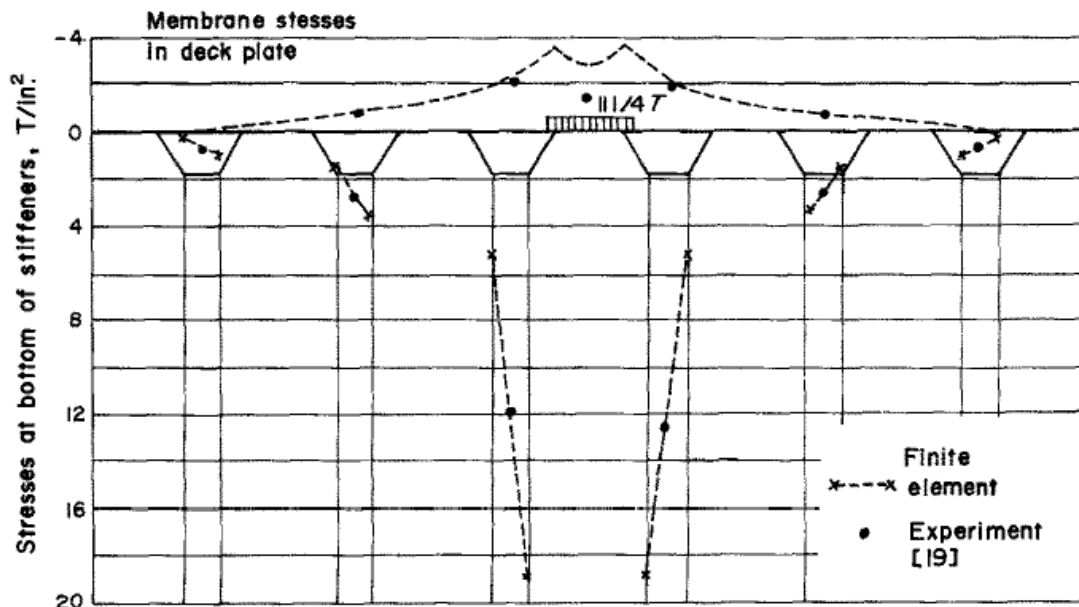


FIGURE 3-50 Stresse results of FE analysis (Tinawi, 1976).

3.5.2 Thickness influence of the deck plate

The increasing of deck plate thickness can reduce the peak stress effectively. Therefore, the fatigue life of an orthotropic deck bridge can be improved. However, thicker deck plate will greatly increase the self weight of orthotropic deck as well, and cost more. A optimized design should make a rational balance between the thickness

and the self weight.

Typology B (one of the optimized designs according to the previous numerical analyses) under load case 3 is analyzed according to the transformation of the deck plate thickness. The vertical displacements at the middle of the deck plates in transversal direction are presented in Figure 3-51. It shows the displacements for the deck plate thickness varies from 10 mm to 20 mm. It is demonstrated that the peak displacements decrease with the increasing of the thickness, and the reduction accelerate with the increasing of the thickness. As well, the peak stress of the deck plate changes with the thickness similar with the displacement, as shown in Figure 3-52. The maximal stress of 10 mm thickness is 179 MPa, while the maximal stress of 20 mm thickness is only 59.5 MPa. Moreover, it is found that when the thickness is more than 16 mm, the maximal stress at the deck plate is more acceptable, but the economy should be considered as well.

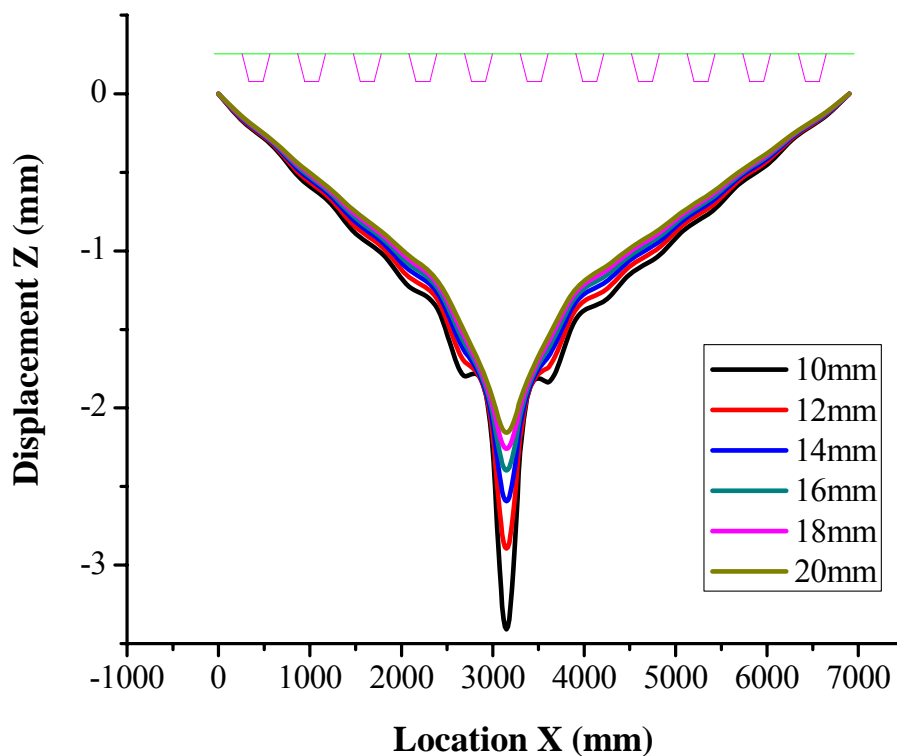


FIGURE 3-51 The thickness influence to the displacement of the deck plate.

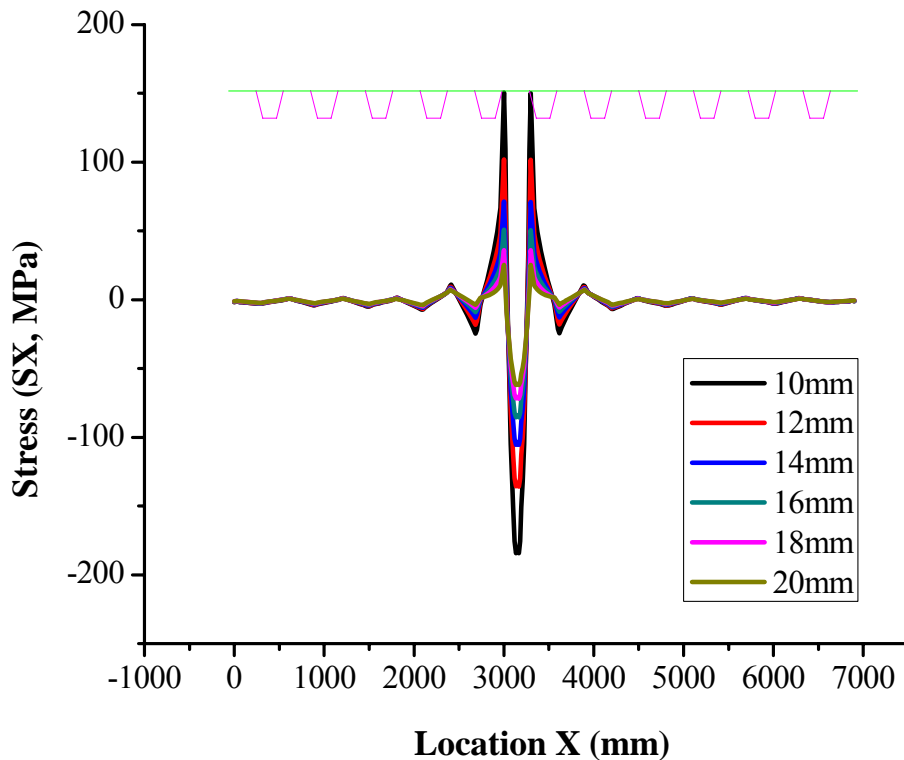
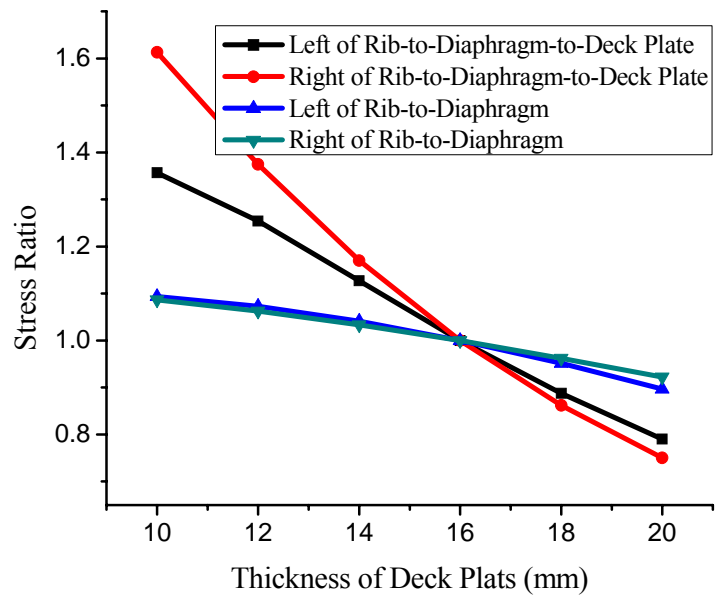
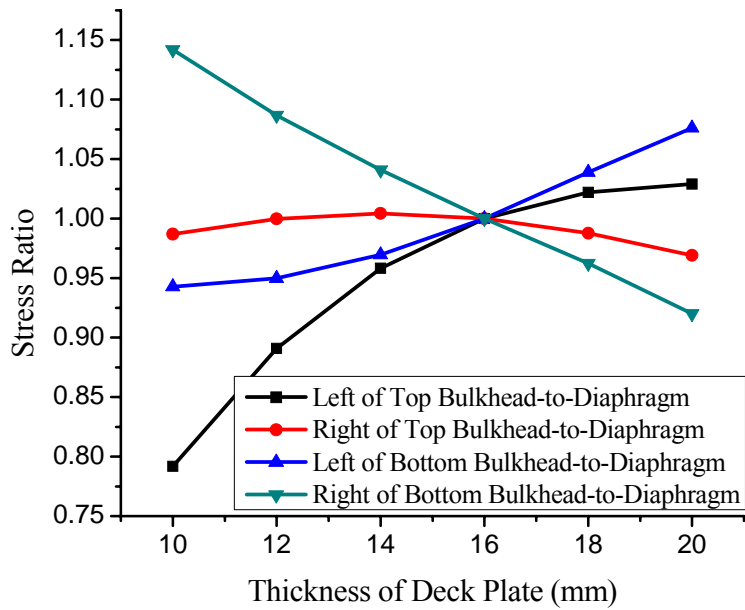


FIGURE 3-52 The thickness influence to the stress of the deck plate.

The thickness influence of the deck plate to the critical connection is also studied, as shown in Figure 3-53. The stress of 16 mm thickness deck plate is taken as the reference point in Figure 3-53. Figure 3-53a shows the stress ratios of the rib-to-diaphragm-to-deck plate connections and the rib-to-diaphragm connections. The stresses at the rib-to-diaphragm-to-deck plate connections vary significantly, while the curve slopes of the rib-to-diaphragm connections are much gentler. The stress at the left of rib-to-diaphragm-to-deck plate connection varies more than two times from 10 mm thickness plate to 20 mm. The thickness influence to the bulkhead-to-diaphragm connection is presented in Figure 3-53b. The stresses at the left of top bulkhead-to-diaphragm and the right of bottom of bulkhead-to-diaphragm connections change greatly with the thickness, while the others are not. Therefore, thicker deck plate can decrease the peak stress at critical connections in orthotropic deck bridge, e.g. rib-to-deck plate, and reduce the stresses at rib-to-diaphragm-to-deck plate and rib-to-diaphragm connections.



a. Rib connections;



b. Bulkhead connections;

FIGURE 3-53 Stress ratio of thickness influence to the connections (typology B, load case 3).

3.5.3 Discussions

Thinner deck plate provides worse performance to the deck plate and a majority of the critical welded connections. Therefore, a minimal thickness is usually defined in specifications. For example, AASHTO-LRFD requires that the minimum deck plate thickness shall not be less than either 14 mm or 4% of the largest rib spacing. Experience from the durability of previously built bridges presents that this requirement is advisable for both constructibility and long-term bridge life.

The minimal thickness of a deck plate may be determined by allowable deflection of the deck plate under a wheel load, which should not exceed 1/300 of the spacing of the deck supports. Based on this criteria, the plate thickness can be determined by Kloeppe's formula:

$$t_p = (0.004a)\sqrt[3]{p} \quad (3.1)$$

where, a is spacing of the open ribs, or the maximum spacing of the walls of the closed ribs; p is wheel load unit pressure, under the AASHTO-LRFD design tandem wheel load 55 kN, including 33% dynamic load allowance, in kPa.

Table 3-7 presents the requirement of width-to-thickness ratio of orthotropic deck plates in major design specifications. It is found in Table 3-7 that the requirement for width-to-thickness ratio of the orthotropic deck system varies obviously between these specifications.

TABLE 3-7 Comparison of design specifications on the thickness of the deck plates.

Specification	Design criteria (mm)
EUROCODE 3	-
AISC [23]	$t \geq a \sqrt{\frac{125}{16} \left(\frac{p}{E} \right)^a}$
AASHTO	$t_{\min} = 14^b, \frac{t_r a^3}{t_{d,eff}^3 h} \leq 400^b$
Japan Road Association [24]	$t_{\min} = 12$

^a Based on out-of-plane deformation under traffic load;

^b Based on distortion-induced fatigue.

Thicker plate produces many advantages, however, its disadvantage is also obvious, that a thicker plate leads heavier self weight to the deck and costs more. Meanwhile, thicker plate also increase the stresses of some critical welded connetions. Thus, bridge designers should balance the the above aspects.

3.6 Future Researches

The investigations conducted in the last 10 years have shown that orthotropic decks have a definite place in the future of bridge structures. Future Code writing and design work must address the issue of what technique to use to correctly assess the fatigue life of these structures. As the initial cost of orthotropic decks will decrease they will come more in competition for deck replacements, not only in suspension bridges, but also in viaducts and overpasses against alternate deck types that take short time to erect and have least impact on the traffic.

Recently, most of long span suspension bridges and cable stayed bridges take use of orthotropic deck box girders by bridge designers because its significant advantages, such as less self weight, higher bending resistance and torsional resistance. Figure 3-54 provides an actual project of an orthotropic deck box girder bridge [25]. Although a large number of orthotropic deck box girders are applied to long span

bridges, the computing theories is far behind compared to the techniques of construction due to the more complex composition. FE analysis maybe used to solve the problem.

The benefits provided by orthotropic decks have not yet been fully discovered. The tools at our disposal for such discoveries are various. Testing is foreseen to build the database where complex geometries and loads obtain are included.

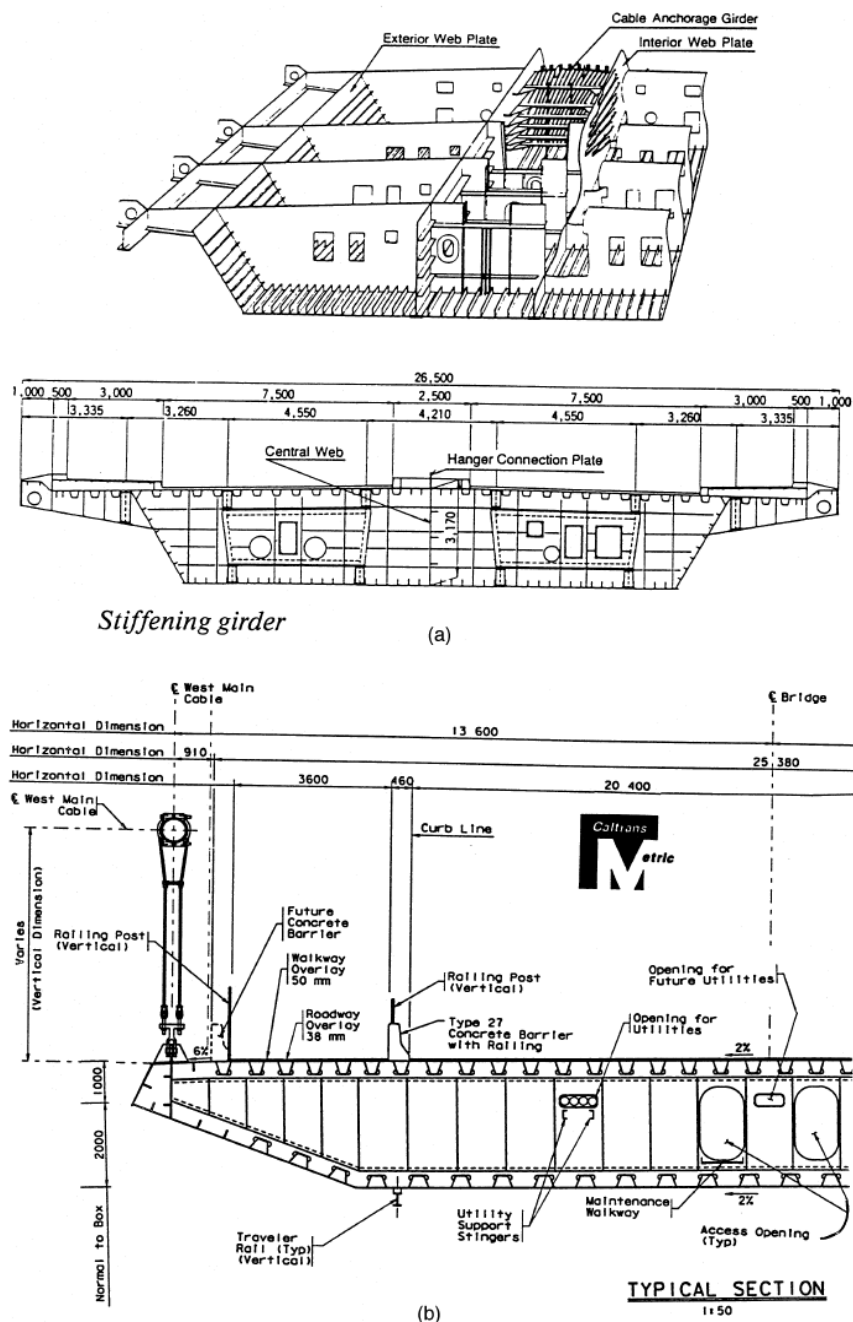


FIGURE 3-54 Examples of orthotropic deck box girder bridges (A.R.Mangus, 2000).

References

- [1] Tsakopoulos PA, Fisher JW. Full-scale fatigue tests of steel orthotropic decks for the Williamsburg Bridge. *Journal of Bridge Engineering*, 2003; 8(5): 323-333.
- [2] Camo S, Ye Q. Orthotropic decks-lesson learned from recent analyses and testing. *International Orthotropic Bridge Conference*, 2004, Sacramento, U.S.A.
- [3] Connor RJ. Influence of cutout geometry on stresses at welded rib to diaphragm connections in the steel orthotropic bridge decks. *Journal of the Transportation Research Board*, 2004; 1892: 78-87.
- [4] Eurocode 3. *Design of Steel Structures*, 2004.
- [5] AASHTO. *AASHTO LRFD Bridge Design Specifications*, 2005.
- [6] Kiss K, Dunai L. Fracture mechanics based fatigue analysis of steel bridge decks by two-level cracked models. *Computers and Structures*, 2002; 80: 2321–2331.
- [7] Xiao ZG. Fatigue cracks in longitudinal stiffeners of steel orthotropic deck. *International Journal of Fatigue*, 2006; 28: 409-416.
- [8] NTC. *Norme Tecniche per le Costruzioni*, 2008 (In Italian).
- [9] Lehrke H. Fatigue tests on large size specimens of stiffener to diaphragm connections. *IABSE Volume: Remaining Fatigue Life of Steel Structures*, ETH-Honggerberg, Zurich; 1990: 249-258.
- [10] Caramelli S, Froli M, Croce P, Sanpaolesi L. Ermudungsverhalten Orthotrope Platten in Stahlbrücken. *IABSE Volume: Remaining Fatigue Life of Steel Structures*, ETH-Honggerberg, Zurich; 1990: 271-280.
- [11] Connor RJ. Influence of cutout geometry on stresses at welded rib to diaphragm connections in the steel orthotropic bridge decks. *Journal of the Transportation Research Board*, No.1892, 2004; 78-87.
- [12] Fryba L, Gajdos L. Fatigue properties of orthotropic decks on railway bridges. *Engineering Structures*, 1999; 21: 639–652.
- [13] Pfeila MS, Battista RC, Mergulhão A JR. Stress concentration in steel bridge orthotropic decks. *Journal of Constructional Steel Research*, 2005; 61: 1172-1184.
- [14] Yarnold MT, Wilson JL, Jen W, Yen BT. Local buckling analysis of trapezoidal rib orthotropic bridge deck systems. *Bridge Structures*, 2007; 3(2): 93-103.

- [15] AASHTO LRFD Bridge Design Specifications. 2005.
- [16] Tinawi R. Orthotropic bridge decks with closed stiffeners-analysis and behaviour. *Computer & Structure*, 1976; 7: 683-699.
- [17] Bocchieri WJ, Fisher JW. Williamsburg Bridge Replacement Orthotropic Deck As-built Fatigue Test. ATLSS Report No. 98-04. May, 1998.
- [18] Connor RJ, Fisher JW. Results of Field Measurements on the Williamsburg Bridge Orthotropic Deck. ATLSS Report No. 01-01. January, 2001.
- [19] Abruzzese D, Qian ZH. Fatigue Problems for Orthotropic Deck Bridges. Handling Exceptions in Structural Engineering: Robustezza Strutturale, Scenari Accidentali, Complessità di Progetto”;University of Rome “La Sapienza”, Italy: DOI: 10.3267/HE2008, (2008).
- [20] Tsakopoulos PA, Fisher JW. Fatigue performance and design refinements of steel orthotropic deck panels based on full-scale laboratory tests. *Steel structures*, 2005; 5: 211-223.
- [21] Connor RJ, Fisher JW. Consistent approach to calculating stresses for fatigue design of welded rib-to-web connections in steel orthotropic bridge decks. *Journal of Bridge Engineering*, 2006; 11(5): 517-525.
- [22] Troitsky MS. Orthotropic Bridges - Theory and Design, 2nd ed., The James F. Lincoln Arc Welding Foundation, Cleveland, 1987.
- [23] AISC. Design manual for orthotropic steel plate bridges. New York: American Institute of Steel Construction; 1963.
- [24] Japanese specification for highway bridges, Part II steel bridge. Tokyo: Japan Road Association, 1996.
- [25] Mangus AR, Sun S. Orthotropic Deck Bridges. *Bridge Engineering Handbook* (Ed. Wai-Fah Chen and Lian Duan). Boca Raton: CRC Press, 2000.

CHAPTER 4

FATIGUE EVALUATION OF ORTHOTROPIC DECK

Fatigue design is an important task in the design of a steel bridge. An orthotropic deck, which has many welded connections, is sensitive to fatigue cracking under repeated vehicle loading. Therefore, more attention should be paid to it.

Metal Fatigue has been studied from the start of the industrial age. Figure 4-1 shows three different cracking modes in materials. The crack front can be subjected to three primary loading modes and their combinations due to different load cases. Idealized planar crack problems are considered, in which the stresses and strains near the crack tip can be expressed in terms of the in-plane coordinates x and y only. As shown in Figure 4-1a, the crack of Mode I (the opening or tensile mode) where the in-plane stresses and strains are symmetric with respect to the x axis. As shown in Figure 4-1b, the crack of Mode II (the sliding or in-plane shearing mode) where the stresses and strains are anti-symmetrical with respect to the x axis. As shown in Figure 4-1c, the crack of Mode III (the tearing or anti-plane shearing mode) where the out-of-plane stresses and strains are anti-symmetrical with respect to the x axis.

The fatigue investigations of steel structures have a long history. The modern study of fatigue is generally dated from the work of Wöhler, a technologist in the German railroad system. He did a large number of fatigue tests from 1852 to 1869, and presented S-N curve to describe the fatigue performance. In memory of his great contribution, S-N curve is also called Wöhler curve. Figure 4-2 shows typical S-N curves.

In 1874, Gerber investigated the design method of fatigue, and introduced mean stress to calculate the fatigue life. Goodman discussed the similar problems. In 1910, Basquin presented the empirical laws of metal S-N curves. He expressed fatigue in this mathematical form $\Delta S \cdot N^b = \text{constant}$. When the logarithm is taken on both sides of the equation the following expression results:

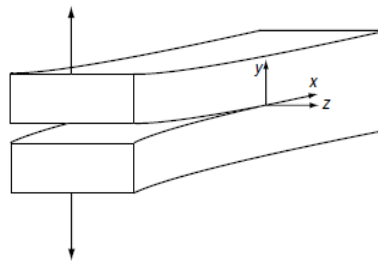
$$C - b \cdot \log(N) = \log(\Delta S)$$

Where N is the number of cycles to failure and ΔS is the stress range applied. This is the form in which the database is given in all modern codes, and in which the slope b is typically -3 at the higher stress levels.

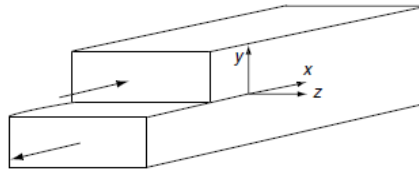
In 1929, Haigh studied the sensitivity of notch. In 1945 Miner presented linear damage cumulative rules based on the investigations of Palmgren. The Miner-Palmgren rule is expressed as follows:

$\sum n_i/N_i = C$ where “ n_i ” is the number of cycles in the load spectrum stressed at ΔS_i , which fail after N_i cycles, and C is a constant typically taken close to 1.

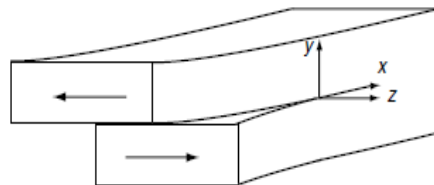
Later, Coffin and Manson presented the relationship between the plastic strain and fatigue life respectively.



a. Mode I (opening mode);



b. Mode II (in-plane shearing mode);



c. Mode III (out-of-plane shearing mode).

FIGURE 4-1 Cracking modes.

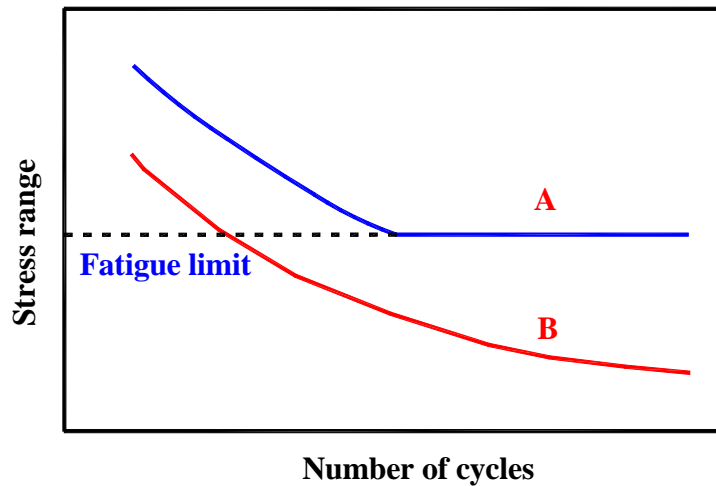


FIGURE 4-2 Typical S-N curves.

Figure 4-3 [1] shows the fatigue damage process that crack nucleation starts at the highest stress concentration position in the persistent slip bands. The second step in the fatigue process is the crack propagating stage. This stage is divided into the propagation of Stage I and Stage II.

In Stage I, crack nucleation and growth (initiation) are usually considered to be the initial short crack propagation across a limit length of the order of a couple of grains on the local maximal shear stress plane. In this stage, the crack tip plasticity is greatly influenced by the slip characteristics, grain size, orientation, and stress level, since the crack size is comparable to the material microstructure.

In Stage II, crack growth refers to long crack propagation normal to the principal tensile stress plane globally and in the maximum shear stress direction locally. In this stage, the characteristics of the long crack are less influenced by the properties of the microstructure than the crack of Stage I. This is because the crack tip plastic zone for Stage II is much larger than the material microstructure. It is noted that the failure stage is not described in Figure 4-3.

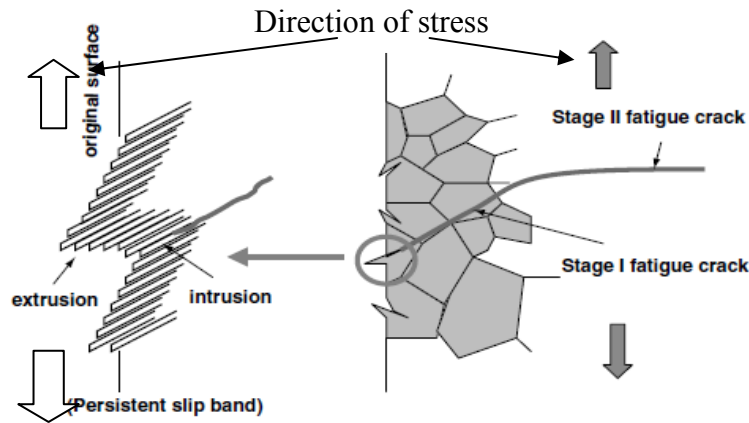


FIGURE 4-3 The fatigue process under cyclic tensile loading (Lee et al., 2005).

Make correction in left of figure (Persistent slip bands)

In welded structures, Stage I is short lived because the defects, microscopic slag inclusions, produced by welding are already present at the toe or the root of the weld, and are equivalent to some degree of crack initiation. Therefore, it can be said that for all practical purposes a weld detail will either propagate or it will not, and that initiation has no life, unless the weld is of a special kind.

The fatigue cracking behavior of many materials can be divided into three regions, as shown in Figure 4-4. Region I is the fatigue threshold region where the stress range is too low to propagate a crack. Region II encompasses data where the rate of crack growth changes roughly linearly with a change in stress intensity fluctuation. In region III, small increases in the stress intensity amplitude will produce relatively large increases in crack growth rate (unstable crack growth) since the material is nearing the point of fracture.

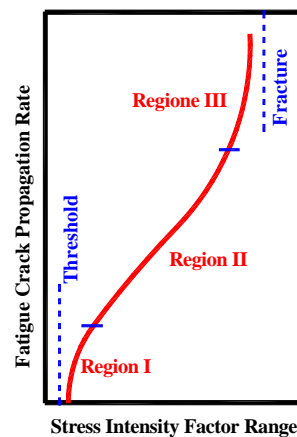


FIGURE 4-4 Fatigue cracking process.

Many factors influence fatigue life. They are:

- Material properties: chemical and physical compositions, textures, and internal defects;
- State of specimen: notch effect, size effect, surface condition, and residual stress condition;
- Work conditions: loading conditions (load mode or combination thereof, load spectrum, load frequency, load history), temperature, and other environmental conditions leading to corrosion, which affects fatigue life.

There are two different methods to obtain the fatigue life of a structure: the experimental method and the analytical method. The experimental method is the traditional way to know the fatigue life, and is very reliable. However, it is difficult to use this method during the design stage due to the possible use of many different geometric shapes, and proportions. It consumes too much time and expenditure. It should be noted that some Bridge authorities have confirmed the viability of prototype designs (derived analytically), using “full-scale” tests in the final design stage of important structures, such as long span bridges.

The analytical method is based on confirmed theories and the results of prior fatigue tests, referred to as database, such as is included in design codes. There are several different analytical methods to evaluate the fatigue life, such as nominal stress approach, local stress-strain approach, stress field intensity approach and hot spot structural stress approach. With the development of the computer technologies and the FE technique, the analytical method is now taking hold in the design stage in structural engineering, while prototype fatigue test is often the prerogative of the owner who wants to ensure the longevity of the structure to justify the initial expenditure.

Today, fatigue design codes are widely applied in the design of bridges, vehicles, offshore structures and other steel structures. In bridge engineering the following come to mind: BS5400, Eurocode3, AASHTO. Although the history of fatigue design codes is very short, fatigue design had already started early in the history of engineering of the industrial age. BS5400 (1980) is a milestone because it is the first

European standard which provided detailed fatigue design specifications. In the U.S., the “Fracture Control Plan was introduced in 1978. These codes contained simple standard bridge details and associated resistance curves. However, orthotropic decks require complex details to reduce fatigue stresses. It follows that some relationship between the resistance of the simple code details and the orthotropic deck details must be found, or some resistance categories must be developed directly by testing for the more complex details.

4.1 Design Codes

Before the 1970’s, there was little fatigue data for the design of welded structures. The databases, which were developed in the late 60’s and 70’s by Fisher (U.S.) and Gurney (U.K.), were based on the mean stress level in the general area of the detail (such as that of a flange near a welded stiffener, for example). The ensuing design approach adopted by the codes of that era, and still in use today, has come to be known the “nominal stress approach”. However, even before the turn of the century, engineers of orthotropic deck projects realized that in orthotropic deck details there are high stress gradients with areas of high stress intensity (otherwise called “hot spots”). It became truly confusing to determine at what point in the geometry of the detail to take the mean stress (presently also referred to as structural stress). Working independently from the bridge industry, researchers for the offshore industry had to develop more accurate and stringent criteria to address the fatigue problems of welded pipes in a sea environment. In the automotive and rail car industries Engineers had to address similar problems. A method had to be found to give a resistance category to unusual details. Researchers who have paid attention to this issue are E. Niemi, W. Fricke, S.J. Maddox, P. Marshall, P. Dong and probably many others. While bridge codes are still trying to deal with the “orthotropic deck issue”, the above named researchers have already published criteria, not yet incorporated into codes, which address the question of the “hot spot” by judicious use of the Finite Element.

In the description of bridge codes which follows, the experimental database is described in graphs on log-log coordinates, where the abscissa is in units of log N (number of cycles) against the log of the stress range on the ordinate. These are called S-N curves. Thus, the specimens were tested at constant stress range cycles.

Each point in any curve represents the logarithm of the number of uniform cycles it takes to fail the detail at the logarithm of the stress range applied.

4.1.1 European codes

4.1.1.1 British standard (BS5400)

The British Standard BS5400 [2] is one of the pioneering fatigue codes in the world. In the 10th part of the British Standard BS5400, it defines the followings:

- The fatigue design loads to be applied;
- The allowable stress ranges for a service life of 120 years;
- The procedure for fatigue evaluation.

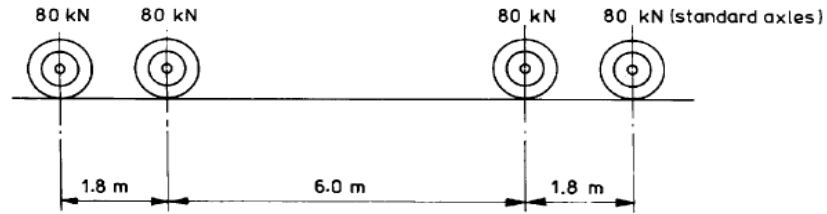
However, this British Standard (1980) takes no account of the possible onset of unstable fracture from a fatigue crack. This possibility should be considered and guarded against by appropriate material selection.

The Standard Fatigue Vehicle is a concept used to represent the effects of the standard load spectrum (i.e. cause equivalent damage as a standard spectrum). For highway bridges this is a single vehicle with a weight of 320 kN. In the BS 5400 code, the vehicle dimensions are provided as shown in Figure 4-5.

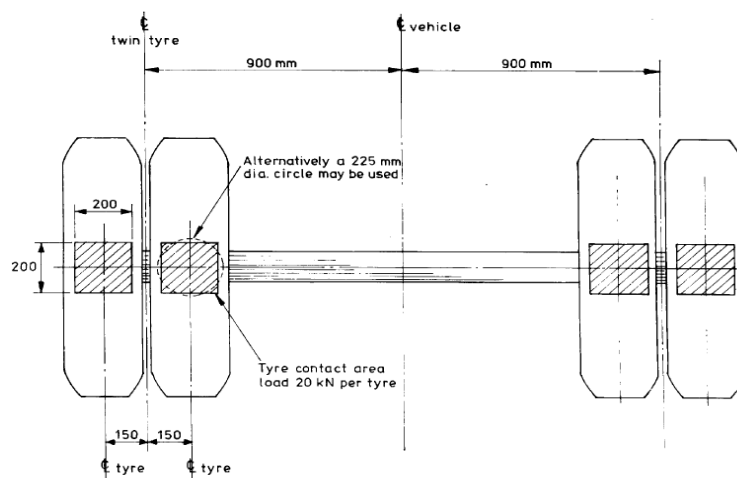
To be correct, the stress effects on the detail being assessed should be derived by passing each vehicle in the truck spectrum along the various lanes. Also, account should be taken of the possibility of higher stress ranges due to some of the vehicles occurring simultaneously in more than one lane (called the effect of multiple occupancy).

The design spectrum may be divided into any convenient number of intervals (of

quantity per unit time vs. stress range). To each interval is assigned a maximum range. Figure 4-6 shows the simplification of a spectrum. It should be noted that the use of small intervals will fatigue assessment more accurate.



a. Axle arrangement of standard fatigue vehicle;



b. Plan of standard axle;

FIGURE 4-5 Vehicle loading (BS5400, 1980).

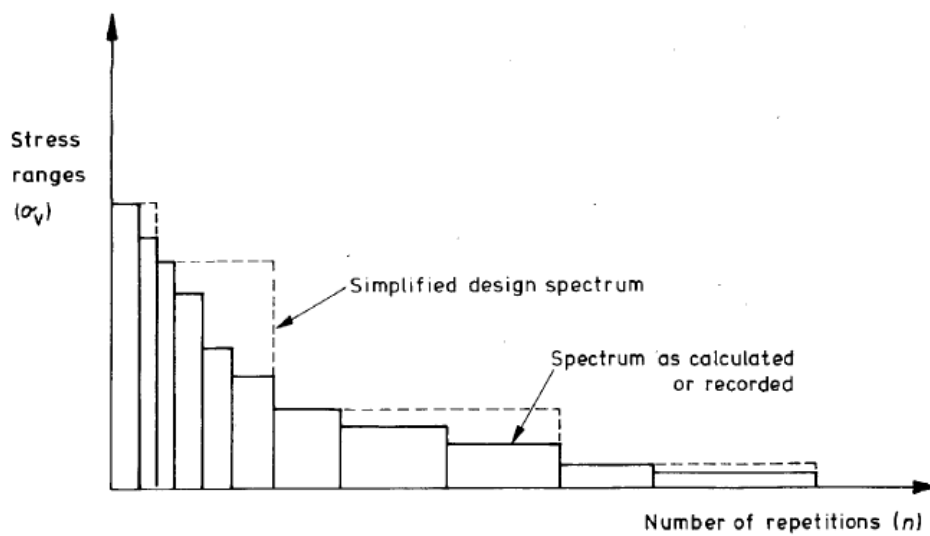
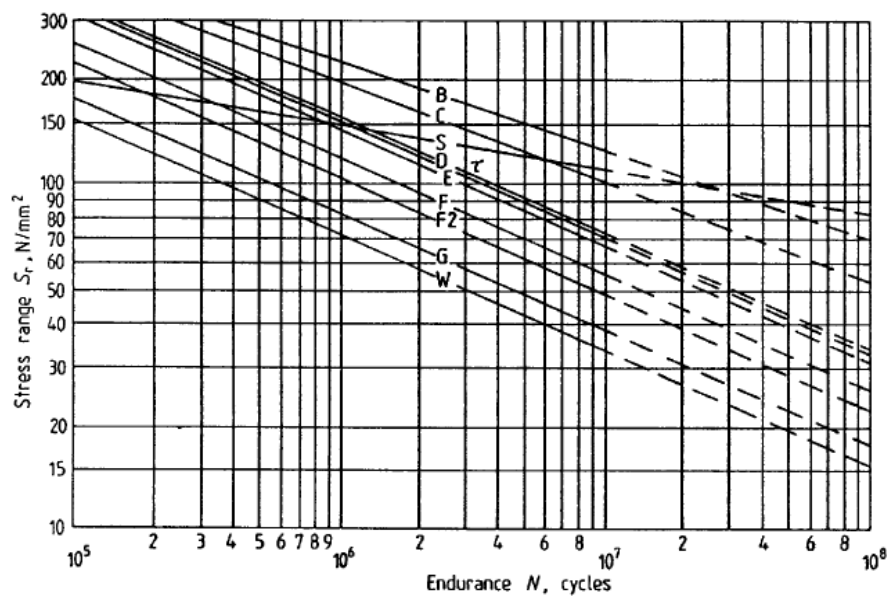


FIGURE 4-6 Simplification of a spectrum (BS5400, 1980).

Highway loading in BS5400 is applicable to the fatigue design of orthotropic deck bridges. However, the stress analyses and classification of details in such bridges is very complex and is beyond the scope of this British Standard.

The classifications (database) given in BS5400, while satisfactory for conventional bridge design may not be applied with full confidence to welded connections in orthotropic decks, because of complex details and stress patterns which occur in such structures.

However, the classifications of welded connections in BS5400 are very important to the fatigue design of conventional bridges because the S-N curves presented therein make assessment simple. Figure 4-7 shows the S-N curves in BS5400.



NOTE. The use of these curves for calculation purposes is not recommended.

FIGURE 4-7 Summary of mean-line S_r -N curves (BS5400, 1980).

Although this British Standard provide information for fatigue design of bridges, it can not be applied to the followings:

- Orthotropic decks;
- Wire ropes;
- Steel reinforcement in concrete;
- Pressure vessels;
- Castings.

The BS5400 (1980) has been updated many times, fatigue design for the welded connections of orthotropic deck are still not fully solved.

4.1.1.2 Eurocode 3

The European fatigue design code-Eurocode 3, part 1.9 [3], developed from the version of EN 1993-1-9, is widely utilized in Europe now. This new version is based on the fatigue investigations in the past 10 years.

The following parts for the fatigue design are taken from Eurocode 3:

- a) More refined S-N curves, compared to BS5400, are presented in this code, as shown in Figure 4-8. In this code, the S-N curves have three regions. The slope of the S-N curve before 5-million cycles is 3, while from 5-million to 10-million is 5 (10-million is the fatigue limit);

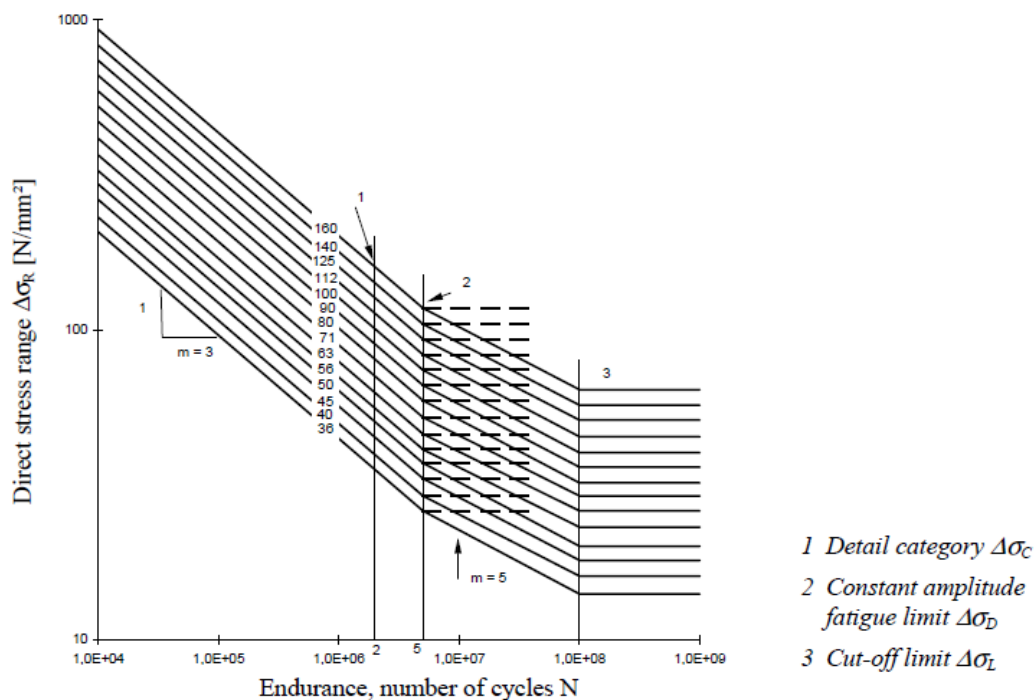


FIGURE 4-8 S-N curves for direct stress ranges (Eurocode 3, 2004).

- b) It provides methods for the evaluation of fatigue resistance of members, connections and joints subjected to the fatigue loading. These methods are derived

from fatigue tests with large scale specimens, including the geometrical effects and structural imperfections from material production and execution (e.g. the effects of tolerances and residual stresses from welding). The evaluation methods given in this code are applicable to all grades of structural steels, stainless steels and unprotected weathering steels except where noted. It only applies to materials which conform to the toughness requirements of EN 1993-1-10;

- c) Fatigue assessment methods other than the $\Delta\sigma_R - N$ methods are not included;
- d) Post fabrication treatments to improve the fatigue strength other than stress relief are not included.

Furthermore, main welded details of orthotropic deck are classified in this code, as shown in Table 4-1 and Table 4-2. Although not all welded connections are included in these two tables, the code provides great benefits to the fatigue design of orthotropic deck bridges.

TABLE 4-1 Orthotropic decks - open ribs.

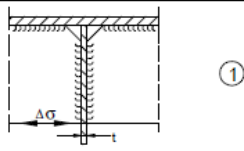
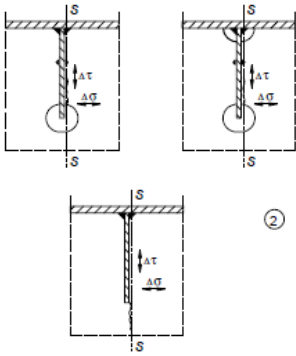
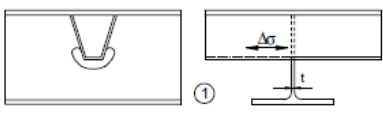
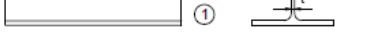
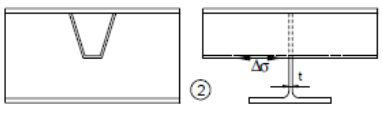
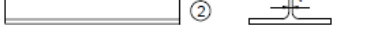

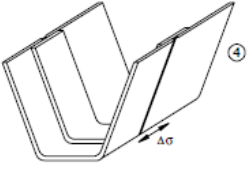
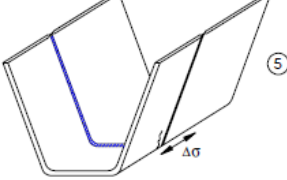
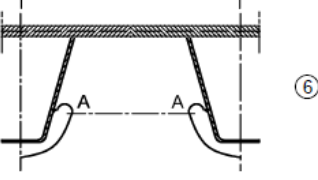
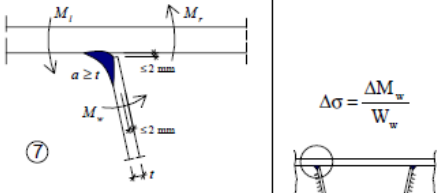
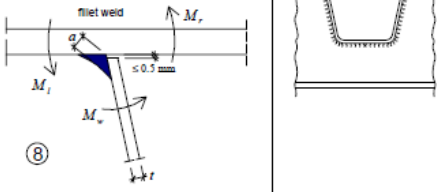
Detail category	Constructional detail		Description	Requirements
80	$t \leq 12\text{mm}$		1) Connection of longitudinal stringer to cross girder.	1) Assessment based on the direct stress range $\Delta\sigma$ in the stringer.
71	$t > 12\text{mm}$			
56			2) Connection of continuous longitudinal stringer to cross girder. $\Delta\sigma = \frac{\Delta M_s}{W_{net,s}}$ $\Delta\tau = \frac{\Delta V_s}{A_{w,net,s}}$ Check also stress range between stringers as defined in EN 1993-2.	2) Assessment based on combining the shear stress range $\Delta\tau$ and direct stress range $\Delta\sigma$ in the web of the cross girder, as an equivalent stress range: $\Delta\sigma_{eq} = \frac{1}{2} \left(\Delta\sigma + \sqrt{\Delta\sigma^2 + 4\Delta\tau^2} \right)$

TABLE4-2 Orthotropic decks – closed ribs.

Detail category	Constructional detail		Description	Requirements
80	$t \leq 12\text{mm}$		1) Continuous longitudinal stringer, with additional cutout in cross girder.	1) Assessment based on the direct stress range $\Delta\sigma$ in the longitudinal stringer.
71	$t > 12\text{mm}$			
80	$t \leq 12\text{mm}$		2) Continuous longitudinal stringer, no additional cutout in cross girder.	2) Assessment based on the direct stress range $\Delta\sigma$ in the stringer.
71	$t > 12\text{mm}$			
36			3) Separate longitudinal stringer each side of the cross girder.	3) Assessment based on the direct stress range $\Delta\sigma$ in the stringer.
71			4) Joint in rib, full penetration butt weld with steel backing plate.	4) Assessment based on the direct stress range $\Delta\sigma$ in the stringer.
112	As detail 1, 2, 4 in Table 8.3		5) Full penetration butt weld in rib, welded from both sides, without backing plate.	5) Assessment based on the direct stress range $\Delta\sigma$ in the stringer. Tack welds inside the shape of butt welds.
90	As detail 5, 7 in Table 8.3			
80	As detail 9, 11 in Table 8.3			
71			6) Critical section in web of cross girder due to cut outs.	6) Assessment based on stress range in critical section taking account of Vierendeel effects. NOTE In case the stress range is determined according to EN 1993-2, 9.4.2.2(3), detail category 112 may be used.
71			<u>Weld connecting deck plate to trapezoidal or V-section rib</u> 7) Partial penetration weld with $a \geq t$	7) Assessment based on direct stress range from bending in the plate.
50			8) Fillet weld or partial penetration welds out of the range of detail 7)	8) Assessment based on direct stress range from bending in the plate.

4.1.1.3 DNV offshore specifications

The Det Norske Veritas (DNV) [4] offshore specifications explain very detailed to the fatigue design, not only including S-N curves, welded connections, and the methods of fatigue analyses, but also the calculation of hot spot stress by FE analyses and improvement technologies of fatigue life. It is not only a specification for offshore structure, but also very helpful to other steel structures, such as orthotropic deck bridges. This specification provides S-N curves both in air and in seawater. Figure 4-9 shows the S-N curves in air.

Compared with BS5400 and Eurocode 3, the S-N curves in this specification are bilinear. Furthermore, it is found that different details may have different slopes of S-N curves, while after experienced more than 10-million cyclic loading the slopes become the same.

The offshore specification also provides some useful information related to orthotropic deck structures. It is known that the orthotropic deck is originated from ship structure, thus, some similar welded connections are found in this specification, as shown in Table 4-3. The detail 9 is almost the same to the rib-to-deck plate connection in the orthotropic deck, which is one of the most important welded connections.

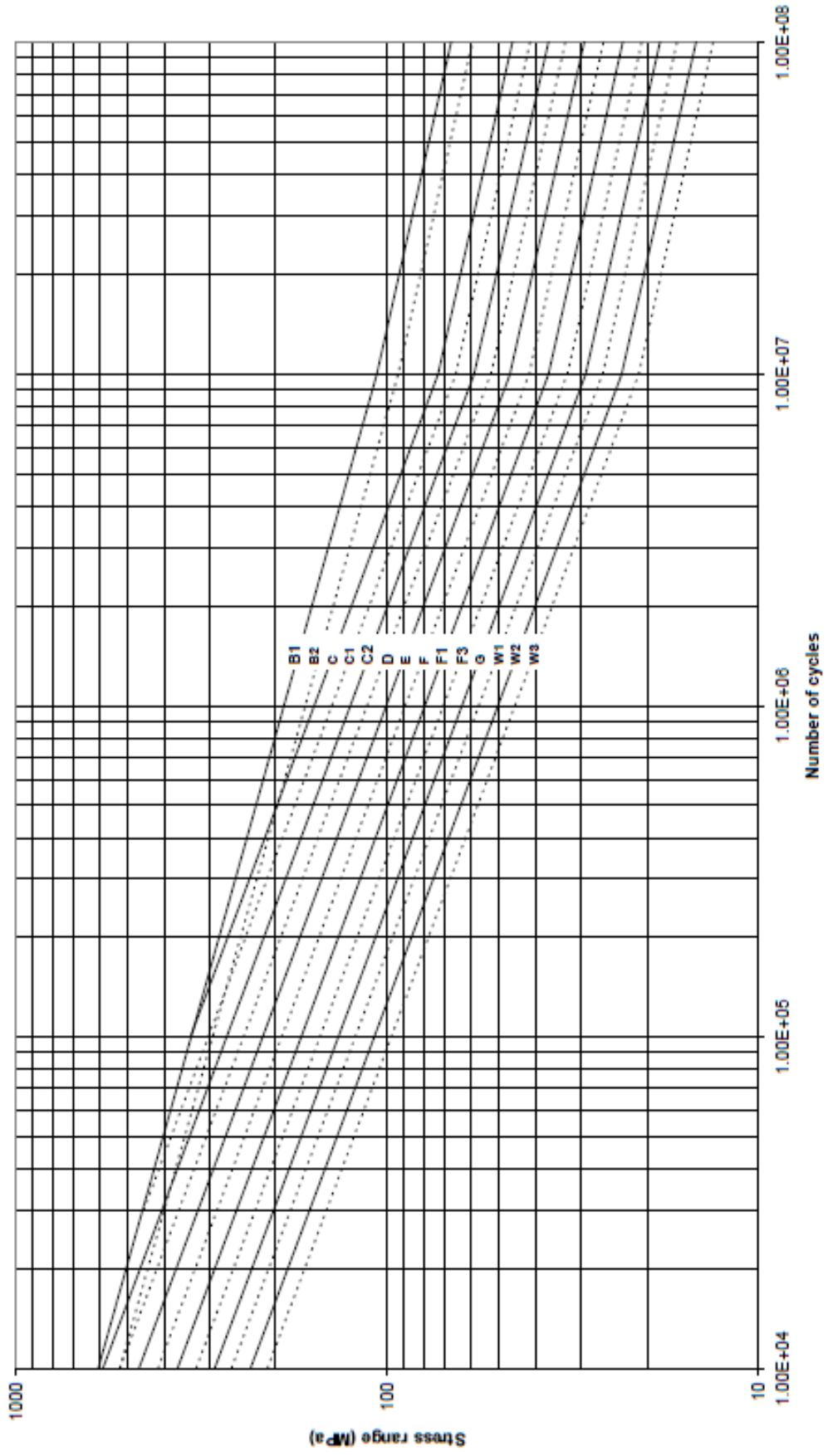
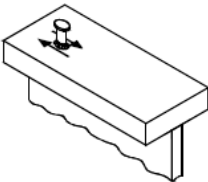
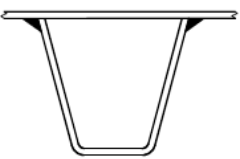
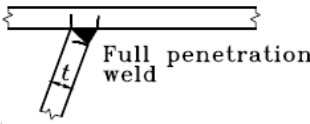
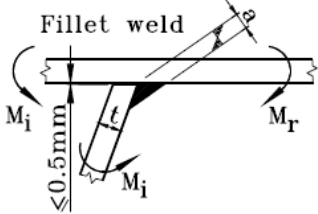


FIGURE 4-9 S-N curve (LRFD, 1999)

TABLE 4-3 Welded connections similar to orthotropic deck (DNV, 2005).

Detail category	Constructional details	Description	Requirement
E	8. 	8. Stud connectors (failure in the weld or heat affected zone).	8. <ul style="list-style-type: none"> — The shear stress to be calculated on the nominal cross section of the stud.
	9. 	9. Trapezoidal stiffener welded to deck plate with fillet weld or full or partial penetration butt weld.	9. <ul style="list-style-type: none"> — For a full penetration butt weld, the bending stress range shall be calculated on the basis of the thickness of the stiffener. — For a fillet weld or a partial penetration butt weld, the bending stress range shall be calculated on the basis of the throat thickness of the weld, or the thickness of the stiffener if smaller.
F			
G			

4.1.2 American specifications

There are several American design specifications/codes that include the fatigue design, such as “LRFD Specification for Structural Steel Buildings, 1999” [5] and “AASHTO LRFD Bridge Design Specifications, 2005” [6].

The AASHTO LRFD Bridge Design Specifications provide more information to the design of orthotropic decks.

The S-N curves in AASHTO provided to the bridge designers are bilinear which are ease to apply in the design stage.

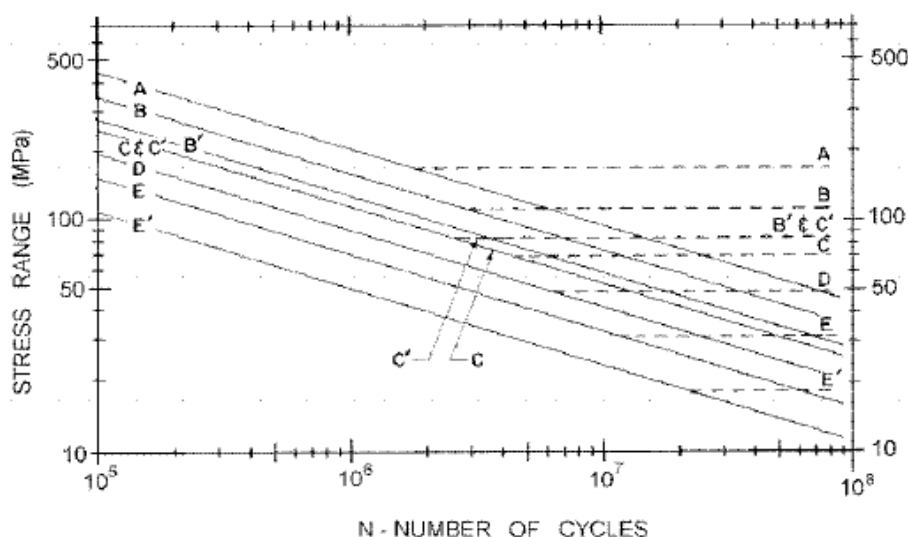


FIGURE 4-10 Stress range versus number of cycles (AASHTO, 2005).

Detail categories for the components in the orthotropic deck are presented in AASHTO. Plate splice, rib splice, rib-to-diaphragm connection and deck plate-to-diaphragm connection are listed in the specification, as shown in Table 4-4. Although still many other welded connections are not included in this specification, it provides great benefits to the bridge designer compared with the previous specifications. Both the Eurocode 3 (2004) and AASHTO (2005) are the milestones in the fatigue design of orthotropic deck bridges.

Propagation thresholds are presented in Table 4-5. It is noted that propagation

thresholds (also called the endurance limits) are also illustrated in figure 4-10 as dashed horizontal lines. It is noted that in AASHTO a category between C and D is the equivalent of Fatigue 71 in Eurocode 3 up to 2 million cycles.

According to AASHTO if all the stress ranges in the load spectrum are below the propagation threshold, then the detail will have an infinite life, i.e. it will never fail by fatigue. The concept of infinite life as described in AASHTO is being contested and may have to be revised as can be intuited from the fact that, at much higher number of cycles, the AASHTO Category C-D does not agree with Eurocode 3 and other European codes.

Table 4-4 Detail categories for load-induced fatigue of orthotropic decks
(AASHTO, 2005).

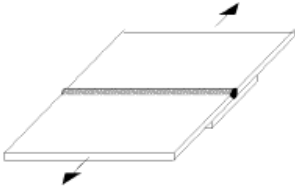
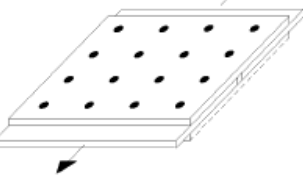

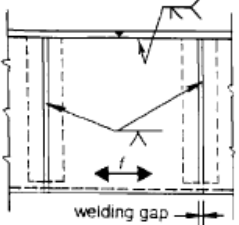
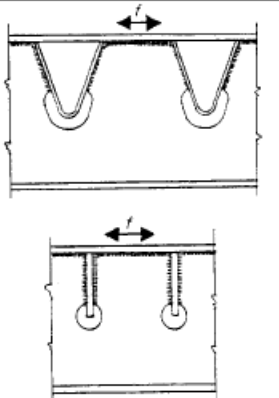
ILLUSTRATIVE EXAMPLE	DETAIL	DESCRIPTION OF CONDITION	DETAIL CATEGORY
	Transverse or longitudinal deck plate splice or rib splice	(1) Ceramic backing bar. Weld ground flush parallel to stress.	B
	Single-groove butt weld	(2) Ceramic backing bar	C
		(3) Permanent backing bar. Backing bar fillet welds shall be continuous if outside of groove or may be intermittent if inside of groove.	D
	Bolted deck plate or rib splice	(4) In unsymmetrical splices, effects of eccentricity shall be considered in calculating stress.	B
	Deck plate or rib splice	(5) Plates of similar cross-section with welds ground flush. Weld run-off tabs shall be used and subsequently removed, plate edges to be ground flush in direction of stress.	B
	Double-groove welds	(6) The height of weld convexity shall not exceed 20% or weld width. Run-off tabs as for (5).	C
	Welded rib "window" field splice	(7) Permanent backing bar for rib splice	D
Single groove butt weld	Welding gap > rib wall thickness f = axial stress range in bottom of rib		
	Deck plate at the connection to floorbeam web	(12) f = axial stress range in the deck plate at the deck/floorbeam weld	E

TABLE 4-5 Fatigue Propagation Thresholds (AASHTO, 2005).

Detail Category	Threshold (MPa)
A	165.0
B	110.0
B'	82.7
C	69.0
C'	82.7
D	48.3
E'	31.0
E'	17.9
M 164M (A 325M) Bolts in Axial Tension	214.0
M 253M (A 490M) Bolts in Axial Tension	262.0

4.1.3 Recommendations of IIW

International Institute of Welding (IIW) presented “Recommendations for Fatigue Design of Welded Joints and Components” in 2003 [7]. Although specific chapter for orthotropic deck bridges is not included, it covers most of general steel structures. Thus, it can be useful to the bridge designers.

The S-N curves for normal stress and shear stress are provided in this specification. The slope of the fatigue strength curves for details assessed on the basis of normal stresses is 3.00, as shown in Figure 4-11. The propagation threshold starts at 5-million cycles. The slope of the fatigue strength curves for details assessed on the basis of shear stresses is 5.00, as shown in Figure 4-12, but in this case the propagation threshold starts at 100-million cycles.

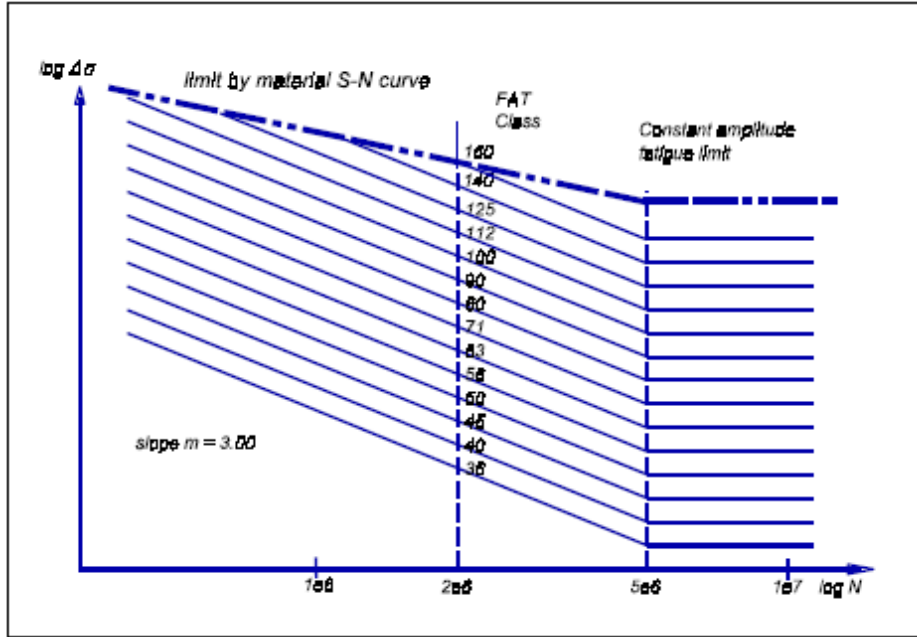


FIGURE 4-11 Fatigue resistance S-N curves, normal stress (IIW, 2003).

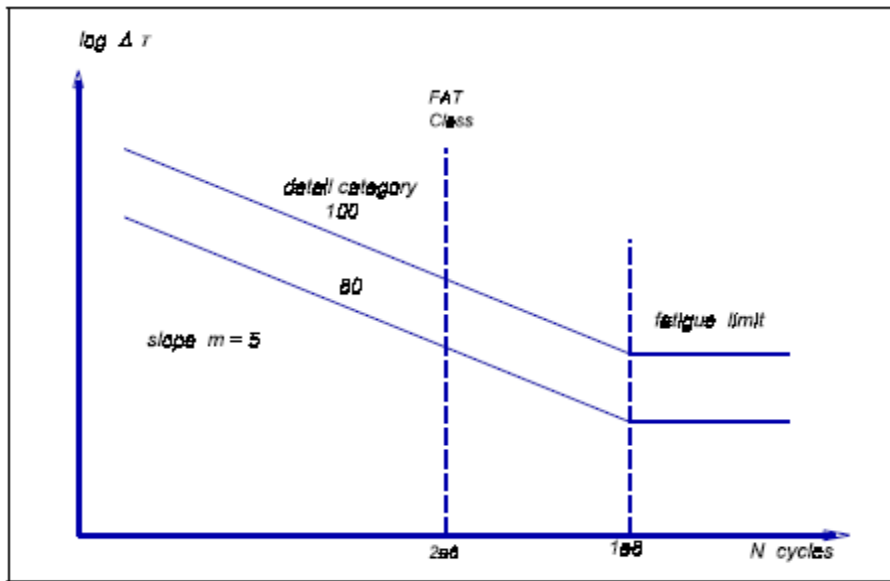


Fig. (3.2)-2 Fatigue resistance S-N curves for shear stress (steel)

FIGURE 4-12 Fatigue resistance S-N curves for shear stress (IIW, 2003).

Although the welded connections of orthotropic deck bridges are not provided, some similar connections can be found. For example, structural detail of No. 515 is almost the same to the rib-to-deck plate connection in orthotropic deck bridges, as shown in Table 4-6.

As well, this specification presents the method of structural hot spot stress. Fatigue resistances against structural hot spot stress are provided in Table 4-7. Detailed information to the welds can be found in Table 4-7.

TABLE 4-6 Welded connections existing in orthotropic deck (IIW, 2003).

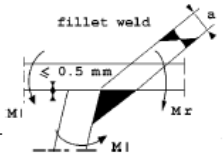
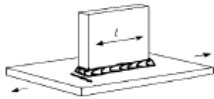
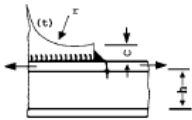


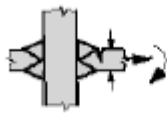
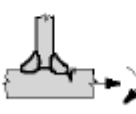
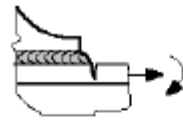

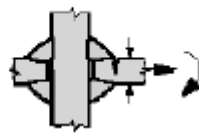
No.	Structural Detail	Description (St.= steel; Al.= aluminium)	FAT St.	FAT Al.	Requirements and Remarks
515		Trapezoidal stiffener to deck plate, fillet or partial penetration weld, calculated on basis of stiffener thickness and weld throat, whichever is smaller	45	16	
521		Longitudinal fillet welded gusset at length l $l < 50$ mm $l < 150$ mm $l < 300$ mm $l > 300$ mm	80 71 63 50	28 25 20 18	For gusset near edge: see 525 "flat side gusset" If attachment thickness $< 1/2$ of base plate thickness, then one step higher allowed (not for welded on profiles!)
522		Longitudinal fillet welded gusset with radius transition, end of fillet weld reinforced and ground, $c < 2t$, max 25 mm $r > 150$ mm	90	32	t = thickness of attachment

TABLE 4-7 Fatigue resistance against structural hot spot stress (IIW, 2003).

No.	Structural detail	Description	Requirements	FAT Steel	FAT Alu.
1		Butt joint, special quality	See details 1) to 3) in table 8.3, for misalignment see note below.	112	45
2		Butt joint, standard quality	See detail 7) in table 8.3, for misalignment see note below.	100	40
3		Cruciform joint with full penetration K-butt welds	Weld toe angle $\leq 60^\circ$, for misalignment see note below.	100	40
4		Non load-carrying fillet welds	Weld toe angle $\leq 60^\circ$, for misalignment see note below	100	40
5		Bracket ends, ends of longitudinal stiffeners	Weld toe angle $\leq 60^\circ$	100	40
6		Cover plate ends and similar joints	Weld toe angle $\leq 60^\circ$	100	40
7		Cruciform joints with load-carrying fillet welds	Weld toe angle $\leq 60^\circ$, for misalignment see note below.	90	36

Note: Table does not cover effects of misalignment. They have to be considered explicitly in determination of stress

4.1.4 Japanese specifications

Bridge engineering became highly developed after World War II in Japan. A large number of long span bridges have been built all over Japan, and many investigations have been carried out with fruitful results. The “Fatigue Design Specifications for Steel Bridges” [8] is one of the most outstanding fruits, which elaborates how to carry out the fatigue design for steel bridges.

S-N curves, both for normal stress and shear stress, are provided in the specifications, as shown in Figure 4-13 and Figure 4-14. Similar with the recommendations of IIW, the slope of the fatigue strength curves for details assessed on the basis of normal stresses is 3.0, as shown in Figure 4-13; while the slope of the fatigue strength curves for details assessed on the basis of shear stresses is 5.0, as shown in Figure 4-14. Furthermore, the S-N curves for both constant amplitude and variable amplitude load cycles are shown.

In addition, the specifications provide the design of some details. For instance, fatigue cracks near the rib-to-diaphragm-to-deck plate connection are shown in Figure 4-15. Different fatigue cracks at that connection are presented.

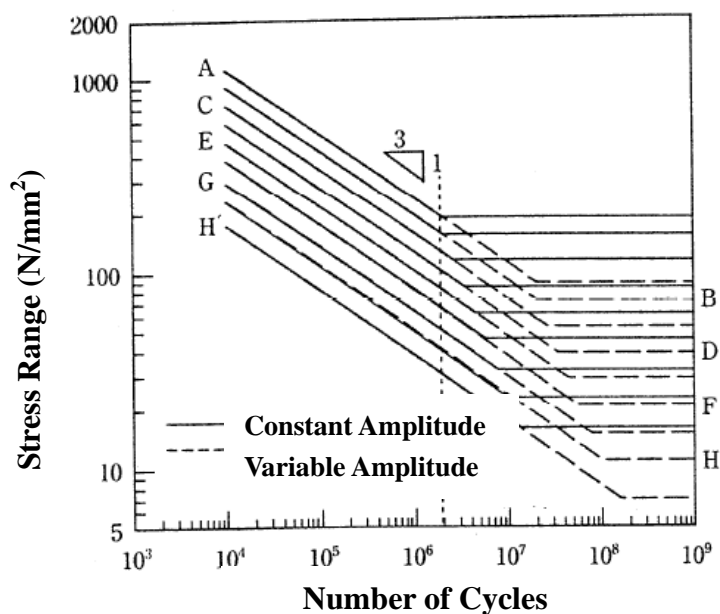


FIGURE 4-13 S-N curves (normal stress) in the Japanese code.

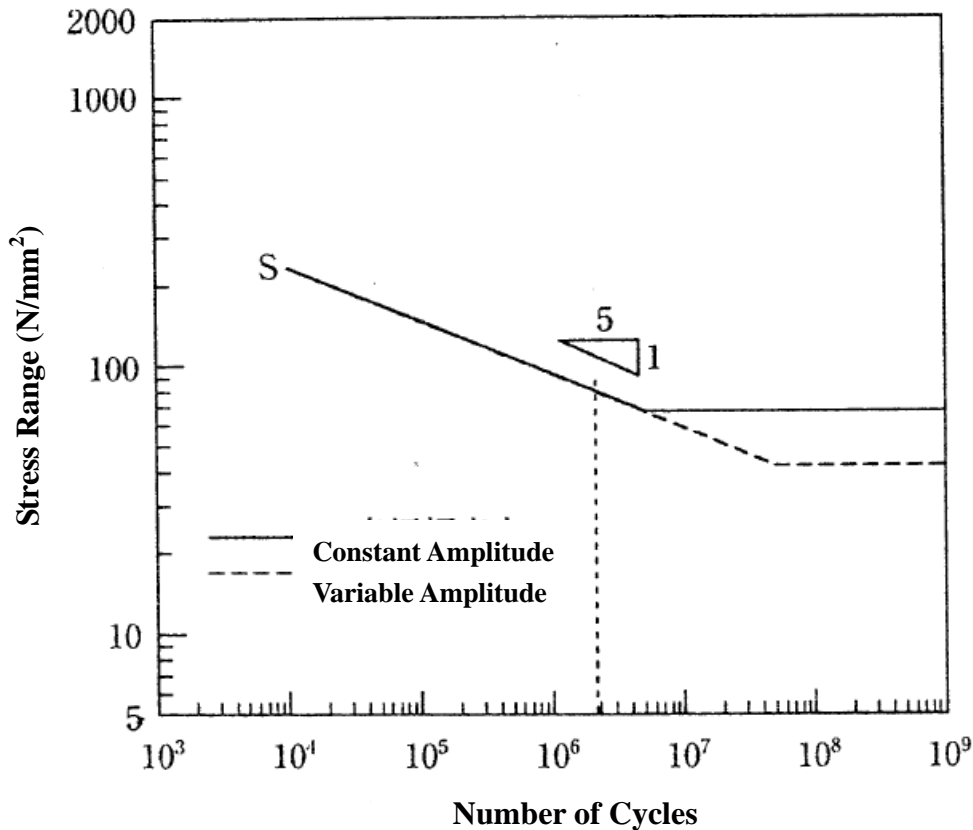


FIGURE 4-14 S-N curves (shear stress) in the Japanese code.

It is noted that at 2 Million cycles Fat 71 of the Eurocode is equivalent to Category G in the Japanese Code. The “knee”, where the propagation threshold starts, for constant amplitude loading is taken at about 30 Mpa. If used with an effective truck this threshold is similar to that of AASHTO (69Mpa/2). However, for variable amplitude loading the threshold is estimated from the graph to be about 17 Mpa and the slope of the line does not change to -5 as in the Eurocode. For limited life, the AASHTO Code is more conservative because the slope of the N curve is assumed to remain -3. But this is the detriment of orthotropic decks which must have long life to be commercially competitive.

It is evident that the Codes are not in agreement at low stress range and high number of cycles. But this is precisely what is of interest in orthotropic deck fatigue analysis, because they must last a long time to be economically competitive against other deck systems.

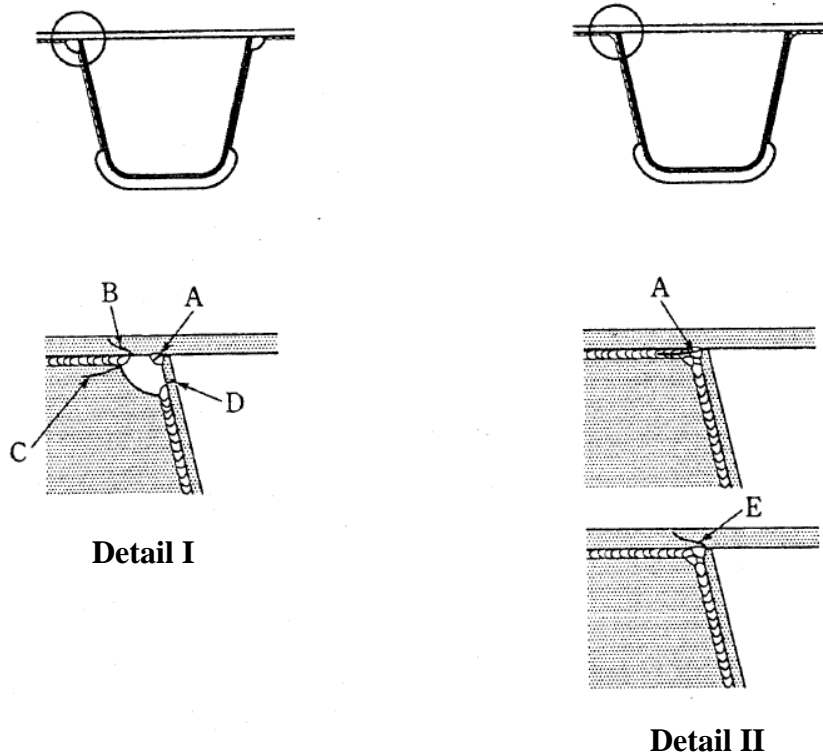


FIGURE 4-15 Fatigue cracks in orthotropic deck (Japanese code, 2002).

4.1.5 Chinese Codes

Fatigue design was introduced to the structural engineering in China only recently. Therefore, there are only few parts of fatigue design covered in the Chinese codes, not like other codes or specifications.

In “Code for Design of Steel Structures (GB 50017-2003)” [9], it is prescribed that when the cycles of repetitive loading is greater than 50,000, fatigue design should be considered. Moreover, stress range is used in fatigue calculation both for constant amplitude and variable amplitude cyclic loading.

For constant amplitude loading,

$$\Delta\sigma < [\Delta\sigma] \quad (4.1)$$

For welded components, $\Delta\sigma = \sigma_{\max} - \sigma_{\min}$; and for non welded components

$$\Delta\sigma = \sigma_{\max} - 0.7\sigma_{\min} .$$

For variable amplitude loading,

$$\Delta\sigma_e \prec [\Delta\sigma] \quad (4.2)$$

$\Delta\sigma_e$ is equivalent stress range calculated according to constant amplitude stress range.

$$\Delta\sigma_e = \left[\frac{\sum n_i (\Delta\sigma_i)^\beta}{\sum n_i} \right]^{1/\beta} \quad (4.3)$$

In “Code for Design on Steel Structure of Railway Bridge (TB10002.2-99)” [10], the theory is the same to that used in “Code for Design of Steel Structures (GB 50017-2003)”. In this code, fatigue resistance formulations for S-N curves are presented according to different components.

However, no figurative S-N curves are provided in these codes, and neither in the other Chinese codes.

4.1.6 Discussion

S-N curves, are the most important fatigue design tools. Figure 4-16 shows the different S-N curve types in the above different codes. These are placed in the same graph for comparison. A comparison of all the categories is shown in Table 4-8 and Table 4-9.

Common and divergent characteristic of these S-N curves may be briefly described as follows:

- The stress range is the only parameter which impacts design life; residual stress falls within the scatter of the test data and is inherent in the S-N curves.
- Fatigue strength is classified based on a large number of laboratory tests, and their resistances are listed in Table 4-8;
- Many different kinds of details are included in the codes;
- All S-N curves of Code databases are obtained by constant amplitude testing.
- Miner’s rule is used to calculate fatigue damage due to variable amplitude loading.

Most of the S-N curves are according to the “normal stress” testing. However the testing apparatus or methodology introduces various degrees of shear in the

specimens. The variability between codes may be in part due to the degree of shear introduced in test methodology.

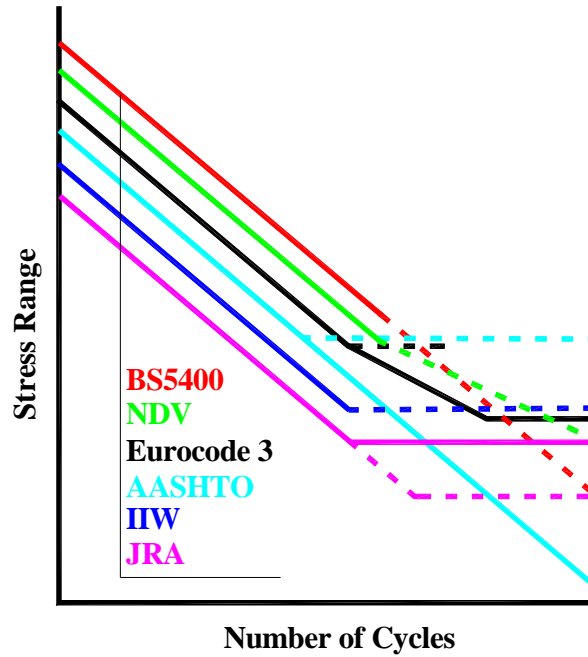


FIGURE 4-16 Different types of S-N curves in different codes/specifications.

- The critical welded details provided in these codes/specifications are insufficient for the fatigue design of orthotropic deck bridges. Many fatigue cracks result from out-of-plane distortion or other secondary stresses at fatigue sensitive details, thus, the above codes/specifications are difficult to use. Therefore, more detailed codes/specifications should be developed to help bridge designers and consulting engineering firms or a technique must be developed to calibrate complex details to equivalent design curves;
- Only some of these codes/specifications cover the improvement techniques to enhance fatigue life. The IIW and DNV are some of these:

TABLE 4-8 Categories of details.

BS5400	Eurocode 3	AASHTO	DNV	IIW	JRA
B, C	160	A	-	160	A, B
S	140	B	B1, B2	140	-
D	125	-	C	125	C
E	112, 100	B'	C1, C2	112, 100	D
F	90	C, C'	D	90	-
F2	80	-	E	80	E
-	71	D	F	71	-
G, W	63, 56	E	F1, F3	63, 56	F
-	50, 45, 40, 36	E'	G, W1, W2, W3	50, 45, 40, 36	G, H, H'

TABLE 4-9 Comparison of different codes/specifications.

Code /Specification	S-N curve	Detail categories to orthotropic deck
BS5400	straight line; m=3; 10 categories.	fatigue categories for orthotropic deck details are not covered.
Eurocode 3	trilinear; less than 5-million cycles, m=3; more between 5-million cycles to 10-millions cycles, m=5; 14 categories.	fatigue categories for orthotropic deck details (both open-rib and closed rib) are covered; including rib-to-deck plate connection, rib-to-diaphragm connection, rib splice, details around cutout, etc.
DNV	bilinear; m=3; 14 categories;	fatigue categories for orthotropic deck details are not covered.
AASHTO	bilinear; m=3; 8 categories.	specific fatigue categories for orthotropic deck details (both open-rib and closed rib) are covered; including rib-to-deck plate connection, rib-to-diaphragm connection, rib splice, etc.
IIW	bilinear; normal stress, m=3; shear stress, m=5; 14 categories.	fatigue categories for orthotropic deck details are not covered.
JRA	bilinear; normal stress, m=3; shear stress, m=5; 9 categories; variable amplitude.	fatigue categories for orthotropic deck details are covered.

4.2 Nominal Stress Approach

There are several approaches that can be used to calculate the fatigue life of the steel structure. These are: Nominal Stress Approach, Local Stress-Strain Approach, Stress Field Intensity Approach and Hot spot Structural Stress method. Among of these approaches, the Nominal Stress Approach is one of the earliest approaches, and is widely applied in structural engineering.

The fatigue life of a structure can be analyzed as shown in Figure 4-17. At first, the fatigue properties of structural materials and the structural responses under repeated loading should be known. Then, the fatigue life can be calculated according to the fatigue cumulative damage law. This law is significant to the analyses of fatigue life.

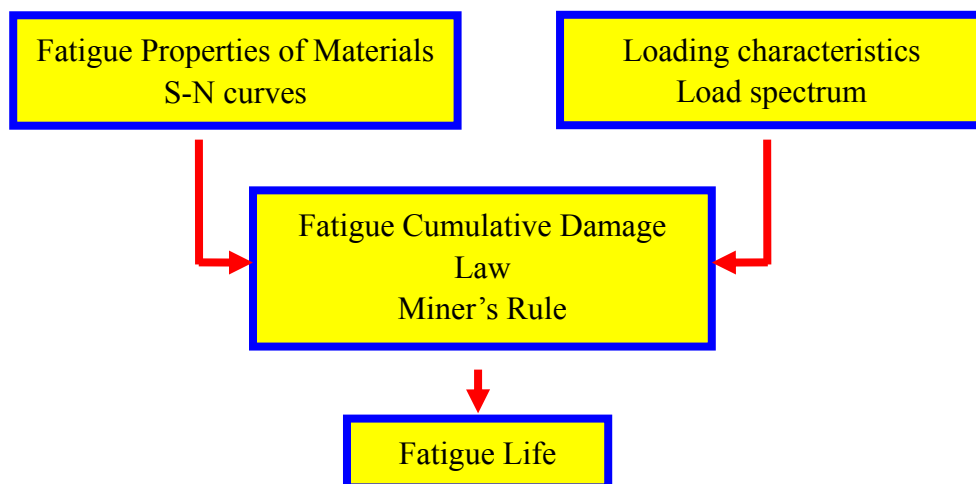


FIGURE 4-17 Analyses of fatigue life.

4.2.1 Fatigue cumulative damage law

Cumulative damage is the core issue in the design of limited life, and it is very important to the fatigue design. In 1924, Palmgren presented the linear hypothesis of fatigue cumulative damage. Then, Miner [11] developed this theory and made a formula, that is Palmgren-Miner theory or for short Miner's theory.

Later, in order to improve the precision many investigations relative to nonlinear cumulative damage were carried out based on laboratory tests, such as Marco-Starkey

theory [12] and Corten-Dolan theory [13].

4.2.1.1 Linear fatigue cumulative damage law

The Palmgren-Miner theory is simple and easy to utilize, thus, it is widely used by design engineers. This theory is a linear fatigue cumulative damage law without considering the loading sequence, as shown in Figure 4-18 (curve 2) [14]. The damage of each cycle loading is

$$D = \frac{1}{N} \quad (4.4)$$

where, D is the damage, and N is the number of total cycles.

Thus, for constant amplitude loading, the damage of n cycles is

$$D = \frac{n}{N} \quad (4.5)$$

for variable amplitude loading, the damage of n cycles is

$$D = \sum_{i=1}^n \frac{1}{N_i} \quad (4.6)$$

where, N_i is the fatigue life based on the relative stress range.

The fracture occurs when the damage arrives 1. Some other linear fatigue cumulative damage theories are presented in Table 4-10.

4.2.1.2 Nonlinear fatigue cumulative damage law

Based on a large number of laboratory tests, the fatigue damage is often proved to be nonlinear, as indicated by curves 1 and 3 in Figure 4-18.

Marco-Starkey cumulative damage theory is one of the first nonlinear theories.

Damage for each cycle can be defined by the following relationship:

$$D = \left(\frac{n}{N} \right)^{m_i} \quad (4.7)$$

where, m_i is a function of the stress level.

The fracture occurs when the damage arrives 1. In addition, the loading sequence is considered in this theory. Some other nonlinear fatigue cumulative damage theories are presented in Table 4-11.

TABLE 4-10 Linear fatigue cumulative damage theories.

Researchers	Cumulative Damage Models	
Palmgren-Miner	Definition of damage	$D_i = 1/N_i$
	Fracture law	$\sum D_i = 1$
Lundberg [15]	Definition of damage	$D = \frac{N_o}{\alpha} [l^{-s} \gamma (s-1) \exp(-ls_0)]$
	Fracture law	$\sum D = 1$
Shanley [16]	Definition of damage	$D = \exp \left[CK \left(\frac{n_i}{N_i} - 1 \right) \right], K = S_{a_i}^n$
	Fracture law	$\sum D = 1$
Grover [17]	Definition of damage	$D_i = 1/(\alpha_i N_i)$
	Fracture law	$\sum D_i = 1$

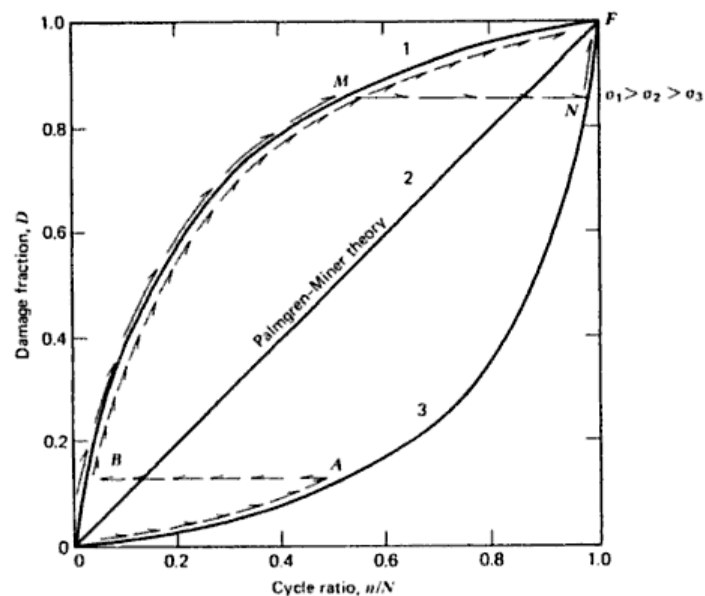


FIGURE 4-18 Fatigue damage as a function of cycle ratio (Collins, 1993).

TABLE 4-11 Nonlinear fatigue cumulative damage theories.

Researchers		Cumulative Damage Models
Marco-Starkey	Definition of damage	$D = (n / N)^{m_i}$
	Fracture law	$D = 1$
Corten-Dolan	Definition of damage	$D = m^c r^d$
	Fracture law	$1 = \sum_{i=1}^p \frac{n_i}{N_i (S_1 / S_i)^d}$
Freudenthal-Heller [18]	Definition of damage	$D = Ar^d$
	Fracture law	$1 = \frac{\bar{N}}{\sum n_i (S_i / \bar{S})^d}$
Henry [19]	Definition of damage	$D = \sum \frac{n}{N} = \frac{n_1}{N_1} + \frac{n_2}{N_2} = \frac{r_2 + (r_2 / r_1) + \beta_1^2 (1 - r_2 / r_1)}{r_1 + (r_2 / r_1) + \beta_1 (1 - r_2 / r_1)}$ $r = (S - S_e) / S_e$
	Fracture law	$D = 1$
Fuller [20]	Definition of damage	$D = (n / N)^{\bar{\beta}}$
	Fracture law	$D = 1$

4.2.2 Traditional nominal stress approach

Nominal stress approach is one of the earliest engineering approaches for the fatigue design. It is based on S-N curves of materials or components, the stress intensity factors, nominal stress, and combined with the fatigue cumulative damage theory. The fatigue resistance or fatigue life of a component or structure can be computed by the nominal stress approach.

4.2.2.1 Assumptions of nominal stress approach

The assumption of the nominal stress approach is that the fatigue lives of components of similar material but with different notches are the same if these notches have the same stress concentration factor and are under the same loading history. Figure 4-19 [21] illustrates details which may have same stress intensity factors.

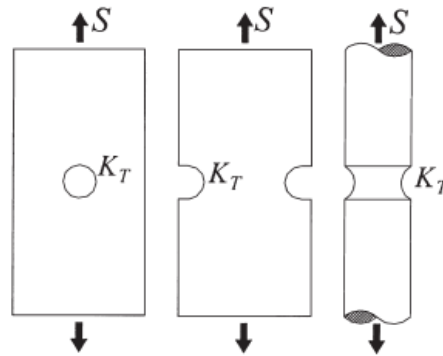


FIGURE 4-19 Nominal stress approach (Yao et al., 2001).

However, it should be noted that there are always some difference between the calculated life and the tested life.

4.2.2.2 Traditional nominal stress approach

The steps to calculate the fatigue lives of critical components are shown in Figure 4-20.

There are two methods to assess the fatigue life of a component. The first method is to calculate the fatigue life directly based on the nominal stress of the component and its own S-N curve. The second method is to calculate the fatigue life based on the nominal stresses and the modified S-N curves which are obtained from the S-N curves of material. Obviously, the first one is much more reliable, but it is impossible in most cases. Thus, the traditional nominal stress approach applies the second one.

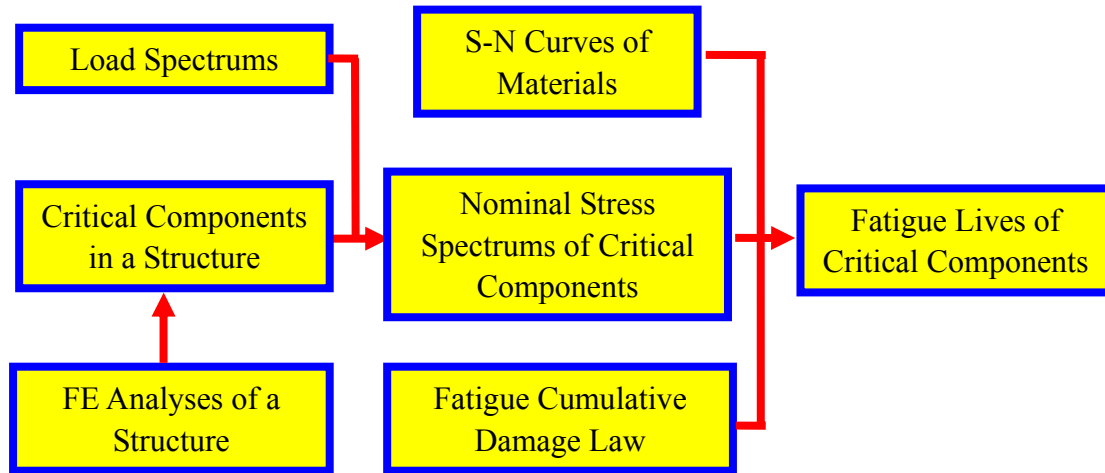


FIGURE 4-20 Flowchart of nominal stress approach.

Usually, the joint classifications and corresponding S-N curves take into account the local stress concentrations created by the joints themselves and by the weld profile. Therefore, the design stress can be regarded as the nominal stress, adjacent to the weld under consideration. However, if the detail is located at a stress concentrated area, this must be taken into account. For example, for the weld shown in Figure 4-21a, the relevant local stress for fatigue design would be the tensile stress, $\sigma_{nominal}$. For the weld shown in Figure 4-21b, the stress concentration factor for the global geometry must be considered, giving the relevant local stress equal to $SCF\sigma_{nominal}$, where SCF is the stress concentration factor due to the hole (SCF is related with the notch factor, the size factor, the quality of the surface and the load spectrum). Thus the local stress can be calculated as

$$\sigma_{local} = SCF\sigma_{nominal} \quad (4.8)$$

σ_{local} shall be used together with the relevant S-N curves, dependent on joint classification.

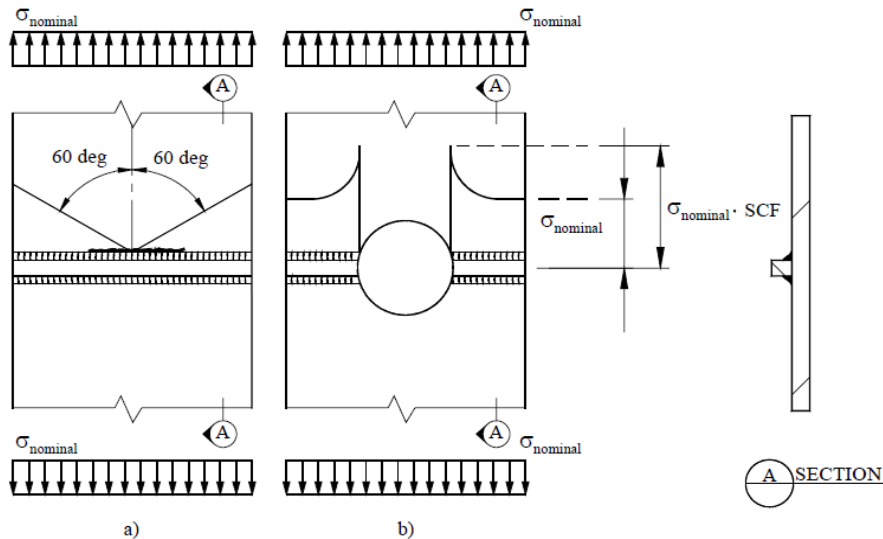


FIGURE 4-21 Explanation of local stresses (DNV, 2005).

There are some other approaches developed from the traditional nominal stress approach, such as the stress severity factor approach.

4.3 Structural Hot Spot Stress Method

4.3.1 The definitions of the structural hot spot stress method

Traditional fatigue evaluation methods are based on a series of S-N curves which are classified by geometries and loadings. For that reason, it is difficult to predict the fatigue life of a complicated component which is not included in the design codes. The structural hot spot stress method focuses on the weld geometry (not global geometry) and the load mode, therefore, it is much simpler than before because less S-N curves are needed. Structural hot spot stresses include nominal stresses and stresses due to structural discontinuities and presence of attachments, but excluding stresses due to presence of welds. Figure 4-22 [6] shows the definition of structural hot spot stress. It is evident that the structural hot spot stress is smaller than the notch stress.

Two different types of hot spots can be distinguished according to their locations on

the plate and their orientations to the weld toe, as shown in Figure 4-23. The two types are described detailed in Table 4-12.

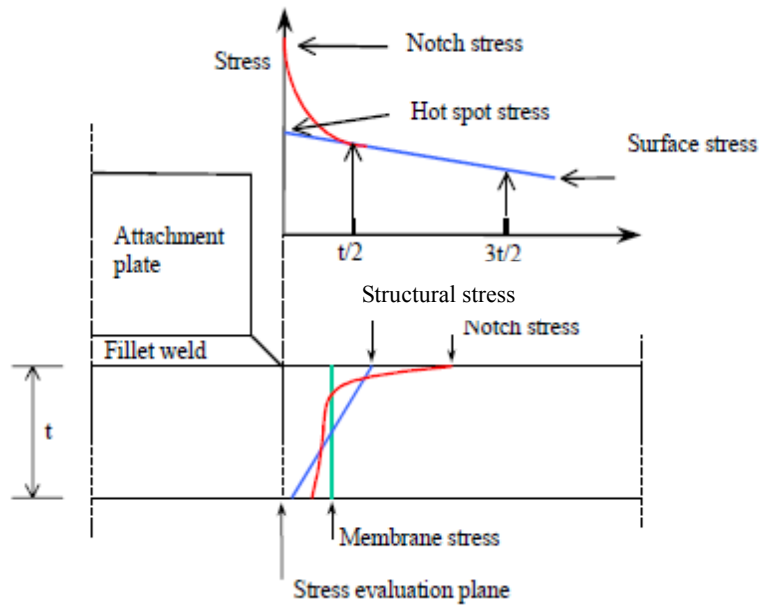


FIGURE 4-22 Definition of structural hot spot stress.

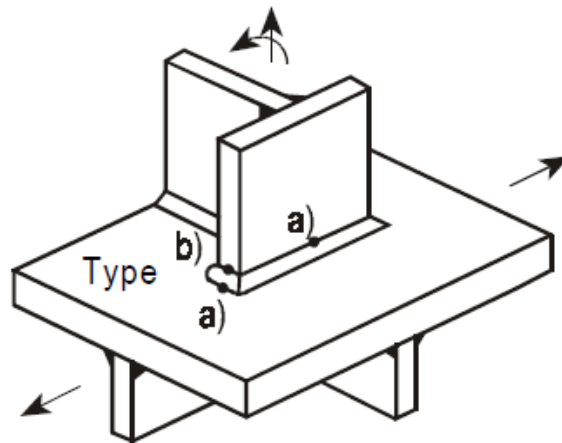


FIGURE 4-23 Types of hot spots (IIW, 2003).

TABLE 4-12 Descriptions of hot spots.

Type	Description	Determination
a	Structural hot spot stress transverse to weld toe on plate surface	Special FE analyses or measurement and extrapolation
b	Structural hot spot stress transverse to weld toe at plate edge	Special FE analyses or measurement and extrapolation

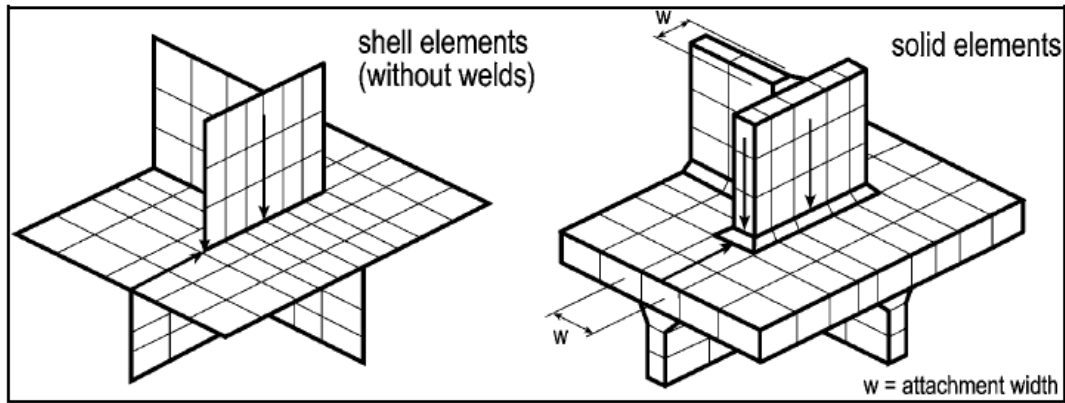


FIGURE 4-24 Typical meshes for a welded detail (IIW, 2003).

In a plate or shell element model, as shown in Figure 4-24, the elements have to be arranged in the mid-plane of the structural components. In FE model, 8-node elements are recommended especially in case of steep stress gradients, while 4-noded elements cannot be used to simulate the welds very well. In 8-node models, the welds may be simulated by vertical or inclined plate elements having appropriate stiffness or by introducing constraint equations or rigid links to couple node displacements. If the weld is not modeled, it is recommended to use the extrapolation method in order to avoid stress underestimation due to the missing stiffness of the weld. Reference points at different types of meshing which are used in the extrapolation method are shown in Figure 4-25 [7].

Solid elements which have a displacement function allowing steep stress gradients as well as plate bending with linear stress distribution in the plate thickness direction can be another recommended selection for complex cases. Modeling of welds is generally recommended as shown in Figure 4-24. It should be noted that solid element model often requires more powerful computers.

The element lengths are determined by the reference points for the subsequent extrapolation. The structural stress closest to the hot spot is usually evaluated at the first or second nodal point in order to avoid an affect of the stress singularity. Therefore, the length of the element at the hot spot should correspond at least to its distance from the first reference point.

Coarser meshes cause errors to the structural hot spot stress, and then change the

evaluation of fatigue life. When a model is meshed by 4-node shell elements larger than $t \times t$, it is recommended to fit a second order polynomial to the element stresses in the three first elements and derive stresses for extrapolation from the $0.5t$ and $1.5t$ points. An example is shown in Figure 4-26.

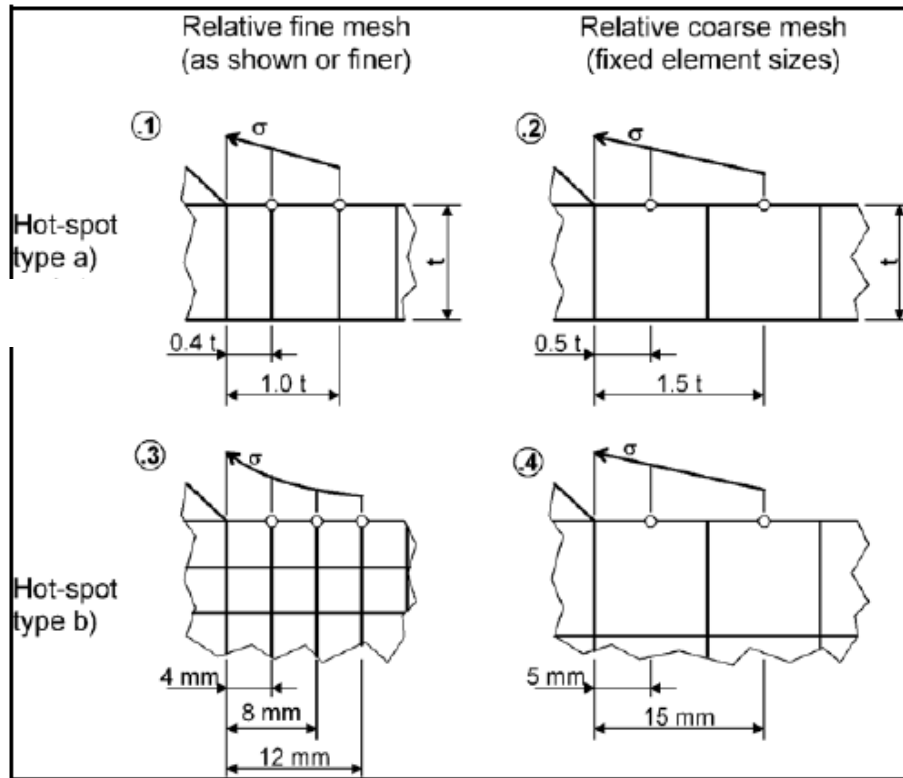


FIGURE 4-25 Reference points at different types of meshing.

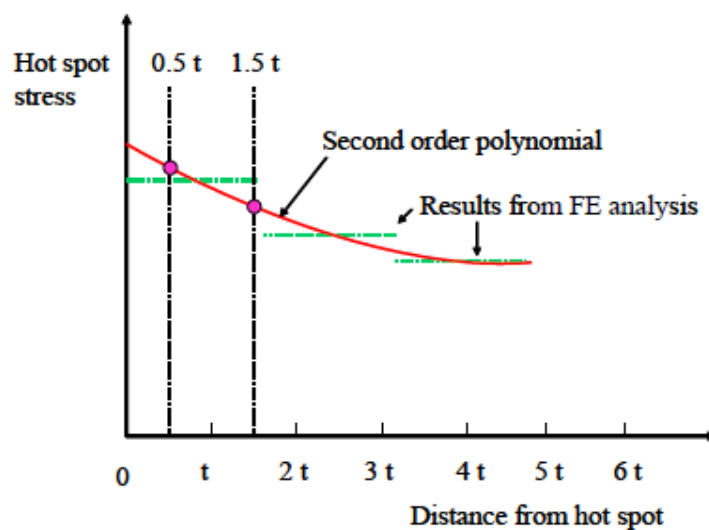
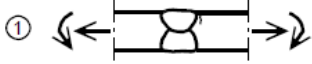
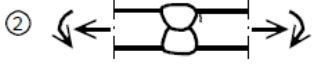
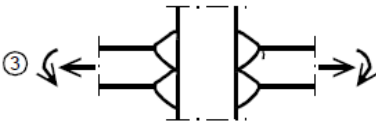
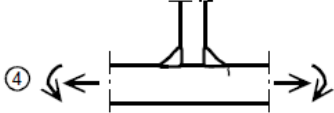
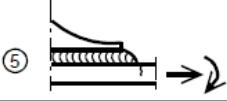
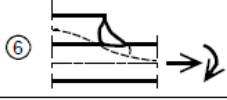
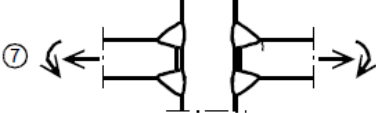


FIGURE 4-26 Derivation of hot spot stress for element size larger than $t \times t$ [7].

Several codes/specifications provide detail categories for the application of the structural hot spot stress method, for example, as shown in Table 4-13, Eurocode 3 (2004). It is found that the detail categories for cracks initiating from:

- toes of butt welds;
- toes of fillet welded attachments;
- toes of fillet welds in cruciform joints.

TABLE 4-13 Detail categories for hot spot stress method (Eurocode 3, 2004).

Detail category	Constructional detail	Description	Requirements
112		1) Full penetration butt joint.	1) -All welds ground flush to plate surface parallel to direction of the arrow. -Weld run-on and run-off pieces to be used and subsequently removed, plate edges to be ground flush in direction of stress. -Welded from both sides, checked by NDT. -For misalignment see NOTE 1.
100		2) Full penetration butt joint.	2) -Weld not ground flush -Weld run-on and run-off pieces to be used and subsequently removed, plate edges to be ground flush in direction of stress. -Welded from both sides. -For misalignment see NOTE 1.
100		3) Cruciform joint with full penetration K-butt welds.	3) -Weld toe angle $\leq 60^\circ$. -For misalignment see NOTE 1.
100		4) Non load-carrying fillet welds.	4) -Weld toe angle $\leq 60^\circ$. -See also NOTE 2.
100		5) Bracket ends, ends of longitudinal stiffeners.	5) -Weld toe angle $\leq 60^\circ$. -See also NOTE 2.
100		6) Cover plate ends and similar joints.	6) -Weld toe angle $\leq 60^\circ$. -See also NOTE 2.
90		7) Cruciform joints with load-carrying fillet welds.	7) -Weld toe angle $\leq 60^\circ$. -For misalignment see NOTE 1. -See also NOTE 2.

NOTE 1 Table 4-13 does not cover effects of misalignment. They have to be considered explicitly in determination of stress.

NOTE 2 Table 4-13 does not cover fatigue initiation from the root followed by propagation through the throat.

The local notch effect is embedded in the S-N curve when the structural hot spot stress method is applied, and the large variation in local notch geometry is accounted for in the scatter of the S-N data. However, it can be difficult in practical design of the structural details to define the nominal stress level to be applied together with the geometry specific S-N curves. Further, the application of a limited number of established S-N curves in fatigue design may complicate the utilization of improved local detail design in the fatigue life evaluation.

4.3.2 Recent investigations of structural hot spot stress method

Dong [22] presented the mesh-intensive structural stress approach. Through his studies, two major implications are found: (a) structural stresses pertaining to weld fatigue behavior can be consistently calculated in a mesh-insensitive manner regardless of types of FE models; (b) transferability of weld S-N test data, regardless of welded joint types and loading modes, can be established using the structural stress based parameters. In addition, a typical lap fillet joint is analyzed, and the structural stress based SCF values calculated with different element mesh sizes is summarized, as shown in Figure 4-27.

Doerk [23] studied the difference of the accuracy and sensitivity between different methods based on several different details through the FE analyses (both 2D and 3D numerical models), as shown in Figure 4-28. The two alternative methods for surface stress extrapolation yield almost the same results. The procedure proposed by Dong [22] for the evaluation of the structural stress directly at the weld toe shows mesh-insensitivity for 2D problems. However, in the case of 3D stress concentration, some scatter is observed in the results evaluated from different mesh densities.

Atzori et al. [24] studied the fatigue of complex welded structures, compared different approaches, such as the nominal stress approach, the structural hot spot stress method, and Notch Stress Intensity Factor (NSIF) approach. The structural hot spot stress approach allows a better definition of a nominal stress, especially when FE analysis is

utilized. While this approach is satisfactory to overcome the problem connected with the complexity of the structure, it is not useful for a problem where there are complex joints. Also, in the case of a joint which can be assimilated to one of the simple geometries considered by the design codes/specifications, attentions should be taken in defining the fatigue strength of the joint, since both the relative and absolute dimensions have a significant effect. It is said that the NSIF approach is more powerful and reliable than more usual approaches, however, the nominal stress approach and the structural hot spot stress approach are more popular to bridge designers because the NSIF approach is more complex to use.

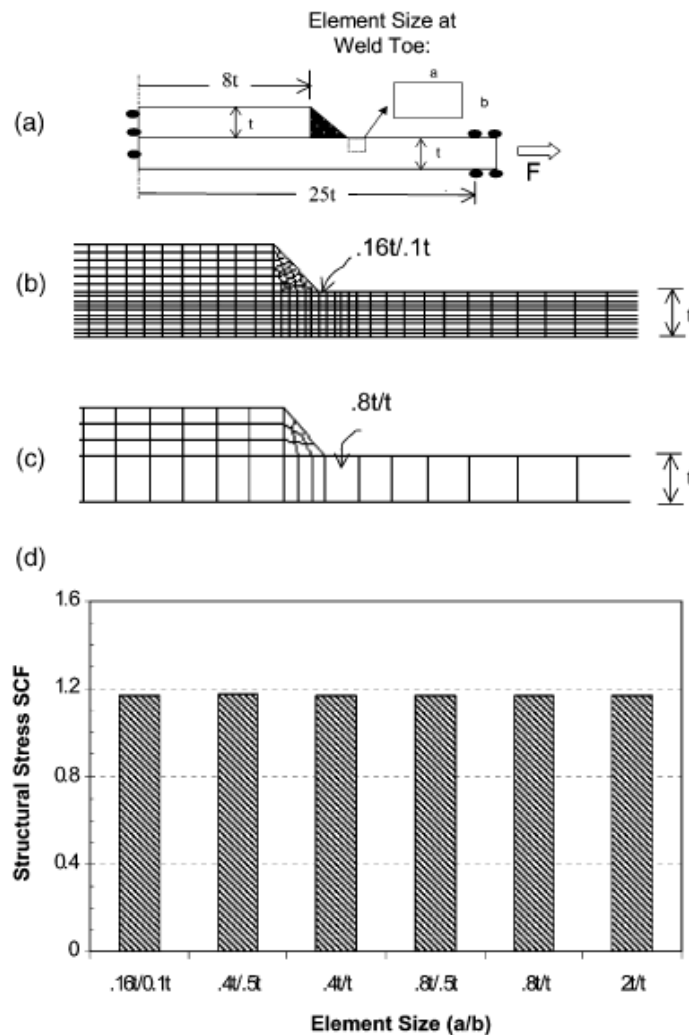


FIGURE 4-27 Structural stress and mesh intensity—single plate lap joint: (a) model definition; (b) a representative FE model with fine mesh ($0.16t/0.1t$) at weld toe; (c) a representative FE model with coarse mesh ($0.8t/t$) at weld toe; and (d) structural stress SCF calculated from six FE models (Dong, 2001).

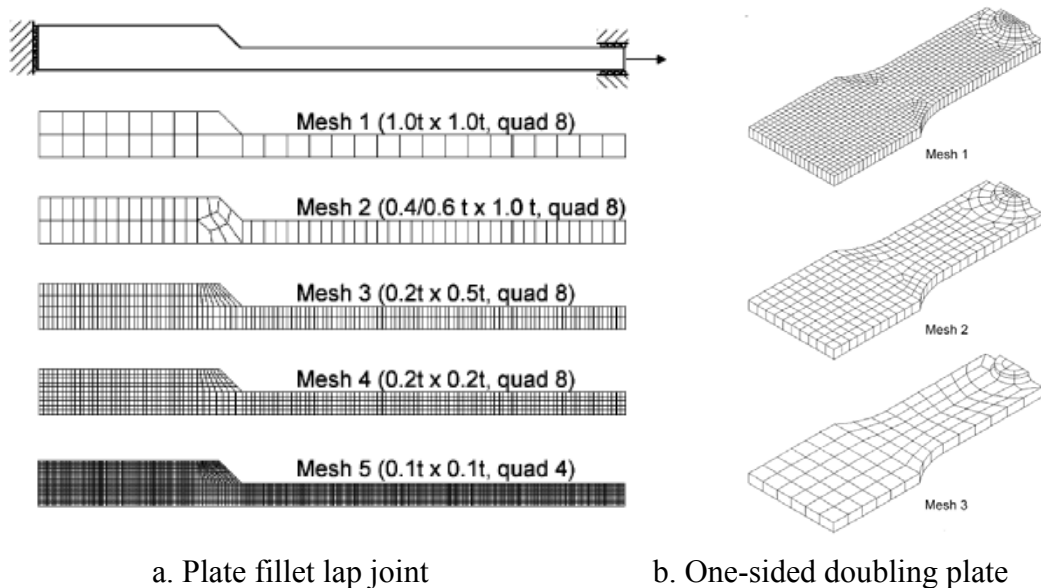


FIGURE 4-28 Examples of numerical models (Doerk et al., 2003).

4.3.3 Discussions

The nominal stress approach and the structural hot spot stress method are the two main methods to calculate the fatigue life in engineering provided in the design codes. these methods are compared in Table 4-14.

TABLE 4-14 Comparisons of the two different methods.

	Nominal Stress Approach	Structural Hot Spot Stress Approach
S-N curve	a series of S-N curves	single S-N curve
Stress	nominal stress, difficult to define in the real projects	hot spot stress: transverse to weld toe on plate surface or at plate edge
Fatigue crack	based on the critical connections	based on the welds
Geometry	not considered	embedded
Potential defect	not considered	considered
FEA	not fully used	fully used
Weld	not considered	not embedded

4.4 Method of analysis

A three-step approach in modeling the structure is often used: a) preparation of a global model, b) a submodel, and c) and a refined model near and around the hot spot. As an example, stress calculation, for evaluating the fatigue resistance of the rib-to-deck plate connections in an orthotropic deck is presented in this study. A model of three-span orthotropic deck, as the global model, is developed to analyze the deformation and stress performance. The submodel of the rib-to-deck plate connections under displacement (not stress) loading is developed with fine mesh based on the results of the global model. In the third step, the structural hot spot stress is calculated according to the results of submodel analyses, and then the fatigue resistance is assessed by the analyzed results of the reference detail according to the recommendations of IIW [7]. Thus, the fatigue resistance of the rib-to-deck plate connection is predicted.

4.4.1 Global model analyses of the orthotropic deck

4.4.1.1 Global model

The general dimensions and boundary conditions of the global model can be found in Chapter 3.1. In this model, normal pavement and different fatigue loads are applied.

The load applied to the model is 140 kN which distributed on a square surface 350 mm*600 mm. This “fatigue load”, according to the Italian code [25], is 30% less than the peak load applied on the deck plate for local loads, i.e. 200 kN. Considering the distribution function of wearing surface, the load area used for analysis is variable. The thickness of pavement is 70 mm. Consequently, the calculated loading area is 506 mm*756 mm. Three different load cases are utilized in order to analyze the most reliable fatigue resistance of orthotropic deck bridge (see Figure 4-29).

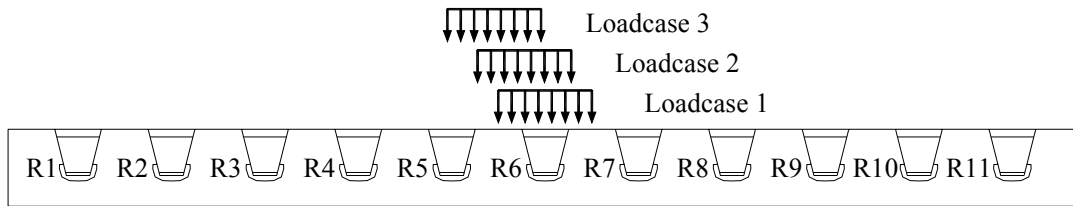


FIGURE 4-29 Wheel loads for fatigue computation (Italian code, 2008).

4.4.1.2 Results of global model analyses

The stress distribution of the deck plate is studied to find the part which is more sensitive to the fatigue cracking.. The global model is simplified by ignoring the weld influence. The stress distribution of deck plate so obtained still provides useful information for further study. Figure 4-30 shows the stress distributions at the center of the deck plate at rib mid span, both at the bottom and the top of the deck plate surfaces. It is displayed that the location near/at R5 is the most highly stressed. In addition, the stresses far from the wheel load appear like waves due to the restriction of longitudinal ribs, and are almost zero in the ends.

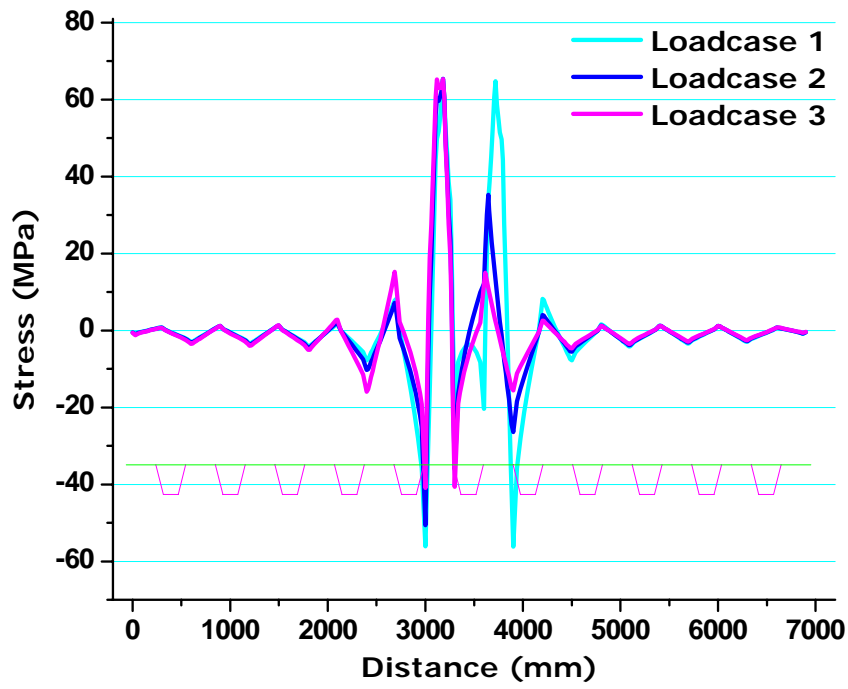
An important observation that should be noted is that although the maximum stresses are located at in the middle of the two ribs, other peak stresses caused by different load cases are produced at the rib-to-deck plate connections, where the fatigue resistance is less. This explains why there are many fatigue cracks occurring at this position in both laboratory tests and actual projects. Furthermore, these peak stresses have very sharp gradients; therefore, the peak stresses are not easily measured either in laboratory tests or field tests.

4.4.2 Submodel analyses of the rib-to-deck plate connection

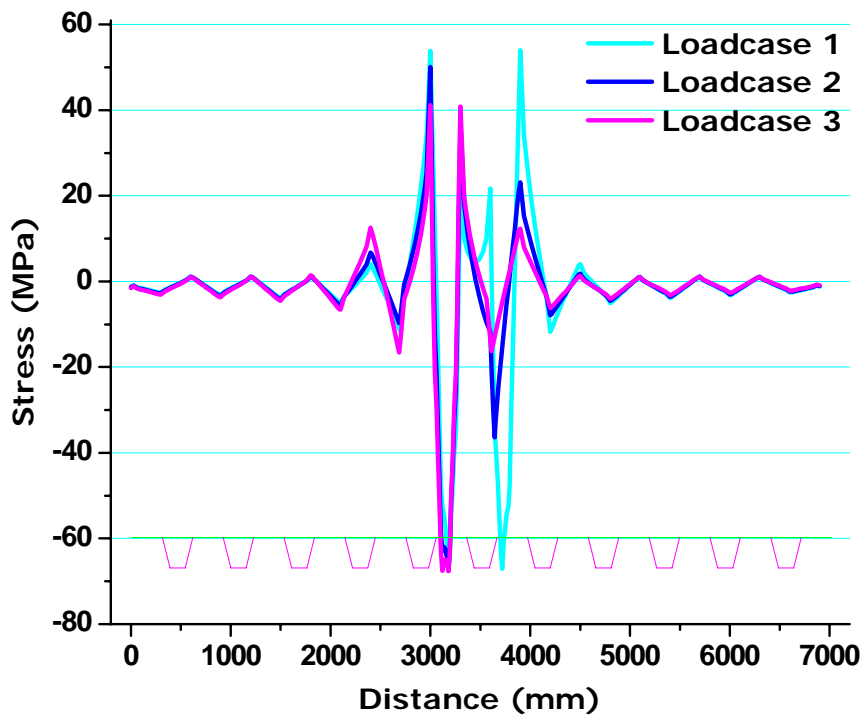
4.4.2.1 Submodel

A submodel of the rib-to-deck plate connection at the middle of the span is

indispensable to study the specific stress status of the joints due to the lack of the weld in the global model. Here, also LUSAS is applied in submodel analysis. Therefore, a two-dimensional submodel was developed to analyze the stress alteration due to the existence of welds between the deck plate and the longitudinal ribs. But, the submodel analyses is necessary for calculating the structural hot spot stress. Therefore a three-rib submodel, including welded joints is developed (as shown in Figure 4-31) and analyzed under three different load cases which were also used in the global analyses. R5, R6 and R7 are the three longitudinal ribs which are more sensitive to the fatigue cracking according to the results of the global analyses. A fillet weld penetrating 75% of the longitudinal rib is modeled. Curved surface instead of straight surface is modeled for the weld in the submodel.



(a) at the bottom of deck plate;



(b) at the top of deck plate.

FIGURE 4-30 Stress distributions at the deck plate.

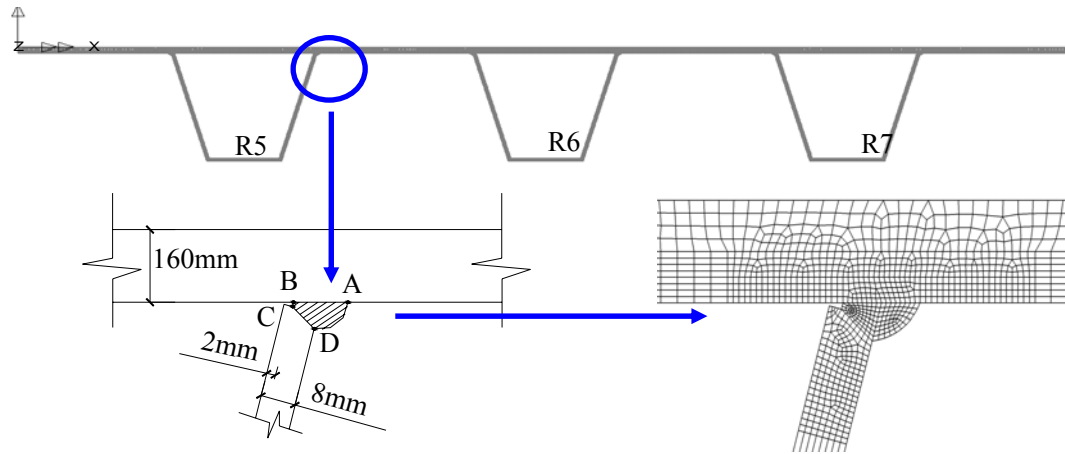


FIGURE 4-31 Submodel of rib-to-deck plate connections.

Points A, B, C, and D will be used extensively for reference in the rest of the text and should be memorized. Fine meshes are used at/near the welds, and the mesh is smaller than 1 mm*1 mm. It helps to obtain more accurate structural hot spot stress. Shell element, the same to the global model, is used in the submodel. Displacement loads, as new loading way, instead of traditional stress loads, are applied to the submodel. The displacements obtained from the global analysis are taken as the “fatigue loads”, as shown in Figure 4-32. The displacement loads obtained from the global analyzed results are based on the three typical wheel loading, as shown in Figure 4-32. The displacements which used on the top of the deck plate in the submodel are all relative values (not the absolute values of the global model analyses), taking the left end point at the mid span as the reference point.

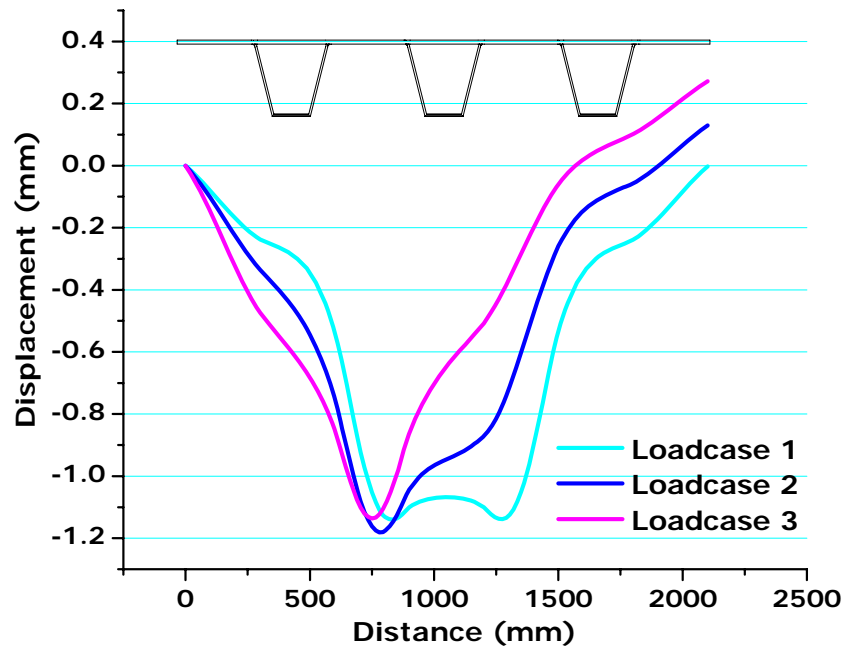


FIGURE 4-32 Displacement load cases for the submodel.

4.4.2.2 Results of submodel analyses

Welded detail is neglected in the global model, and the real stress status at this connection is still indistinct. Therefore, the submodel is necessary to investigate the stress at/near the weld toe or root.

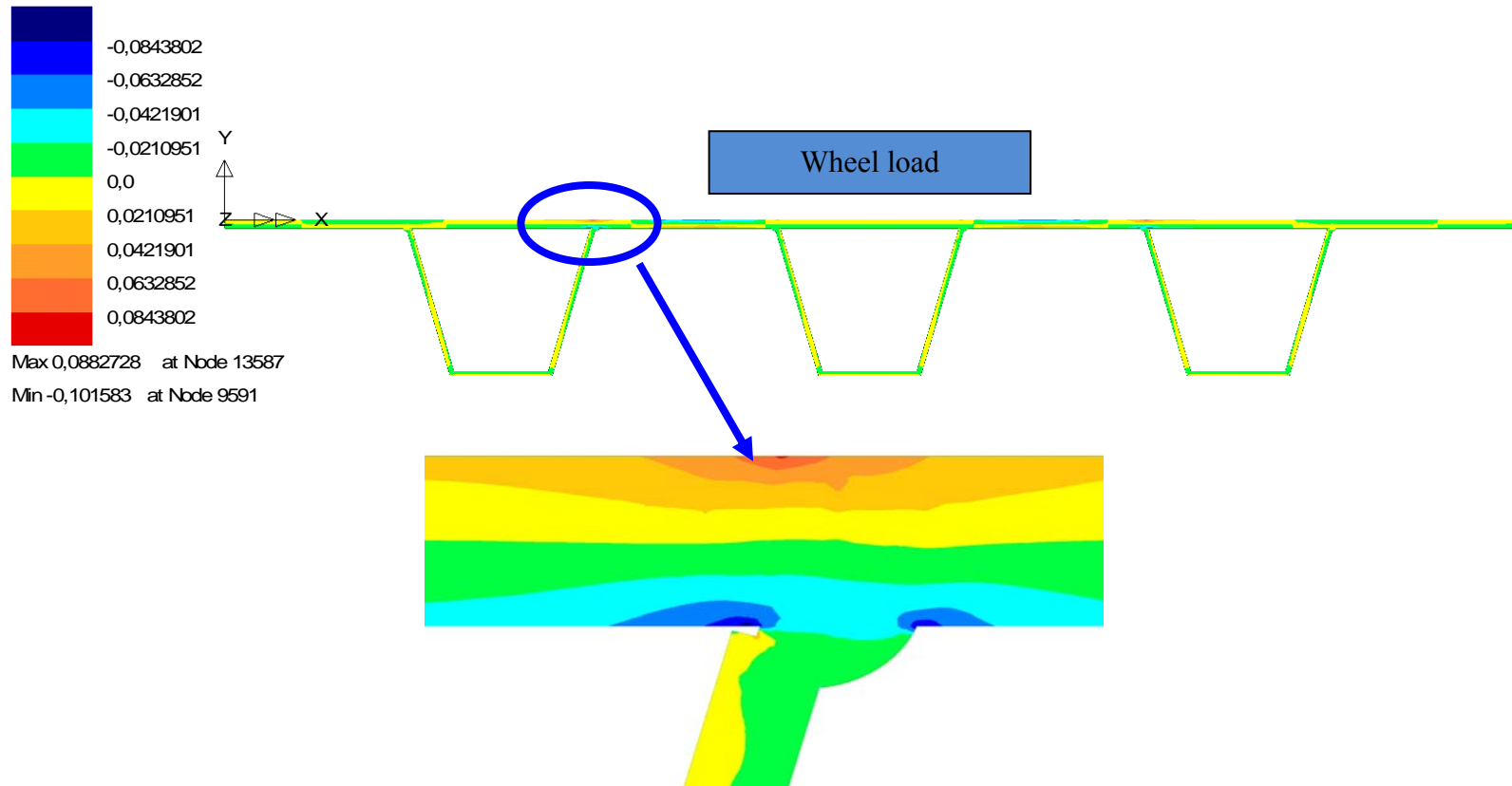
The stress distributions of the submodel under the three different load cases are very similar, as shown in Figure 4-33. However, it is found that the loading position influences the magnitude of the stress significantly. Moreover, peak stresses are located at the welded connection, at Points of A, B and C. High stress also exists at the top of the deck plate where there is no welds.

Figure 4-34 shows the stress distributions at the bottom of the deck plate of submodel which are compared to the results of the global model, while Figure 4-35 shows the stress distributions at the top of the deck plate. The stress distributions are similar according to the two different model results. However, a significant distinction exists at the rib-to-deck plate connection. The stresses have a sudden change exactly at the welded connections while the stresses are almost the same at the other places in both models. For the three different load cases, the maximal change occurs at the right

rib-to-deck plate connection of R5, while for load case 1 also occurs at the left of R7 and for load case 3 at the left of R6 taken accounting into the symmetrical loading at the local positions. The other welded connections far from the vehicle loading have a sudden change as well, but much smaller than the above ones.

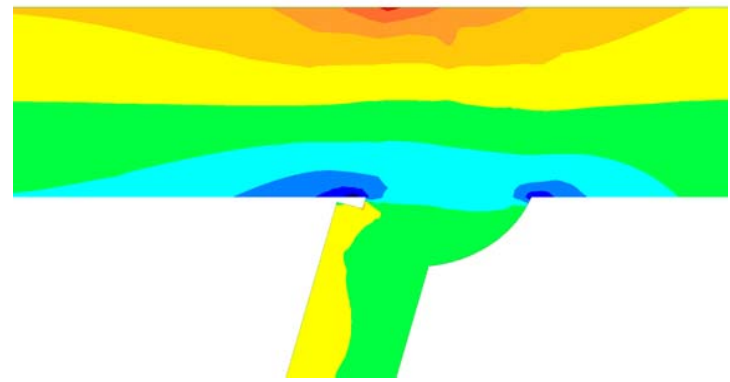
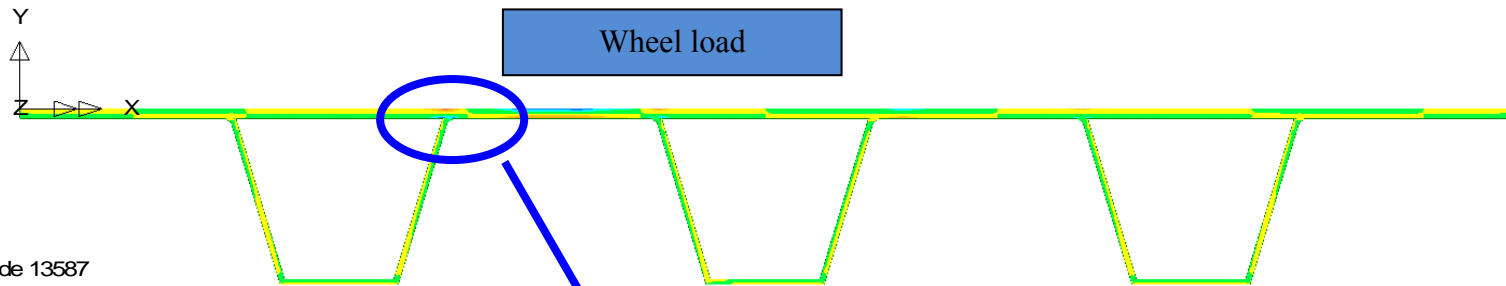
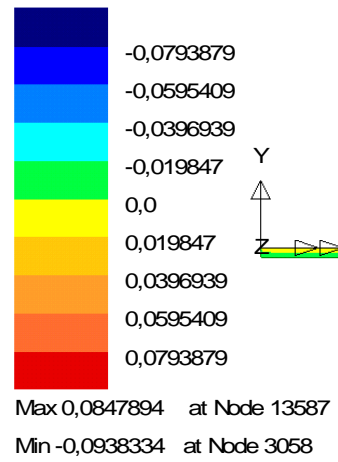
From Figure 4-34 and 4-35, it is also obvious that the welded joints not only influence the bottom stress but also change the top stress. However, the sudden change at the bottom of the deck plate is higher than that at the top of deck plate due to the presence of the welds which impact the stress path and concentration.

Loadcase: 1
Title: Loadcase 1
Results File: 0
Entity: Mid Stress
Component: SX



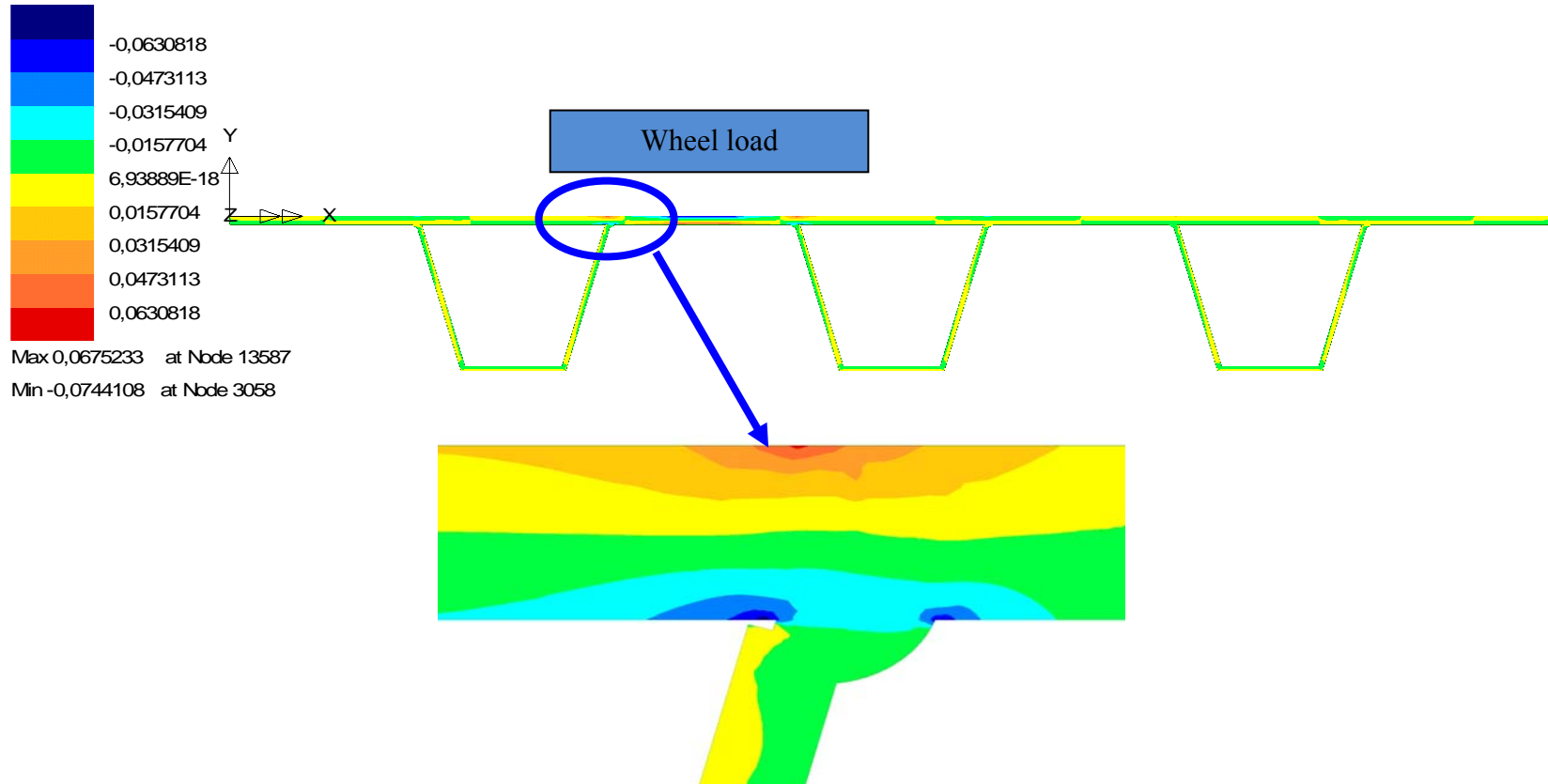
a. load case 1;

Loadcase: 2
Title: Loadcase 2
Results File: 0
Entity: Mid Stress
Component: SX



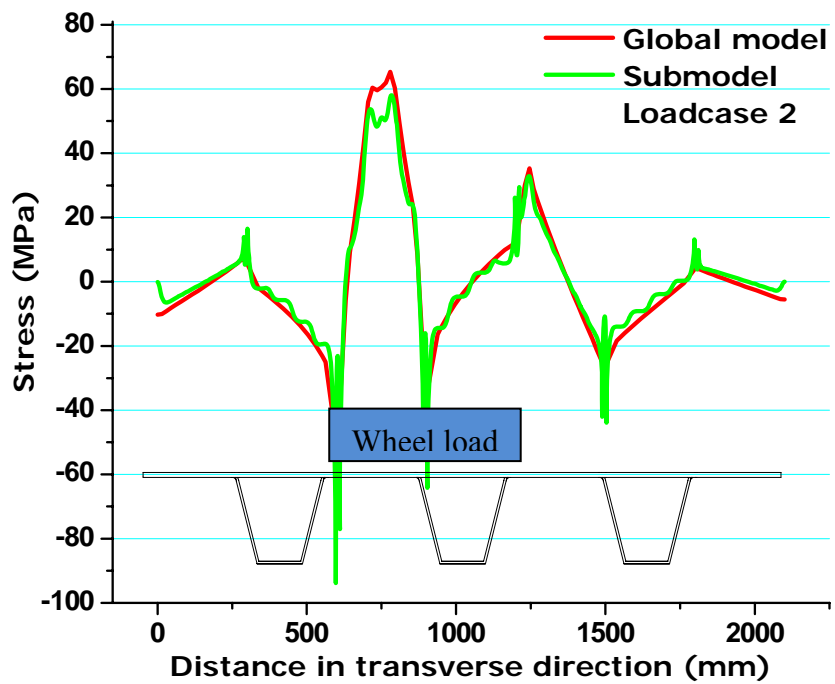
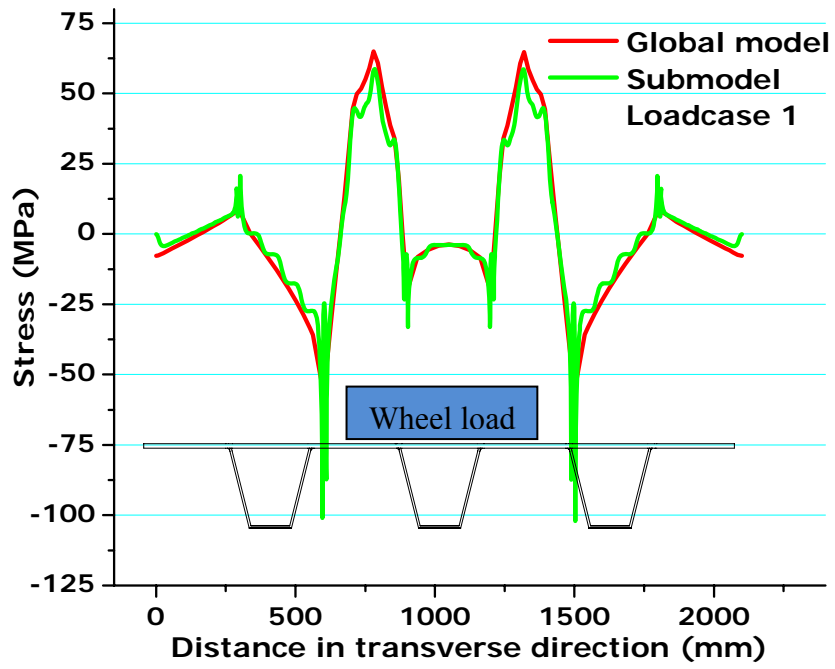
b. load case 2;
187

Loadcase: 3
Title: Loadcase 3
Results File: 0
Entity: Mid Stress
Component: SX



a. load case 3;

FIGURE 4-33 Stress distributions for the different load cases ($\times 10^3$ MPa).



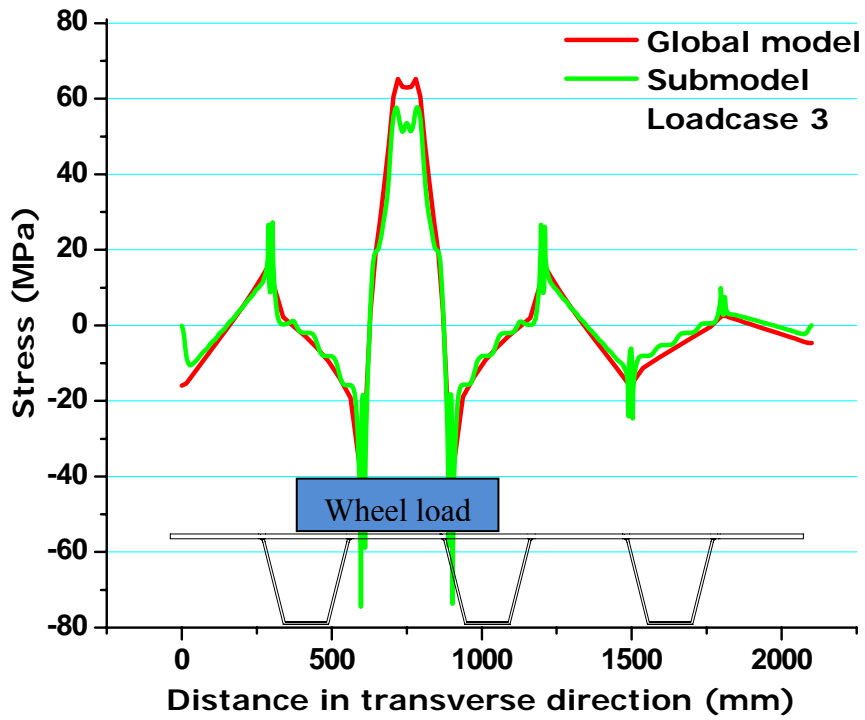
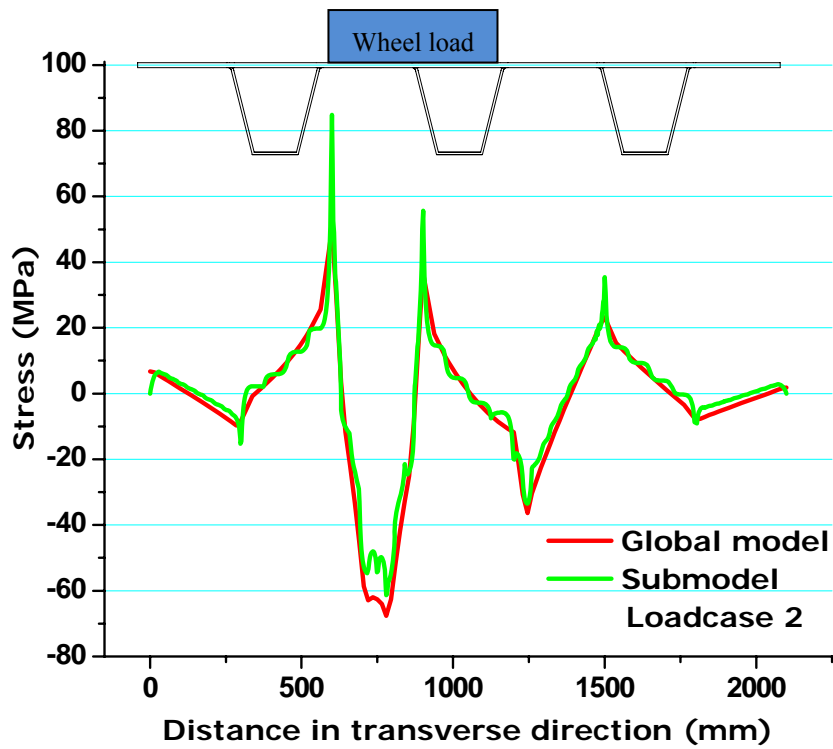
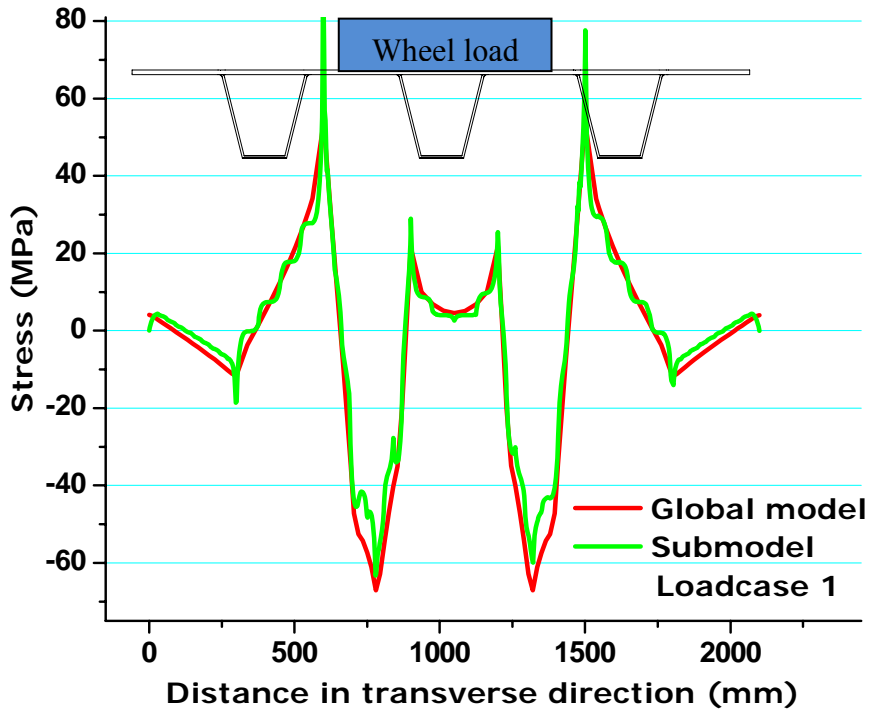


FIGURE 4-34 Stress comparison between global model and submodel analysis at the bottom of deck plate.



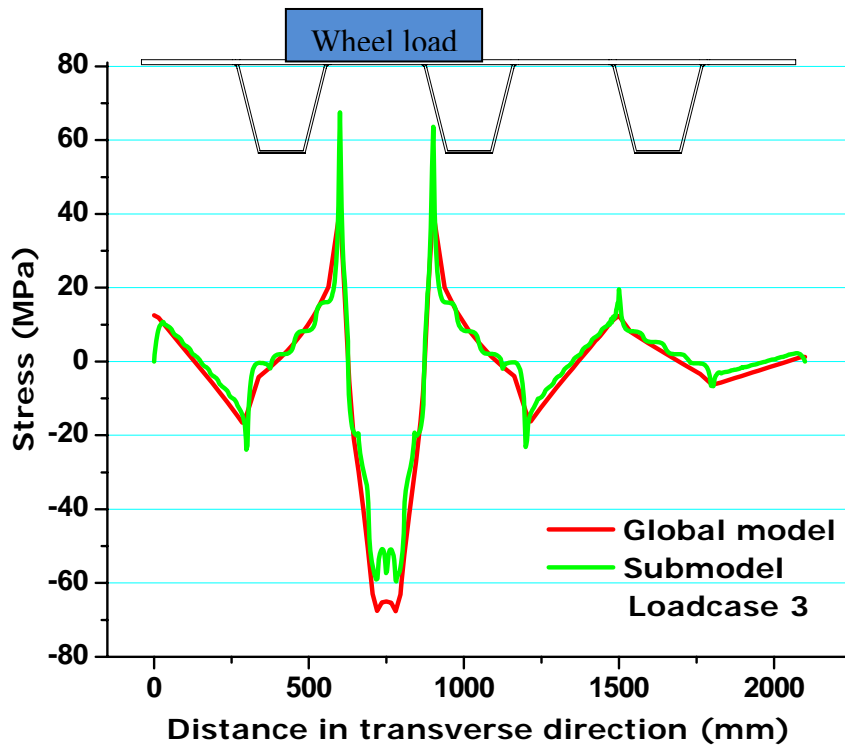


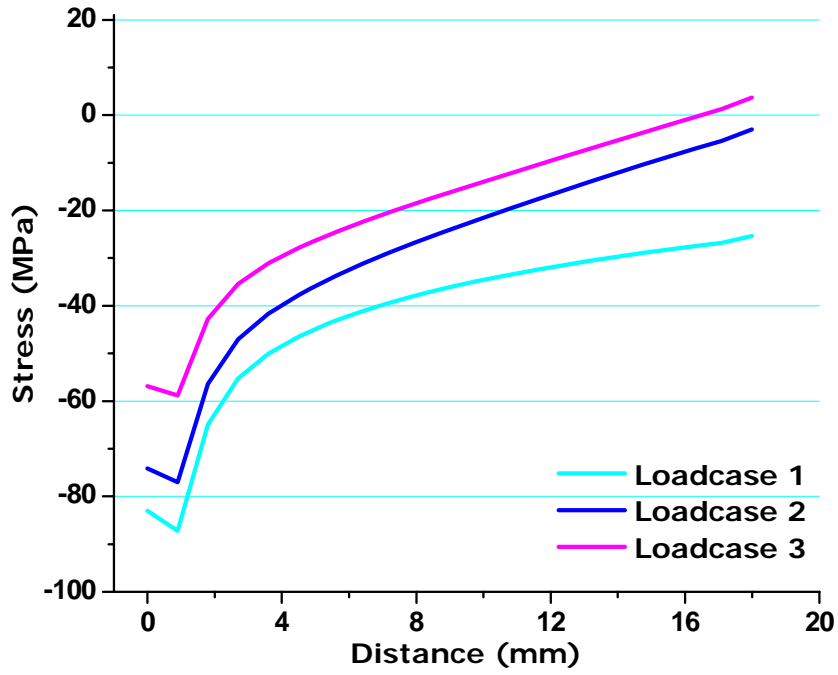
FIGURE 4-35 Stress comparison between global model and submodel analysis at the top of deck plate.

Submodel analysis indicates that high stresses exist at Point A, B and C, however, among of these points the stress of Point A and B are much higher than that of Point C. Stress distributions of Point A, B and interface C-D are shown in Figures 4-36, 4-37 and 4-38.

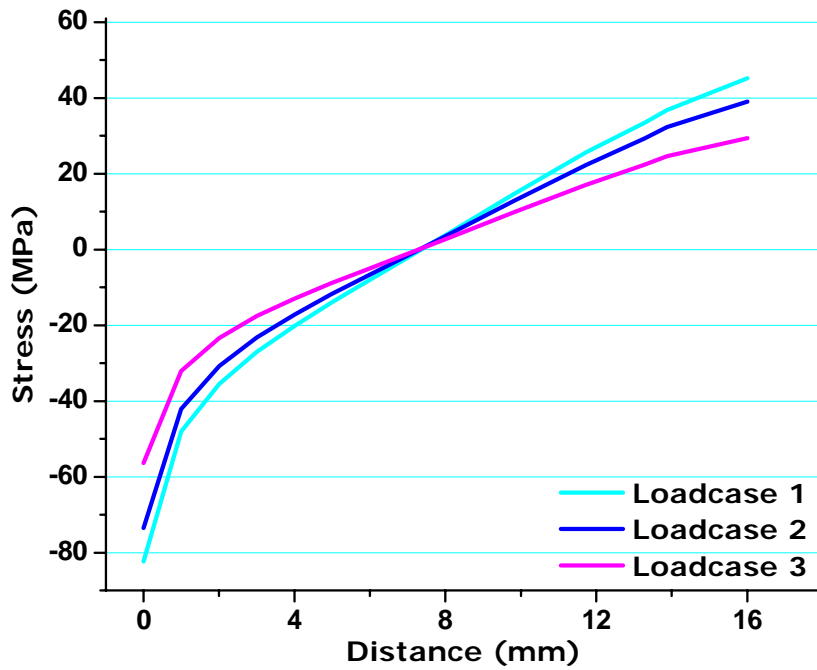
A sharp gradient is found at the welded connection along the bottom of deck plate, as shown in Figure 4-36*a* and 4-37*a*. The sudden change occurs in the region of 2 mm along the bottom of deck plate. Therefore, the peak stress is very difficult to measure in both of laboratory test and field test. Figure 4-36*a* implies that a highly localized and small stress area exist near Point A, while it is not found near Point B.

The stress distribution through the deck plate thickness shows that there is a sharp gradient near Point A, which becomes less sharp far from the weld, as shown in Figure 4-35*b*. The steep gradient is not found near Point B, where stress is more even (see Figure 4-36*b*). The stresses at the neutral axis of the deck plate are almost zero. Compared with Point A and B, it is apparent that higher peak stress occurs at Point B. Another significant phenomenon should be pointed out is that load case 1 is the most critical loading to the rib-to-deck plate connections according to the global analysis and submodel analysis. However, it should be noted that this can be influenced significantly by the load distribution area. Different load distribution areas will change the local stress distinctly. In the previous chapters, it is found that load case 1 produces lower stress in the orthotropic deck.

Through the FE analysis, it is found that the magnitude of peak stress is influenced significantly by the load distribution area and the distance/span of longitudinal rib.

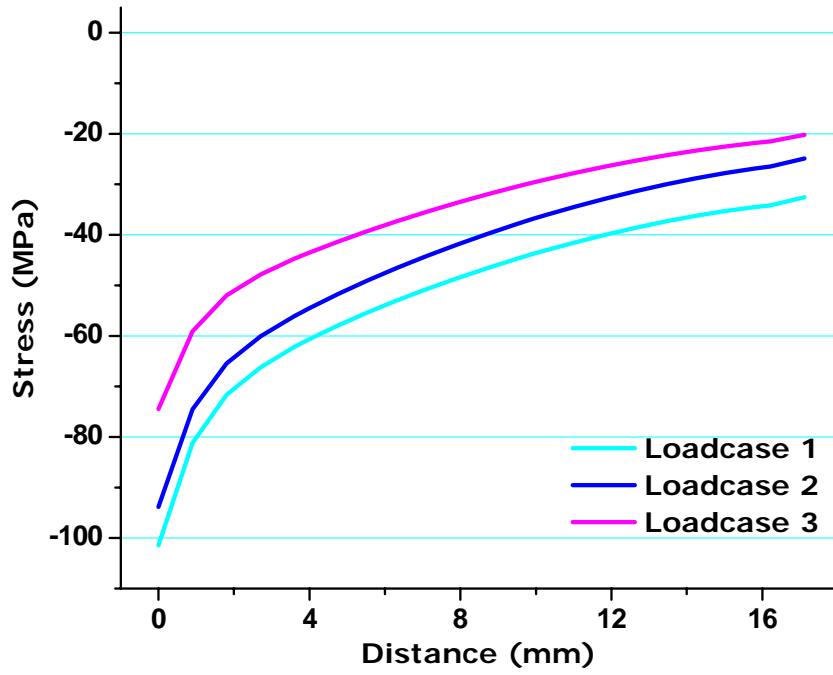


(a) along the bottom of deck plate near the welded toe;

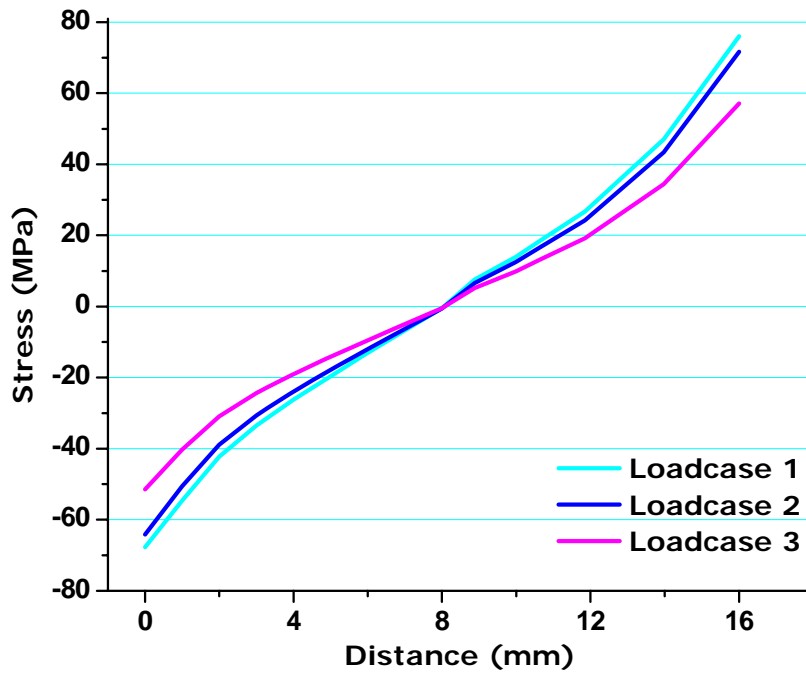


(b) through the deck plate thickness;

FIGURE 4-36 Stress distributions at Point A (the direction to R6).



(a) along the bottom of deck plate near the welded toe;



(b) through the deck plate thickness;

FIGURE 4-37 Stress distributions at Point B (inside R5).

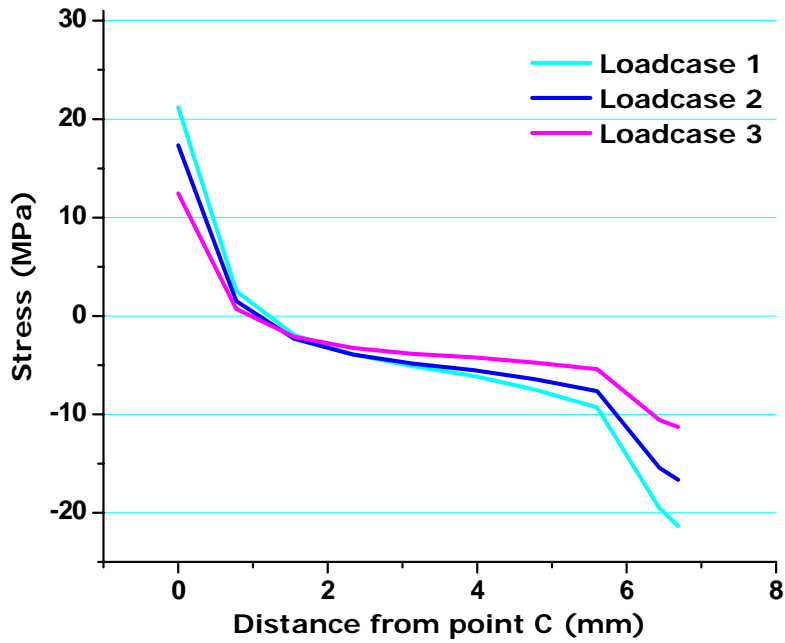


FIGURE 4-38 Stress distributions along the interface C-D.

4.4.3 Structural hot spot stresses

Traditional fatigue evaluation is carried out according to a series of S-N curves classified by global geometries and loadings. For that reason, it is difficult to predict the fatigue life of the complicated component which is not included in the design codes. The Structural Hot Spot stress method focuses on the weld geometries (not global geometry) and loadings, by the use of the Finite Element. It is simple to the extent that it needs only one single S-N curve for the toe of the weld. Figure 4-39 [7] shows the definition of structural hot spot stress.

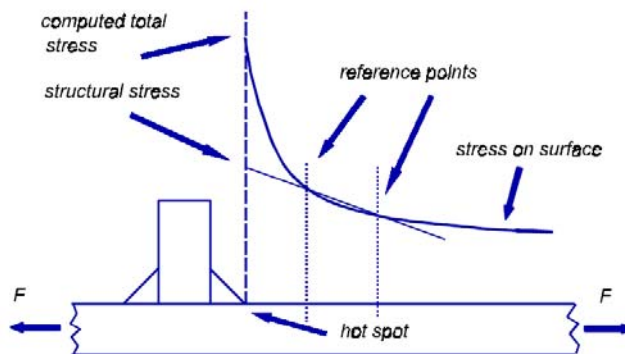


FIGURE 4-39 Definition of structural hot spot stress (IIW, 2003).

The S-N curve for the structural hot spot method is for the material at the toe of the weld with all its microscopic inclusions at the interface between the weld nugget and the heat affected zone (HNZ); the curve contains the inherent residual stress, and it may be similar to a Fat 71 (Eurocode) or a Category C (AASHTO). The structural hot spot stress at the rib-to-deck plate connection is calculated according to the results of submodel analyses. The linear extrapolation method, two reference points ($0.4t$ and $1.0t$, t is the plate thickness), is used:

$$\sigma_{hs} = 1.67 \cdot \sigma_{0.4t} - 0.67 \cdot \sigma_{1.0t} \quad (4.9)$$

The stresses of Point A and B are calculated since they are more sensitive to fatigue cracking. The results of structural hot spot stresses are shown in Table 4-15. It is evident that Point B is more sensitive than Point A.

Based on the submodel analyses and the structural hot spot stress analyses, stress concentration factor (SCF) k is calculated through Eq. (4.9):

$$\sigma_{hs} = k \cdot \sigma_{nom} \quad (4.10)$$

SCFs of Point A and B are calculated because the stresses are much higher than Point C and D, see Table 4-15. It is found that the SCFs of the three load cases are approximate.

TABLE 4-15 Structural hot spot stresses calculated by linear extrapolation method.

		Loadcase 1	Loadcase 2	Loadcase 3
Stresses of Poing A (MPa)	Submodel	87.2	77.0	58.8
	Hot-spot	50.1	46.5	36.2
	SCF k	1.74	1.66	1.62
Stresses of Poing B (MPa)	Submodel	101.4	93.8	74.4
	Hot-spot	65.1	59.5	47.3
	SCF k	1.56	1.57	1.57

In order to apply the structural hot spot stress calculated from the submodel analysis, the reference detail is chosen as similar as possible to the submodel to assess

according to the recommendation of IIW, as shown in Figure 4-40. The same mesh type (shell element) is used in the FE model. Fine meshes are utilized in this model which is similar to the submodel. The displacement loading is applied based on the results of submodel analysis. The length of the deck plate model in this analysis is 300 mm, and the height of the rib is 60 mm.

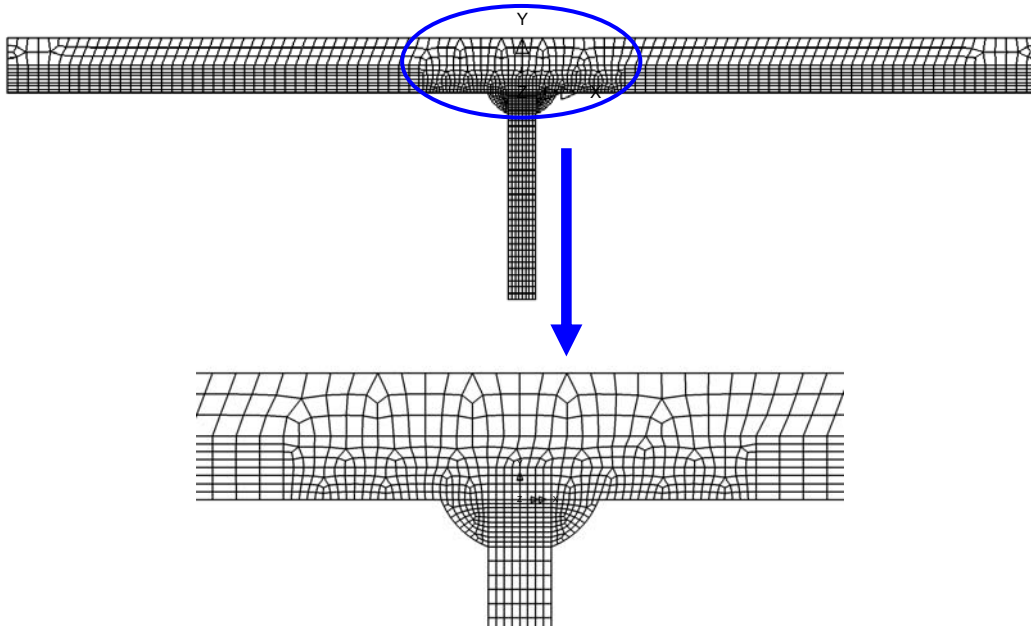


FIGURE 4-40 FE model of the reference detail.

The structural hot spot stresses of the three difference load cases for the reference detail are shown in Table 4-16. The fatigue resistance for 2-million cycles of the rib-to-deck plate connection to be assessed is then calculated based on the fatigue class of the reference detail by:

$$FAT_{assess} = \frac{\sigma_{hs,ref}}{\sigma_{hs,assess}} \cdot FAT_{ref} \quad (4.11)$$

where, $\sigma_{hs,ref}$ is the structural hot spot stress of the reference detail, $\sigma_{hs,assess}$ is the structural hot spot stress of the detail to be assessed, FAT_{assess} is the fatigue resistance of the detail to be assessed, and FAT_{ref} is the fatigue resistance of the reference detail.

The calculated fatigue resistances of Point A and B are listed in Table 4-16. It is found

that the fatigue resistances for different load cases are close. The fatigue resistance of Point B is lower which is close to 70 MPa which is in consistent with the same detail in the Eurocode [3]. Therefore, this approach can be an effective way to predict the fatigue resistance of the rib-to-deck plate connection.

TABLE 4-16 Structural hot spot stresses of the reference detail

		Loadcase 1	Loadcase 2	Loadcase 3
$\sigma_{hs,ref}$ (MPa)		46.6	44.8	33.1
FAT_{assess} (MPa)	Point A	93.1	96.5	91.4
	Point B	71.6	75.5	69.8

4.4.4 Three-step approach

Three-step approach for evaluating the fatigue resistance of an orthotropic deck, as well as to other similar welded structures, is concluded based on the global model, the submodel and the structural hot spot stress. The three-step approach can be carried out as following:

- a) **Global model analyses.** Build a global FE model to simulate an orthotropic deck system under the actual wheel loading, and obtain the results of FE analysis for the second step, such as displacements and stresses;
- b) **Submodel analyses.** A reasonable submodel should be developed based on the previous analyzed results, and displacements, moments or stresses of the global model are taken as loadings to simulate the real problem. Displacement is proved to be a good choice in this study. The geometry of welded joint should be modeled precise, and fine mesh at/near the joint should be applied in order to achieve real structural hot spot stress;
- c) **Fatigue evaluation.** The structural hot spot stress is calculated based on the submodel analyses according to the recommendation of IIW. Then, a reference detail, as similar as possible to the submodel, should be chosen to analyze, and

obtain its structural hot spot stress. After that, the fatigue resistance at 2-million cycles is calculated based on the fatigue class of the reference FAT_{ref} by Eq. (4.11).

The fatigue evaluation of the rib-to-deck plate connection in this study manifests that this approach is reliable. Therefore, it is supposed that the three-step approach can be helpful to analyze other complex welded connections in orthotropic deck bridges, such as rib-to-diaphragm and rib-to-diaphragm-deck plate.

However, attentions should be paid to the model simulation. Different hypothesis and simplifications can cause significant difference. Therefore, the designer should be familiar with both professional knowledge and FE software. In addition, it should be noted that structural hot spot stress approach has some deficiencies, such as few reference details are presented in the recommendation of IIW [7].

4.4.5 Conclusions

The fatigue resistance of the rib-to-deck plate connection is assessed through a series of FE analyses and calculations in this study. As similar as possible of loadings and other conditions should be applied to the global model, the submodel, and the reference detail model. From this study, the following conclusions can be drawn:

- a) The three-step approach based on the global model, the submodel and the structural hot spot stress can be used to evaluate the fatigue resistance of rib-to-deck plate connections in the orthotropic deck. Structural hot spot stress can be helpful to predict the fatigue resistance of other similar welded joints;
- b) The submodel analyses show that sudden change of stress occurs at/near the rib-to-deck plate connection, not only at the bottom of deck plate but also at the top. Sudden change of stress is found at/near the weld toe where the peak stress area is very small and, therefore, structural stress is difficult to find by test;
- c) Displacement instead of moment or stress from the global analysis can be taken as the loading for the submodel, as well as to the reference detail model;

- d) Different loading position causes different critical connection;
- e) Different points at the same connection also have different fatigue resistance. For example, Point B is more sensitive to fatigue failure than Point A and Point C according to the evaluation of the three-step approach.

References

- [1] Lee YL, Pan J, Richard Hathaway, Mark Barkey. Fatigue Testing and Analyses: Theory and Practice. Elsevier Butterworth–Heinemann, 2005
- [2] Steel, concrete and composite bridges - Part 10: Code of practice for fatigue, 1980.
- [3] Eurocode 3: Design of Steel Structures, Part 1.9: Fatigue, 2004.
- [4] Fatigue Design of Offshore Steel Structures Recommended Practice. Det Norske Veritas DNV-RP-C203, 2005.
- [5] AISC. Load and Resistance Factor Design Specification for Structural Steel Buildings, 1999.
- [6] AASHTO LRFD Bridge Design Specifications, 2005.
- [7] Hobbacher A. Recommendations for fatigue design of welded joints and components. IIW document XIII-1965-03/XV-1127-03. International Institute of Welding; 2003.
- [8] Japan Road Association (JRA). Fatigue Design Specifications for Steel Bridges. Japan Road Association, 2002 (in Japanese).
- [9] Ministry of Housing and Urban-Rural Development of the People's Republic of China (MOHURD). Code for Design of Steel Structures, GB 50017-2003. MOHURD, 2003 (in Chinese).
- [10] China Zhongtie Major Bridge Reconnaissance & Design Institute. Code for Design on Steel Structure of Railway Bridge, TB10002.2-99. Ministry of Railway (MOR), 2000 (in Chinese).
- [11] Miner MA. Cumulative damage in fatigue. Journal of Applied Mechanics, 1945; 12(3):159-164.
- [12] Marco SM, W.L. Starkey. A concept of fatigue damage. ASME Transactions, 1954; 76: 627-632.
- [13] Corten HT, Dolan TJ. Cumulative fatigue damage. Proceedings of International Conference on Fatigue of metals, ASME and IME, 1956; 235-246.
- [14] Collins JA. Failure of materials in mechanical design: analyses, prediction, prevention. Wiley-Interscience Publication, 1993.
- [15] Lundberg G, Palmgren A. Dynamic capacity of rolling bearings. Acta Polytechnica Mechanical Engineering Series, Stockholm, Sweden, 1947; 1(3).

- [16] Shanley FR. A theory of fatigue based on unbonding during reversed slip. Report No. P350, The Rand Corporation, 1952.
- [17] Grover HJ. An observation concerning the cycle ratio in cumulative damage. Fatigue in Aircraft Structures, STP-274, American Society for Testing and Materials, Philadelphia, 1960: 120-124.
- [18] Freudenthal AM, Heller RA. On stress interaction in fatigue and a cumulative damage rule. Journal of the institute of Aeronautical Sciences, 1954; 26(7): 431-442.
- [19] Henry DL. Theory of fatigue damage accumulation in steel. ASME Transactions, 1955; 99: 913-918.
- [20] Fuller JR. Research on techniques of establishing random type fatigue curves for broad band sonic loading. National Aeronautical Meeting, Society of Automotive Engineers and American Society of Naval Engineers, 1963; Paper 761C.
- [21] Yao WX, Ye B, Zheng LC. A verification of the assumption of anti-fatigue design. International Journal of Fatigue, 2001; 23: 271–277.
- [22] Dong P. A structural stress definition and numerical implementation for fatigue analyses of welded joints. International Journal of Fatigue, 2001; 23: 865-876.
- [23] Doerk O, Fricke W, Weissenborn C. Comparison of different calculation methods for structural stresses at welded joints. International Journal of Fatigue, 2003; 25: 359-369.
- [24] Atzori B, Lazzarin P, Meneghetti G, Ricotta M. Fatigue design of complex welded structures. International Journal of Fatigue, 2009; 31: 59–69.
- [25] Norme Tecniche per le Costruzioni; 2008 (In Italian).

CHAPTER 5

FATIGUE ENHANCEMENT TECHNIQUES

The fatigue life of an orthotropic deck bridge can be improved by better designs or by weld enhancement techniques. Developing details which reduce stress is the first and most important step to increase the service-life of an orthotropic deck. With the use of FE method, the more accurate analyses of detail prototype can be obtained and tested. This is especially useful in low resistance details where small analytical error can be a large percentage error for low resistance categories. Fatigue behavior is still not well understood at low stress ranges and high number of cycles. Most codes are not in agreement where the number of cycles exceeds 10 Million. This becomes evident when reviewing the S-N curves shown for various codes as illustrated in Chapter 4. The second method is to provide enhancement of the weld by fabrication techniques. Enhancement techniques have not been used in orthotropic deck fabrication. However, considering the current uncertainties relative to resistance at high number of cycles, and that in highway bridges, especially long span bridges, 10,000 fatigue cycles per day are not uncommon, such that 100 Million cycles is reached in, say, 30 years, appropriate enhancement techniques only in areas of hot spots provides much greater certainty relative to the postulated life of the structure, and may even allow for weight reduction of the structure, from which other benefits are derived.

Fatigue performance of an orthotropic deck bridge can be improved by the following methodologies:

a) Introduce beneficial compressive stress

Large numbers of tests and investigations have reveal that beneficial compressive stress in steel structures, especially in welded structures, can improve the fatigue life dramatically. There are several surface treatment techniques that introduce compression and eliminate or reduce the tensile residual stresses thus reducing the mean stress improving the fatigue life of welded structures.

b) Reduce stress concentration

Fatigue cracks are easy to initiate at the connection where produces high stress concentration and the stress state is very complicated. Therefore, to reduce the stress concentration by designing more reasonable geometry, such as shape of cutout, can be helpful to improve the fatigue life.

c) Remove the defects in component

Defects in welds cause stress concentrations and are sites of crack propagation thus reducing the service life, especially the defects in welded area. Grinding is one of the effective treatments removing defects, particularly for welded components. Grinding and weld repair at the toe of the weld removes microscopic slag inclusions which are the causes of stress concentration at toe of welds.

d) Increase the rigidity of the connection

To increase the rigidity of the connection is beneficial to resist fatigue cracking. High strength bolts can be applied to places where are susceptible to fatigue cracking. Large numbers of experiments and repairing cases in the last century had already shown that it is one of the most effective methods to improve the fatigue life.

The weld toe is a primary source of fatigue cracking due to the severity of the stress concentration. Apart from a relatively sharp transition from the plate surface to the weld, dependent on the weld profile, the stress concentration effect is aggravated by the crack-like flaws. Fatigue cracks readily initiate at these flaws.

In general, the weld fatigue improvement methods can be described in two main groups:

- a) Stress methods. To introduce a beneficial compressive stress to the area where cracks are likely to initiate;
- b) Weld geometry modification methods. To remove weld toe defects and/or reduce the stress concentration.

It should be noted that the enhancement of the toe will not improve the fatigue life if fatigue cracks occur at the weld root.

5.1 Stress Methods

A summary of the various improvement techniques is shown in Figure 5-1.

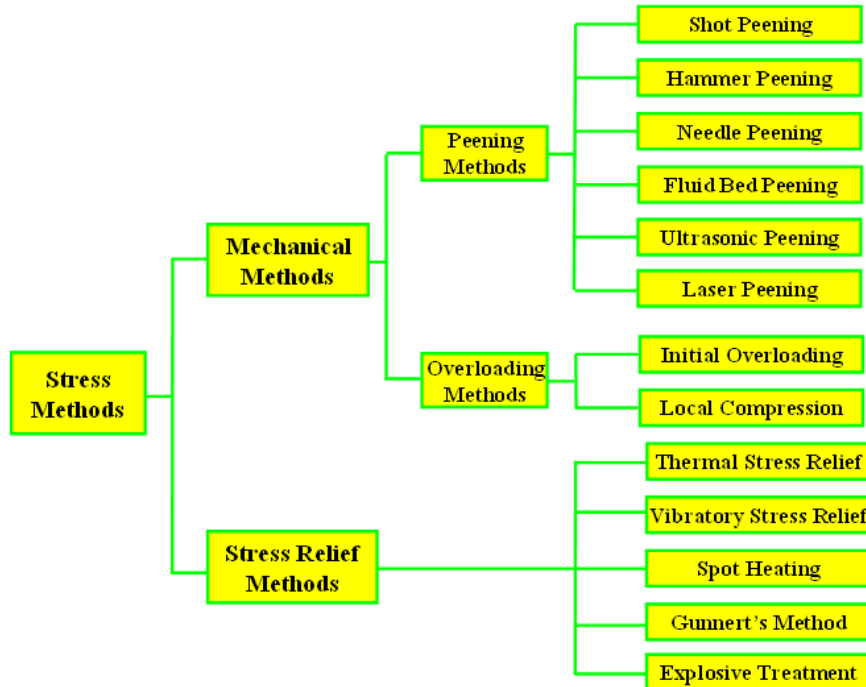


FIGURE 5-1 Classification of stress improvement techniques.

It is obvious that peening is one of the principle methods to introduce the beneficial compressive residual stress to welded joints. Peening is a process which plastically deforms the surface by impacting it with a tool or small metal balls. Several different peening methods are demonstrated in the following.

5.1.1 Shot peening

Shot peening, as cold-work process, has been widely applied recently to try to improve the fatigue strength of material, and also it is becoming a common method to reduce fatigue cracks in steel structures [1]. Through impacting the surface of material by small balls at high speed, the beneficial compressive residual stress is introduced to the surface, as shown in Figure 5-2. Moreover, shot peening process is an effective method to postpone crack initiation and crack propagation.

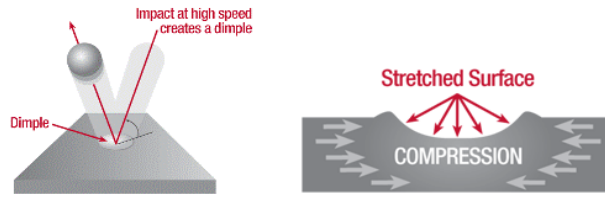


FIGURE 5-2 The theory of shot peening
(www.metalimprovement.com/shot_peening.php).

Based on a larger number of investigations, it is shown that shot peening can increase fatigue strength obviously. Maddox [2] reported an increase of 33% in the fatigue strength at 2-million cycles of joints with longitudinal attachments and fabricated from 260 and 390 MPa yield strength steel while the improvement was 70% for higher strength QT steels with yield strengths of 730 and 820 MPa. Bignonnet et al. [3] reported typical improvements produced by shot peening as shown in Figure 5-3, however, these joints were also fabricated with improved profiles using special electrodes.

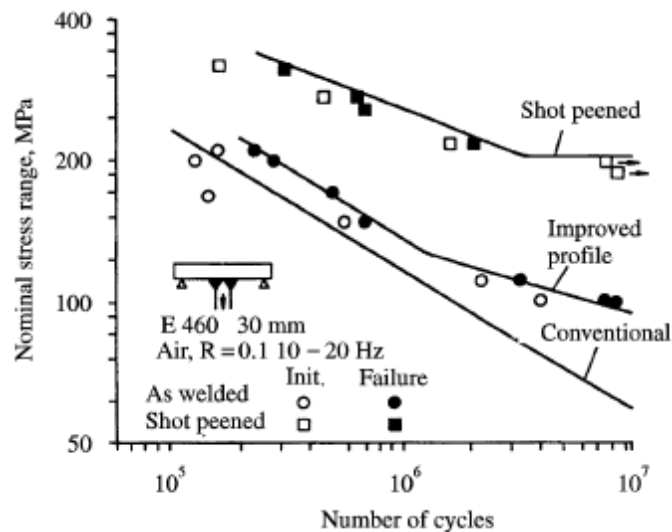


FIGURE 5-3 Fatigue strength improvements obtained by improved profile and shot peening (Bignonnet et al., 1984).

In recent years, some novel shot peening methodologies have been investigated. Cavitation shotless peening (CSP) can increase the fatigue limit more than 11%, while the shot peened specimen gave an increment of 52 MPa (7%) to the fatigue limit

compared to the non-peened specimen [4]. Through the fatigue tests of the aluminum alloy treated by the ceramic and glass shots, residual stresses were created and the axial fatigue strength increased, and an increase in the axial fatigue strength of 25% and 50% of ceramic and glass shots, respectively was observed [5].

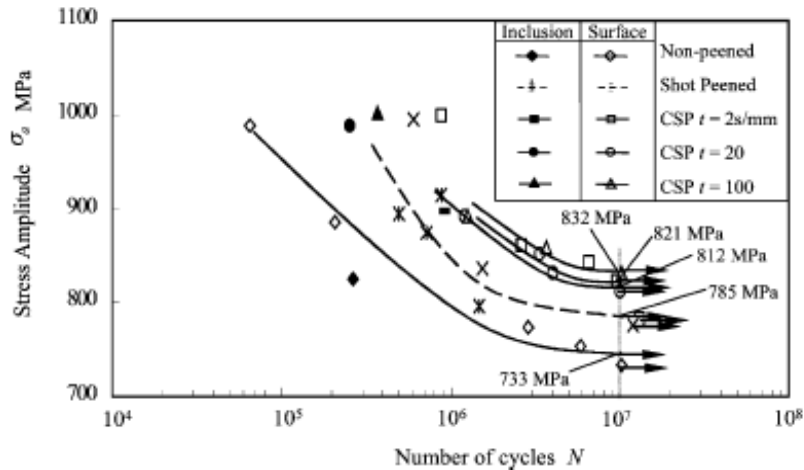


Fig. 7. Cyclic-stress curves.

FIGURE 5-4 Experimental results of the different peening processes (Odhiambo et al., 2003).

The effectiveness of shot peening is affected by many factors, such as part geometry, part material, shot material, shot quality, shot intensity and shot coverage. The effectiveness of shot peening is difficult to be controlled, in general, two parameters are used to specify the process, the Almen intensity and the surface coverage.

5.1.2 Hammer peening

Hammer peening is another cold-work process to improve the fatigue strength. In certain cases it can be applied more readily than other cold working treatments, such as shot peening. The operation of hammer peening can be performed by hand with a ball-peen hammer or with various punches and a hammer; or by a pneumatically operated hammer. The IIW recommendations [6] provided detailed operational information to hammer peening. Figure 5-5 shows the operation of hammer peening.

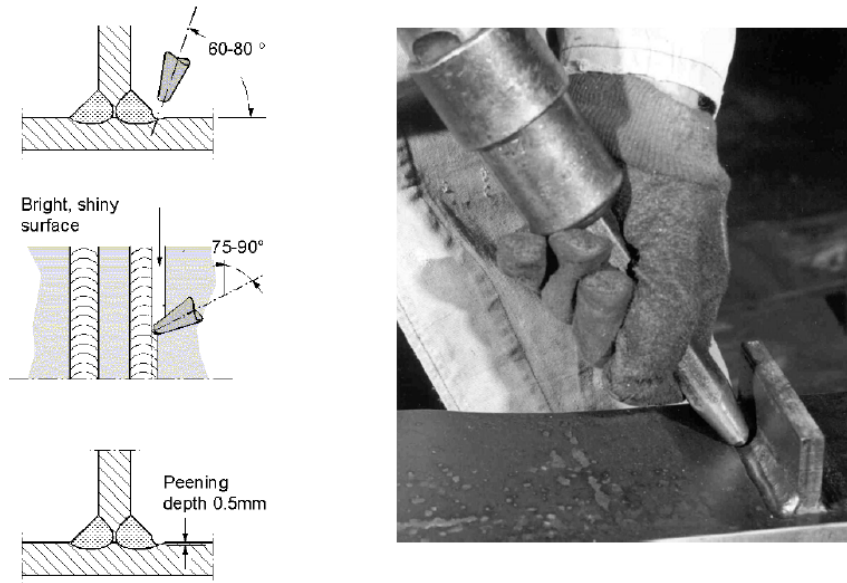


FIGURE 5-5 Operation of hammer peening (IIW recommendations, 2002).

In hammer peening, the beneficial compressive residual stress is induced by repeatedly hammering the weld toe region with a blunt-nosed chisel. It is known that the benefit from hammer peening of steel components can only be claimed for details in design Class FAT 90 or lower in the IIW notation for S-N curves. This limitation is due to the fact that the higher classes include non-welded details, details whose lives are not governed by weld toe failure or the welds that have been already been improved. Typical improvements in fatigue strength are shown in Figure 5-6 [7].

It should be noted that hammer peening produces the noise, and for some industrial environments it would not be allowed for health reasons. An alternative process which is quieter, easier to operate is needle peening.

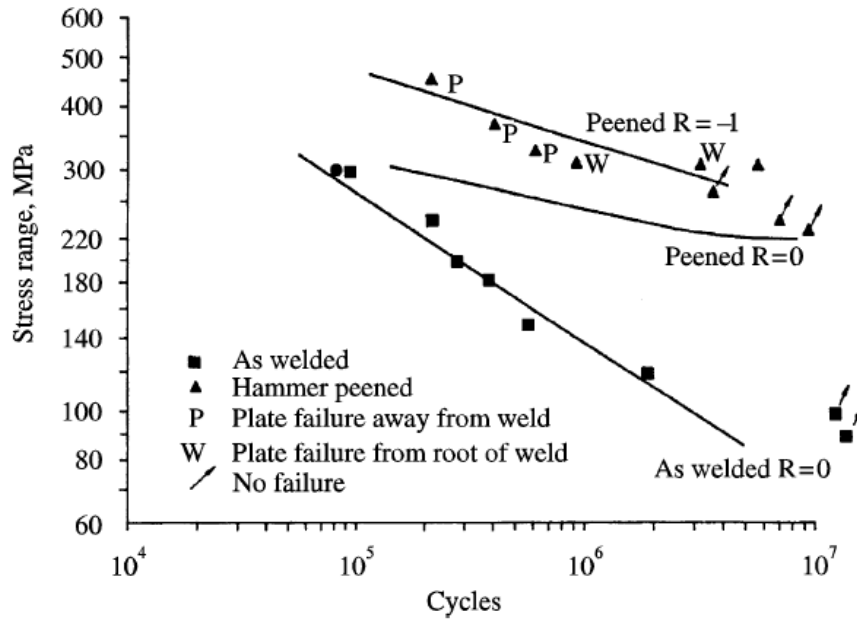


FIGURE 5-6 Improvement in fatigue strength due to hammer peening (Booth, 1977).

5.1.3 Needle peening

Needle peening is a similar process to hammer peening except that the solid tool is substituted by a bundle of steel wires of approximately 2 mm diameter with rounded ends.

In needle peening, the beneficial compressive residual stress is induced by repeatedly hammering the weld toe region with a bundle of round-tipped rods. Compared with hammer peening, it is more suitable when large areas need to be treated.

Based on the IIW recommendations, it is known that the benefit from the needle peening of steel components can only be claimed for details in design Class FAT 90 or lower in the IIW notation for S-N curves, as shown in Figure 5-7 [8]. This is same as hammer peening.

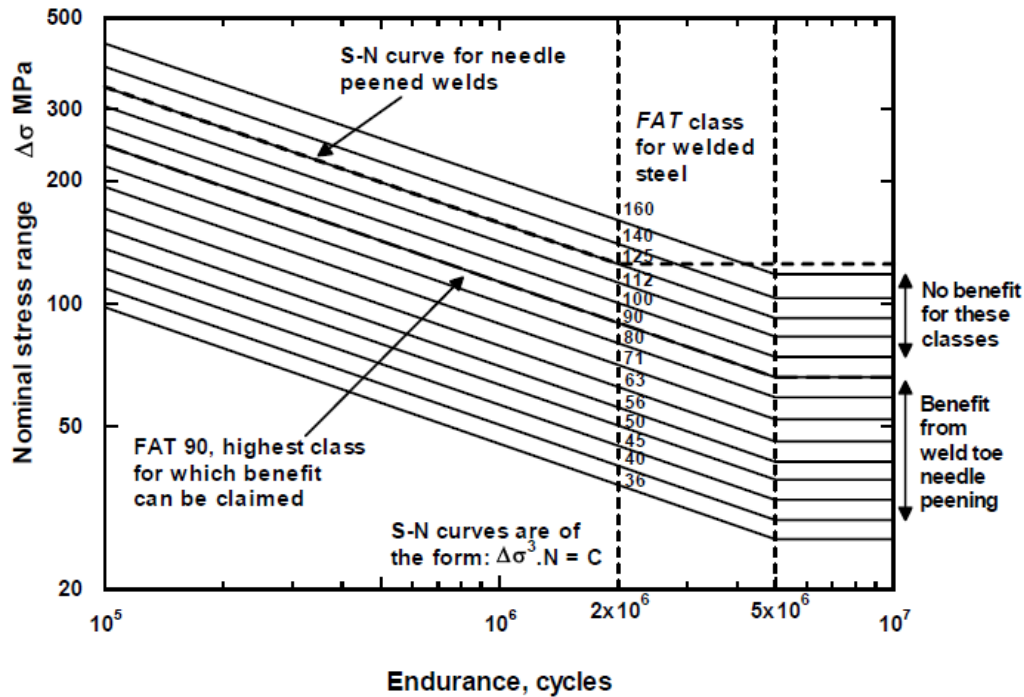


FIGURE 5-7 Design S-N curves for needle peened welds in steels (IIW recommendations, 2002).

It should be noted that the improvement obtained from needle peening is often slightly less than that of hammer peening.

5.1.4 Ultrasonic Impact Treatment

Recently, the Ultrasonic Impact Treatment (UIT) becomes more and more widely used as a method of surface treatment.

In the past decade, UIT of the weld toe had evolved as a promising technique for enhancement of fatigue strength of welded joints [8]. The post-weld enhancement of welded details by UIT involves deformation treatment of the weld toe surface by needle impacts that are excited at ultrasonic frequency. Thus, UIT is a possible way to effectively improve the beneficial compressive residual stress to a detail weld toe. Test results [9] indicated that UIT enhanced the fatigue performance of all treated details by improving the weld toe profile, changing microstructure and introducing

beneficial compressive residual stresses at the treated weld toe. The UIT tool is shown in Figure 5-8.



FIGURE 5-8. Detail of UIT tool (Roy, 2003).

The Category C (AASHTO) transverse stiffener details on the tension flange and web of orthotropic deck can achieve Category B fatigue resistance or better, as shown in Figure 5-9 [9]. The fatigue strength of welded joints treated by ultrasonic peening [10] under constant amplitude loading was improved about 84% at 2×10^6 cycles, and the fatigue life was increased about 3.5~27 times.

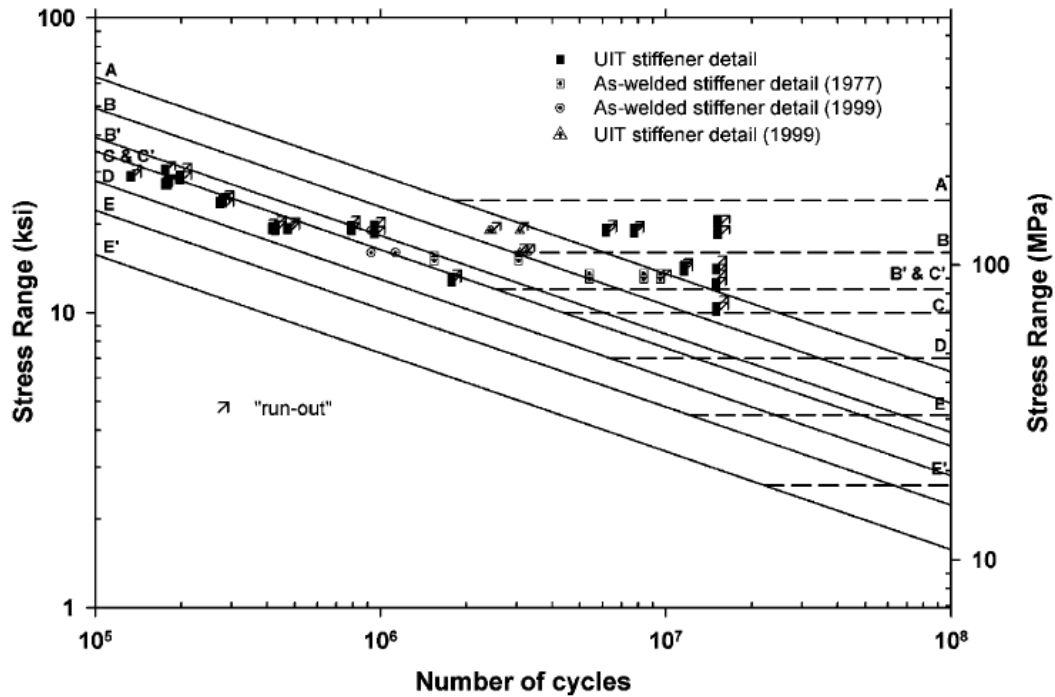


FIGURE 5-9 S-N curves for stiffener details (Roy et al., 2003).

5.1.5 Laser peening

Laser peening (LP) is an emerging surface treatment technology, and it is an extension of conventional shot peening. LP is a rapidly expanding technology capable of developing deep, high compressive stresses in the materials. Prototype laser peening machines were developed in the 1970s, but they and the subsequent versions in the later decades were not updated effectively because the lasers lacked the high repetition rate required for treating parts rapidly.

The beneficial compressive residual stress produced by LP can significantly increase fatigue life and fatigue strength by inhibiting the initiation and propagation of cracks. The LP process is illustrated in Figure 5-10 [11].

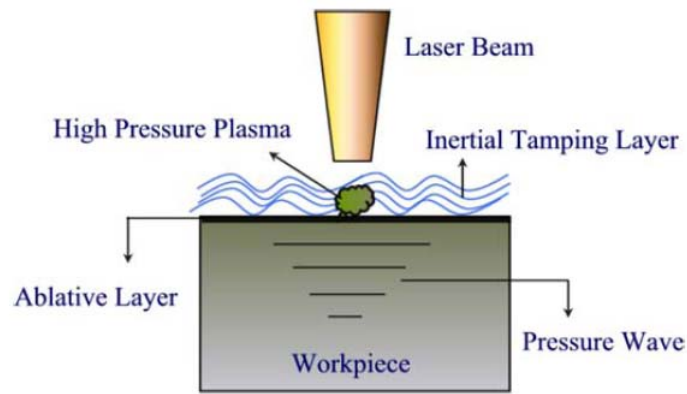


FIGURE 5-10 A schematic of the laser peening process (Hatamleh, et al., 2007).

Specimens[11] treated by LP had an increase of about 146% over the non-peened the friction stir welding specimens, as shown in Figure 5-11.

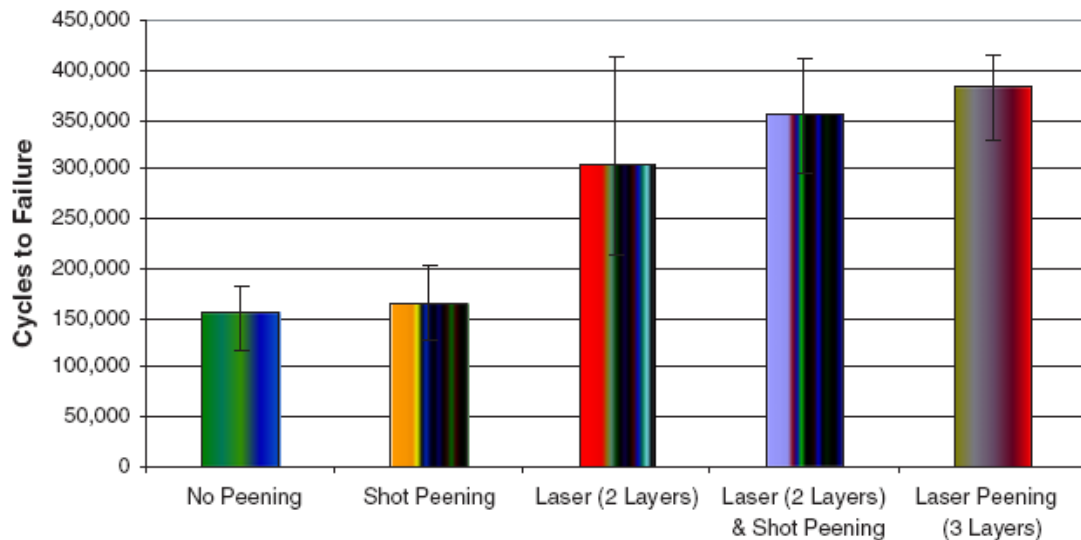


FIGURE 5-11 High cycle fatigue test results (Hammersley et al., 2000).

5.1.6 Fluid Bed Peening

The fluidized bed has been used to coat the components with powders more than half century. In fluidized bed powder coating, heated parts are either dipped directly into a container of fluidized powder or passed through an electrically charged cloud of powder, which is created above a container of fluidized powder, as shown in Figure 5-12.

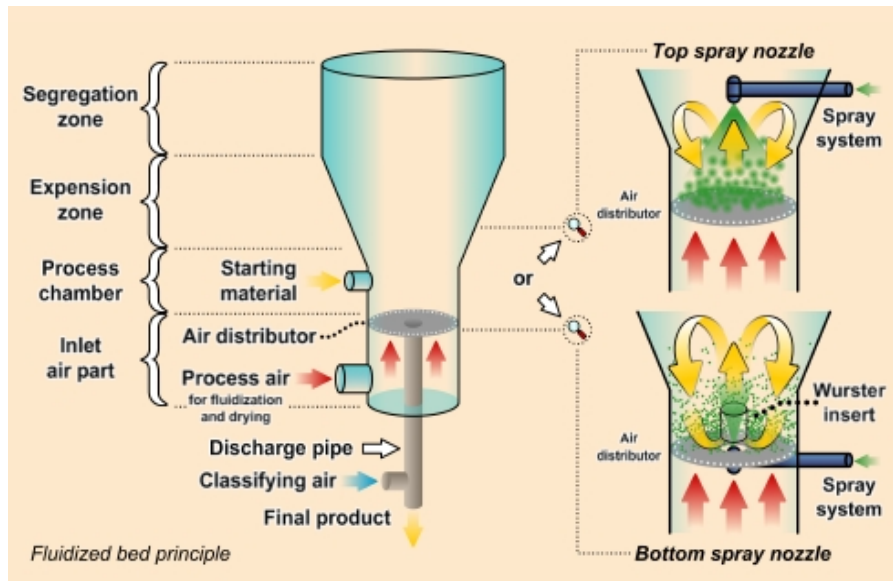


FIGURE 5-12 Fluidized bed principle

(http://www.gate2tech.com/article.php3?id_article=6).

The fluidized bed coating technology is a simple dipping process that can be either conventional or electrostatic. In the conventional fluidized bed process, the fluidized bed is a tank with a porous bottom plate. The electrostatic fluidized bed is essentially a fluidized bed with a high voltage DC grid installed above the porous plate to charge the finely divided particles. Once charged, the particles are repelled by the grid, and they repel each other, forming a cloud of powder above the grid. The advantages of electrostatic fluidized bed coating is that preheating of parts is generally not necessary and small products, such as electrical components, can be coated uniformly and quickly.

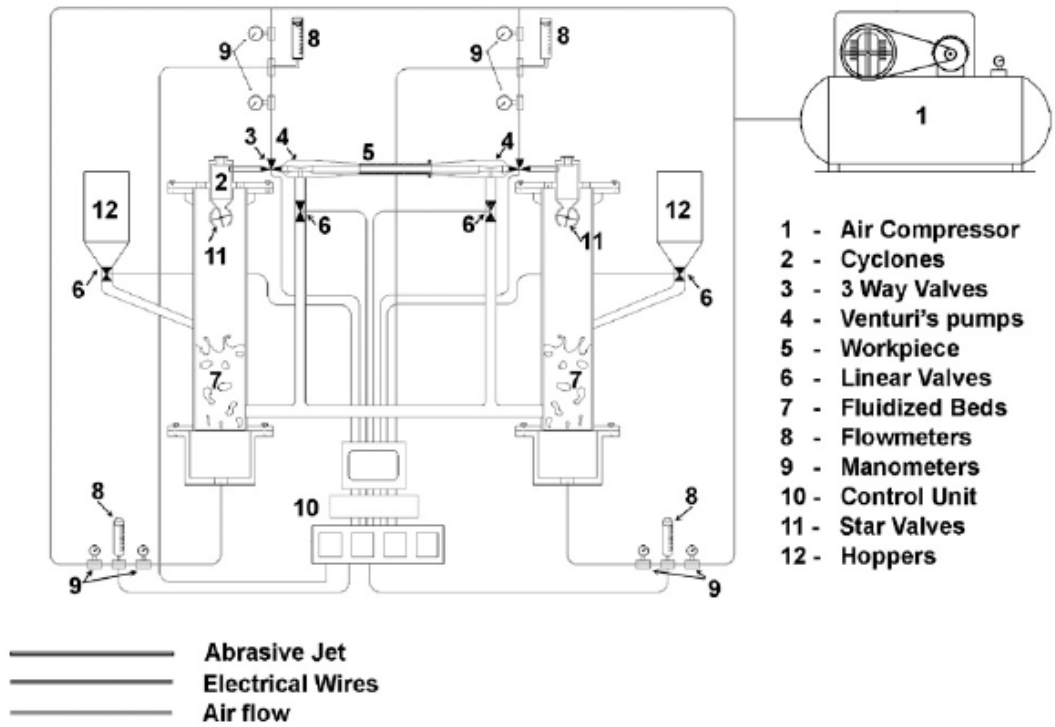
The fluid bed peening (FBP) is developed from the electrostatic fluidized bed technology as one kind of cold-work surface treatments. FBP technique is relatively novel treatment to coat metal substrates, change the surface properties, and induce micro-structural changes. This technique is studied by Department of Mechanics, at University of Rome “Tor Vergata”, and a larger number of tests have been done in the laboratory and obtained fruitful achievements.

FBP is performed in a cold three-dimensional fluidization column. The machine system is shown in Figure 5-13. The fluidization column consists of a circular column

with a cross-section of 25 cm in diameter, respectively, and a height of 120 cm. The column is made of Plexiglas so that the fluidization process can be visible during the peening process. At the base of the column, there is an inlet section, usually called the homogenization section. This section is designed to produce a uniform air flux throughout the whole cross section of the tubular reactor in order to avoid deviations from ideal hydrodynamic behavior in the fluid bed. To produce a uniform air flux inside the tubular reactor, the homogenization section was filled with porous material. Situated in the bottom part of the fluidization column, the air distributor is composed of a 1mm thick stainless steel mesh. The powders should be supported when they are not fluidized and, at the same time, to assure the passage of the fluidization air. The design of the air distributor has not to modify the velocity distribution produced by the homogenizing section.

Specimens in fluid bed machine are kept in a fixed position in the inner bed, and are subjected to strikes from abrasive grains driven by the fluid onto their surfaces (see Figure 5-14). The investigations of Barletta et al. [13-15] revealed a progressive change in both the surface topography of the metal and in superficial properties (surface hardness, residual stress, density of the dislocations) can be induced. Figure 5-15 shows the treatment effective to the surface morphology under different temperature (*a*, 110°C; *b*, 130°C; *c*, 150°C; *d*, 170°C; *e*, 200°C; *f*, 230°C;). Furthermore, progressive smoothing of specimen surface associated with remarkable material removal can be expected.

After FBP treatment, the crack initiation and crack propagation are postponed. The previous investigations also showed that the peening time and the alternating stress were the only two important experimental factors. Therefore, FBP technique is more convenient to control due to less operational parameters demanded.



Fluidized bed assisted abrasive jet machining (FB-AJM) system

(Barletta et al., 2007)



Figure 5-13 Fluid bed machining system.

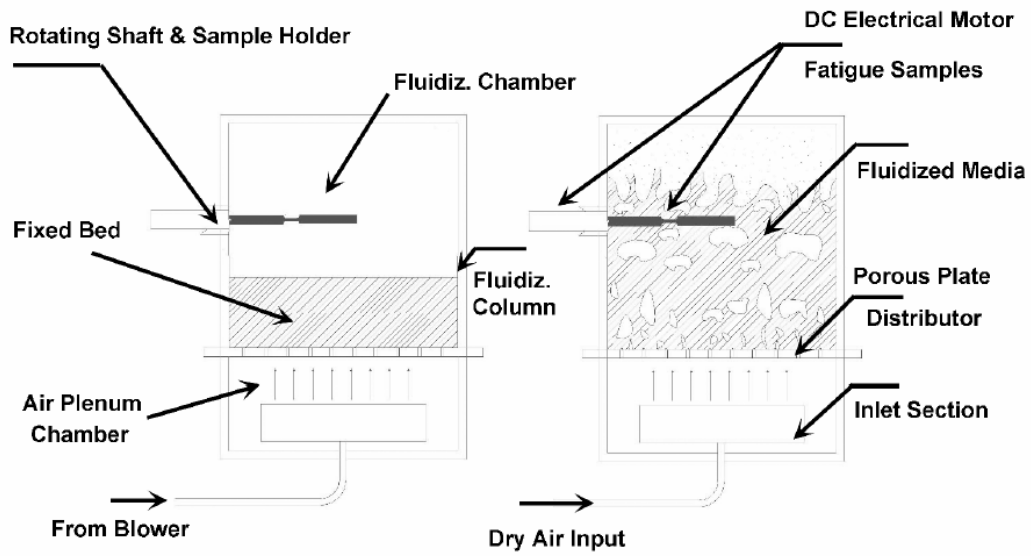


Figure 5-14 Location during fluidized bed processing (Barletta et al., 2007).

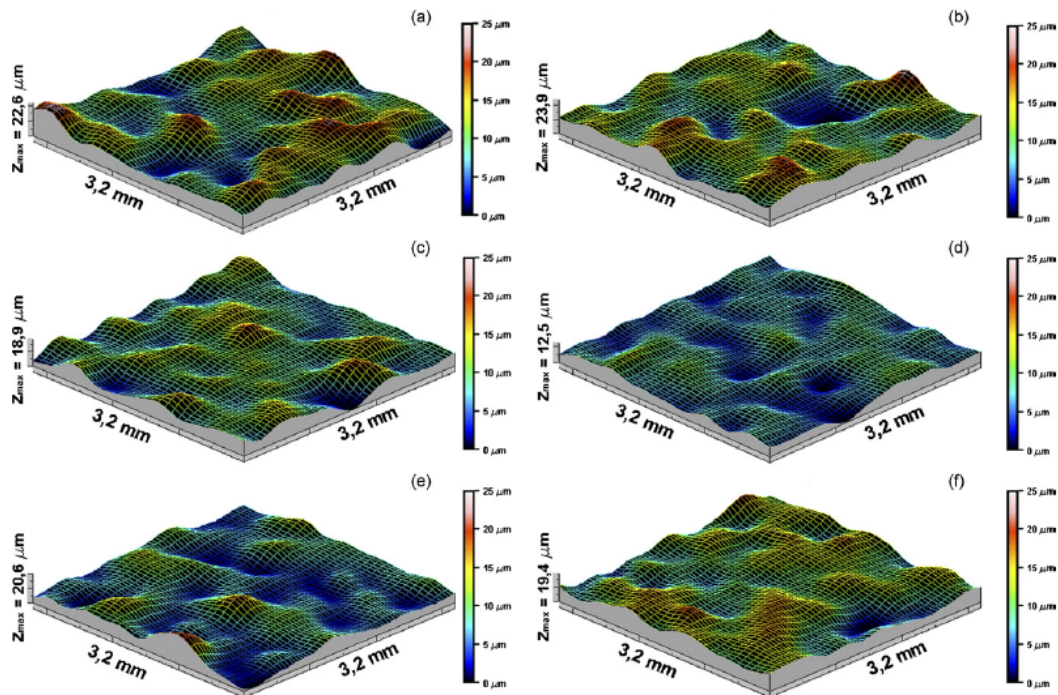


Figure 5-15 Surface morphology of untreated and FB treated fatigue samples (Barletta et al., 2007).

5.1.7 Discussions

Peening methods often bring beneficial compressive residual stresses, thus, the fatigue life can be improved. These post-weld improvement methods influence beneficially, within certain limits, the fatigue strengths of the treated joints are shown in Figure 5-16 [16]. It is found that the effect of hammer peening is better than that of shot peening.

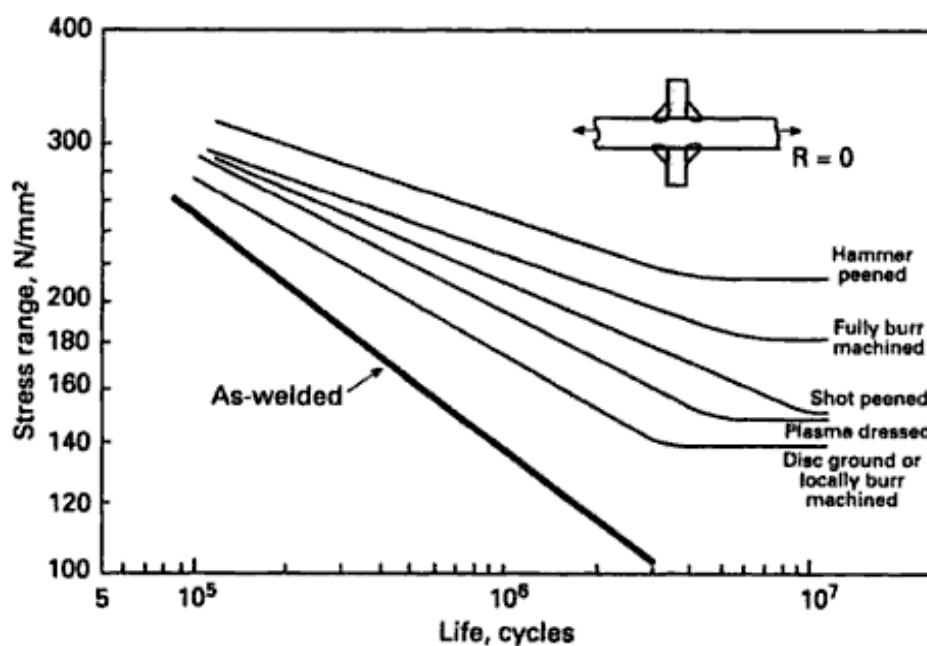


FIGURE 5-16 Typical improvement in fatigue strength of mild steel fillet welds resulting from toe dressing or peening (Maddox, 1991)

The investigations of Maddox [16] do not cover all the previous improvement methods, such as UIT, laser peening and FBP. In order to make a better comparison, some detailed information of all the above peening methods are presented in Table 5-1. Peening method does not work well in high-tensile conditions because the residual stress plays less important role to the fatigue life. The effect of diverse peening has a distinguished difference, sometimes maybe several times. It is found that the UIT can provide the maximal improvement. In addition, the effect of peening is often restrained by many factors. Compared to the other peening methods, FBP needs less

control parameters. The improvement of fatigue life of FBP will be discussed in Chapter 6.

TABLE 5-1 Comparison of the different peening methods.

	Description	Control parameter
Shot Peening	effect: normal; almost does not work in high-tensile condition; travel speed: normal; noisy	intensity, coverage, pressure, flow distance, angle, depth, ball radius, elastic properties of ball
Hammer Peening	effect: good; almost does not work if larger than Class FAT 90; travel speed: normal; noisy	diameter of tool tip, coverage, pressure, angle, depth, speed
Needle Peening	effect: good; almost does not work if larger than Class FAT 90; travel speed: normal; noisy	diameter of needle, temperature, coverage, pressure, angle, depth, speed
Ultrasonic Impact Peening	effect: excellent; almost does not work when stress larger than 200MPa; travel speed: normal; noisy	pulse energy, pulse time, speed, amplitude, frequency, duration, speed
Laser Peening	effect: good; almost does not work in high-tensile condition; travel speed: normal; noisy	pulse energy, pulse time, number of laser pulses, focal lens, working distance, thickness of the energy absorbing coating, curable resin, transparent overlay to control the laser shock process
Fluid Bed Peening	discussed in Chap. 5.3	peening time, alternating stress

5.2 Geometric Methods

Geometric methods remove weld toe defects, thereby, stress concentrations are reduced. A summary of the various geometric improvement techniques are presented in Figure 5-17. The main ones are burr grinding and TIG dressing, and both of them have been adopted by the recommendations of IIW [6]. Therefore, the two improvement techniques are presented in the following.

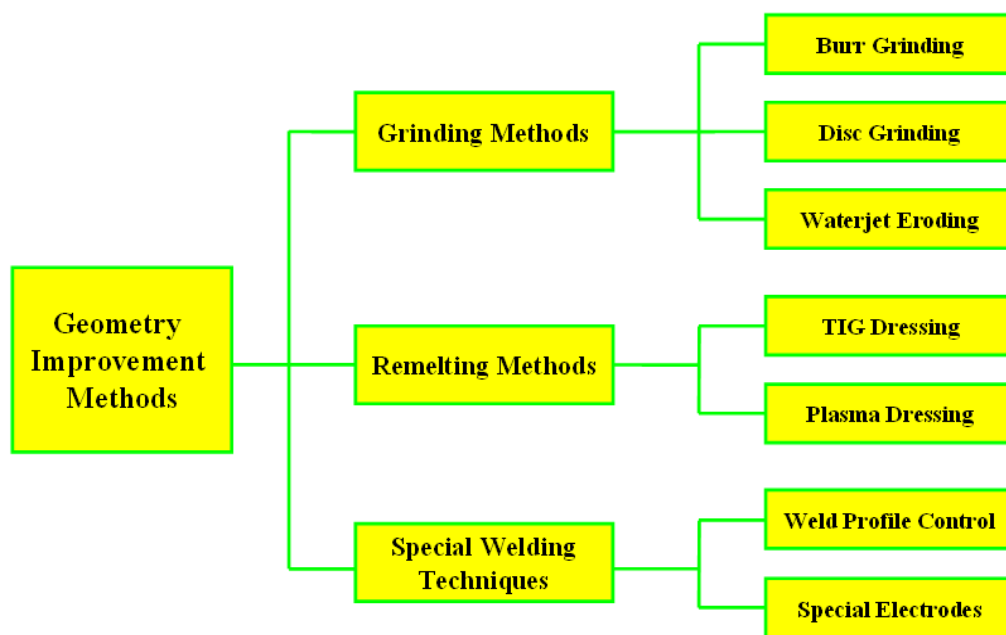


FIGURE 5-17 Classification of geometric improvement techniques.

5.2.1 Burr grinding

The first aim of burr grinding is to remove/reduce the weld toe flaws from where fatigue cracks may initiate and propagate. Meanwhile, it aims to decrease the local stress concentration of the weld profile through smoothly blending the transition between the plate and the weld.

The effect of burr grinding to the fatigue life of the weld has been studied for a long time. A comparison of the improvement in fatigue strength obtained from laboratory tests is shown in Figure 5-18 [17]. Although the effect is not as good as hammer

peening, burr grinding also provides significant improvement. Moreover, burr grinding is more frequently used to improve the fatigue life due to the flexibility of implement.

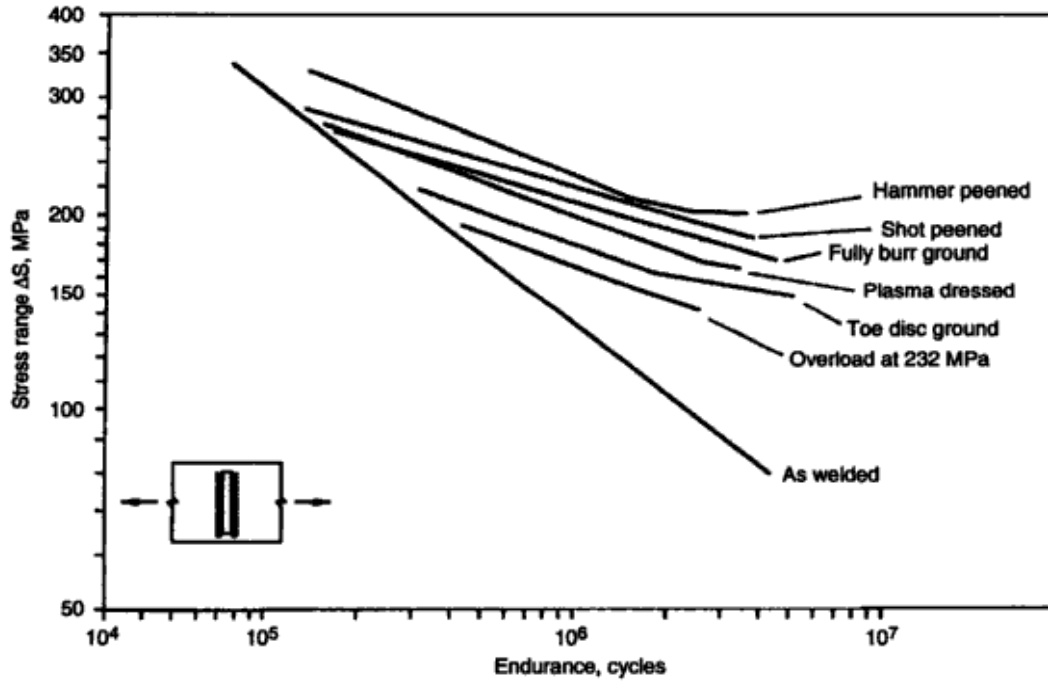


FIGURE 5-18 Comparison of different improvement techniques (ASM, 1997).

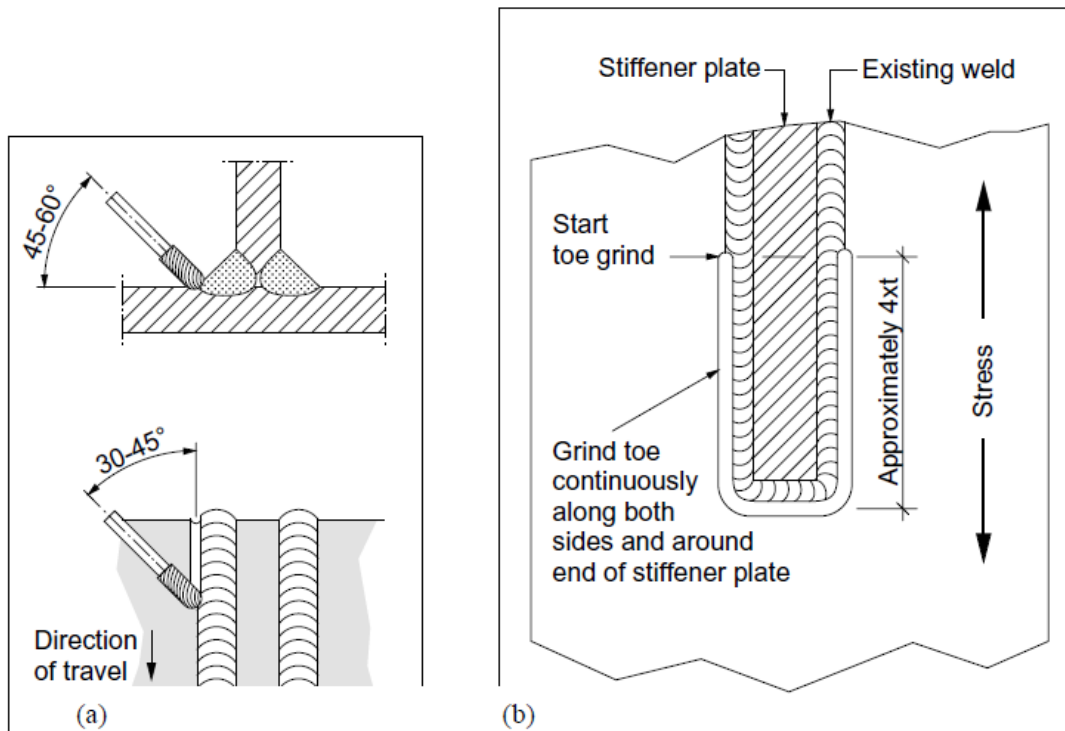


FIGURE 5-19 The weld toe burr grinding technique (IIW recommendations, 2002).

The burr grinding procedure is illustrated in Figure 5-19. In order to obtain better effect, many parameters are necessary to be controlled, such as the treated depth, the operational angle of the grinder, and the rotational speed and the pressure of the grinder. In general, grinding must extend to a depth of at least 0.5 mm below any visible undercut, as shown in Figure 5-20.

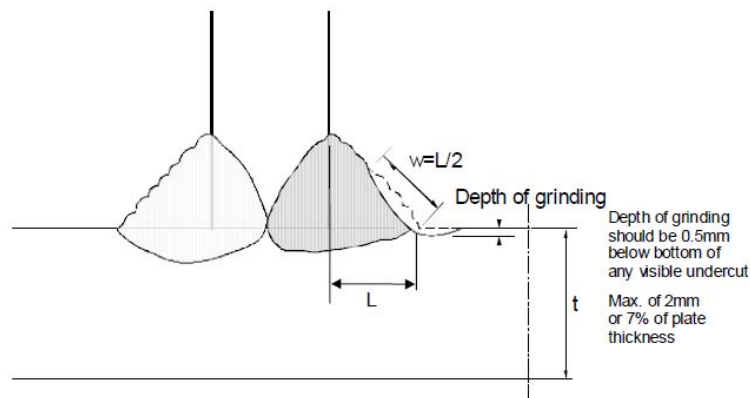


FIGURE 5-20 The burr grinding technique, showing depth and width of groove in stressed plate (IIW recommendations, 2002).

For IIW FAT 90 Class or lower details the benefit of burr grinding corresponds to an increase in allowable stress range by a factor of 1.5, corresponding to a factor of 3.4 on life. Furthermore, it can be assumed that the constant amplitude fatigue limit corresponds to an endurance of 2×10^6 .

5.2.2 TIG dressing

In Tungsten Inert Gas (TIG) dressing, the weld toe region is remelted to improve the weld profile. As well, it aims to reduce the local stress concentration effect of the local weld toe profile by providing a smooth transition between the plate and the weld face.

The effect of TIG dressing to the fatigue life is evident. Huo et al. [10] investigated the welded joints treated by TIG dressing. It is found that the fatigue strength of the specimens at 2-million cycles are increased 34% under constant amplitude loading, as shown in Figure 5-21.

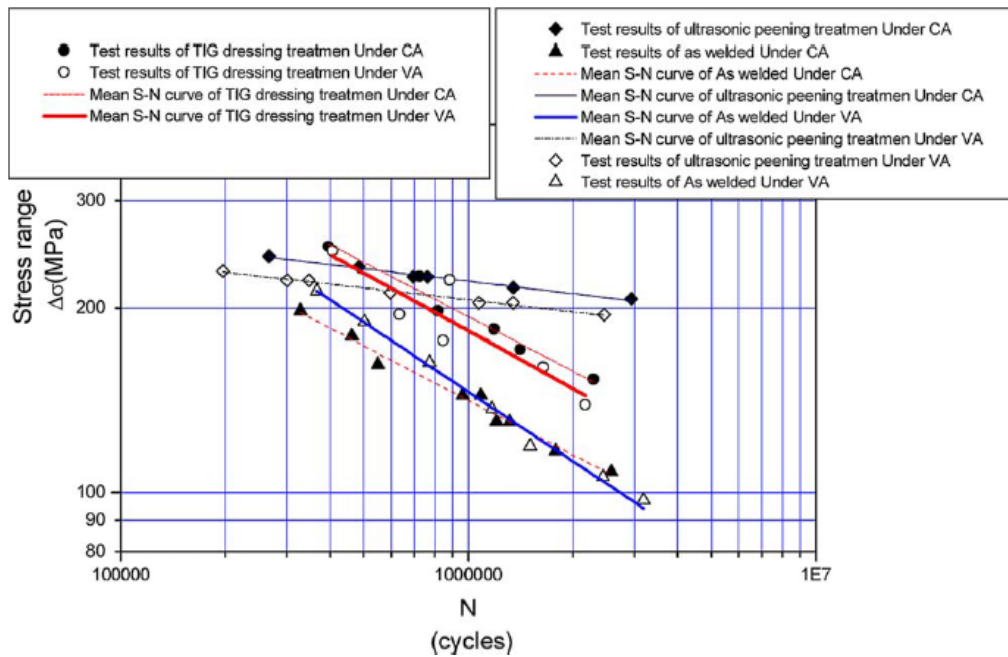


FIGURE 5-21 S-N curves of fillet welds (Huo et al., 2005).

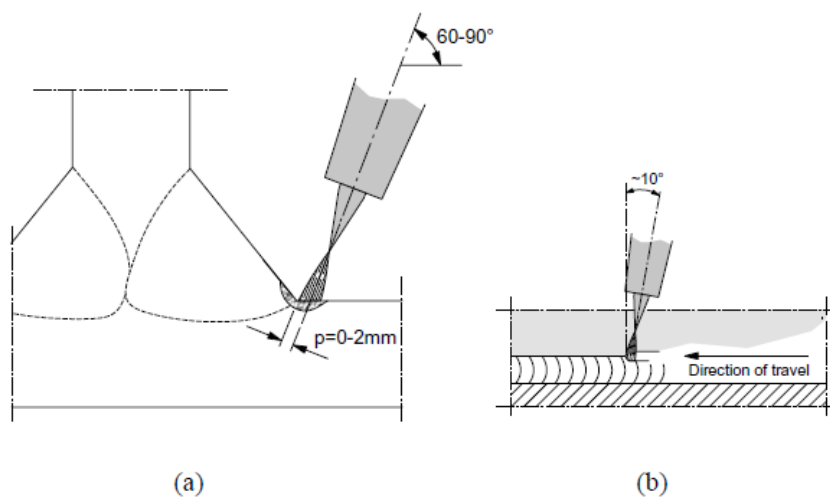


FIGURE 5-22 Typical position of torch and dressing zone (IIW recommendations, 2002).

In general, the best improved result is obtained when the arc centre is located a small distance away from the weld toe, as shown in Figure 5-22a. Furthermore, the small backward tilt shown in Figure 5-22b may help to maintain an adequate gas shield. The benefit from TIG dressing of steel components can only be claimed for details in FAT 90 Class or lower in the IIW notation for S-N curves.

5.3 Fatigue tests applied FBP

Sixteen specimens are tested in the laboratory of University of Rome “Tor Vergata”. The specimens are divided into four different groups: simple (group A), simple and treated by FBP (group B), notched (group C), notched and treated by FBP (group D), and they are tested under cyclic constant amplitude fatigue loading. The notched groups are designed to simulate fatigue cracks on steel components. There are many different methods to retrofit fatigue cracks, such as hole-drilling, air-hammer peening, cover plate installation, high strength bolt [18, 19]. Therefore, group D is designed to study whether FBP technology is effective to retrofit the fatigue cracks in steel components.

5.3.1 Material tests

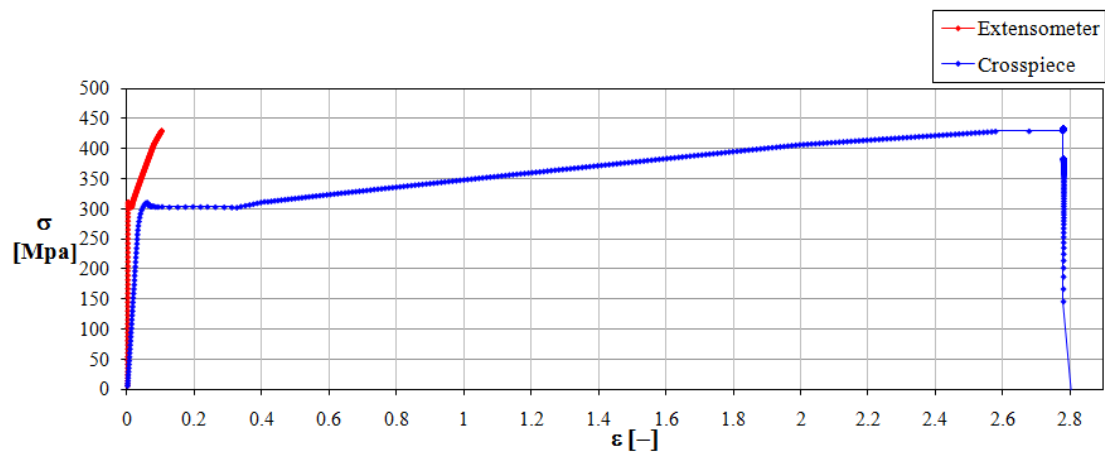
The material of specimen utilized in the tests is Fe 360 steel. The actual properties of the material are tested by MTS Insight machine, as shown in Figure 5-23. In order to measure the deformation of the steel, an extensometer is used during the material tests.



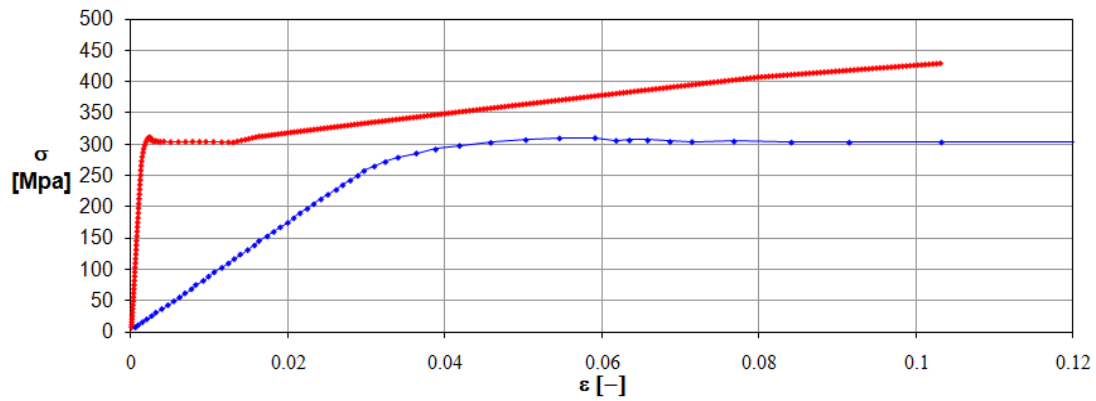
FIGURE 5-23 Material tests.

The strain-stress curves of the steel are obtained through the laboratory tests, as shown in Figure 5-24a. In order to show the curve better, the parts of two curves while the strain is less than 0.12% are demonstrated in Figure 5-24b.

The yield strength is measured at 38.2 kN, the corresponded tensile stress is 310 MPa and the strain is 0.237%. The fracture stress obtained from the test is 47.1 kN, and the corresponded tensile stress is 434 MPa. Figure 5-25 shows the fracture of the test specimen.



a



b

FIGURE 5-24 Strain-stress curves of Fe 360 steel.



FIGURE 5-25 Fracture in the tensile test.

5.3.2 Surface treatment

The section parameters of the first two groups are as following, the length varies from 19 cm to 30 cm, widths 3 cm, and thickness 0.3 cm. The section parameters of the latter two groups are in the following, the length varies from 20 cm to 30 cm, widths 3 cm, and thicknesses 0.3 cm. Furthermore, the sections of the notches are the same, with “V” shape, the height is 0.05 cm, and the angle is 120° , as shown in Figure 5-26. The treatments are carried out by Fluid Bed machine, as shown in Figure 5-13. Al_2O_3 powders are used to treat the surfaces of specimens. The diameter of the Al_2O_3 powder is 1 mm. Peening time is an important parameter to control FBP treatment, therefore, an empirical peening time is chosen in the tests. The specimens are treated 8 hours totally in order to obtain good effect, 6 hours for the tensile surfaces and other 2 hours for the compressive surfaces.

Table 5-2 Detailed sizes of the four groups.

Group	Length (cm)	Width (cm)	Height (cm)	Notch
A	18;	3	0.3	-
	21.5;			
	23;			
	25.5			
B	17.5;	3	0.3	-
	19;			
	19.5			
	18;			
C	20;	3	0.3	“V”
	21.5;			
	23;			
	25.5;			
D	28	3	0.3	“V”
	18;			
	23;			
	25.5			

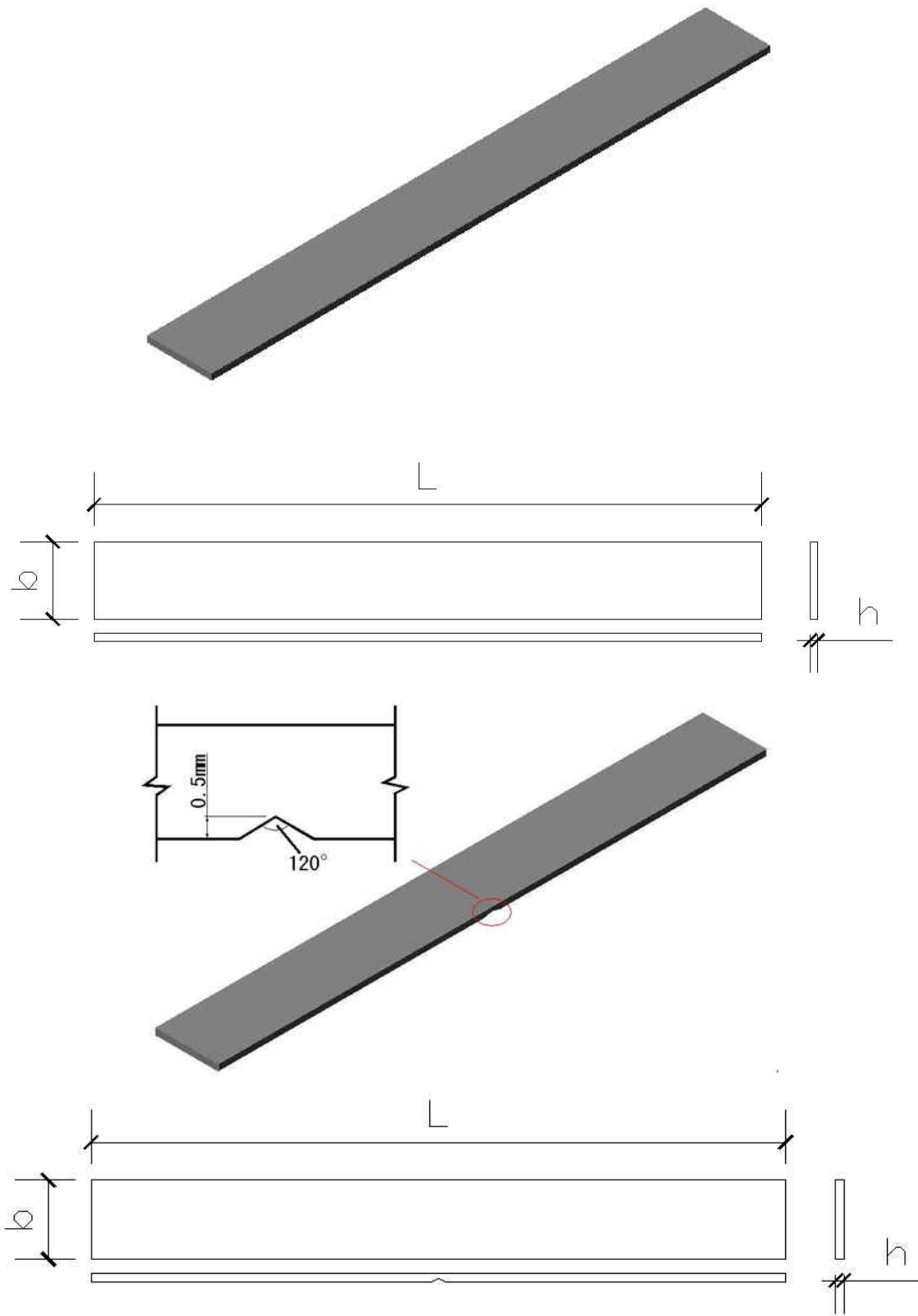


FIGURE 5-26 Configurations of the specimens for fatigue tests.

The machine which was used to measure the surfaces of the specimens is Talysurf-Hobson, CLI 2000, as shown in Figure 5-27. This machine has the capability to measure and analyze surfaces in three dimensions using either contact (range from 3 μm to 3 mm) or non contact gauging technology. In this study, the contact gauging technology is applied to measure the surfaces of specimens. The roughness measured is a map of 10 mm*0.5 mm, and the scanning velocity is 200 $\mu\text{m/s}$. The system offers powerful measurement and analysis capability in 3D and 2D and it is easy to operate.

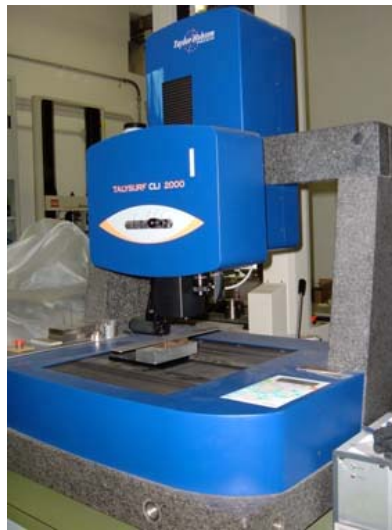


FIGURE 5-27 Talysurf-Hobson, CLI 2000.

Significant difference of the surface performances among the four groups can be found in Figure 5-28. The specimens with notch are much coarser than that without notch according to the tested results.

The average roughness of the four groups is shown in Figure 5-29. It is found that the average roughness of group A is much larger than group B, and group C is larger than group D. The average roughness of group B after being treated 6 hours (tensile stress side) is only one third of group A, and the roughness of group D also treated 6 hours is half of group C. As known, fatigue cracking is greatly influenced by surface roughness. Smooth surface can offer a good performance to the fatigue life since it can delay the cracking initiation and propagation, while rough surface will accelerate the cracking initiation and propagation. Therefore, better fatigue performance of the specimens treated by FBP under cyclic loading are expected.

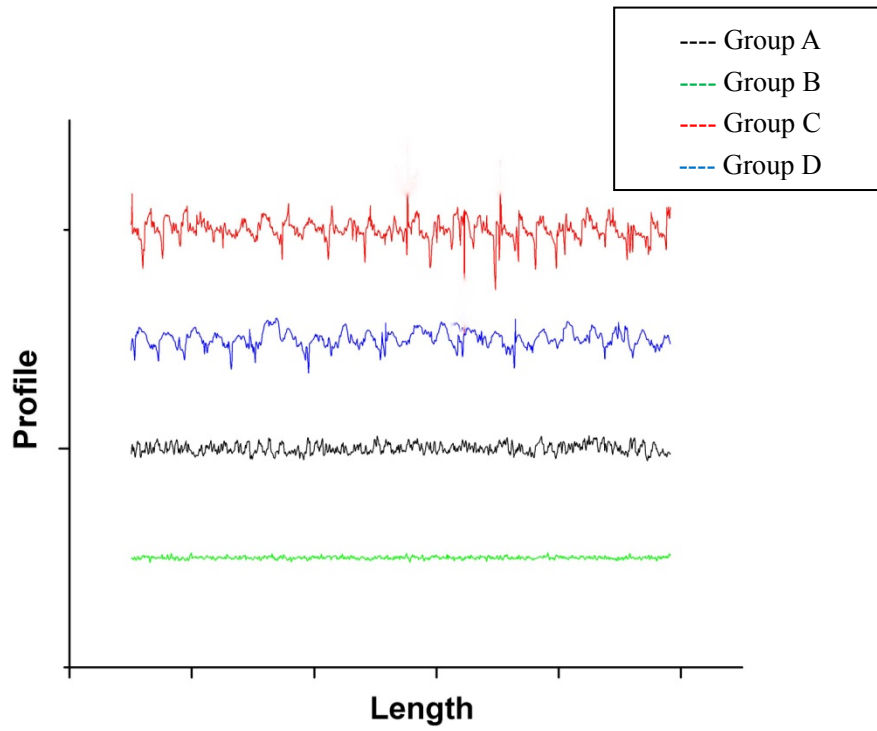


FIGURE 5-28 Surface performances of the four groups.

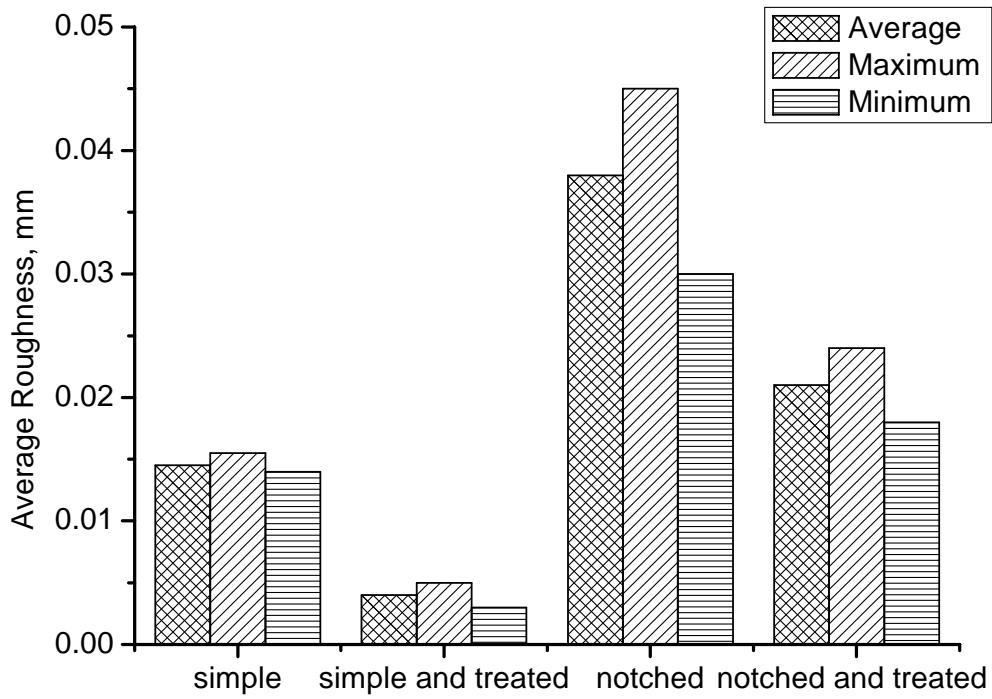


FIGURE 5-29 Surface roughness of four different types.

In addition, the average roughness of notched groups (C and D) was much larger than the simple groups (A and B). The fatigue life of notched specimen will be much shorter than specimen without notch taking accounting into the surface performance and the stress concentration produced by the notch.

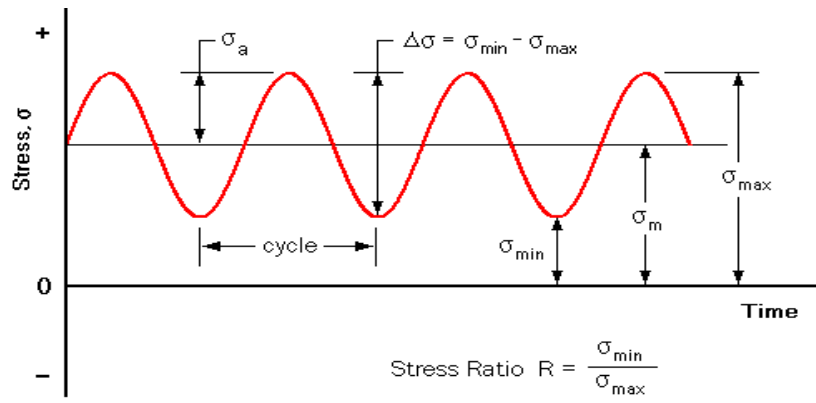
5.3.3 Fatigue tests

5.3.3.1 Loading Spectrum

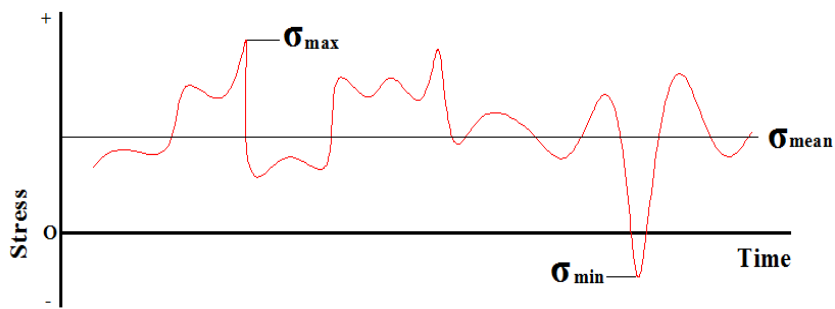
Fatigue loading in a real situation is usually very complicated due to the random vehicle loading in the service and, thus, it very difficult to simulate in the design stage. Therefore, variable amplitude loading is often simplified as constant amplitude loading in order to count the number of repeated cycles. Constant amplitude loading and variable amplitude loading are shown in Figure 5-30. Rain-flow counting method [20] is widely used in the fatigue analyses to reduce a spectrum of varying stress into a set of simple stress reversals, and then the Miner's rule is utilized to evaluate the fatigue life of a structure.

Constant amplitude loading is utilized in the fatigue tests. The fatigue loading acted at the middle of the specimen, as shown in Figure 5-31. The frequency of the fatigue machine is 10 Hz.

The stress ranges applied during the tests for these two groups varied from 285 MPa to 572 MPa. The stress ranges applied during the tests for these two groups varied from 237 MPa to 572 MPa (with notch).



a. Constant amplitude;



b. Variable amplitude.

FIGURE 5-30 Loading scheme.

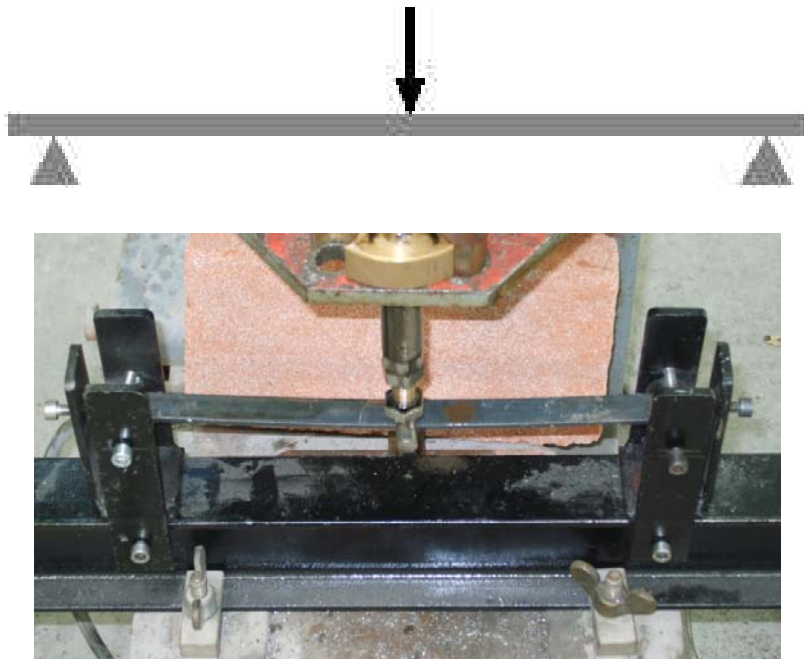


FIGURE 5-31 Fatigue tests.

5.3.3.2 Test Results

Cracks

In the tests, it was found that all the failures of specimens were brittle fractures. The fatigue cracking occurred in the middle of the bottom of the specimens due to the maximal stress range. The cracks at simple specimens initiated from the edge side and ended in the middle, while the cracks at notched specimens crossed through the bottom of the specimens along the notches, as shown in Figure 5-32. Compared to the simple and notched groups, the failure of notched group are more serious.

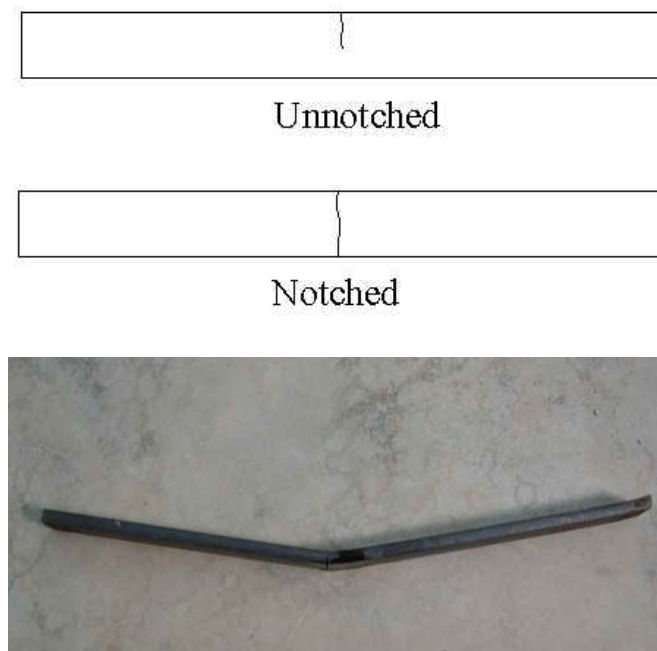


FIGURE 5-32 Cracks and fracture in the fatigue tests.

Fatigue performances

The test results for specimens of the four groups under fatigue loading are shown in Figure 5-33, 5-34 and Table 5-3.

Figure 5-33 shows the number of repeated cycles of group A and B under fatigue loading. At the stress range of 401 MPa, the simple specimen didn't occur any fracture before experienced 5-million cycles. The fatigue lives of the treated specimens are improved dramatically when the stress range is less than 500 MPa,

while it is not so efficient at high stress range. The fatigue strength of specimens after treated 8 hours by fluid bed peening had a distinct increasing for both of the two groups, particularly at low stress range.

Figure 5-34 shows the number of cycles of group C and D under the fatigue loading. At the stress range of 285 MPa, the cyclic number of notched specimen is 705-thousand, while that of the notched and treated specimen is 2.75 millions, about 3.90 times than before. At the stress range of 351 MPa, group D suffered 1.03 million cycles, while group C experienced 105 thousand cycles, 11.8 times than before. At the high stress range of 572 MPa, group C experienced 44 thousands cycles, while group D suffered 73 thousand cycles, 1.66 times than before. The notched specimens treated 8 hours by fluid bed have longer fatigue lives, especially at low stress range, while the effect at high stress range is much less because the stress concentration plays less important role to the fatigue life.

According to the tests, the fatigue lives of notched and simple specimens after peened 8 hours can have a better fatigue performance. FBP has a remarkable effect to postpone the initiation and propagation of fatigue cracking in steel, particularly under low stress range. Therefore, FBP technology can be used to prolong the fatigue life of steel structures, as well for small cracked steel structures.

TABLE 5-3 Tested results of the four different groups.

Group	Stress Range (MPa)	Number of Cycles (10³)	Notes
A	285	8,000 (unfailed)	SIMPLE
	351	8,000 (unfailed)	
	401	1,290	
	572	500/400	
B	495	8,000 (unfailed)	TREATED (8 hrs)
	514	6,500	
	610	800	
C	237	8,000 (unfailed)	NOTCHED
	285	705	
	351	105	
	401	87	
	464	51	
	572	44	
D	285	2,750	NOTCHED+TREATED (8 hrs)
	351	1,030	
	572	73	

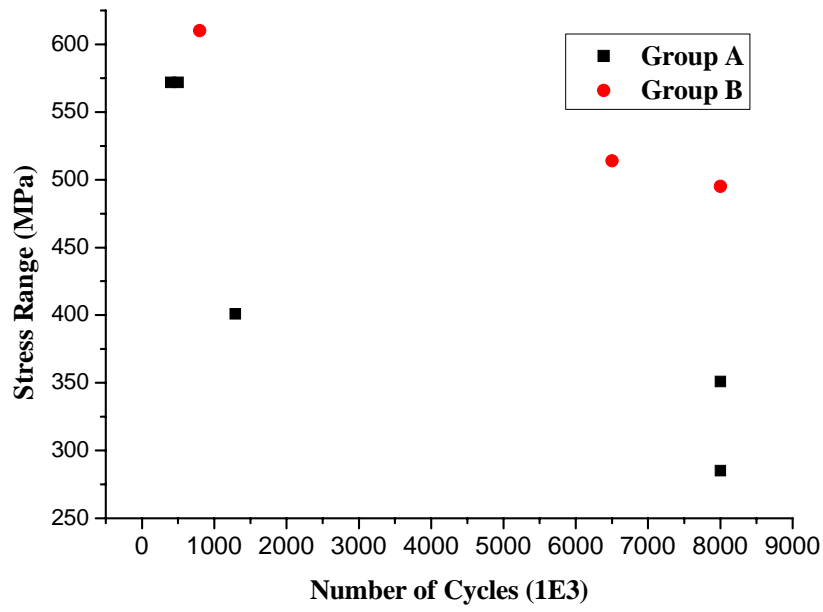


FIGURE 5-33 Fatigue lives of group A and B.

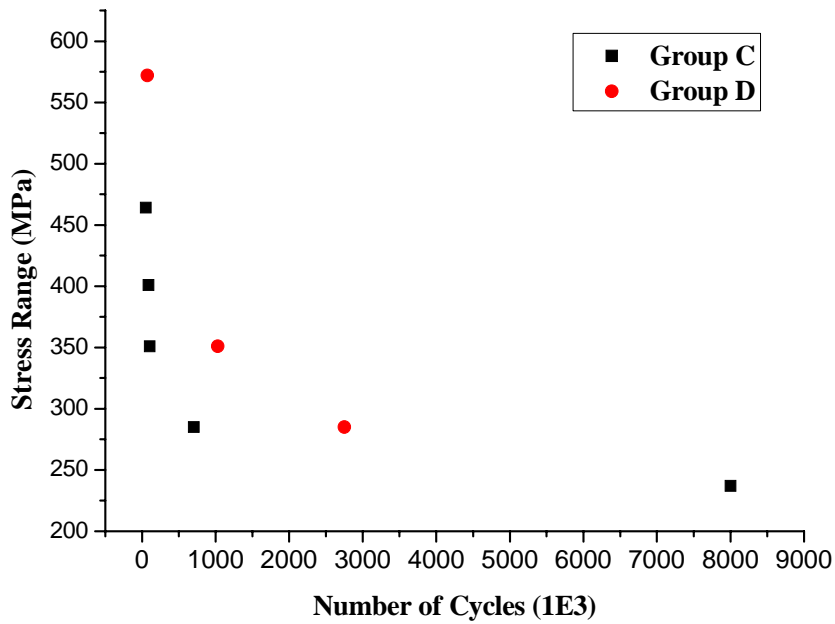


FIGURE 5-34 Fatigue lives of group C and D.

5.3.4 Discussions and conclusions

Shot peening postpones both crack initiation and crack propagation significantly, however, high accuracy of operational parameters are demanded, such as shot material, peening settings, intensity and coverage of components [9]. These parameters can influence the effect of shot peening dramatically. However, it is known that peening time and alternating stress are the only two significant factors for FBP. Therefore, the typical advantages of shot peening and less strict control are available for FBP technique.

The results of the fatigue tests confirm that FBP is an effective technique to improve the fatigue life of steel components. At low stress range fatigue loading the effect of treatment is more significant, the most effective can be 11.8 times than before. However, at high stress range, the fatigue life is improved much less, about 1.6 times than before. The tested results can be helpful to fatigue resistance design and to reduce fatigue crack occurrence in not even surface of the structural elements.

Although the fatigue limit of element after treated was not obtained yet, the investigation demonstrated that FBP is useful to improve the fatigue strength to steel element, for both small cracked and non-cracked structures. The further research should focus on efficiency of the treatment presented for welded elements where exist initial defects.

References

- [1] Kirkhope KJ, Bell R, Caron L, Basu RI, Ma KT. Weld detail fatigue life improvement techniques. Part 1: review. *Marine Structures*, Vol. 2(1999), p. 447-474.
- [2] Maddox SJ. Improving the fatigue lives of fillet welds by shot peening. Proceedings IABSE Colloquium on Fatigue of Steel and Concrete Structures, Lausanne, Switzerland, 1982.
- [3] Bignonnet A, Lieurade HP, Picouet L. Improvement of the fatigue life for offshore welded connections. IIW Conference. *Welding of Tubular Structures*, Boston, 1984.
- [4] Odhiambo D, Soyama H. Cavitation shotless peening for improvement of fatigue strength of carbonized steel. *International Journal of Fatigue*, 2003; 25: 1217–1222.
- [5] Carvalho ALM, Voorwald HJC. Influence of shot peening and hard chromium electroplating on the fatigue strength of 7050-T7451 aluminum alloy. *International journal of fatigue*, 2007; 29: 1282-1291.
- [6] Haagensen PJ, Maddox SJ. IIW recommendations on post weld improvement of steel and aluminium structures. IIW Commission XIII, 2002.
- [7] Booth GS. The effect of mean stress on the fatigue lives of ground or peened fillet welded steel joints. Report 34/1977/E, The Welding Institute, Cambridge, UK, 1977.
- [8] Trufyakov VI, Mikheev PP, Kudryavtsev FY, Statnikov ES. Ultrasonic Impact Treatment of Welded Joints. IIW Doc. No. XIII-1609-95, Paris: International Institute of Welding, 1995.
- [9] Roy S, Fisher JW, Yen BT. Fatigue resistance of welded details enhanced by ultrasonic impact treatment (UIT). *International Journal of Fatigue*, 2003; 25: 1239–1247.
- [10] Huo L, Wang D, Zhang Y. Investigation of the fatigue behaviour of the welded joints treated by TIG dressing and ultrasonic peening under variable-amplitude load. *International journal of fatigue*, 2005; 27: 95-101.
- [11] Hatamleh O, Lyons L, Forman R. Laser peening and shot peening effects on fatigue life and surface roughness of friction stir welded 7075-T7351 aluminum. *Fatigue Fract Engng Mater Struct*, 2007; 30: 115–130.
- [12] Hammersley G, Hackel LA, Harris F. Surface prestressing to improve fatigue strength of components by laser shot peening. *Optics and Lasers in Engineering*, 2000; 30: 327-337.

- [13] Barletta M, Guarino S, Rubino G, Tagliaferri V. Progress in fluidized bed assisted abrasive jet machining (FB-AJM): Internal polishing of aluminium tubes. *International Journal of Machine Tools & Manufacture*, 2007; 47: 483–495.
- [14] Barletta M, Lambiase F, Tagliaferri V. Improvement of fatigue behaviour high strength aluminium alloys by Fluid Bed Peening (FBP). *Key Engineering Materials*, 2007; 344: 87-95.
- [15] Barletta M, GBolelli G, Guarino S, Lusvarghi L. Development of matte finishes in electrostatic (EFB) and conventional hot dipping (CHDFB) fluidized bed coating process. *Progress in Organic Coatings*, 2007; 59: 53–67.
- [16] Maddox SJ. *Fatigue strength of welded structures*. Abington, Cambridge, Abington Publishing; 1991.
- [17] ASM International. *Weld Integrity and Performance: A Source Book Adapted from Asm International Handbooks, Conference Proceedings, and Technical Books (ASM Handbook) (Hardcover)*. ASM International, 1997.
- [18] Fisher JW. Evolution of fatigue-resistant steel bridge. Distinguished Lectureship. *Transportation Research Board, 76th Annual Meeting, Washington DC, 1997: 12-16.*
- [19] Bowman MD. Fatigue design and retrofit of steel bridge. *Structural Engineering and Material*, 1997; 1(1): 107-114.
- [20] Matsuiski M, Endo T. *Fatigue of metals subjected to varying stress*. Japan Soc. Mech. Engineering, 1969.

CHAPTER 6

CONCLUSIONS AND RECOMMENDATIONS

6.1 Conclusions

Fatigue problem of orthotropic deck bridges is being investigated widely in the world. For example, fatigue tests under the guide of Fisher are continuing at ATLSS center (Lehigh University, U.S.A.). When the author visited ATLSS, they were preparing a fatigue test of a full scaled model of bridge deck. Although the problem is studied widely, there are still many difficulties not solved.

In this study, the stress performances of the orthotropic deck were carried out through the numerical analyses (both the global model and the submodel). Then, the evaluation of the fatigue resistance was conducted by the structural hot spot stress approach. Furthermore, the fatigue tests for the specimens treated by FBP were carried out in the laboratory, and it is found that FBP technique can improve the fatigue life of the steel specimen.

In terms of the numerical analyses, the following can be concluded:

- The analyzed results shows that the shape of the cutout has an important influence on the hot spot stress, and particularly to the peak stress on the cutout termination at the rib;
- The shape of cutout influences slightly to the deformation of the diaphragm, the deck plate and the ribs;
- Orthotropic deck with cutout developed from Eurocode3, and which is formed by bulkhead is a good choose to the bridge designer;
- Wheel transverse position relative to its mean has an impact on the stress range spectrum. The worst position to give worst effects for a particular detail must be determined by trial and error;
- Connection details, such as rib-to-diaphragm-to-deck plate, rib-to-diaphragm and rib-to-deck plate, are sensitive to fatigue cracking due to high concentrated stress

- and residual stress;
- Bulkhead can change significantly the stress at the rib-to-diaphragm-to-deck plate connection, the rib-to-diaphragm connection, and the stress at the rib-to-bulkhead connection;
 - Thicker deck plate can decrease the peak stress at critical connections in orthotropic deck bridge, e.g. rib-to-deck plate, and reduce the stresses at rib-to-diaphragm-to-deck plate and rib-to-diaphragm connections. Thinner deck plate provides worse performance to the deck plate and a majority of the critical welded connections.
 - The three-step approach based on the global model, the submodel and the structural hot spot stress can be used to evaluate the fatigue resistance of rib-to-deck plate connections in the orthotropic deck. Structural hot spot stress can be helpful to predict the fatigue resistance of other welded joints;
 - The submodel analyses show that sudden change of stress occurs at/near the rib-to-deck plate connection, not only at the bottom of deck plate but also at the top. Sudden change of stress is found at/near the weld toe where the area is very small and therefore is difficult to be measured;
 - Displacement instead of moment or stress based on the global analysis as the load to the submodel is feasible, as well as to the reference detail model;
 - Different points at the same connection also have different fatigue resistance. For example, Point B is more sensitive to fatigue failure than Point A and Point C according to the evaluation of the three-step approach.

Based on state-of-the-art literature review, the following can be concluded:

- Most of the S-N curves are according to the normal stress in these codes/specifications, and only some of them are based on the shear stress;
- There are not many codes/specifications cover the S-N curves of variable amplitude loading since the test results from laboratory are very discrete;
- The critical welded details provided in these codes/specifications are insufficient for the fatigue design of orthotropic deck bridges. More detailed codes/specifications should be provided to help bridge designers and consulting engineering firms;

Furthermore, the following can be concluded based on the fatigue tests:

- The test results showed that FBP can be helpful to improve the fatigue resistance of steel components, both for notched and non-notched specimens;
- At low stress range fatigue loading the effect of treatment is more significant, the most effective can be 11.8 times than before. However, at high stress range, the fatigue life is improved much less, about 1.6 times than before. It means that the effect of treatment is related with the stress range.

6.2 Recommendations

The FE analyses of this study are based on the typical orthotropic deck. Although it is very helpful to bridge designers, the fatigue test of full-scale model is necessary for long span bridge. Recently, most of long span suspension bridges and cable stayed bridges become to take use of the orthotropic deck box girder by bridge designers because its significant advantages, such as less self weight, higher bending resistance and torsional resistance. Although many orthotropic deck box girders have been applied to long span bridges, the basic theories are behind compared to the techniques of construction due to the more complex composition. The benefits that orthotropic decks provide have not yet been fully discovered. The tools at our disposal for such discoveries are various. Testing is foreseen to round out the database where complex geometries and loads obtain. Meanwhile, the current codes/specifications are not sufficient to the fatigue design, and more welded details should be tested and investigated.

The investigation demonstrated that FBP is useful to improve the fatigue strength to steel element, for both small cracked and non-cracked structures. The further research should focus on efficiency of the treatment presented for welded elements where exist initial defects. Meanwhile, a suitable instrument should be designed for practical projects.

REFERENCES

- AASHTO. AASHTO LRFD Bridge Design Specifications, 2005.
- Abruzzese D, Grimaldi A, Qian ZH. Fatigue Behaviors of Cutout at Crossbeam of Trapezoidal Rib Orthotropic Deck; International Orthotropic Bridge Conference, U.S.A., 2008: 256-266.
- Abruzzese D, Qian ZH. Fatigue Problems for Orthotropic Deck Bridges. Handling Exceptions in Structural Engineering: Robustezza Strutturale, Scenari Accidentali, Complessità di Progetto”; University of Rome “La Sapienza”, Italy: DOI: 10.3267/HE2008, (2008).
- AISC. Design manual for orthotropic steel plate bridges. New York: American Institute of Steel Construction; 1963.
- AISC. Load and Resistance Factor Design Specification for Structural Steel Buildings, 1999.
- ASM International. Weld Integrity and Performance: A Source Book Adapted from Asm International Handbooks, Conference Proceedings, and Technical Books (ASM Handbook) (Hardcover). ASM International, 1997.
- Atzori B, Lazzarin P, Meneghetti G, Ricotta M. Fatigue design of complex welded structures. International Journal of Fatigue, 2009; 31: 59–69.
- Barletta M, Bolelli G, Guarino S, Lusvarghi L. Development of matte finishes in electrostatic (EFB) and conventional hot dipping (CHDFB) fluidized bed coating process. Progress in Organic Coatings, 2007; Vol. 59: 53–67.
- Barletta M, Guarino S, Rubino G, Tagliaferri V. Progress in fluidized bed assisted abrasive jet machining (FB-AJM): Internal polishing of aluminium tubes. International Journal of Machine Tools & Manufacture, 2007; 47: 483–495.
- Barletta M, Lambiase F, Tagliaferri V. Improvement of fatigue behaviour high strength aluminium alloys by Fluid Bed Peening (FBP). Key Engineering Materials, 2007; Vol.344: 87-95.
- Barletta M, Lambiase F, Tagliaferri V. Improvement of fatigue behaviour high strength aluminium alloys by Fluid Bed Peening (FBP). Key Engineering Materials, 2007; 344: 87-95.
- Battista RC, Pfeila MS, Carvalho E. ML. Fatigue life estimates for a slender orthotropic steel deck. Journal of Constructional Steel Research, 2008; 64: 134–143.
- Bignonnet A, Lieurade HP, Picouet L. Improvement of the fatigue life for offshore welded connections. IIW Conference. Welding of Tubular Structures, Boston, 1984.
- Bocchieri WJ, Fisher JW. Williamsburg Bridge Replacement Orthotropic Deck As-built Fatigue Test. ATLSS Report No. 98-04. May, 1998.
- Booth GS. The effect of mean stress on the fatigue lives of ground or peened fillet welded

- steel joints. Report 34/1977/E, The Welding Institute, Cambridge, UK, 1977.
- Bowman MD. Fatigue design and retrofit of steel bridge. *Structural Engineering and Material*, 1997; 1(1): 107-114.
- Camo S, Ye Q. Orthotropic decks-lesson learned from recent analyses and testing. International Orthotropic Bridge Conference, 2004, Sacramento, U.S.A.
- Caramelli S, Froli M, Croce P, Sanpaolesi L. Ermudungsverhalten Orthotrope Platten in Stahlbrücken. IABSE Volume: Remaining Fatigue Life of Steel Structures, ETH-Honggerberg, Zurich; 1990: 271-280.
- Carvalho ALM, Voorwald HJC. Influence of shot peening and hard chromium electroplating on the fatigue strength of 7050-T7451 aluminum alloy. *International journal of fatigue*, 2007; 29: 1282-1291.
- Chen W, Duan L. *Bridge Engineering Handbook*. Boca Raton: CRC Press, 2000.
- Cheung YK. The finite strip method in the analysis of elastic plates with two opposite simply supported ends. *Proc. Inst. Civ. Eng.*, May 1968: 1-7.
- China Zhongtie Major Bridge Reconnaissance & Design Institute. Code for Design on Steel Structure of Railway Bridge, TB10002.2-99. Ministry of Railway (MOR), 2000 (in Chinese).
- Collins JA. *Failure of materials in mechanical design: analyses, prediction, prevention*. Wiley-Interscience Publication, 1993.
- Connor RJ, Fisher JW. Consistent approach to calculating stresses for fatigue design of welded rib-to-web connections in steel orthotropic bridge decks. *Journal of Bridge Engineering*, 2006; 11(5): 517-525.
- Connor RJ, Fisher JW. Results of Field Measurements on the Williamsburg Bridge Orthotropic Deck. ATLSS Report No. 01-01. January, 2001.
- Connor RJ. Influence of cutout geometry on stresses at welded rib to diaphragm connections in the steel orthotropic bridge decks. *Journal of the Transportation Research Board*, 2004; 1892: 78-87.
- Cornelius W. Die berechnung der ebener flachentragwerke mit hilfe der theorie der orthogonal anisotropen platten. *Der Stahlbau*, 1952; 2: 21-26.
- Corten HT, Dolan TJ. Cumulative fatigue damage. *Proceedings of International Conference on Fatigue of metals*, ASME and IME, 1956; 235-246.
- De Fries-Suene A, Scordelis AC. Direct stiffness solution for folded plates. *J. Strut. Div. ASCE*, 1964; 90 (ST4): 15-47.
- De Jong FBP. Overview fatigue phenomenon in orthotropic bridge decks in the Netherlands. Orthotropic Bridge Conference, Sacramento, California, USA, 2004: 489-512.

- Doerk O, Fricke W, Weissenborn C. Comparison of different calculation methods for structural stresses at welded joints. *International Journal of Fatigue*, 2003; 25: 359-369.
- Dong P. A structural stress definition and numerical implementation for fatigue analyses of welded joints. *International Journal of Fatigue*, 2001; 23: 865-876.
- Eurocode 3: Design of Steel Structures, Part 1.9: Fatigue, 2004.
- Fatigue Design of Offshore Steel Structures Recommended Practice. Det Norske Veritas DNV-RP-C203, 2005.
- Fisher JW. Evolution of fatigue-resistant steel bridge. Distinguished Lectureship. Transportation Research Board, 76th Annual Meeting, Washington DC, January 12-16. Paper No. 971520.1-22, 1997.
- Freudenthal AM, Heller RA. On stress interaction in fatigue and a cumulative damage rule. *Journal of the institute of Aeronautical Sciences*, 1954; 26(7): 431-442.
- Fryba L, Gajdos L. Fatigue properties of orthotropic decks on railway bridges. *Engineering Structures*, 1999; 21: 639–652.
- Fuller JR. Research on techniques of establishing random type fatigue curves for broad band sonic loading. National Aeronautical Meeting, Society of Automotive Engineers and American Society of Naval Engineers, 1963; Paper 761C.
- Grover HJ. An observation concerning the cycle ratio in cumulative damage. *Fatigue in Aircraft Structures*, STP-274, American Society for Testing and Materials, Philadelphia, 1960: 120-124.
- Guagliano M, Vergani L. An approach for prediction of fatigue strength of shot peened components, *Engineering Fracture Mechanics*, 2004; Vol. 71: 501-512
- Gurney T. *Cumulative damage of welded joints*. Woodhead Publishing Limited, 2006.
- Guyon Y. Calcul De Ponts Larges a Prouties Multiples Solidarisees Par des Entretoises. *Ann. De Ports et Chavsees de France*, 1946; 24(5):553-612.
- Haagensen P.J, Maddox S J. IIW recommendations post weld improvement steel and aluminium structures. IIW Commission XIII-1815-00. International Institute of Welding, 2002.
- Hammersley G, Hackel LA, Harris F. Surface prestressing to improve fatigue strength of components by laser shot peening. *Optics and Lasers in Engineering*, 2000; 30: 327-337.
- Hatamleh O, Lyons L, Forman R. Laser peening and shot peening effects on fatigue life and surface roughness of friction stir welded 7075-T7351 aluminum. *Fatigue Fract Engng Mater Struct*, 2007; 30: 115–130.
- Henry DL. Theory of fatigue damage accumulation in steel. *ASME Transactions*, 1955; 99: 913-918.

- Hobbacher A. Recommendations for fatigue design of welded joints and components. IIW document XIII-1965-03/XV-1127-03. International Institute of Welding; 2003.
- Huo L, Wang D, Zhang Y. Investigation of the fatigue behaviour of the welded joints treated by TIG dressing and ultrasonic peening under variable-amplitude load. *International journal of fatigue*, 2005; 27: 95-101.
- Japan Road Association (JRA). *Fatigue Design Specifications for Steel Bridges*. Japan Road Association, 2002 (in Japanese).
- Japanese specification for highway bridges, Part II steel bridge. Tokyo: Japan Road Association, 1996.
- Jen W. *Strength of steel orthotropic deck with trapezoidal shaped longitudinal stiffeners*. Lehigh University, 2006.
- Kirkhope KJ, Bell R, Caron L, Basu RI, Ma KT. Weld detail fatigue life improvement techniques. Part 1: review. *Marine Structures*, Vol. 2(1999), p. 447-474.
- Kiss K, Dunai L. Fracture mechanics based fatigue analysis of steel bridge decks by two-level cracked models. *Computers and Structures*, 2002; 80: 2321–2331.
- Lee YL, Pan J, Richard Hathaway, Mark Barkey. *Fatigue Testing and Analyses: Theory and Practice*. Elsevier Butterworth–Heinemann, 2005
- Lehrke H. Fatigue tests on large size specimens of stiffener to diaphragm connections. IABSE Volume: *Remaining Fatigue Life of Steel Structures*, ETH-Honggerberg, Zurich; 1990: 249-258.
- Lundberg G, Palmgren A. *Dynamic capacity of rolling bearings*. Acta Polytechnica Mechanical Engineering Series, Stockholm, Sweden, 1947; 1(3).
- Maddox SJ. *Fatigue strength of welded structures*. Abington, Cambridge, Abington Publishing; 1991.
- Maddox SJ. Improving the fatigue lives of fillet welds by shot peening. *Proceedings IABSE Colloquium on Fatigue of Steel and Concrete Structures*, Lausanne, Switzerland, 1982.
- Mahmoud HN, Connor RJ, Fisher JW. Finite Element Investigation of the Fracture Potential of Highly Constrained Details in Steel Plate Members. *Computer-Aided Civil and Infrastructure Engineering*, 2005; 20: 383–392.
- Mangus AR, Sun S. *Orthotropic Deck Bridges*. Bridge Engineering Handbook (Ed. Wai-Fah Chen and Lian Duan). Boca Raton: CRC Press, 2000.
- Marco SM, W.L. Starkey. A concept of fatigue damage. *ASME Transactions*, 1954; 76: 627-632.
- Massonnet C. *Methods of Calculation of Bridges with Several Longitudinal Beams Taking Into Consideration Their Torsional Resistance*. International Association for Bridge

- and Structural Engineering Publications, 1950; 10: 147-182.
- Matsuiski M, Endo T. Fatigue of metals subjected to varying stress. Japan Soc. Mech. Engineering, 1969.
- Miner MA. Cumulative damage in fatigue. Journal of Applied Mechanics, 1945; 12(3):159-164.
- Ministry of Housing and Urban-Rural Development of the People's Republic of China (MOHURD). Code for Design of Steel Structures, GB 50017-2003. MOHURD, 2003 (in Chinese).
- Morice PB, Little G, Rowe RE. Design curves for the effects of concentrated loads on concrete bridge decks. Publication DB11a, Cement and Concrete Association, 1956.
- Mutoh Y, Fair GH, Noble B, Waterhouse RB. The effect of residual stresses induced by shot-peening on fatigue crack propagation in two high strength aluminum alloys. Fatigue Fract Eng Mater Struct, 1987; Vol. 10(4): 216–72.
- Norme Tecniche per le Costruzioni; 2008 (In Italian).
- NTC. Norme Tecniche per le Costruzioni, 2008 (In Italian).
- Odhiambo D, Soyama H. Cavitation shotless peening for improvement of fatigue strength of carbonized steel. International Journal of Fatigue, 2003; 25: 1217–1222.
- Paik JK, Thayamballi AK. Ultimate limit state design of steel plated structures. John Wiley & Sons, 2003.
- Pelikan W, Esslinger M. Die Stahlfahrbahn Berechnung und Konstruktion. MAN ForschHeft, 1957, 7.
- Pfeila MS, Battista RC, Mergulhão A JR. Stress concentration in steel bridge orthotropic decks. Journal of Constructional Steel Research, 2005; 61: 1172-1184.
- Powell GH, Ogden DW. Analysis of orthotropic steel plate bridge decks. J. Strut. Div. ASCE 1969; 95: 909–922.
- Qian ZH, Abruzzese D. Fatigue Failure of Welded Connections at Orthotropic Bridges. Frattura ed Integrità Strutturale. Gruppo Italiano Frattura, 2009; 9: 105-112.
- Rowe RE. Concrete bridge design. C. R. Books, London, 1962.
- Roy S, Fisher JW, Yen BT. Fatigue resistance of welded details enhanced by ultrasonic impact treatment (UIT). International Journal of Fatigue, 2003; 25: 1239–1247.
- Seim C, Ingham T. Influence of wearing surfacing on performance of orthotropic steel plate decks. Transportation Research Record: Journal of the Transportation Research Board, National Research Council, Washington, D.C., 2004; 1892: 98–106.
- Shanley FR. A theory of fatigue based on unbonding during reversed slip. Report No. P350, The Rand Corporation, 1952.

- Steel, concrete and composite bridges - Part 10: Code of practice for fatigue, 1980.
- Tekeli S. Enhancement of fatigue strength of SAE 9245 steel by shot peening. *Mater Lett.*, 2002; Vol. 57: 604–608.
- Timoshenko S, Woinowsky-Krieger S. *Theory of plates and shells*. McGraw-Hill Book Company, 1959.
- Tinawi R, Redwood RG. Orthotropic bridge decks with closed stiffeners - analysis and behaviour. *Computers & Structures*, 1977; 7: 683-699.
- Troitsky MS. *Orthotropic Bridges - Theory and Design*, 2nd ed., The James F. Lincoln Arc Welding Foundation, Cleveland, 1987.
- Troitsky MS. *Stiffened Plates, Bending, Stability and Vibrations*, Elsevier, 1976, New York.
- Trufyakov VI, Mikheev PP, Kudryavtsev FY, Statnikov ES. *Ultrasonic Impact Treatment of Welded Joints*. IIW Doc. No. XIII-1609-95, Paris: International Institute of Welding, 1995.
- Tsakopoulos PA, Fisher JW. Fatigue performance and design refinements of steel orthotropic deck panels based on full-scale laboratory tests. *Steel structures*, 2005; 5: 211-223.
- Tsakopoulos PA, Fisher JW. Full-scale fatigue tests of steel orthotropic decks for the Williamsburg Bridge. *Journal of Bridge Engineering*, 2003; 8(5): 323-333.
- Tvergaard V, Needleman A. Buckling of eccentrically stiffened elastic-plastic panels on two simple supports or multiply supported, *Int. J. Solids Structures*, 1975, Vol. 11: 647-663.
- Vlasov VZ. *Thin-walled elastic beams*. Israel Program for Scientific Translation, NSF, Jerusalem, 1967. (in English; original Russian edition, 1959)
- Xanthakos DP. *Theory and design of bridges*. John Wiley & Sons, Inc. 1994.
- Xiao ZG. Fatigue cracks in longitudinal stiffeners of steel orthotropic deck. *International Journal of Fatigue*, 2006; 28: 409-416.
- Yao WX, Ye B, Zheng LC. A verification of the assumption of anti-fatigue design. *International Journal of Fatigue*, 2001; 23: 271–277.
- Yarnold MT, Wilson JL, Jen W, Yen BT. Local buckling analysis of trapezoidal rib orthotropic bridge deck systems. *Bridge Structures*, 2007; 3(2): 93-103.